nagra.

Arbeitsbericht NAB 22-04

TBO Bachs-1-1: Data Report

Dossier VIII
Rock Properties, Porewater Characterisation and Natural Tracer Profiles

August 2023

E. Gaucher, L. Aschwanden, T. Gimmi,
A. Jenni, M. Kiczka, M. Mazurek, P. Wersin,
C. Zwahlen, U. Mäder & D. Traber

National Cooperative
for the Disposal of
Radioactive Waste

Hardstrasse 73
P.O. Box
5430 Wettingen
Switzerland
Tel. +41 56 437 11 11

nagra.ch

nagra.

Arbeitsbericht NAB 22-04

TBO Bachs-1-1: Data Report

Dossier VIII Rock Properties, Porewater Characterisation and Natural Tracer Profiles

August 2023

E. Gaucher[1], L. Aschwanden[1], T. Gimmi[1], A. Jenni[1], M. Kiczka[1], M. Mazurek[1], P. Wersin[1], C. Zwahlen[1], U. Mäder[1,2] & D. Traber[3]

[1] Rock-Water Interaction, University of Bern

[2] Rock-Water Consulting, Boll

[3] Nagra

Keywords:
BAC1-1, Nördlich Lägern, TBO, deep drilling campaign, rock properties, petrophysical parameters, water content, porosity, mineralogy, clay content, clay mineral composition, porewater chemistry, natural tracer profiles

National Cooperative for the Disposal of Radioactive Waste

Hardstrasse 73
P.O. Box
5430 Wettingen
Switzerland
Tel. +41 56 437 11 11

nagra.ch

Nagra Arbeitsberichte ("Working Reports") present the results of work in progress that have not necessarily been subject to a comprehensive review. They are intended to provide rapid dissemination of current information.

This NAB aims at reporting drilling results at an early stage. Additional borehole-specific data will be published elsewhere.

In the event of inconsistencies between dossiers of this NAB, the dossier addressing the specific topic takes priority. In the event of discrepancies between Nagra reports, the chronologically later report is generally considered to be correct. Data sets and interpretations laid out in this NAB may be revised in subsequent reports. The reasoning leading to these revisions will be detailed there.

This Dossier was prepared by the Rock-Water Interaction Group of the University of Bern (authors are listed in the individual chapters). D. Traber was the responsible Nagra project manager.

The authors warmly acknowledge the laboratory work of:
P. Bähler and C. Pichler efficiently produced a substantial part of the data presented in this report.
U. Eggenberger, J. Krbanjevic, M. Wolffers J.W. Zucha and F. Gfeller provided data for mineralogical and BET analyses as well as evaluation tools.
D. Roos, J. Richards and L. de Doliwa Zielinski performed sampling and processing of the cores.
T. Oyama (CRIEPI, Japan) kindly collaborated in the context of porewater squeezing.

We also acknowledge the experimental and analytical work performed at Hydroisotop GmbH.

We are also grateful for the excellent work of the drill-site team who successfully provided sealed core samples according to our specifications.

N. Schwendener from IRM (University of Bern) provided X-ray CT scans of a substantial number of core samples, with support by L. Keller (ZHAW) for some of the CT sessions.

We thank P. Blaser and M. Unger for editorial work.

The comments and suggestions of Andreas Gautschi on an earlier version of the manuscript are gratefully acknowledged.

Table of Contents

List of Tables

List of Figures

Electronic Appendices

App. A: Comprehensive database with results of laboratory analyses (xls format)

App. B: Detailed documentation of advective-displacement experiments (xls format)

Note: Appendices are available upon request.

1 Introduction

1.1 Context

To provide input for site selection and the safety case for deep geological repositories for radioactive waste, Nagra has drilled a series of deep boreholes ("Tiefbohrungen", TBO) in Northern Switzerland. The aim of the drilling campaign is to characterise the deep underground of the three remaining siting regions located at the edge of the Northern Alpine Molasse Basin (Fig. 1-1).

In this report, we present the results from the Bachs-1-1 borehole.

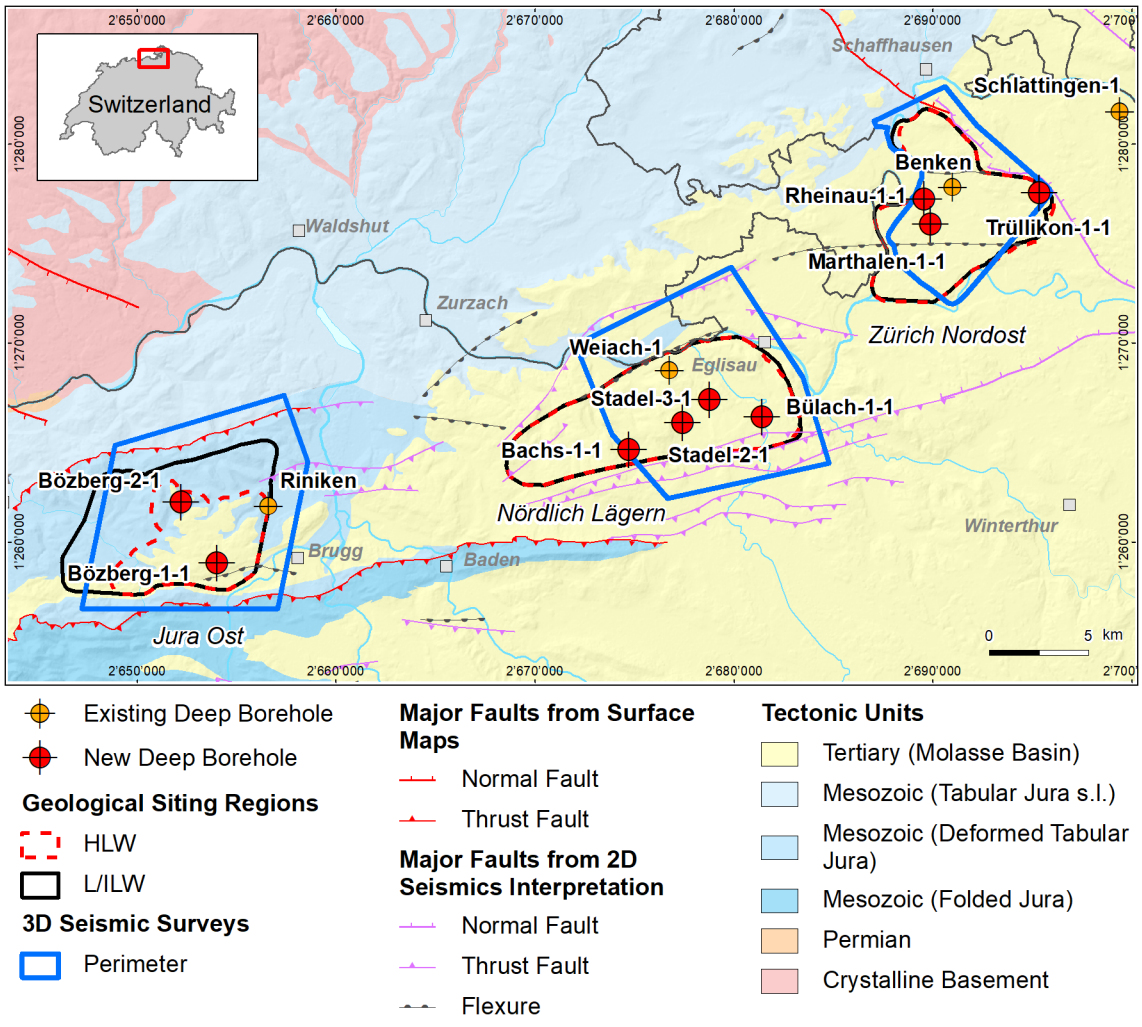

Fig. 1-1: Tectonic overview map with the three siting regions under investigation

1.2 Location and specifications of the borehole

The Bachs-1-1 (BAC1-1) exploratory borehole is the ninth (and last) borehole drilled within the framework of the TBO project. The drill site is located in the western part of the Nördlich Lägern siting region (Fig. 1-2). The vertical borehole reached a final depth of 1'306.26 m (MD)[1]. The borehole specifications are provided in Tab. 1-1.

Due to a loss of a measurement tool (dilatometer), the borehole was cemented up to 500 m MD and a sidetrack was initiated with a kickoff point (KOP) at about 600 m MD. This sidetrack was labelled Bachs-1-1B (BAC1-1B). BAC1-1B reached a final depth of 952 m MD but was abandoned during borehole reaming operations due to entering the original borehole BAC1-1. Therefore, the vertical borehole BAC1-1 was used again for the remaining investigations. For easier communication and labelling, the name BAC1-1 is generally used for this borehole, including the sidetrack, unless stated otherwise. A detailed description of all technical details about the drilling process can be found in Dossier I.

Tab. 1-1: General information about the BAC1-1 borehole

Siting region	Nördlich Lägern
Municipality	Bachs (Canton Zürich / ZH), Switzerland
Drill site	Bachs-1 (BAC1)
Borehole	Bachs-1-1 (BAC1-1) including sidetrack Bachs-1-1B (BAC1-1B)
Coordinates	LV95: 2'674'769.089 / 1'264'600.698
Elevation	Ground level = top of rig cellar: 450.35 m above sea level (asl)
Borehole depth	1'306.26 m measured depth (MD) below ground level (bgl)
Drilling period	10th September 2021 – 23rd April 2022 (spud date to end of rig release)
Drilling company	Daldrup & Söhne AG
Drilling rig	Wirth B 152t
Drilling fluid	Water-based mud with various amounts of different components such as[2]: 0 – 700 m: Bentonite & polymers 700 – 1'057 m: Potassium silicate & polymers[3] 1'057 – 1'129 m: Water & polymers 1'129 – 1'306.26 m: Sodium chloride brine & polymers

The lithostratigraphic profile and the casing scheme are shown in Fig. 1-3. The comparison of the core versus log depth[4] of the main lithostratigraphic boundaries in the BAC1-1 borehole is shown in Tab. 1-2.

[1] Measured depth (MD) refers to the position along the borehole trajectory, starting at ground level, which for this borehole is the top of the rig cellar. For a perfectly vertical borehole, MD below ground level (bgl) and true vertical depth (TVD) are the same. In all Dossiers depth refers to MD unless stated otherwise.

[2] For detailed information see Dossier I.

[3] Including sidetrack.

[4] Core depth refers to the depth marked on the drill cores. Log depth results from the depth observed during geophysical wireline logging. Note that the petrophysical logs have not been shifted to core depth, hence log depth differs from core depth.

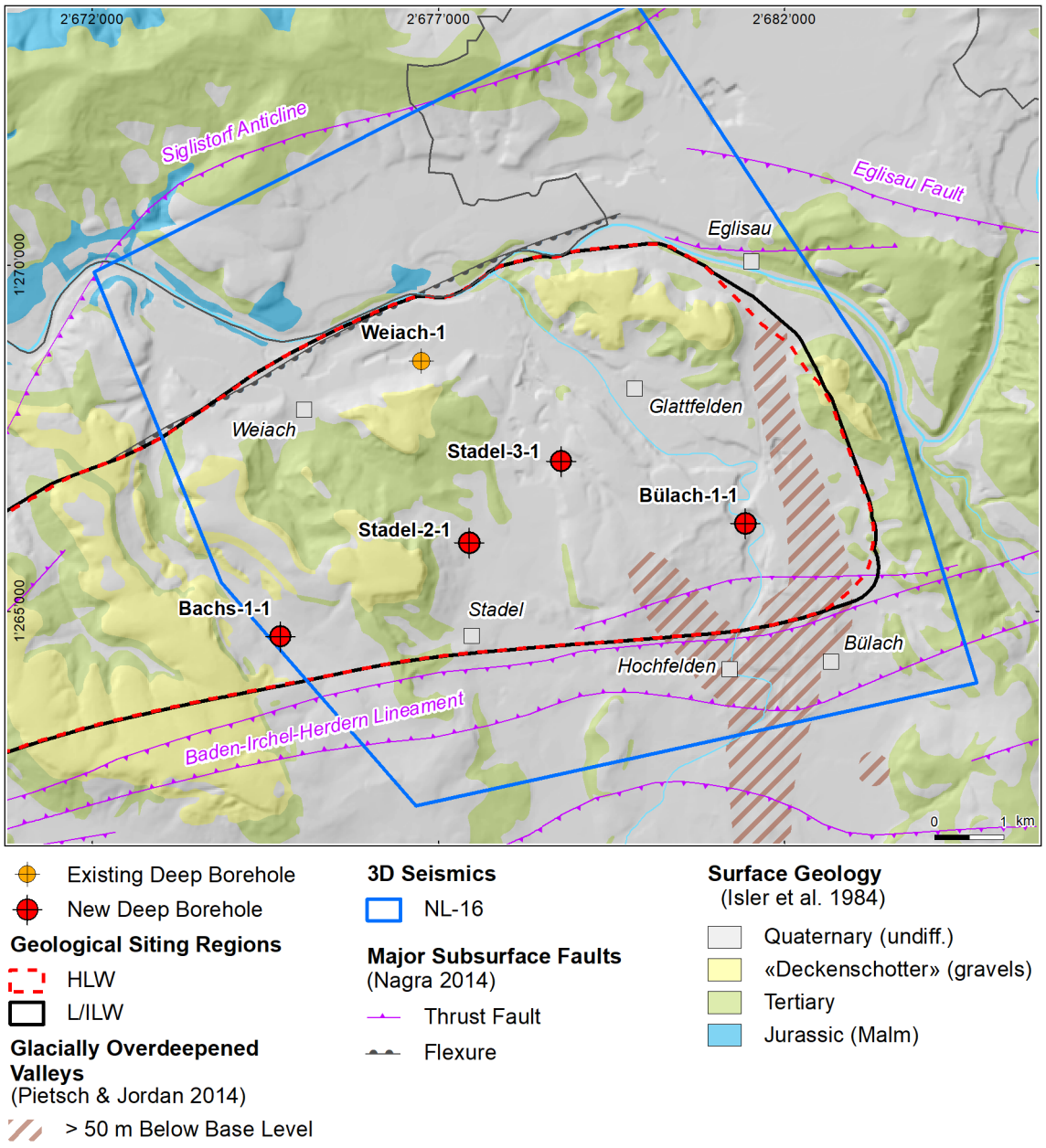

Fig. 1-2: Overview map of the investigation area in the Nördlich Lägern siting region with the location of the BAC1-1 borehole in relation to the boreholes Weiach-1, BUL1-1, STA3-1 and STA2-1

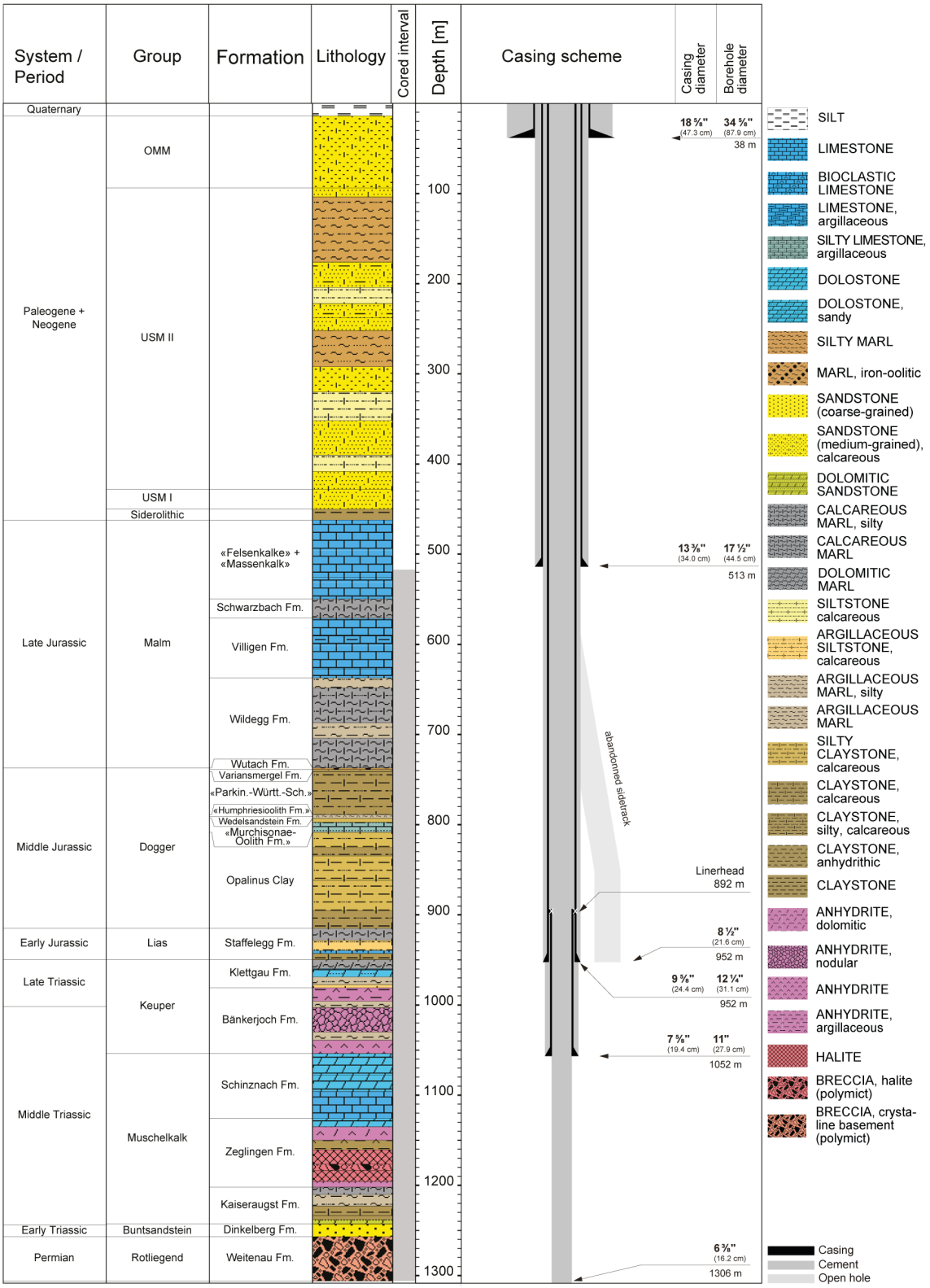

Fig. 1-3: Lithostratigraphic profile and casing scheme for the BAC1-1 borehole[5]

[5] For detailed information see Dossier I and III.

Tab. 1-2: Core and log depth for the main lithostratigraphic boundaries in the BAC1-1 borehole[6]

System / Period	Group	Formation		Core top depth in m (MD)	Log top depth in m (MD)	
Quaternary				**14**		—
Paleogene + Neogene	OMM			94		—
	USM			450		—
	Siderolithic			**462**		—
Jurassic	Malm	«Felsenkalke» + «Massenkalk»		549.69	550.03	—
		Schwarzbach Formation		570.98	571.29	—
		Villigen Formation		637.31	637.55	—
		Wildegg Formation		737.05	737.32	—
	Dogger	Wutach Formation		738.81	739.08	—
		Variansmergel Formation		741.22	741.47	—
		«Parkinsoni-Württembergica-Schichten»		788.92	789.12	—
		«Humphriesioolith Formation»		791.05	791.25	—
		Wedelsandstein Formation		793.11	793.31	—
		«Murchisonae-Oolith Formation»		808.34	808.57	—
		Opalinus Clay		914.91	915.30	—
	Lias	Staffelegg Formation		**949.73**	**950.07**	—
Triassic	Keuper	Klettgau Formation		980.93	981.27	—
		Bänkerjoch Formation		1053.90	1054.30	—
	Muschelkalk	Schinznach Formation		1125.75	1126.20	—
		Zeglingen Formation		1202.03	1202.43	—
		Kaiseraugst Formation		1242.82	1243.12	—
	Buntsandstein	Dinkelberg Formation		**1256.86**	**1257.26**	—
Permian	Rotliegend	Weitenau Formation	final depth	1306.26	1306.77	

[6] For details regarding lithostratigraphic boundaries see Dossier III and IV; for details about depth shifts (core goniometry) see Dossier V.

1.3 Documentation structure for the BAC1-1 borehole

NAB 22-04 documents the majority of the investigations carried out in the BAC1-1 borehole, including laboratory investigations on core material. The NAB comprises a series of stand-alone dossiers addressing individual topics and a final dossier with a summary composite plot (Tab. 1-3).

This documentation aims at early publication of the data collected in the BAC1-1 borehole. It includes most of the data available approximately one year after completion of the borehole. Some analyses are still ongoing (e.g. diffusion experiments, analysis of veins, hydrochemical interpretation of water samples) and results will be published in separate reports.

The current borehole report will provide an important basis for the integration of datasets from different boreholes. The integration and interpretation of the results in the wider geological context will be documented later in separate geoscientific reports.

Tab. 1-3: List of dossiers included in NAB 22-04

Black indicates the dossier at hand.

Dossier	Title	Authors
I	TBO Bachs-1-1: Drilling	P. Hinterholzer-Reisegger
II	TBO Bachs-1-1: Core Photography	D. Kaehr, M. Stockhecke & Hp. Weber
III	TBO Bachs-1-1: Lithostratigraphy	P. Jordan, P. Schürch, M. Schwarz, R. Felber, H. Naef, T. Ibele & F. Casanova
IV	TBO Bachs-1-1: Microfacies, Bio- and Chemostratigraphic Analyses	S. Wohlwend, H.R. Bläsi, S. Feist-Burkhardt, B. Hostettler, U. Menkveld-Gfeller, V. Dietze & G. Deplazes
V	TBO Bachs-1-1: Structural Geology	A. Ebert, E. Hägerstedt, S. Cioldi, L. Gregorczyk & F. Casanova
VI	TBO Bachs-1-1: Wireline Logging, Micro-hydraulic Fracturing and Pressure-meter Testing	J. Gonus, E. Bailey, J. Desroches & R. Garrard
VII	TBO Bachs-1-1: Hydraulic Packer Testing	R. Schwarz, R. Beauheim, L Schlicken-rieder, E. Manukyan & A. Pechstein
VIII	TBO Bachs-1-1: Rock Properties, Porewater Characterisation and Natural Tracer Profiles	E. Gaucher, L. Aschwanden, T. Gimmi, A. Jenni, M. Kiczka, M. Mazurek, P. Wersin, C. Zwahlen, U. Mäder & D. Traber
IX	*The geomechanical campaign in BAC-1-1 was limited to two oedometric tests. Hence, no dedicated Dossier IX was produced for NAB 22-04. The hydraulic conductivity values derived from the oedometric tests are documented in the Summary Plot.*	
X	TBO Bachs-1-1: Petrophysical Log Analysis	S. Marnat & J.K. Becker
	TBO Bachs-1-1: Summary Plot	Nagra

1.4 Scope and objectives of this dossier

The dossier at hand summarises the laboratory work of the Rock-Water Interaction Group (RWI) of the University of Bern, Institute of Geological Sciences, dedicated to rock and porewater characterisation of core materials obtained from the BAC1-1 borehole. The level of ambition is to document observations and measurements and to provide a quality-assured dataset.

Data are evaluated and discussed to some degree, including consistency and plausibility checks. An in-depth discussion, sophisticated modelling efforts and regional comparisons with data from other sites are beyond the scope of this report. Additional data obtained by other groups (e.g. hydraulic tests, groundwater sampling, geophysical borehole and core logging, structural logging) are considered in several cases but not in a comprehensive way. An integrated interpretation of all available data is deferred to a later stage of the TBO programme, when results from several boreholes can be synthesised for a siting region.

Throughout this report, rock samples used for analysis are identified by their mid-sample depth in m.

Note that in this report «Brauner Dogger» is used for the Dogger units overlying the Opalinus Clay. In the Sectoral Plan Stages 1 and 2, «Brauner Dogger» is referred to the clay-rich rock sequence east of the lower Aare valley only (Nagra 2008).

2 Geoscientific data of interest and drilling conditions for the BAC1-1 borehole

Eric Gaucher, Lukas Aschwanden, Martin Mazurek.

2.1 Geological information

The BAC1-1 borehole is located at the south-western periphery of the siting region Nördlich Lägern north-west of the village of Bachs (Canton Zürich; Fig. 1-1). Nördlich Lägern lies in the Deformed Eastern Tabular Jura between the autochthonous Tabular Jura in the NW and the Folded Jura in the SW. The siting area is delineated by some major tectonic structures, the Siglistorf Anticline and the Eglisau Fault in the north and the Baden – Irchel – Herdern Lineament and the Jura Main Thrust in the south. Tectonically, the Deformed Tabular Jura is compressively overprinted by the alpine forefront. This is for example manifested by the thrust of the Mesozoic sediments about 200 m to the north assumed to have occurred in the Triassic salt layers of the Zeglingen Formation (Nagra 2014). However, according to seismic interpretations, no relevant faults were identified in the Mesozoic sediment stack at the borehole location. The regional dip of the bedding is subhorizontal towards SE.

2.2 Structural logging

The results of the structural core logging are documented in Dossier V, where the following types of structural features are distinguished:

- Fault planes and fault zones (shear structures); mainly oriented bedding-subparallel and SSE-dipping (average at 163/06).
- Brittle extensional fractures (structures without shear or slip indication, e.g., joints, veins, tension gashes); these exhibit large variation in orientation and dip (3 – 90°), however, one orientation cluster can be distinguished showing mean orientations of 276/78.
- Stylolites show one well-developed, sub-horizontal to moderate (1° to 25°) SE-dipping cluster (overall mean: 147/02) and two subordinate, steep to sub-vertical (50° to 90°) clusters with dip directions towards the N and S (overall means: 355/78; and 176/77)
- Larger open pores

The interpreted structures are unevenly distributed among the stratigraphic units. Highest frequencies of structures are observed in the carbonates of the Malm and the Schinznach Formation, but also of the Bänkerjoch Formation. The Dogger and the Liassic show distinctly less structures, especially the Opalinus Clay shows only few. However, a distinct deformation zone (911.63 m to 912.16 m log depth) was found in the Opalinus Clay (Fig. 2-1). This 0.53 m thick zone is characterised by numerous fault planes and tension gashes forming a prominent fault zone. All fault planes are mineralised (i.e. closed) with synkinematic calcite, generally < 4 mm thick and NW-SE striking (Dossier V).

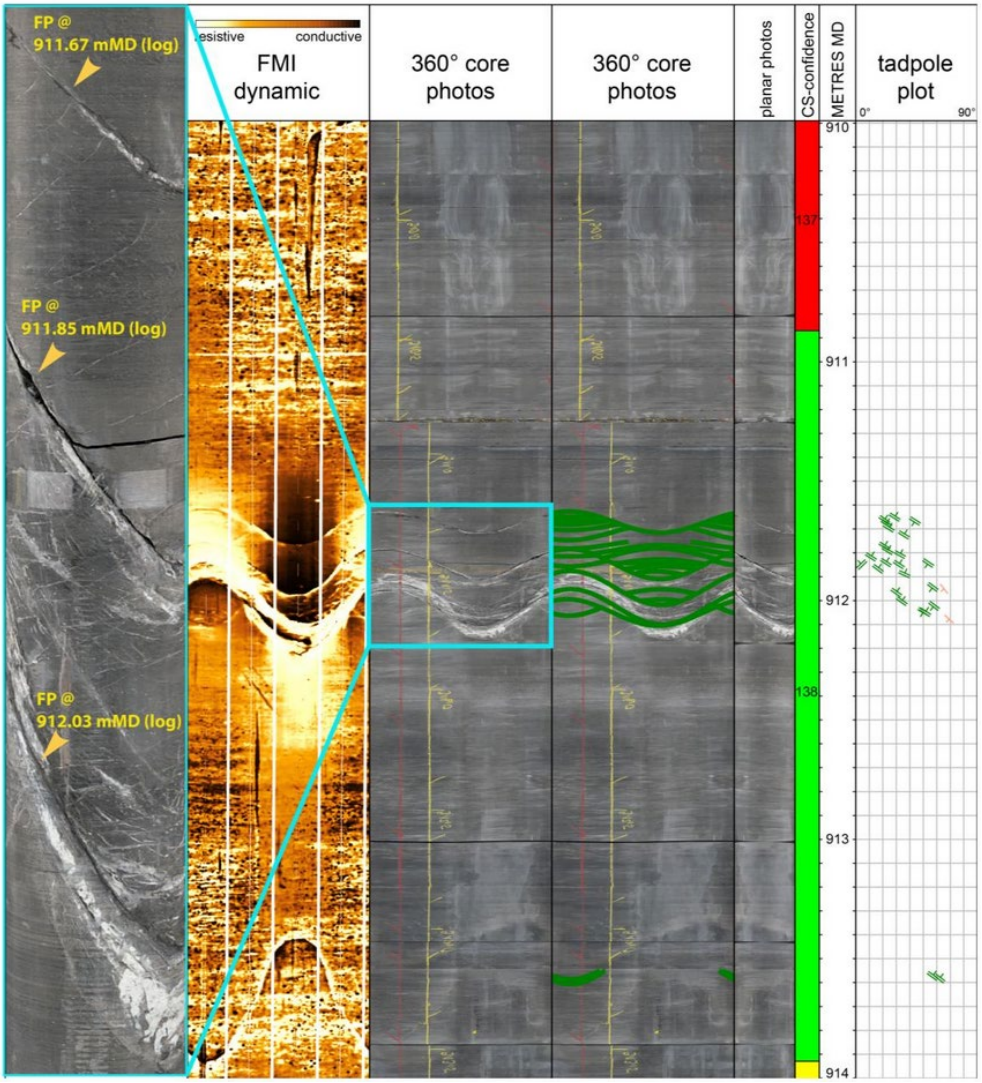

Fig. 2-1: Illustration of a distinct fault zone at 911.63 m – 912.16 m within the Opalinus Clay

Three other prominent structures were identified, one in the Staffelegg Formation (940.58 – 942.78 m) and two in the Schinznach Formation (1'060.82 m and 1'099.40 – 1'103.98 m; Dossier V). They include sets of subvertical, partly open joints.

A compilation of all individual fault zones, shear bands and mirror-like fault planes encountered in the cored section at BAC1-1 is provided in Tab. 2-1.

Tab. 2-1: Fault zones, mirror-like fault planes and shear bands in the cored section of the BAC1-1 borehole

From Dossier V. SB = shear bands.

Fault zones				
Top [m MD log depth]	**Bottom** [m MD log depth]	**Thickness** [m]	**Formation**	**Type**
568.71	568.87	0.16	Schwarzbach Formation	Fault zone
581.66	581.70	0.04	Villigen Formation	Fault zone
585.86	586.02	0.16	Villigen Formation	Fault zone
726.83	726.89	0.06	Wildegg Formation	Fault zone
911.63	912.16	0.53	Opalinus Clay	Fault zone
942.35	942.38	0.03	Staffelegg Formation	Fault zone
969.51	970.04	0.53	Klettgau Formation	Fault zone
976.27	977.75	1.48	Klettgau Formation	Fault zone
977.22	978.31	1.09	Klettgau Formation	Fault zone
977.69	977.75	0.06	Klettgau Formation	Fault zone
981.73	981.95	0.22	Bänkerjoch Formation	Fault zone
1'018.18	1'018.26	0.08	Bänkerjoch Formation	Fault zone
1'161.61	1'164.15	2.54	Zeglingen Formation	Salt SB zone
1'170.26	1'176.65	6.39	Zeglingen Formation	Salt SB zone
1'186.24	1'186.90	0.66	Zeglingen Formation	Salt SB zone

2.3 Hydrogeological conditions

Thirteen hydraulic packer tests were conducted in the BAC1-1 borehole (Dossier VII), and selected results for the more permeable Keuper and Muschelkalk aquifer sections are summarised in Tab. 2-2. Hydraulic conductivities for the clay-rich section «Brauner Dogger» to Staffelegg Formation range from 2×10^{-14} to 1×10^{-11} m/s (best estimates). Enhanced hydraulic conductivities were identified in the Keuper and Muschelkalk aquifers. The Malm section is of low transmissivity and did not yield any groundwater for sampling (Dossier VII).

Tab. 2-2: Selected results from hydraulic packer tests for the more permeable sections of the BAC1-1 borehole

The best estimates for transmissivity *T*, hydraulic conductivity *K* and hydraulic head are indicated. Data are from Dossier VII.

Top [m MD]	**Bottom** [m MD]	**Length** [m]	**Geological unit**	***T*** [m^2/s]	***K*** [m/s]	**Head** [m asl]
957.20	979.00	21.80	Klettgau Formation (Keuper aquifer)	2×10^{-7}	8×10^{-9}	350
1'080.90	1'129.00	48.10	Schinznach Fm. (Muschelkalk aquifer)	2×10^{-5}	4×10^{-7}	353

2.4 Groundwater samples

Groundwater samples with variable degrees of drilling-fluid contamination were obtained from the Keuper and Muschelkalk aquifers. For the present report, values for the chemically conservative parameters Cl and Br and the water-isotope ratios $\delta^{18}O$ and $\delta^{2}H$ are of major interest, as these serve as boundary conditions for the porewater data. These values were corrected by Lorenz (*in prep.*) for (minor) drilling-fluid contamination (< 1%) and are reproduced in Tab. 2-3 along with information on the chemical water type and mineralisation of the groundwaters.

Tab. 2-3: Conservative parameters for groundwater from the Keuper and Muschelkalk aquifers in borehole BAC1-1 corrected for drilling-fluid contamination

Parameter	**Unit**	**Keuper aquifer**	**Muschelkalk aquifer**
Chemical type		Na-Cl	Na-Ca-Cl-SO_4[*]
Mineralisation (TDS)	[g/L]	20.3[*]	4.23[*]
Chloride (Cl)	[mg/L]	9'745[**]/ 9'964[***]	1'221[**]/ 1'246[****]
Bromide (Br)	[mg/L]	24.4[**]/ 25.0[***]	0.20[**]/ 0.19[****]
1000·Br/Cl	[molal]	1.11[**]/ 1.11[***]	0.07[**]/ 0.07[****]
$\delta^{18}O$ of water	[‰VSMOW]	–5.47[**]/ –5.43[***]	–11.80[**]/ –11.83 [****]
$\delta^{2}H$ of water	[‰VSMOW]	–45.4 [**]/ –45.4 [***]	–86.0 [**]/ –86.2 [****]
Test interval	[m MD]	957.20 – 979.00	1'080.90 – 1'129.00

[*] Considering the ignition residue at 600°C.
[**] Corrected based on uranine (Lorenz *in prep.*)
[***] Corrected based on 1.5-NDSA (Lorenz *in prep.*)
[****] Corrected based on Tritium (Lorenz *in prep.*)

2.5 Drilling conditions and drilling fluids

Three different types of drilling fluid were used in the BAC1-1 borehole (Dossier I). A bentonite polymer mud was used for the Quaternary and most of the Malm (until 700 m MD), a potassium silicate polymer mud for the Dogger, Lias and Keuper, a water-based mud with polymers for the upper part of the Muschelkalk, and a sodium chloride polymer mud for the Muschelkalk further down until the final depth within the upper part of the Rotliegendes. Key information is listed in Tab. 2-4. Minor losses of drilling mud occurred in the «Murchisonae-Oolith Formation» (15 m^3) in a section with drilling-induced fractures at around 807 m MD depth. Below 1'105 m MD several mud losses have been observed, starting with 15m^3/h between 1'105 m and 1'114 m MD. While coring down to 1'306.77 m MD, static and dynamic mud losses have been measured but reduced constantly with depth until reaching 0.5 – 1.1 m^3/h, resulting in 15 m^3 mud losses per day on average. Mud losses added up to 763 m^3 while coring.

Detailed information on the composition of the drilling muds used at BAC1-1 is only available for the Keuper and the Muschelkalk (Lorenz *in prep.*) and is listed in Tab. 2-5.

Tab. 2-4: Drilling muds and main mud loss events

Based on Dossier I.

Depth interval [m MD]	**Geological unit**	**Drilling mud**	**Comments** Reactive chemicals / mud losses
0 – 515	Quaternary – «Felsen-kalke» + «Massenkalk»	Bentonite, polymers	+ Na_2CO_3
515 – 700	«Felsenkalke» + «Massen-kalk» – Wildegg Fm.	Bentonite, polymers	+ Na_2CO_3 + citric acid
700 – 1'057	Wildegg Fm. – Schinznach Fm.	Potassium silicate, polymers	+ $CaCO_3$ + citric acid + soda ash Losses at 807 m MD (see text)
1'057 – 1'129	Schinznach Fm. – Zeglingen Fm.	Water, polymers	
1'129 – 1'306.8	Zeglingen Fm. – Weitenau Fm.	NaCl brine, polymers	+ $CaCO_3$ +barite + soda ash

Tab. 2-5: Composition of drilling mud used in the Keuper and Muschelkalk

From Lorenz (*in prep.*)

Parameter	**Units**	**Keuper: K-Si polymer mud**	**Muschelkalk: Na-Cl polymer mud**
pH		12.9	10.4
EC	[µS/cm]	87'450	13'962
uranine	[ppb]	1'246	1'962
^3H-H_2O	[TU]	9.2	5.1
Alk (pH 4.3)	[meq/L]	1'488	74.2
TOC	[mg/L]	4'213	4'849
Na	[mg/L]	2'947	3'505
K	[mg/L]	63'817	1'093
NH_4	[mg/L]	< 1	< 1
Ca	[mg/L]	53.3	2.8
Mg	[mg/L]	4.75	< 1
Si	[mg/L]	31'517	315
Cl	[mg/L]	1'230	2'231
SO_4	[mg/L]	2'117	449
NO_3	[mg/L]	13.0	21.4
Br	[mg/L]	0.80	0.37
F	[mg/L]	0.68.1	< 1
Sr	[mg/L]	0.47	0.08
Ba	[mg/L]	0.50	0.09
$\delta^{18}O$ of water	[‰VSMOW]	-7.31	-9.02
$\delta^{2}H$ of water	[‰VSMOW]	-49.7	-65.9

The values are the mean of 6 (KEU) or 8 (MUK) analyses of samples taken in the suction pit and in the shaker for the mud monitoring. First Keuper sample: 07/02/2022 04:00, last Keuper sample 08/02/2022 03:45. First Muschelkalk sample: 26/03/2022 12:00, last Muschelkalk sample 27/03/2022 20:00.

3 Sampling and applied methods

3.1 Sampling strategy

Lukas Aschwanden, Martin Mazurek

A suite of four different sample types were investigated (Tab. 3-1). No diffusion experiments were performed, but measurements on an experimentally demanding anhydrite (Keuper) and an AD post-mortem sample are in progress. Sample types and the general procedures of core sampling, sample conditioning and storage are described by Rufer (2019).

Tab. 3-1: Sample types and sampling strategy

This table includes on-site conditioned samples relevant for the present report.

Sample type	**Main study targets**	**Sampling (by on-site team)**
PW (porewater chemistry)	Characterisation of rock and porewater chemistry	Sample lithology representative of the current lithofacies and the sampled core section (usually 3 m). Sampling with a regular spacing in order to obtain a representative dataset
SQ (squeezing)	Characterisation of porewater chemistry	Focussed on clay-rich lithologies due to methodological constraints
AD (advective displacement)	Characterisation of porewater chemistry	Focussed on clay-rich lithologies due to methodological constraints
GM (geomechanics)	Mineralogy and grain density of samples studied for their geomecha-nical properties by other laboratories	-

3.2 Laboratory programme

Eric Gaucher

A total of 95 core segments were prepared on-site and designated for our studies. Except 2 samples designated for geomechanical tests (GM), the segments were analysed for geochemical and petrophysical characterisation (porewater: PW, squeezing: SQ, advective displacement: AD). Tab. 3-2 provides an overview, the analytical programme for the various sample types is shown in more detail in Tab. 3-3.

Tab. 3-2: Number of samples analysed for the different geological units

Unit	**PW**	**SQ**	**AD**	**GM**	**Total**
Malm	17				17
«Brauner Dogger»	13	3	2	2	20
Opalinus Clay	17	5	2		24
Staffelegg Formation	6	3	2		11
Klettgau Formation	6	1			7
Bänkerjoch Formation	9				9
Schinznach Formation	6				6
Zeglingen Formation	1				1
Kaiseraugst Formation					
Dinkelberg Formation					
Weitenau Formation					
All	**75**	**12**	**6**	**2**	**95**

Tab. 3-3: Analytical programme performed for the different sample types
×× = standard programme, × = selected samples only, calc. = calculated.

Method	**PW**	**SQ**	**AD**	**GM**
Bulk mineralogical composition including CNS analysis	××	××	××	××
Clay mineralogy	×	×	××	
Bulk wet density	××		calc.	
Grain density	××		calc.	××
Water content	××	××	××	
BET surface area				
Cation-exchange properties (Ni-en method)	×		××	
Aqueous extraction	××	××	××	
Pore-water squeezing		××		
Advective displacement of porewater			××	
Stable water isotopes	××	××	××	

3.3 Analytical methods and methods of raw-data processing

Eric Gaucher

Experimental procedures and associated analytical methods, formalisms to process measured data and quantification of propagated errors are documented in Waber (ed.) (2020) and are not repeated here. Moreover, Mazurek et al. (2021) provide additional information for situations where the current practice is not documented or deviates from that described in Waber (ed.) (2020).

4 Results

4.1 Documentation of measured and calculated data

Martin Mazurek

Raw data collected in the framework of the analytical programme of BAC1-1 are organised in a FileMaker database, including raw-data files (e.g. XRD quantification not corrected for C/N/S analysis), graphics (e.g. XRD patterns) and photographs. The main purpose of this database is to ensure the full documentation and traceability of original and derived data presented in this report. From this database, the relevant data were exported into a comprehensive Excel sheet, which is attached as Appendix A (Excel file). The full dataset for advective-displacement experiments is provided as Appendix B (Excel file).

The objective of the Excel summary sheet is not to fully document all analyses made but, per parameter and sample, to indicate the "best" or most representative value in case multiple measurements were made, and to list parameters calculated from the original measurements. For example, only one composition is given for squeezed and advectively displaced porewaters in a sample, even though multiple aliquots were collected and analysed. Explanatory notes for this sheet follow here.

Bulk mineralogy (X-ray diffraction and CNS analysis)

- Contents of minerals not detected by X-ray diffraction are set to zero, as the actual detection limits are difficult to quantify. 'tr' = present in trace amounts.
- Clay-mineral content is not measured directly but is calculated by difference to 100%.
- Pyrite content is calculated from the measured S content, assuming that pyrite is the main S reservoir in the rock. This is not the case in anhydrite-bearing rocks, which are typically free of pyrite. Here, the S is used to calculate the content of anhydrite.
- Column 'Füchtbauer name' refers to the nomenclature of clastic rocks as defined in Naef et al. (2019). Names are listed only for rock compositions that have < 10 wt.-% minerals not represented in the Füchtbauer triangle (i.e. minerals other than clays, calcite, dolomite/ankerite, siderite, quartz, K-feldspar, plagioclase). In particular, this means that evaporitic rocks are not given a Füchtbauer name. If a rock contains ≥ 90 wt.-% minerals represented in the Füchtbauer triangle but also contains anhydrite, this is stated in brackets.
- The Füchtbauer triangle does not distinguish between limestones and dolostones. When the content of calcite exceeds that of dolomite/ankerite, the terms "limestone" or "calcareous" are used in this report, and "dolostone" or "dolomitic" are used if the opposite applies.

Clay mineral groups

- All data refer to wt.-% of the total rock.
- Illite/smectite ML (85-90) refers to a mixed-layer phase with 85 – 90% illite layers, Chl/Sm ML (85-95) designates a chlorite-smectite mixed-layer phase with 85 – 95% chlorite (analogous for the other listed mixed-layer phases).

End-member clays

- All data refer to wt.-% of the total rock.
- Illite, smectite and chlorite partially occur in mixed-layer phases. Here, the respective total contents of the end-members are calculated. For example, if a sample contains 10 wt.-% illite and 8 wt.-% illite/smectite mixed layers containing 75% illite, the end-member illite content would be 16 wt.-%.

Petrophysical parameters

- Bulk wet density was measured, and bulk dry density was calculated using equation 5-14 in Waber (ed.) (2020).
- Pycnometer porosity was calculated from densities using equation 5-16 in Waber (ed.) (2020).
- Water content (dry) was calculated from water content (wet) using $w_d = w_w/(1-w_w)$.
- Water-loss porosity was calculated using bulk wet density (equation 5-9 in Waber ed. 2020) or grain density (equation 5-7 in Waber ed. 2020).
- The formalisms to calculate the water content from isotope diffusive-exchange experiments are given in equation 76 of Appendix A of Waber (ed.) (2020) and are detailed in Mazurek et al. (2021).

Chloride and bromide from aqueous extracts recalculated to porewater concentrations using water content

- Concentrations are given relative to bulk porewater as well as relative to various assumptions regarding anion accessibility in the pore space. The calculation is made using equation 6-1 in Waber (ed.) (2020). The variants pertaining to the dependence of anion accessibility on the clay-mineral content are discussed in Chapter 5.

Errors

- The error columns refer to analytical uncertainty or instrument precision for measured parameters and to propagated errors for calculated parameters, following the formalisms documented in Waber (ed.) (2020).

4.2 Mineralogical composition

Martin Mazurek

4.2.1 Whole rock data

A total of 86 mineralogical analyses were performed in the section Wildegg Formation (Malm) – Zeglingen Formation (Triassic). The full dataset is documented in Appendix A, and Tab. 4.2-1 provides formation-specific summaries. Plots against depth for the most relevant minerals are shown in Fig. 4.2-1, and a representation in the Füchtbauer triangle is given in Fig. 4.2-3.

The Triassic section is lithologically heterogeneous, mainly due to the variable contents of dolomite, calcite and anhydrite. Systematic depth trends cannot be resolved. The overlying Dogger – Lias section is discussed in detail further below.

Minor or trace amounts of the following phases have been identified:

- Goethite in the «Murchisonae-Oolith Formation» (up to 19 wt.-%) and in the Ergolz Member of the Klettgau Formation
- Haematite in the «Murchisonae-Oolith Formation» and in the Ergolz and Gruhalde Members of the Klettgau Formation.

The depth profiles of the contents of S and N (based on CNS analysis) are shown in Fig. 4.2-2. Variable but often high S contents, mostly related to the presence of pyrite, are seen in the Dogger – Lias section. In the Triassic, high S contents are related to anhydrite. N contents above the quantification limit of 0.01 wt.-% are only found in the Villigen Formation (Malm) but mainly in the Dogger, Lias and in the underlying Klettgau Formation. The highest N content is observed in the Rietheim Member of the Staffelegg Formation, likely related to the presence of abundant organic matter.

Tab. 4.2-1: Bulk-rock mineralogy: formation-specific means, medians, standard deviations and ranges

For the calculation of statistical parameters, values below the limit of quantification were set to 0.

Formation (number of analyses)	**Member**		**S** [wt.-%]	**N** [wt.-%]	**C(inorg)** [wt.-%]	**C(org)** [wt.-%]	**Quartz** [wt.-%]	**K-feldspar** [wt.-%]	**Plagioclase** [wt.-%]	**Calcite** [wt.-%]	**Dolomite / Ank.** [wt.-%]	**Siderite** [wt.-%]	**Anhydrite** [wt.-%]	**Goethite** [wt.-%]	**Haematite** [wt.-%]	**Pyrite** [wt.-%]	**Clay minerals** [wt.-%]
Wildegg Fm. (8)		Mean	0.05	0.00	7.73	0.70	8.6	1.7	0.8	62.9	1.4	0.0	0.0	0.0	0.0	0.1	23.8
		Median	0.05	0.00	8.01	0.69	6.1	1.6	0.0	64.4	1.4	0.0	0.0	0.0	0.0	0.1	24.1
		Stdev	0.03	0.00	1.07	0.12	6.4	0.6	1.9	8.9	1.5	0.0	0.0	0.0	0.0	0.1	5.8
		Min	0.00	0.00	6.15	0.50	4.1	1.0	0.0	48.7	0.0	0.0	0.0	0.0	0.0	0.0	15.9
		Max	0.11	0.00	9.04	0.85	23.6	3.1	5.5	73.8	4.4	0.0	0.0	0.0	0.0	0.2	32.6
«Parkinsoni-Württembergica-Sch.» (14)		Mean	0.68	0.03	2.55	0.80	18.4	2.6	1.6	19.9	1.0	0.2	0.0	0.0	0.0	1.3	54.1
		Median	0.45	0.04	2.57	0.79	17.8	3.1	2.0	19.2	0.0	0.0	0.0	0.0	0.0	0.8	52.0
		Stdev	0.52	0.02	0.74	0.21	4.8	2.0	1.1	5.3	1.4	0.9	0.0	0.0	0.0	1.0	8.5
		Min	0.00	0.00	1.44	0.46	10.7	0.0	0.0	12.0	0.0	0.0	0.0	0.0	0.0	0.0	41.6
		Max	1.65	0.07	4.50	1.17	28.1	5.4	3.1	33.3	3.7	3.3	0.0	0.0	0.0	3.1	68.1
Wedelsst. Fm. (1)		Mean	0.44	0.05	0.85	0.95	24.3	0.0	0.0	7.1	0.0	0.0	0.0	0.0	0.0	0.8	66.8
«Murchisonae-Oolith Fm.» (5)		Mean	0.10	0.02	6.06	0.38	13.4	1.4	0.9	41.2	8.3	0.3	0.0	7.7	1.0	0.2	25.3
		Median	0.00	0.00	7.48	0.21	5.9	0.0	0.0	51.8	9.5	0.0	0.0	9.0	1.3	0.0	22.1
		Stdev	0.21	0.03	3.49	0.34	11.6	2.0	1.3	26.3	5.2	0.7	0.0	7.7	0.6	0.4	23.1
		Min	0.00	0.00	0.32	0.20	4.3	0.0	0.0	1.4	0.0	0.0	0.0	0.0	0.0	0.0	7.3
		Max	0.48	0.05	9.00	0.98	28.5	4.2	3.0	66.1	14.3	1.5	0.0	18.8	1.3	0.9	64.9
Opalinus Clay (24)	All	Mean	0.35	0.06	1.31	1.14	21.1	2.3	1.7	8.7	0.0	2.6	0.0	0.0	0.0	0.7	61.9
		Median	0.29	0.07	1.00	1.07	20.5	2.2	1.6	6.4	0.0	2.2	0.0	0.0	0.0	0.5	64.7
		Stdev	0.30	0.02	1.21	0.41	4.5	0.5	0.4	10.1	0.0	1.5	0.0	0.0	0.0	0.6	10.3
		Min	0.00	0.00	0.00	0.54	15.1	1.4	1.0	0.0	0.0	0.0	0.0	0.0	0.0	0.0	24.0
		Max	1.06	0.09	6.59	2.86	36.6	3.4	2.8	53.7	0.0	6.1	0.0	0.0	0.0	2.0	73.1
Opalinus Clay (6)	'Sub-unit with silty calc. beds'	Mean	0.54	0.04	2.05	1.30	22.8	2.2	1.6	15.3	0.0	2.1	0.0	0.0	0.0	1.0	53.7
		Median	0.37	0.06	1.38	1.09	20.3	2.2	1.6	9.9	0.0	1.4	0.0	0.0	0.0	0.7	55.0
		Stdev	0.38	0.03	2.37	0.80	7.0	0.7	0.4	19.6	0.0	2.1	0.0	0.0	0.0	0.7	17.2
		Min	0.24	0.00	0.00	0.54	17.4	1.4	1.0	0.0	0.0	0.0	0.0	0.0	0.0	0.4	24.0
		Max	1.06	0.07	6.59	2.86	36.6	3.4	2.3	53.7	0.0	6.1	0.0	0.0	0.0	2.0	73.1
Opalinus Clay (7)	'Upper silty sub-unit'	Mean	0.19	0.06	1.18	1.04	23.6	2.3	1.8	7.4	0.0	2.9	0.0	0.0	0.0	0.4	60.6
		Median	0.18	0.06	1.11	1.05	23.4	2.4	1.8	6.4	0.0	2.1	0.0	0.0	0.0	0.3	61.4
		Stdev	0.16	0.01	0.40	0.12	2.3	0.2	0.5	2.9	0.0	1.6	0.0	0.0	0.0	0.3	5.0
		Min	0.00	0.05	0.68	0.83	20.4	1.9	1.2	4.5	0.0	1.3	0.0	0.0	0.0	0.0	52.0
		Max	0.43	0.07	1.76	1.19	27.1	2.6	2.6	11.8	0.0	6.0	0.0	0.0	0.0	0.8	65.4

Tab. 4.2-1: continued

Formation (number of analyses)	**Member**		**S** [wt.-%]	**N** [wt.-%]	**C(inorg)** [wt.-%]	**C(org)** [wt.-%]	**Quartz** [wt.-%]	**K-feldspar** [wt.-%]	**Plagioclase** [wt.-%]	**Calcite** [wt.-%]	**Dolomite / Ank.** [wt.-%]	**Siderite** [wt.-%]	**Anhydrite** [wt.-%]	**Goethite** [wt.-%]	**Haematite** [wt.-%]	**Pyrite** [wt.-%]	**Clay minerals** [wt.-%]
Opalinus Clay (5)	'Mixed clay-silt-carbonate sub-unit'	Mean	0.38	0.07	0.95	1.17	20.6	2.3	1.8	5.7	0.0	2.6	0.0	0.0	0.0	0.7	65.1
		Median	0.22	0.08	0.92	1.08	20.5	2.1	1.7	6.4	0.0	2.1	0.0	0.0	0.0	0.4	66.7
		Stdev	0.40	0.01	0.25	0.20	0.8	0.5	0.3	1.3	0.0	1.6	0.0	0.0	0.0	0.7	3.1
		Min	0.00	0.07	0.71	1.00	19.7	2.0	1.5	3.7	0.0	1.4	0.0	0.0	0.0	0.0	61.2
		Max	1.01	0.08	1.33	1.50	22.0	3.1	2.2	6.8	0.0	5.4	0.0	0.0	0.0	1.9	68.1
Opalinus Clay (6)	'Clay-rich sub-unit'	Mean	0.32	0.07	1.02	1.09	16.8	2.2	1.7	6.1	0.0	2.8	0.0	0.0	0.0	0.6	68.8
		Median	0.34	0.07	1.04	1.09	16.6	2.1	1.6	5.9	0.0	2.9	0.0	0.0	0.0	0.6	68.8
		Stdev	0.17	0.01	0.19	0.19	1.2	0.5	0.6	1.0	0.0	1.0	0.0	0.0	0.0	0.3	2.6
		Min	0.00	0.06	0.80	0.84	15.1	1.8	1.3	4.7	0.0	1.2	0.0	0.0	0.0	0.0	64.4
		Max	0.52	0.09	1.24	1.36	18.7	3.2	2.8	7.6	0.0	4.1	0.0	0.0	0.0	1.0	71.4
Staffel-egg Fm. (11)		Mean	0.58	0.05	2.72	1.83	27.2	2.4	1.8	21.7	0.9	0.0	0.0	0.0	0.0	1.1	43.1
		Median	0.38	0.00	1.47	0.67	30.6	2.2	1.8	12.2	0.0	0.0	0.0	0.0	0.0	0.7	40.0
		Stdev	0.95	0.09	2.50	2.66	17.0	1.5	0.8	21.2	1.5	0.0	0.0	0.0	0.0	1.8	14.1
		Min	0.00	0.00	0.95	0.39	3.1	0.0	0.0	4.8	0.0	0.0	0.0	0.0	0.0	0.0	21.5
		Max	3.29	0.29	8.98	8.60	46.0	4.5	3.2	74.8	3.4	0.0	0.0	0.0	0.0	6.2	71.0
Klettgau Fm. (7)		Mean	0.05	0.01	4.23	0.28	17.1	4.1	4.6	3.3	29.4	0.0	0.0	0.1	0.7	0.1	40.2
		Median	0.00	0.00	5.27	0.17	11.0	1.8	2.4	0.0	32.5	0.0	0.0	0.0	0.0	0.0	42.8
		Stdev	0.11	0.02	3.98	0.26	11.6	3.5	4.0	5.0	29.6	0.0	0.0	0.3	1.1	0.2	12.2
		Min	0.00	0.00	0.00	0.05	5.4	1.4	0.6	0.0	0.0	0.0	0.0	0.0	0.0	0.0	24.7
		Max	0.28	0.04	8.58	0.74	31.1	10.7	10.1	12.1	65.8	0.0	0.0	0.9	2.9	0.5	54.2
Bänker-joch Fm. (9)		Mean	9.55	0.00	1.79	0.37	7.6	2.5	1.2	0.1	13.6	0.0	40.5	0.0	0.0	0.0	34.1
		Median	10.00	0.00	1.69	0.34	6.9	2.7	0.8	0.0	13.0	0.0	42.5	0.0	0.0	0.0	33.6
		Stdev	6.52	0.00	1.59	0.13	8.5	2.4	1.7	0.3	12.3	0.0	27.7	0.0	0.0	0.0	10.4
		Min	0.07	0.00	0.10	0.24	0.0	0.0	0.0	0.0	0.0	0.0	0.0	0.0	0.0	0.0	19.3
		Max	18.00	0.00	4.93	0.65	28.0	6.1	5.1	0.8	37.8	0.0	76.4	0.0	0.0	0.1	50.5
Schinz-nach Fm. (6)	All	Mean	0.48	0.00	11.83	0.32	1.7	0.0	0.0	26.8	66.1	0.0	1.4	0.0	0.0	0.3	3.5
		Median	0.13	0.00	11.82	0.36	2.0	0.0	0.0	22.8	69.0	0.0	0.0	0.0	0.0	0.1	3.7
		Stdev	0.78	0.00	0.39	0.16	0.9	0.0	0.0	29.7	29.8	0.0	3.5	0.0	0.0	0.5	2.3
		Min	0.00	0.00	11.33	0.00	0.0	0.0	0.0	0.0	33.6	0.0	0.0	0.0	0.0	0.0	-0.5
		Max	2.00	0.00	12.44	0.45	2.4	0.0	0.0	58.0	95.5	0.0	8.5	0.0	0.0	1.2	5.8
Schinz-nach Fm. (3)	Stamberg Mb.	Mean	0.72	0.00	12.12	0.27	1.2	0.0	0.0	0.0	93.0	0.0	2.8	0.0	0.0	0.1	2.6
		Median	0.16	0.00	12.00	0.38	1.3	0.0	0.0	0.0	92.0	0.0	0.0	0.0	0.0	0.0	2.5
		Stdev	1.11	0.00	0.28	0.24	1.2	0.0	0.0	0.0	2.2	0.0	4.9	0.0	0.0	0.2	3.1
		Min	0.00	0.00	11.92	0.00	0.0	0.0	0.0	0.0	91.5	0.0	0.0	0.0	0.0	0.0	-0.5
		Max	2.00	0.00	12.44	0.43	2.3	0.0	0.0	0.0	95.5	0.0	8.5	0.0	0.0	0.3	5.8

Tab. 4.2-1: continued

Formation (number of analyses)	**Member**		**S** [wt.-%]	**N** [wt.-%]	**C(inorg)** [wt.-%]	**C(org)** [wt.-%]	**Quartz** [wt.-%]	**K-feldspar** [wt.-%]	**Plagioclase** [wt.-%]	**Calcite** [wt.-%]	**Dolomite / Ank.** [wt.-%]	**Siderite** [wt.-%]	**Anhydrite** [wt.-%]	**Goethite** [wt.-%]	**Haematite** [wt.-%]	**Pyrite** [wt.-%]	**Clay minerals** [wt.-%]
Schinznach Fm. (3)	Lied. + Leutschenb. + Kienb. Mb.	Mean	0.25	0.00	11.53	0.36	2.1	0.0	0.0	53.6	39.1	0.0	0.0	0.0	0.0	0.5	4.3
		Median	0.10	0.00	11.53	0.34	2.3	0.0	0.0	57.1	37.4	0.0	0.0	0.0	0.0	0.2	3.9
		Stdev	0.35	0.00	0.20	0.07	0.4	0.0	0.0	6.9	6.6	0.0	0.0	0.0	0.0	0.6	1.0
		Min	0.00	0.00	11.33	0.31	1.6	0.0	0.0	45.6	33.6	0.0	0.0	0.0	0.0	0.0	3.6
		Max	0.64	0.00	11.73	0.45	2.4	0.0	0.0	58.0	46.5	0.0	0.0	0.0	0.0	1.2	5.5
Zeglingen Fm. (1)		Mean	0.38	0.00	11.98	0.56	2.6	0.0	0.0	0.0	92.0	0.0	0.0	0.0	0.0	0.7	4.2

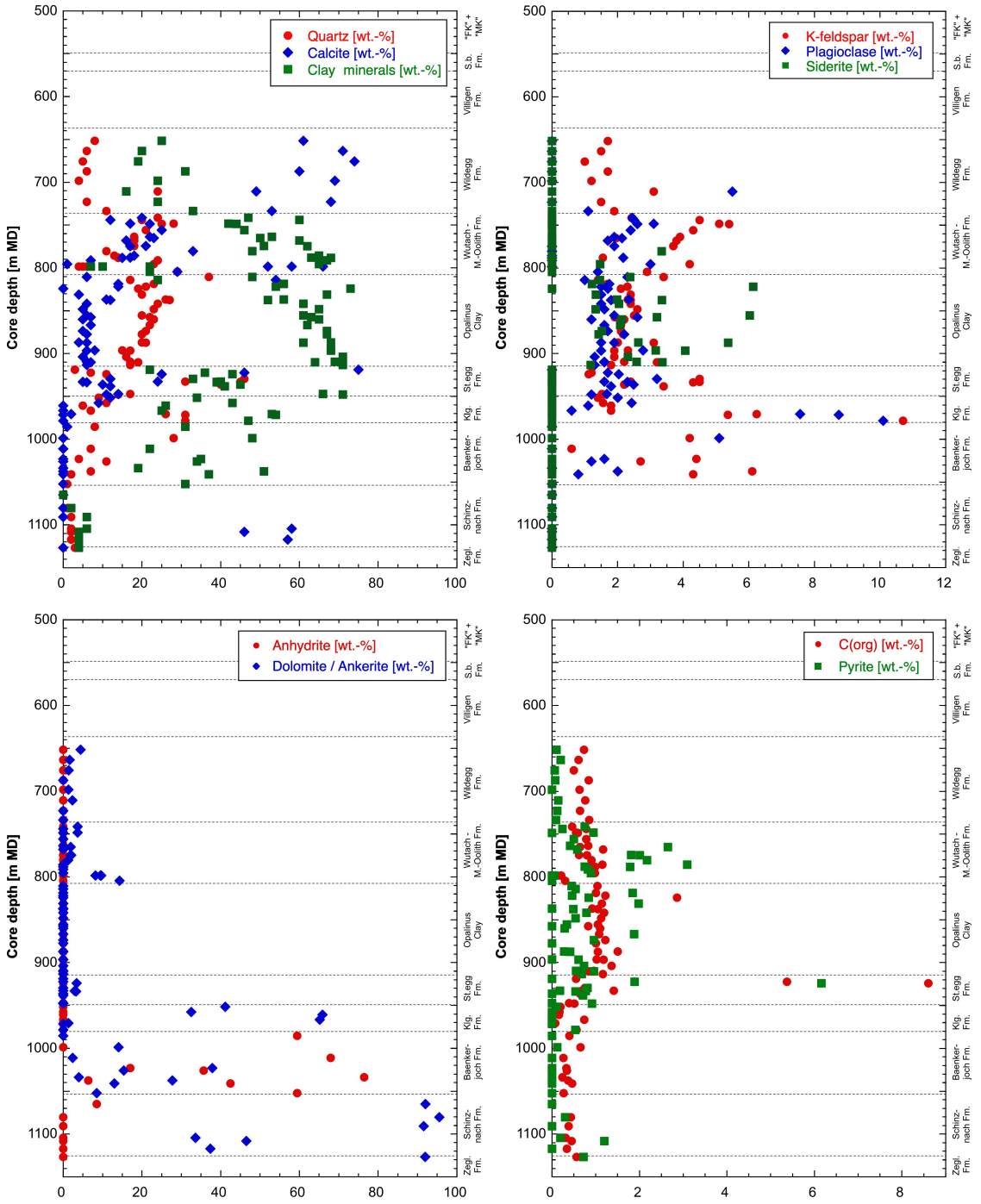

Fig. 4.2-1: Mineral contents in the bulk rock as a function of depth

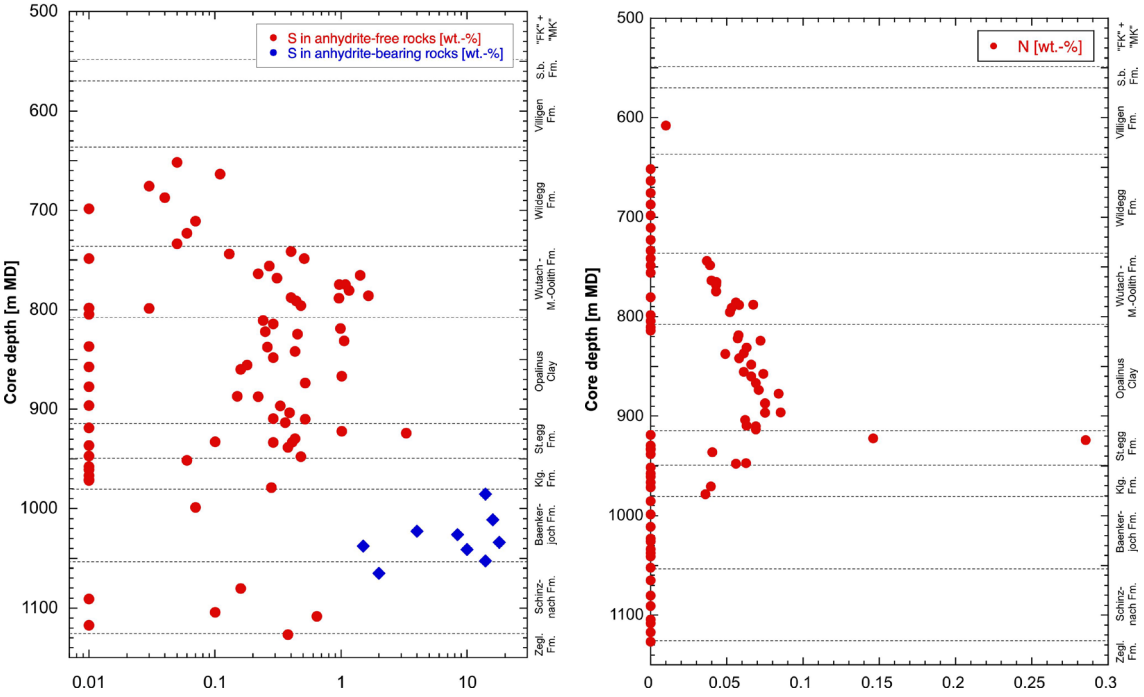

Fig. 4.2-2: Contents of S and N in the bulk rock as a function of depth

S contents below the detection limit of 0.05 wt.-% are represented by data points shown at 0.01 wt.-%. N contents below the detection limit of 0.01 wt.-% are represented by data points shown at 0 wt.-%.

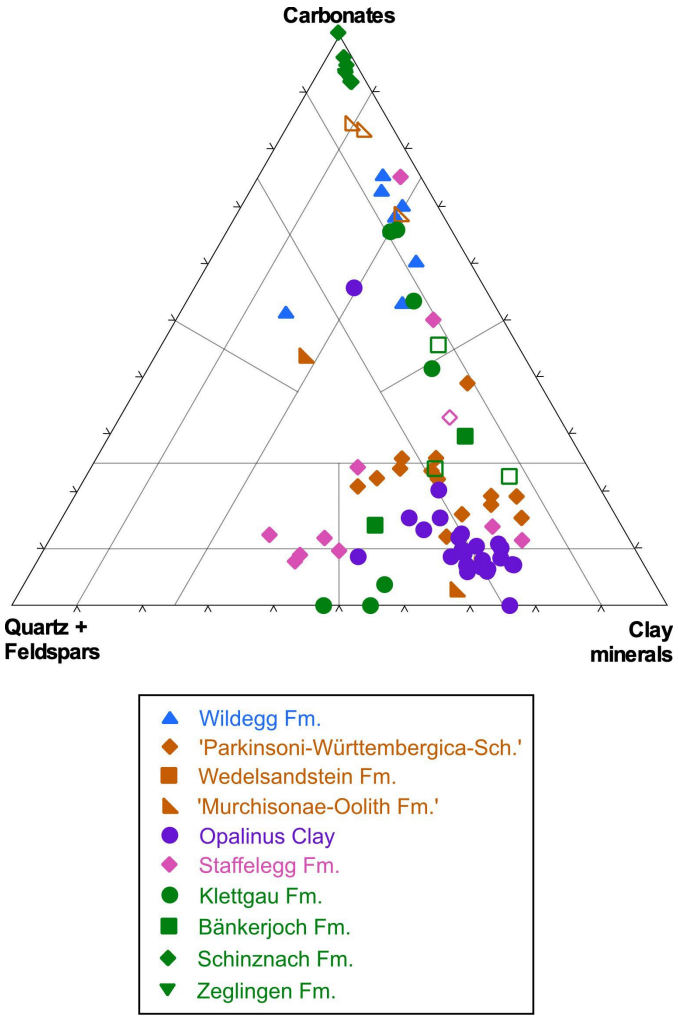

Fig. 4.2-3: Mineralogical composition of studied samples in the Füchtbauer triangle

Open symbols indicate samples containing 10 – 50 wt.-% minerals other than those represented by the Füchtbauer triangle (which are clay minerals, calcite, dolomite/ankerite, siderite, magnesite, quartz, K-feldspar, plagioclase). Samples with > 50 wt.-% of such minerals are excluded. The additional phases are goethite and haematite in the «Murchisonae-Oolith Formation», organic C and pyrite in the Staffelegg Formation (Rietheim Member), and anhydrite in the Bänkerjoch Formation.

A closer look at the section Staffelegg Formation – Opalinus Clay – «Brauner Dogger»

The graphs shown in Fig. 4.2-4 indicate systematic depth trends of the contents of quartz, clay minerals, siderite and the ratio quartz/clay, whereas other minerals show no evident systematic variability.

Staffelegg Formation

Lithological heterogeneity is a characteristic in the Staffelegg Formation, which, according to the Füchtbauer nomenclature, contains claystone, marl, limestone and sandstone/siltstone. Overall, the clay content decreases upwards throughout the formation, while the quartz content increases from the base until the top of the Frick Member. High contents of pyrite and C(org) are observed in samples from the Rietheim Member (919.64 – 925.49 m).

Opalinus Clay

Informal sub-units within the Opalinus Clay were defined by Mazurek & Aschwanden (2020) on a regional basis, and this scheme was successfully applied to several TBO boreholes. In borehole BAC1-1, however, mineralogical trends are less well expressed, in particular when compared to the findings from the BUL1-1 profile (Mazurek et al. 2021). The subdivision of the 'Mixed clay-silt-carbonate sub-unit' in two sections with distinct trends is not evident.

«Murchisonae-Oolith Formation»

No distinct trends could be identified.

«Parkinsoni-Württembergica-Schichten»

Clear trends of upwards increasing quartz and decreasing clay minerals are evident, similar to the situation in borehole STA2-1. In addition, an increase of dolomite/ankerite was also observed.

Conclusion

A number of mineralogical discontinuities and changes in depth trends were identified and generally correlate well with the lithostratigraphic subdivision defined in Dossier III. Quartz and clay-mineral contents show the most pronounced trends in their depth profiles. In the Opalinus Clay, mineralogical trends are less well expressed than in other TBO boreholes.

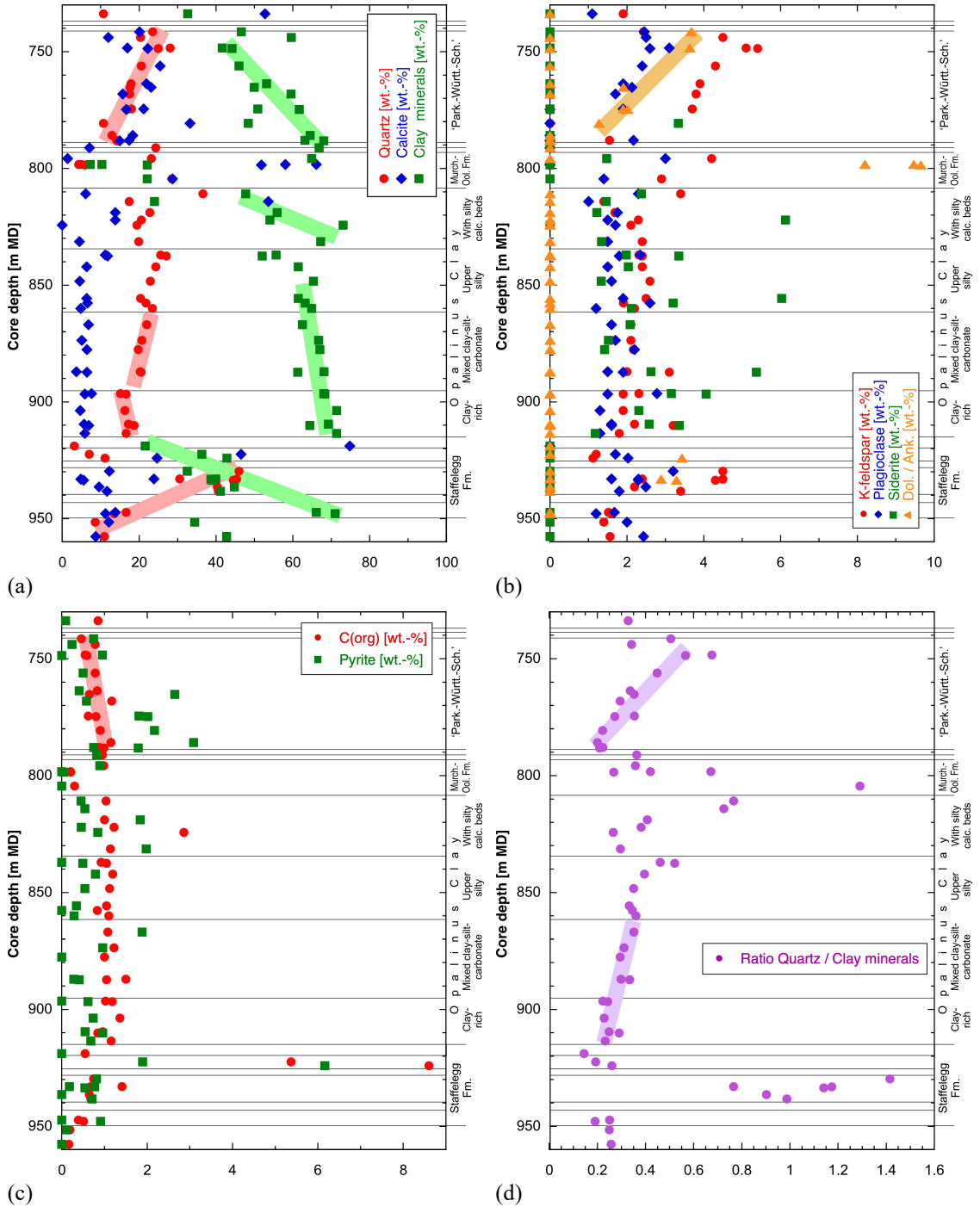

Fig. 4.2-4: Depth trends of mineral contents in the bulk rock in the Lias – Dogger interval
Coloured bars highlight systematic trends.

4.2.2 Clay minerals

A total of 38 mineralogical analyses of the clay fraction were performed in the section Wildegg Formation – Klettgau Formation. The full dataset is documented in Appendix A. Tab. 4.2-2 provides formation-specific summaries, normalising the contents of individual clay phases to the sum of all clay minerals.

The identified clay-mineral species include illite, smectite, illite/smectite mixed layers, kaolinite, chlorite and chlorite/smectite mixed layers. The identification of chlorite/smectite mixed layers in all samples is in contrast with previous data from northern Switzerland where this mineral was rarely reported (Mazurek 2017). However, this is not a real difference but due to the improved methodology of the evaluation of X-ray patterns that was applied for the TBO campaign (details in Waber ed. 2020). Because the chlorite/smectite mixed-layer phase contains 85 – 95% chlorite layers, its XRD reflections are close to those of pure chlorite. The new methodology also allows to better resolve the fraction of smectite layers in the illite/smectite mixed-layer phase. As seen in Tab. 4.2-2, illite-rich mixed layers dominate, but minor amounts of illite-poorer mixed layers also occur. Given the fact that the contents of mixed-layer phases and the smectite fractions in these are known, the end-member compositions of illite, smectite, chlorite and kaolinite (whether in mixed layers or as a discrete phase) can be calculated and are also listed in Tab. 4.2-2.

Depth trends of the relative proportions of clay minerals are shown graphically in Fig. 4.2-5 for individual clay phases (a) and end-member clays (b). The depth plot of the latter is less noisy than that of the individual clay minerals. Smectite as a discrete phase occurs only in small proportions, and most smectite is found in illite/smectite mixed-layer minerals. Variability of the smectite and chlorite end-members is limited. In contrast, the relative proportions of the two main end-member clays, namely illite and kaolinite, vary substantially over the profile (Figs. 4.2-5 and 4.2-6). The Klettgau Formation is characterised by the dominance of the illite end-member, while the proportions of kaolinite are low (illite/kaolinite ratios are in the range of 16 – 60). The overlying Dogger – Lias interval will be explored in more detail below.

Tab. 4.2-2: Mineralogical composition of the clay fraction: formation-specific means, medians, standard deviations and ranges

Formation (number of analyses)	**Member**		**Individual clay phases** [wt.-% of clay fraction]										**End-member clays** [wt.-% of clay fraction]			
			Illite	**Ill/Sm ML (85-90)**	**Ill/Sm ML (75-80)**	**Ill/Sm ML (50-70)**	**Ill/Sm ML (20-40)**	**Total Ill/Sm**	**Smectite**	**Kaolinite**	**Chlorite**	**Chl/Sm ML (85-95)**	**Illite**	**Smectite**	**Kaolinite**	**Chlorite**
Wildegg Fm. (4) (4)		Mean	34.7	19.1	7.5	13.5	0.0	40.1	0.8	13.4	1.6	9.4	65.0	11.6	13.4	10.0
		Median	34.4	16.6	7.2	12.5	0.0	40.1	0.8	14.5	1.6	9.5	65.1	11.1	14.5	10.2
		Stdev	2.3	5.9	6.4	4.1	0.0	7.5	0.6	6.5	0.5	1.2	5.2	2.4	6.5	1.4
		Min	32.6	15.4	0.0	9.7	0.0	33.0	0.1	4.9	1.1	7.8	59.1	9.6	4.9	8.1
		Max	37.5	27.9	15.5	19.2	0.0	47.1	1.5	19.7	2.1	10.8	70.8	14.5	19.7	11.5
«Parkinsoni-Württembergica-Schichten» (10)		Mean	31.8	16.9	9.8	5.5	0.0	32.2	0.6	24.0	2.0	9.4	57.4	8.2	24.0	10.4
		Median	32.0	18.0	2.5	4.1	0.0	33.2	0.0	22.3	2.2	9.3	60.5	7.8	22.3	9.4
		Stdev	4.0	9.1	12.4	4.7	0.0	4.7	1.3	5.1	1.0	2.7	5.8	2.1	5.1	2.7
		Min	26.9	0.0	0.0	0.0	0.0	24.3	0.0	19.0	0.4	5.0	46.4	5.9	19.0	7.0
		Max	41.6	26.6	29.8	14.4	0.0	37.5	4.3	34.6	3.3	14.9	63.2	13.2	34.6	15.6
«Murchisonae-Oolith Fm.» (2)		Mean	26.5	11.3	15.5	2.9	3.4	32.9	0.4	23.8	9.2	7.3	51.2	9.2	23.8	15.9
		Median	26.5	11.3	15.5	2.9	3.4	32.9	0.4	23.8	9.2	7.3	51.2	9.2	23.8	15.9
		Stdev	4.7	15.9	11.7	1.3	4.7	0.8	0.6	3.3	9.9	1.6	8.2	2.8	3.3	8.7
		Min	23.1	0.0	7.2	1.9	0.0	32.3	0.0	21.4	2.2	6.2	45.4	7.2	21.4	9.7
		Max	29.8	22.5	23.7	3.8	6.7	33.5	0.8	26.1	16.2	8.4	57.0	11.2	26.1	22.0
Opalinus Clay (10)	All	Mean	29.2	10.5	8.1	5.5	0.2	24.2	0.1	33.3	2.2	11.0	48.0	6.6	33.3	12.1
		Median	27.2	12.6	7.2	5.5	0.0	24.5	0.0	35.2	2.1	11.1	46.1	6.5	35.2	11.8
		Stdev	4.7	7.6	8.0	4.1	0.5	4.2	0.2	5.6	0.7	1.3	4.2	1.1	5.6	1.3
		Min	24.0	0.0	0.0	0.0	0.0	16.6	0.0	21.5	1.5	9.6	43.6	4.9	21.5	10.9
		Max	39.0	19.8	19.5	14.1	1.6	32.3	0.5	39.6	3.9	13.8	55.3	8.7	39.6	14.5
Opalinus Clay (2)	'Sub-unit with silty calcareous beds'	Mean	30.1	18.2	3.9	7.8	0.0	29.8	0.3	25.5	3.0	11.4	53.3	7.9	25.5	13.2
		Median	30.1	18.2	3.9	7.8	0.0	29.8	0.3	25.5	3.0	11.4	53.3	7.9	25.5	13.2
		Stdev	0.1	2.3	5.4	0.4	0.0	3.5	0.4	5.7	1.3	0.4	2.8	1.1	5.6	1.8
		Min	30.0	16.5	0.0	7.5	0.0	27.3	0.0	21.5	2.1	11.1	51.3	7.2	21.5	12.0
		Max	30.2	19.8	7.7	8.1	0.0	32.3	0.5	29.5	3.9	11.6	55.3	8.7	29.5	14.5
Opalinus Clay (3)	'Upper silty sub-unit'	Mean	26.3	6.7	15.3	2.4	0.0	24.4	0.0	37.4	2.3	9.6	45.6	6.0	37.4	11.1
		Median	26.5	5.2	15.8	2.4	0.0	24.5	0.0	37.1	2.3	9.6	45.7	5.8	37.1	11.0
		Stdev	0.7	3.8	4.2	0.3	0.0	1.3	0.0	1.0	0.2	0.1	0.8	0.3	1.0	0.2
		Min	25.5	3.9	10.9	2.1	0.0	23.1	0.0	36.5	2.2	9.6	44.8	5.8	36.5	10.9
		Max	26.8	11.0	19.3	2.6	0.0	25.6	0.0	38.5	2.5	9.7	46.4	6.3	38.5	11.3

Tab. 4.2-2: continued

Formation (number of analyses)	**Member**		**Individual clay phases** [wt.-% of clay fraction]										**End-member clays** [wt.-% of clay fraction]			
			Illite	**Ill/Sm ML (85-90)**	**Ill/Sm ML (75-80)**	**Ill/Sm ML (50-70)**	**Ill/Sm ML (20-40)**	**Total Ill/Sm**	**Smectite**	**Kaolinite**	**Chlorite**	**Chl/Sm ML (85-95)**	**Illite**	**Smectite**	**Kaolinite**	**Chlorite**
Opalinus Clay (2)	'Mixed clay-silt-carbonate sub-unit'	Mean	29.8	7.1	3.8	8.9	0.8	20.6	0.0	36.1	1.8	11.8	44.7	6.8	36.0	12.4
		Median	29.8	7.1	3.8	8.9	0.8	20.6	0.0	36.1	1.8	11.8	44.7	6.8	36.0	12.4
		Stdev	8.2	10.0	4.0	7.4	1.1	5.6	0.0	5.0	0.4	2.8	1.6	1.3	5.0	2.1
		Min	24.0	0.0	0.9	3.7	0.0	16.6	0.0	32.5	1.5	9.8	43.6	5.9	32.5	11.0
		Max	35.5	14.2	6.6	14.1	1.6	24.5	0.0	39.6	2.1	13.8	45.8	7.8	39.6	13.9
Opalinus Clay (3)	'Clay-rich sub-unit'	Mean	31.2	11.4	6.5	4.9	0.0	22.8	0.0	32.7	1.9	11.5	48.9	6.1	32.7	12.3
		Median	27.3	16.5	0.0	7.3	0.0	23.9	0.0	35.1	2.0	11.6	46.6	6.7	35.1	12.3
		Stdev	6.8	9.9	11.3	4.2	0.0	2.9	0.0	4.3	0.2	0.4	4.9	1.0	4.3	0.6
		Min	27.2	0.0	0.0	0.0	0.0	19.5	0.0	27.7	1.7	11.1	45.7	4.9	27.7	11.6
		Max	39.0	17.6	19.5	7.4	0.0	24.9	0.0	35.3	2.0	11.8	54.5	6.7	35.3	12.9
Staffelegg Fm. (8)		Mean	40.9	12.1	7.3	7.0	0.0	26.4	0.9	18.4	2.1	11.4	60.9	8.2	18.4	12.6
		Median	40.6	9.6	2.9	8.8	0.0	25.9	0.3	18.3	2.1	11.3	61.1	8.1	18.3	12.8
		Stdev	10.7	13.3	8.7	5.4	0.0	12.6	1.5	4.6	0.9	1.9	4.9	2.0	4.6	2.4
		Min	29.5	0.0	0.0	0.0	0.0	9.0	0.0	12.1	0.9	9.0	54.6	5.4	12.1	8.9
		Max	53.9	30.7	19.8	14.1	0.0	48.0	4.1	25.6	3.6	14.7	67.3	11.5	25.6	17.2
Klettgau Fm. (4)		Mean	47.8	30.2	6.0	5.5	0.0	41.7	0.2	3.1	1.2	6.1	81.5	8.7	3.1	6.7
		Median	40.5	29.4	0.0	3.0	0.0	49.3	0.2	3.0	1.2	6.5	81.9	8.1	3.0	6.2
		Stdev	16.5	21.3	12.1	6.8	0.0	17.9	0.2	1.7	1.0	1.9	2.5	4.1	1.7	1.8
		Min	37.8	10.8	0.0	0.5	0.0	15.2	0.0	1.3	0.2	3.5	78.2	4.3	1.3	5.2
		Max	72.3	51.3	24.1	15.3	0.0	52.9	0.4	5.1	2.1	7.9	84.1	14.1	5.1	9.3

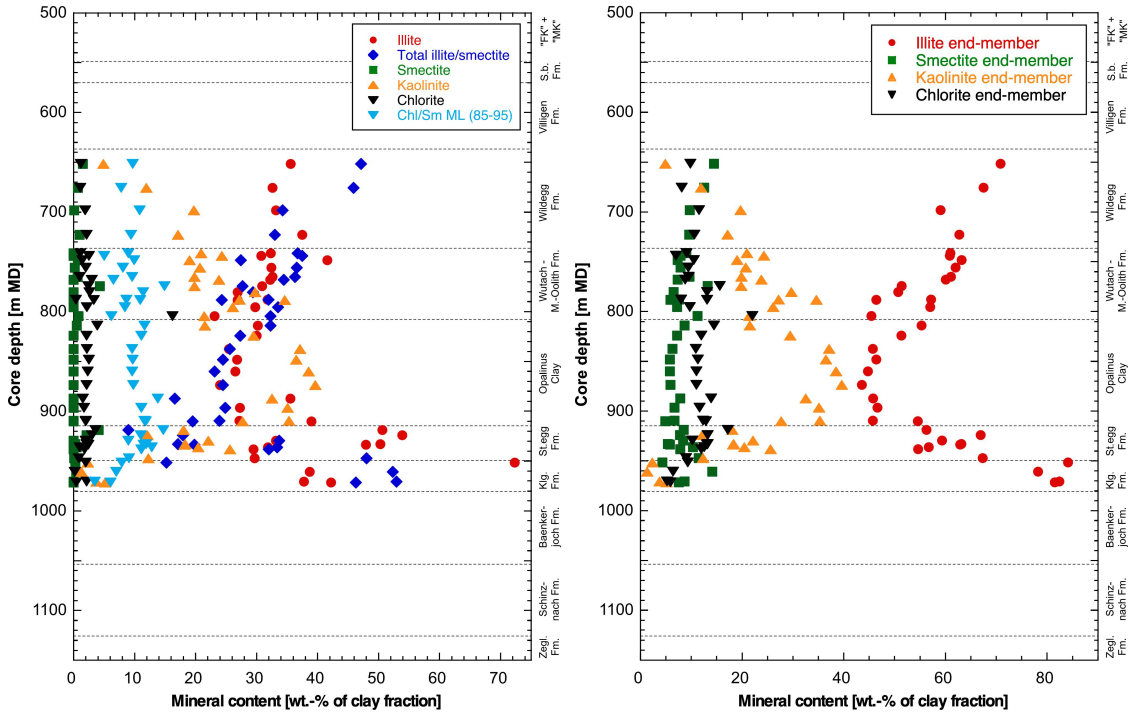

Fig. 4.2-5: Mineralogical composition of the clay fraction as a function of depth: (a) individual clay minerals, (b) end-member clays

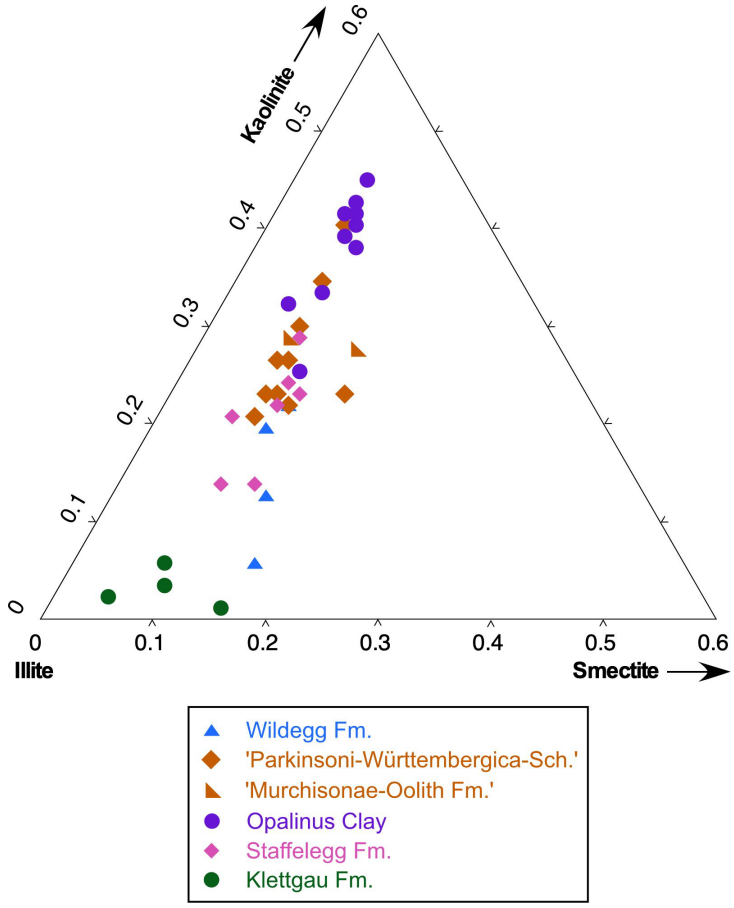

Fig. 4.2-6: Relative mass proportions of illite, smectite and kaolinite end-member clays

A closer look at the section Staffelegg Formation – Opalinus Clay – «Brauner Dogger»

The composition of the clay fraction in this interval shows some distinct depth trends (Figs. 4.2-7 and 4.2-8). In the Staffelegg Formation, a general upward decrease of the illite end-member contents is observed, and the opposite is seen for kaolinite. The ratio illite to kaolinite end-member is low and remarkably constant in the Opalinus Clay, except in the 'Sub-unit with silty calcareous beds' where it begins to increase, a trend that persists until the top of the Dogger. Similar profiles of the illite and kaolinite contents were also observed in several other TBO boreholes, e.g. STA2-1 and STA3-1.

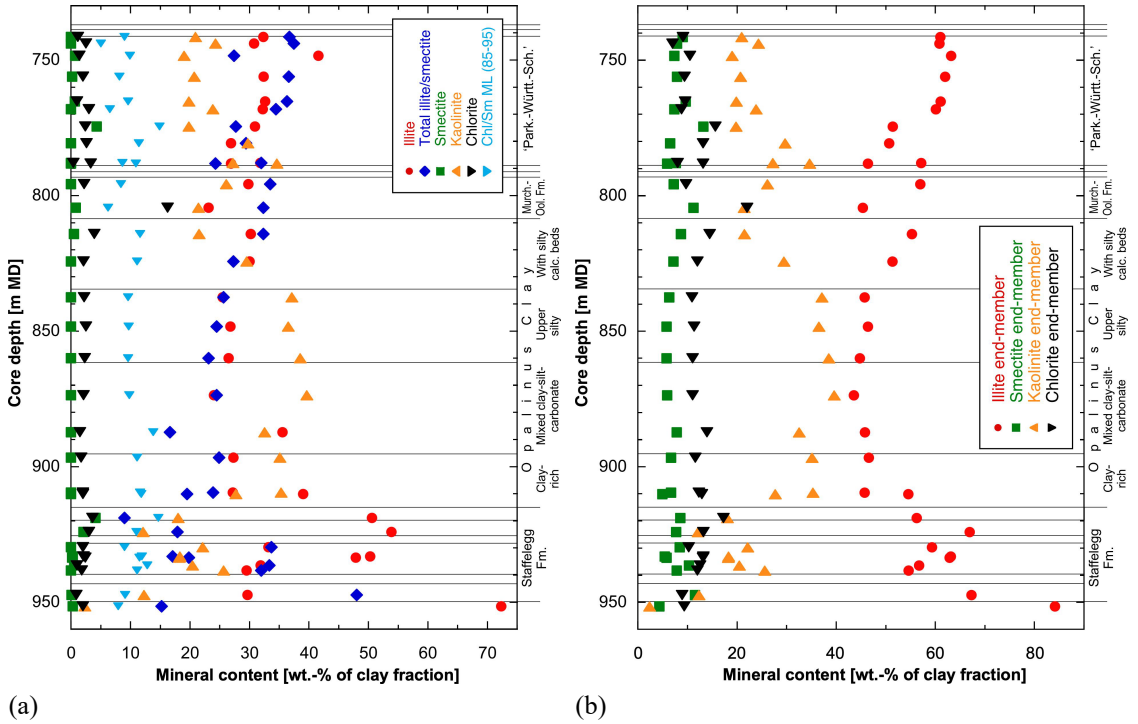

Fig. 4.2-7: Mineralogical composition of the clay fraction as a function of depth in the Lias – Dogger interval: (a) individual clay minerals, (b) end-member clays

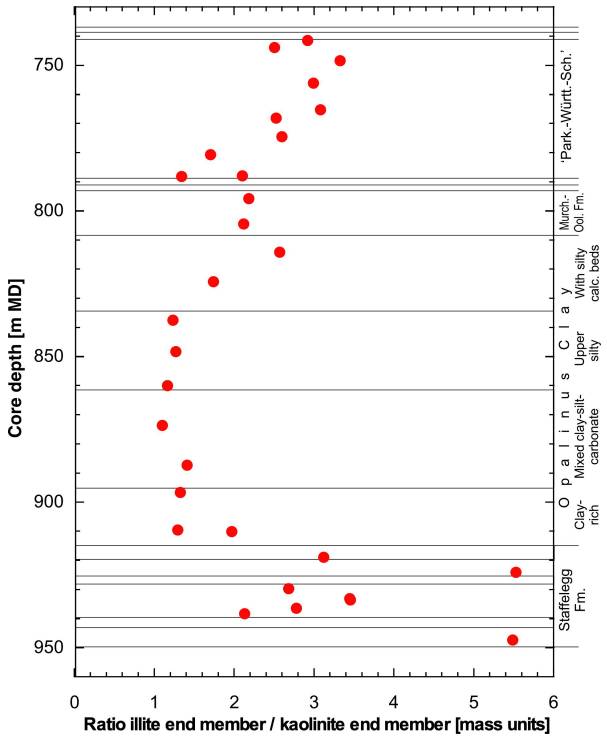

Fig. 4.2-8: Ratio of the illite to kaolinite end-member clays as a function of depth

4.3 Petrophysical parameters

Martin Mazurek & Lukas Aschwanden

All petrophysical measurements were performed at the University of Bern, and the acquired parameters are listed in Tab. 4.3-1. The formalisms to calculate additional parameters from measured data (such as porosity) are detailed in Waber (ed.) (2020). Formation-specific statistical data are summarised in Tab. 4.3-2, and the full dataset is documented in Appendix A. In cases where gravimetric water content was available, but density data were missing, water-loss porosity was calculated assuming a grain density of 2.7 g/cm^3. The uncertainty related to this assumption is small.

Tab. 4.3-1: Analytical programme for petrophysical measurements

	Number of samples
Bulk wet density	76
Grain density	77
Gravimetric water content	94
Water content from isotope mass balance	73
N_2 adsorption (BET external surface + full isotherm)	11

Tab. 4.3-2: Summary of measured and calculated petrophysical data

Listed water contents are averages of measurements performed on typically 3 subsamples. n = number of samples per geological unit.

Formation	**Member / Sub-unit**		**Bulk wet density** [g/cm^3]	**Bulk dry density, calculated** [g/cm^3]	**Grain density** [g/cm^3]	**Pycnometer porosity** [–]	**Gravimetry**				**Isotope mass balance**			**External surface area (BET)** [m^2/g dry rock]
							Water content (wet) (105 °C) [wt.-%]	**Water content (dry)** (105 °C) [wt.-%]	**Water-loss porosity** using bulk wet density [–]	**Water-loss porosity** using grain density [–]	**Water content (wet)** based on isotope diff. exch. [wt.-%]	**Porosity based on isotope diff. exch.** using bulk wet density [–]	**Porosity based on isotope diff. exch.** using grain density [–]	
«Felsenkalke» + «Massenkalk»		Mean	2.653	2.619	2.701	0.030	1.278	1.295	0.034	0.034	1.853	0.049	0.049	
		n	1	1	1	1	1	1	1	1	1	1	1	0
Schwarzbach Fm.		Mean	2.609	2.539	2.702	0.060	2.682	2.756	0.070	0.069	2.950	0.077	0.076	
		Median	2.609	2.539	2.702	0.060	2.682	2.756	0.070	0.069	2.950	0.077	0.076	
		Stdev	0.010	0.015	0.002	0.006	0.221	0.234	0.006	0.006	0.081	0.002	0.002	
		Min	2.602	2.528	2.700	0.056	2.525	2.590	0.066	0.065	2.892	0.076	0.074	
		Max	2.616	2.550	2.703	0.065	2.838	2.921	0.074	0.073	3.007	0.078	0.077	
		n	2	2	2	2	2	2	2	2	2	2	2	0

Tab. 4.3-2: continued

Formation	Member / Sub-unit						Gravimetry				Isotope mass balance			
			Bulk wet density [g/cm³]	**Bulk dry density, calculated** [g/cm³]	**Grain density** [g/cm³]	**Pycnometer porosity** [–]	**Water content (wet)** (105 °C) [wt.-%]	**Water content (dry)** (105 °C) [wt.-%]	**Water-loss porosity** using bulk wet density [–]	**Water-loss porosity** using grain density [–]	**Water content (wet)** based on isotope diff. exch. [wt.-%]	**Porosity based on isotope diff. exch.** using bulk wet density [–]	**Porosity based on isotope diff. exch.** using grain density [–]	**External surface area (BET)** [m²/g dry rock]
Villigen Fm.		Mean	2.671	2.647	2.702	0.020	0.921	0.935	0.024	0.024	1.013	0.027	0.027	
		Median	2.690	2.679	2.701	0.010	0.464	0.466	0.012	0.012	0.521	0.014	0.014	
		Stdev	0.036	0.057	0.006	0.019	0.818	0.840	0.021	0.021	0.856	0.022	0.022	
		Min	2.610	2.550	2.692	0.008	0.378	0.379	0.010	0.010	0.454	0.012	0.012	
		Max	2.697	2.685	2.708	0.053	2.309	2.364	0.060	0.060	2.465	0.064	0.064	
		n	5	5	5	5	5	5	5	5	5	5	5	0
Wildegg Fm.		Mean	2.597	2.528	2.709	0.067	2.662	2.737	0.069	0.069	2.905	0.075	0.075	
		Median	2.606	2.540	2.708	0.063	2.524	2.589	0.066	0.066	2.864	0.074	0.074	
		Stdev	0.027	0.038	0.010	0.013	0.542	0.573	0.014	0.013	0.511	0.013	0.012	
		Min	2.539	2.461	2.693	0.051	1.954	1.993	0.051	0.051	2.328	0.061	0.061	
		Max	2.622	2.571	2.729	0.086	3.549	3.680	0.091	0.090	3.860	0.099	0.098	
		n	9	9	9	9	9	9	9	9	9	9	9	0
«Parkinsoni-Württembergica-Schichten»		Mean	2.511	2.387	2.716	0.121	4.951	5.213	0.124	0.124	5.463	0.137	0.135	29.67
		Median	2.517	2.387	2.710	0.125	5.074	5.345	0.130	0.126	5.860	0.147	0.144	28.92
		Stdev	0.032	0.046	0.018	0.015	0.589	0.650	0.016	0.013	0.864	0.020	0.020	2.70
		Min	2.459	2.326	2.699	0.103	3.897	4.055	0.100	0.101	3.815	0.098	0.099	27.00
		Max	2.573	2.473	2.756	0.145	5.834	6.195	0.145	0.143	6.374	0.158	0.155	33.82
		n	9	9	9	9	14	14	9	14	9	9	9	5
Wedelsandstein Fm.		Mean	2.486	2.349	2.702	0.131	5.529	5.853	0.137	0.137	6.084	0.151	0.149	
		n	1	1	1	1	1	1	1	1	1	1	1	0
«Murchisonae-Oolith Fm.»		Mean	2.508	2.367	2.847	0.155	5.643	5.992	0.141	0.143	5.782	0.145	0.146	6.73
		Median	2.515	2.343	2.882	0.135	5.663	6.003	0.140	0.140	6.071	0.151	0.149	
		Stdev	0.026	0.045	0.103	0.038	1.213	1.362	0.030	0.032	1.566	0.039	0.039	
		Min	2.479	2.339	2.704	0.130	4.420	4.624	0.112	0.114	4.091	0.104	0.106	
		Max	2.530	2.418	2.947	0.199	6.846	7.349	0.172	0.177	7.183	0.181	0.185	
		n	3	3	5	3	3	3	3	3	3	3	3	1
Opalinus Clay	All	Mean	2.509	2.390	2.704	0.116	4.745	4.985	0.119	0.119	5.301	0.133	0.131	
		Median	2.507	2.382	2.704	0.117	4.894	5.146	0.123	0.122	5.490	0.138	0.136	
		Stdev	0.028	0.041	0.011	0.014	0.600	0.654	0.015	0.014	0.736	0.018	0.017	
		Min	2.476	2.343	2.683	0.067	2.764	2.843	0.072	0.072	3.053	0.080	0.079	
		Max	2.607	2.535	2.726	0.132	5.357	5.660	0.133	0.132	6.008	0.149	0.147	
		n	17	17	17	17	24	24	17	24	17	17	17	0
Opalinus Clay	'Sub-unit with silty calc. beds'	Mean	2.515	2.403	2.707	0.112	4.440	4.654	0.112	0.111	4.980	0.125	0.124	
		Median	2.505	2.393	2.707	0.117	4.518	4.731	0.117	0.114	5.186	0.130	0.129	
		Stdev	0.054	0.077	0.009	0.026	0.927	1.006	0.024	0.022	1.190	0.028	0.028	
		Min	2.476	2.343	2.695	0.067	2.764	2.843	0.072	0.072	3.053	0.080	0.079	
		Max	2.607	2.535	2.718	0.132	5.357	5.660	0.133	0.132	6.008	0.149	0.147	
		n	5	5	5	5	6	6	5	6	5	5	5	0

Tab. 4.3-2: continued

Formation	Member / Sub-unit		Bulk wet density [g/cm³]	Bulk dry density, calculated [g/cm³]	Grain density [g/cm³]	Pycnometer porosity [–]	Gravimetry: Water content (wet) (105 °C) [wt.-%]	Gravimetry: Water content (dry) (105 °C) [wt.-%]	Gravimetry: Water-loss porosity using bulk wet density [–]	Gravimetry: Water-loss porosity using grain density [–]	Isotope mass balance: Water content (wet) based on isotope diff. exch. [wt.-%]	Isotope mass balance: Porosity based on isotope diff. exch. using bulk wet density [–]	Isotope mass balance: Porosity based on isotope diff. exch. using grain density [–]	External surface area (BET) [m²/g dry rock]
Opalinus Clay	'Upper silty sub-unit'	Mean	2.508	2.391	2.702	0.115	4.502	4.716	0.117	0.113	5.149	0.129	0.128	
		Median	2.508	2.388	2.700	0.113	4.640	4.866	0.121	0.116	5.447	0.136	0.135	
		Stdev	0.005	0.013	0.016	0.007	0.508	0.555	0.010	0.012	0.547	0.014	0.013	
		Min	2.500	2.379	2.683	0.110	3.622	3.758	0.101	0.092	4.252	0.107	0.107	
		Max	2.514	2.407	2.726	0.127	5.036	5.303	0.126	0.125	5.555	0.139	0.137	
		n	5	5	5	5	7	7	5	7	5	5	5	0
Opalinus Clay Opalinus Clay	'Mixed clay-silt-carbonate sub-unit'	Mean	2.505	2.382	2.701	0.118	5.007	5.271	0.124	0.125	5.534	0.139	0.137	
		Median	2.504	2.381	2.704	0.117	5.092	5.365	0.123	0.127	5.425	0.136	0.134	
		Stdev	0.006	0.011	0.011	0.005	0.194	0.215	0.006	0.004	0.312	0.008	0.007	
		Min	2.500	2.371	2.689	0.114	4.719	4.953	0.119	0.118	5.292	0.133	0.132	
		Max	2.512	2.393	2.711	0.123	5.179	5.462	0.129	0.129	5.886	0.147	0.145	
		n	3	3	3	3	5	5	3	5	3	3	3	0
Opalinus Clay	'Clay-rich sub-unit'	Mean	2.507	2.380	2.704	0.120	5.117	5.393	0.127	0.127	5.718	0.143	0.141	
		Median	2.509	2.381	2.706	0.120	5.112	5.388	0.127	0.127	5.711	0.144	0.141	
		Stdev	0.012	0.016	0.011	0.003	0.161	0.179	0.004	0.003	0.193	0.004	0.004	
		Min	2.491	2.358	2.690	0.117	4.887	5.138	0.123	0.122	5.520	0.138	0.137	
		Max	2.521	2.398	2.715	0.123	5.320	5.619	0.133	0.131	5.931	0.148	0.145	
		n	4	4	4	4	6	6	4	6	4	4	4	0
Staffelegg Fm.		Mean	2.516	2.416	2.678	0.098	4.287	4.491	0.100	0.107	4.366	0.109	0.108	25.35
		Median	2.545	2.446	2.700	0.094	4.091	4.265	0.098	0.103	4.350	0.112	0.109	22.84
		Stdev	0.091	0.109	0.077	0.027	1.038	1.134	0.027	0.024	1.161	0.027	0.027	11.12
		Min	2.347	2.237	2.523	0.065	2.319	2.374	0.060	0.061	2.336	0.061	0.061	14.72
		Max	2.596	2.536	2.734	0.142	6.049	6.439	0.143	0.148	5.723	0.142	0.142	41.01
		n	6	6	6	6	11	11	6	11	6	6	6	4
Klettgau Fm.		Mean	2.527	2.393	2.748	0.130	5.377	5.695	0.134	0.134	5.970	0.150	0.148	29.08
		Median	2.554	2.414	2.754	0.126	5.614	5.948	0.140	0.138	6.378	0.163	0.158	
		Stdev	0.090	0.110	0.063	0.022	1.086	1.199	0.027	0.024	1.399	0.032	0.030	
		Min	2.367	2.216	2.661	0.099	3.200	3.306	0.084	0.085	3.436	0.090	0.091	
		Max	2.611	2.527	2.821	0.167	6.403	6.841	0.159	0.155	7.285	0.181	0.175	
		n	6	6	6	6	7	7	6	7	6	6	6	1
Bänkerjoch Fm.		Mean	2.773	2.723	2.860	0.057	1.911	1.985	0.051	0.056	2.802	0.074	0.073	
		Median	2.785	2.744	2.869	0.063	1.278	1.297	0.035	0.048	2.146	0.059	0.059	
		Stdev	0.140	0.188	0.085	0.038	1.943	2.045	0.050	0.049	1.830	0.046	0.045	
		Min	2.573	2.432	2.706	0.009	0.057	0.057	0.002	0.002	0.699	0.020	0.020	
		Max	2.933	2.931	2.956	0.122	5.510	5.831	0.142	0.139	5.772	0.149	0.145	
		n	10	10	9	9	10	10	10	9	7	7	7	0
Schinznach Fm.	All	Mean	2.647	2.582	2.832	0.088	2.517	2.622	0.065	0.067	2.567	0.067	0.068	
		Median	2.682	2.644	2.832	0.062	1.637	1.665	0.044	0.045	1.760	0.048	0.048	
		Stdev	0.087	0.137	0.047	0.059	2.084	2.244	0.051	0.053	2.086	0.051	0.053	
		Min	2.497	2.339	2.776	0.042	0.696	0.701	0.019	0.019	0.707	0.019	0.020	
		Max	2.731	2.682	2.884	0.189	6.318	6.744	0.158	0.163	6.285	0.157	0.162	
		n	6	6	6	6	6	6	6	6	6	6	6	0

Tab. 4.3-2: continued

Formation	Member / Sub-unit		Bulk wet density [g/cm³]	Bulk dry density, calculated [g/cm³]	Grain density [g/cm³]	Pycnometer porosity [–]	Gravimetry: Water content (wet) (105 °C) [wt.-%]	Gravimetry: Water content (dry) (105 °C) [wt.-%]	Gravimetry: Water-loss porosity using bulk wet density [–]	Gravimetry: Water-loss porosity using grain density [–]	Isotope mass balance: Water content (wet) based on isotope diff. exch. [wt.-%]	Isotope mass balance: Porosity based on isotope diff. exch. using bulk wet density [–]	Isotope mass balance: Porosity based on isotope diff. exch. using grain density [–]	External surface area (BET) [m²/g dry rock]
Schinznach Fm.	Stamberg Mb.	Mean	2.606	2.507	2.873	0.127	3.862	4.057	0.099	0.102	3.982	0.102	0.105	
		Median	2.591	2.501	2.870	0.129	3.487	3.613	0.090	0.094	3.677	0.095	0.099	
		Stdev	0.118	0.172	0.010	0.062	2.292	2.495	0.055	0.057	2.167	0.052	0.054	
		Min	2.497	2.339	2.866	0.064	1.781	1.813	0.049	0.049	1.984	0.054	0.055	
		Max	2.731	2.682	2.884	0.189	6.318	6.744	0.158	0.163	6.285	0.157	0.162	
		n	3	3	3	3	3	3	3	3	3	3	3	0
Schinznach Fm.	Lied. + Leu-tschenb. + Kienb. Mb.	Mean	2.687	2.656	2.790	0.048	1.171	1.187	0.031	0.032	1.152	0.031	0.031	
		Median	2.692	2.656	2.797	0.043	1.324	1.342	0.036	0.036	1.215	0.033	0.033	
		Stdev	0.015	0.025	0.013	0.010	0.420	0.429	0.011	0.011	0.418	0.011	0.011	
		Min	2.671	2.631	2.776	0.042	0.696	0.701	0.019	0.019	0.707	0.019	0.020	
		Max	2.699	2.680	2.798	0.059	1.494	1.516	0.040	0.041	1.535	0.041	0.042	
		n	3	3	3	3	3	3	3	3	3	3	3	0
Zeglingen Fm.		Mean	2.496	2.307	2.897	0.203	7.561	8.180	0.189	0.192	7.480	0.187	0.190	
		n	1	1	1	1	1	1	1	1	1	1	1	0

4.3.1 Water content

The distribution of gravimetric water content in the studied section Malm – Triassic is shown in Fig. 4.3-1. Note that the error bars on gravimetric water content reflect the variability among 3 aliquots of the samples, i.e. they are a measure of the lithological heterogeneity of the sample on the cm-scale. In contrast, the propagated analytical error is shown for data obtained from isotope diffusive exchange. The following systematics of the water content can be observed in the Triassic and in the Malm (the Dogger – Lias section is detailed further below):

- In the Schinznach Formation, an upwards increasing trend is identified, similar to findings in other boreholes, e.g. STA2-1 and STA3-1.
- The water content varies widely in the Bänkerjoch Formation, reflecting the lithological heterogeneity in this unit.
- The water content is high in the Klettgau Formation, without evident depth trends.
- In the Wildegg Formation, no systematic depth trend can be identified. Low water contents with a decreasing trend are seen towards the top within the Villigen Formation.
- The Schwarzbach Formation shows distinctly higher water contents in comparison to its neighbouring units.

Water contents from gravimetry and from isotope diffusive exchange correlate well (Fig. 4.3-2), but the latter show values that are consistently higher, about 9%$_{rel}$ on the average.

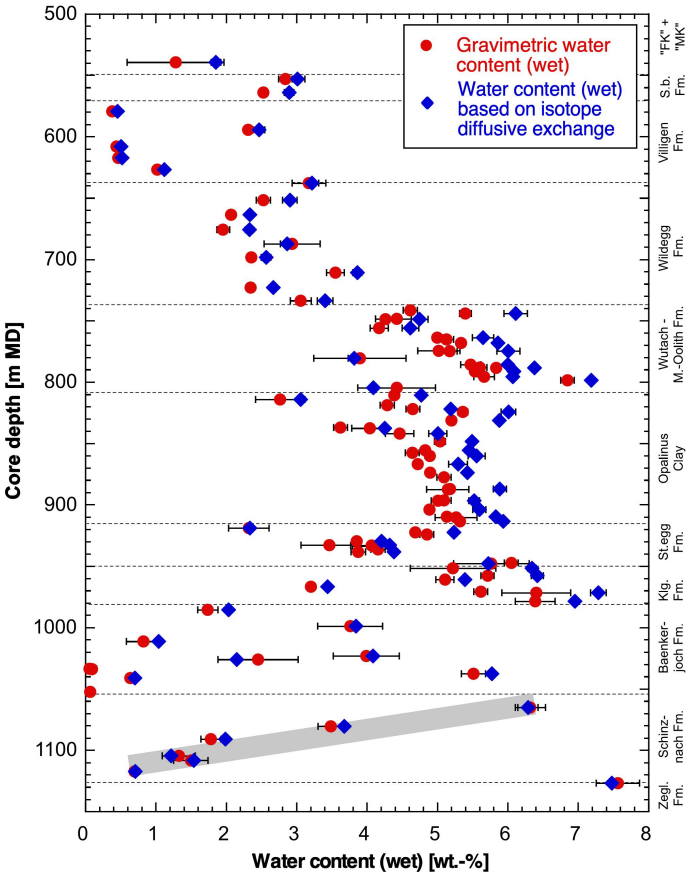

Fig. 4.3-1: Water content as a function of depth

Trends (thick grey bars), if present, are only indicated for the Malm and Triassic sections, the Dogger and Lias are detailed in Fig. 4.3-3. Black bars for gravimetric water content indicate 1σ variability among 3 aliquots of the same sample. Black bars for water content from isotope diffusive exchange represent the propagated analytical error.

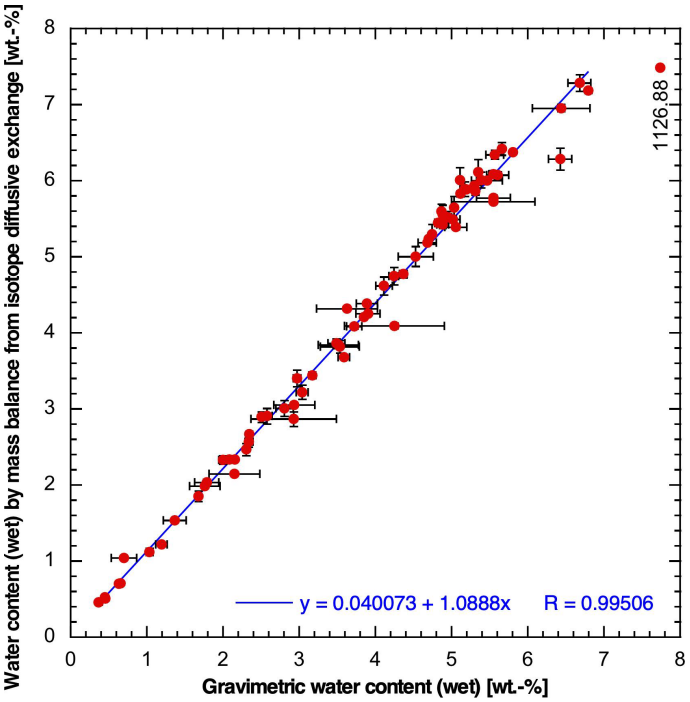

Fig. 4.3-2: Correlation of water contents based on gravimetry and on isotope diffusive exchange

Black bars for gravimetric water content indicate 1σ variability among 2 aliquots of the same sample. Black bars for water content from isotope diffusive exchange represent the propagated analytical error. Note that only the 2 gravimetric water contents obtained from the aliquots used for the isotope diffusive-exchange experiments were considered in this graph, so the correlation refers to identical sample materials. This is particularly important for anhydrite-bearing samples, given the fact that only the anhydrite-poorest portions of such samples were used for diffusive-exchange experiments. Sample 1'126.88 from the Zeglingen Formation (porous dolostone) falls off the trend and was not considered for the linear regression line.

A closer look at the clay-rich Lias – Dogger section

As shown in Fig.4.3-3, water contents in the Lias – Dogger section show several systematic trends with depth. These are similar for gravimetric water content and that obtained from isotope mass balance:

- All four sub-units of the Opalinus Clay show upward trends towards lower water content.
- Another cycle of decreasing water content is observed in the «Parkinsoni-Württembergica-Schichten».

The observed trends of the water content correlate reasonably well with those identified for clay-mineral contents (Section 4.2.1, Fig. 4.2-4), and tend to be even clearer.

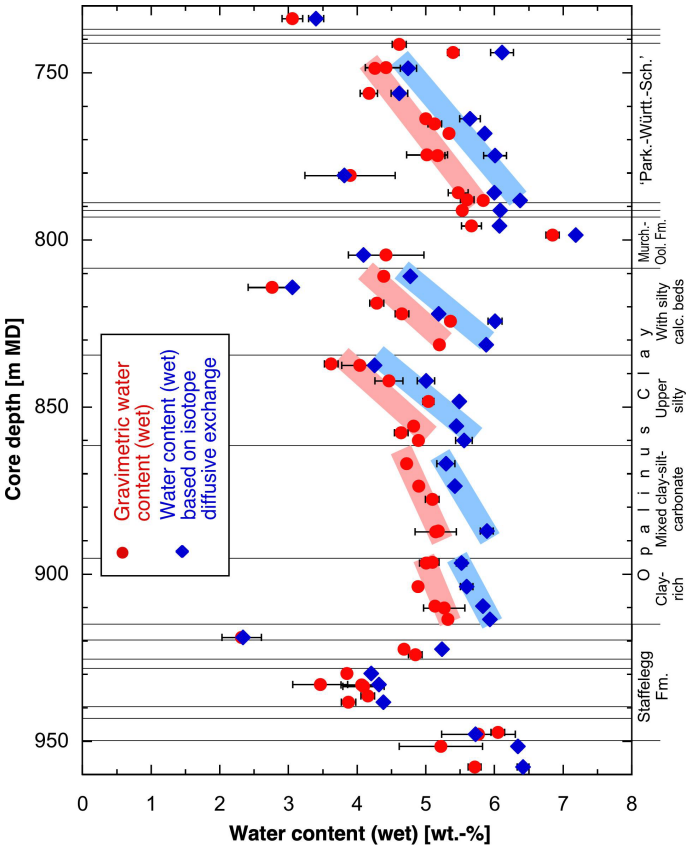

Fig. 4.3-3: Water content (wet) as a function of depth in the Lias – Dogger interval

Black bars for gravimetric water content indicate 1σ variability among 3 aliquots of the same sample. Black bars for water content from isotope diffusive exchange represent the propagated analytical error.

4.3.2 Grain density

The grain-density profile is shown in Fig. 4.3-4. Throughout the Malm, Dogger and Lias units, values are around 2.7 g/cm^3, with only limited scatter. Distinct outliers towards higher values are observed in the «Murchisonae-Oolith Formation» and are due to the presence of goethite and haematite. The only other conspicuous excursion is identified in the Rietheim Member of the Staffelegg Formation («Posidonienschiefer»), where the high content of organic matter (C_{org} = 5.4 wt.-%) leads to a markedly lower grain-density value.

In the underlying Triassic section, values become higher, as does variability. This reflects the lithological heterogeneity, in particular the variable contents of dolomite and anhydrite with their high mineral densities (2.85 and 2.97 g/cm^3, respectively). Fig. 4.3-5 shows the correlation between grain density and dolomite/ankerite contents. Grain density increases linearly with dolomite concentration, and outliers are due to the presence of goethite, anhydrite or organic carbon.

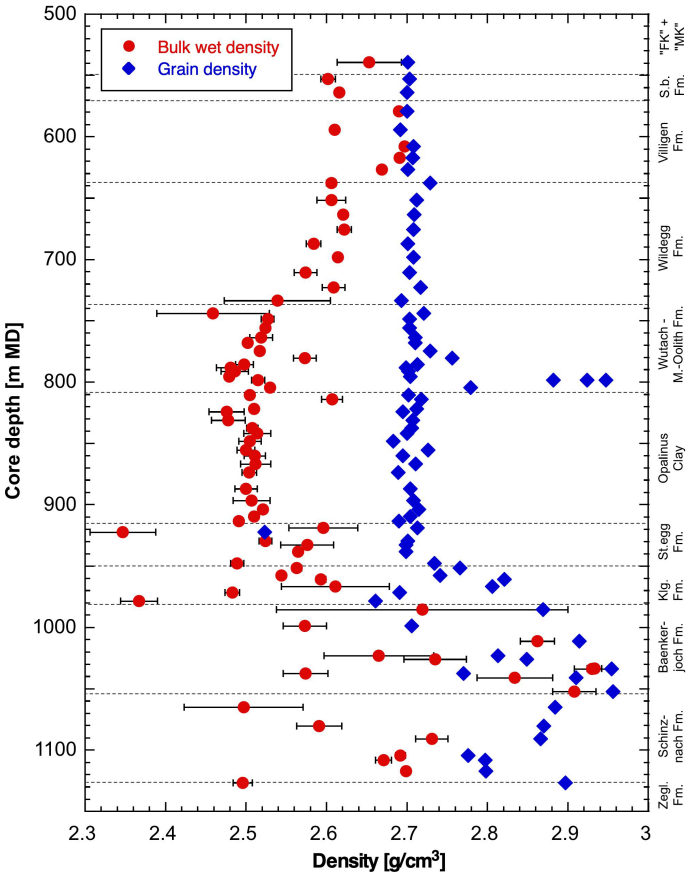

Fig. 4.3-4: Depth profile of bulk wet and grain densities

Black bars for bulk wet density indicate 1σ variability among 3 pieces of the same sample. Analytical error bars for grain density are smaller than the symbol size.

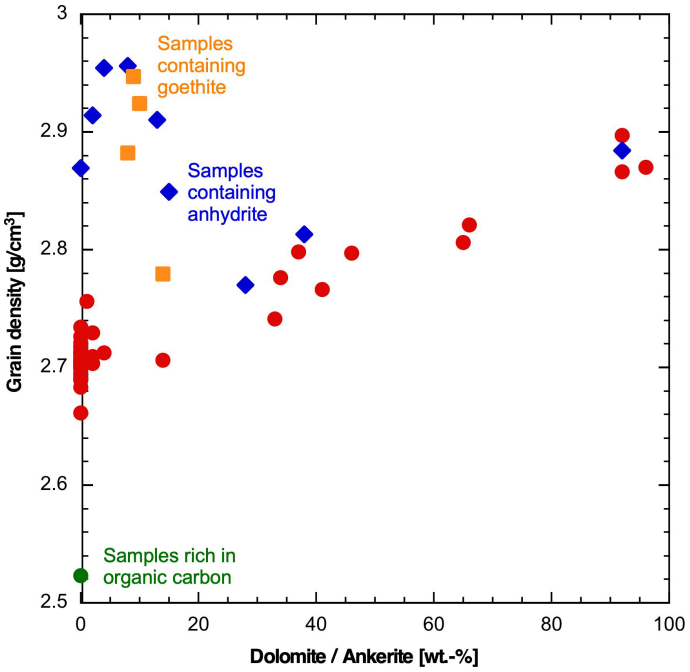

Fig. 4.3-5: Grain density as a function of the contents of dolomite/ankerite

Anhydrite-bearing samples are from the Schinznach and Bänkerjoch Formations. Goethite-bearing samples are from the «Murchisonae-Oolith Formation». The organic-rich sample is from the Rietheim Member of the Staffelegg Formation.

4.3.3 Bulk wet density

Data are shown in Fig. 4.3-4 as a function of depth. Large error bars for some samples reflect heterogeneity on the cm scale.

4.3.4 Porosity

Three different approaches were used to constrain rock porosity (for details see Waber ed. 2020):

- *Water-loss porosity:* calculation from the gravimetric water content using either bulk wet or grain density.
- *Porosity from isotope diffusive exchange:* calculation from the water content obtained by mass balance using either bulk wet or grain density.
- *Pycnometer porosity:* calculation from bulk dry and grain densities; bulk dry density is calculated from bulk wet density and water content.

Water-loss porosity and porosity from isotope diffusive exchange were calculated using bulk wet density by default. If the latter was not available, grain density was used, by which full water saturation of the pore space was assumed. The graphic in Fig. 4.3-6 shows that the two densities yield near-identical porosities, so the choice of the type of density for the calculation incurs no additional uncertainty.

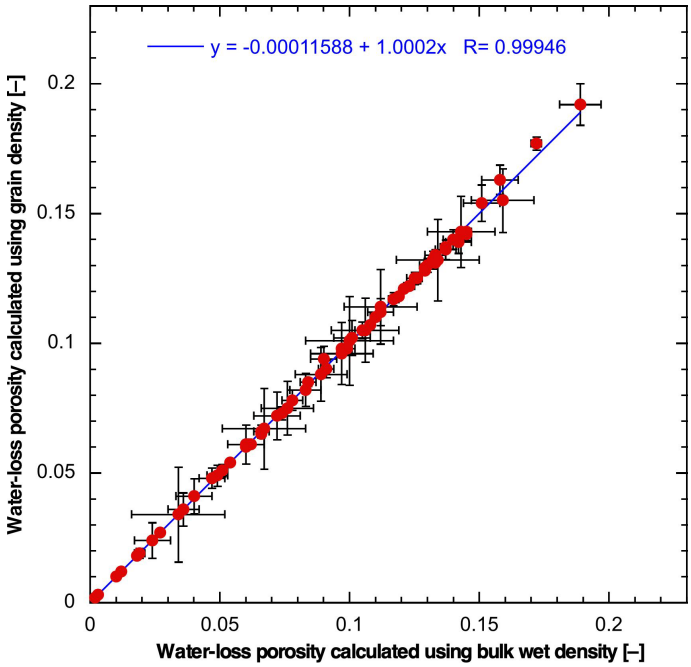

Fig. 4.3-6: Water-loss porosity calculated from gravimetric water content using either bulk wet or grain density

Bars indicate propagated errors, which are dominated by local heterogeneity of water content.

Comparison of porosities obtained by different methods

- An excellent linear correlation is observed between water-loss porosity and porosity from isotope diffusive exchange (Fig. 4.3-7). The latter yields about 7% higher values. Only sample 1'126.80 from the Zeglingen Formation (a dolostone with a heterogeneously distributed macroporosity) falls off the general trend.
- A slightly less good linear correlation is found between pycnometer porosity and porosity from isotope diffusive exchange (Fig. 4.3-8). The latter yields about 10% higher values. Four outliers are explained by sample heterogeneity (see illustrations in Fig. 4.3-9).
- The correlation between water-loss and pycnometer porosity is shown in Fig. 4.3-10. Again, the same samples fall off the trend (see illustrations in Fig. 4.3-9). Excluding these outliers yields a slope for the regression line of about 0.92.

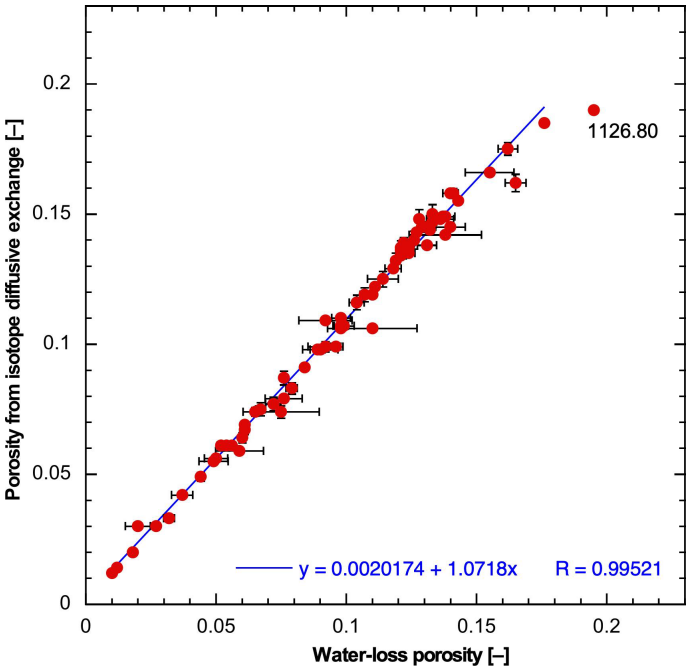

Fig. 4.3-7: Correlation of water-loss porosity and porosity from isotope diffusive exchange

Bars indicate propagated errors. Note that only the gravimetric water contents obtained from the aliquots used for the isotope diffusive-exchange experiments were considered for the x-axis of this graph, so the correlation refers to identical sample materials. Sample 1'126.88 from the Zeglingen Formation (porous dolostone) falls off the trend and was not considered for the linear regression line.

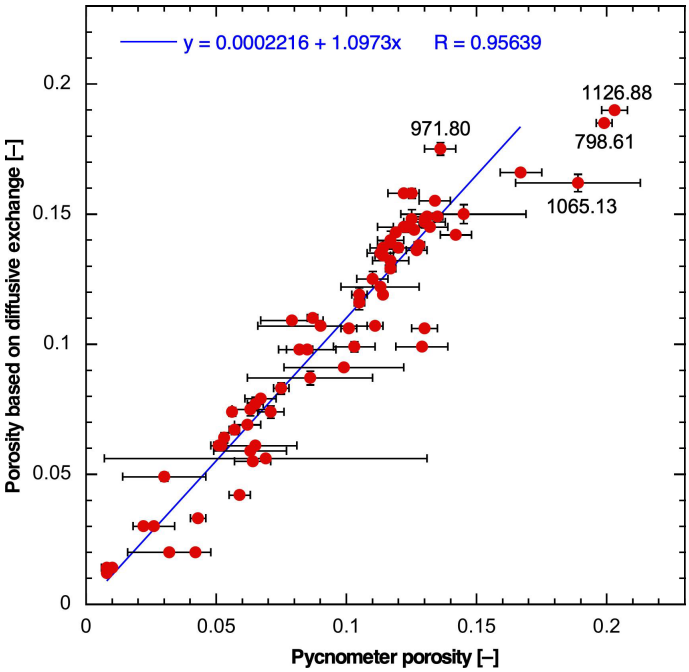

Fig. 4.3-8: Correlation of pycnometer porosity and porosity from isotope diffusive exchange

Bars indicate propagated errors. Indicated outliers were excluded from the regression line.

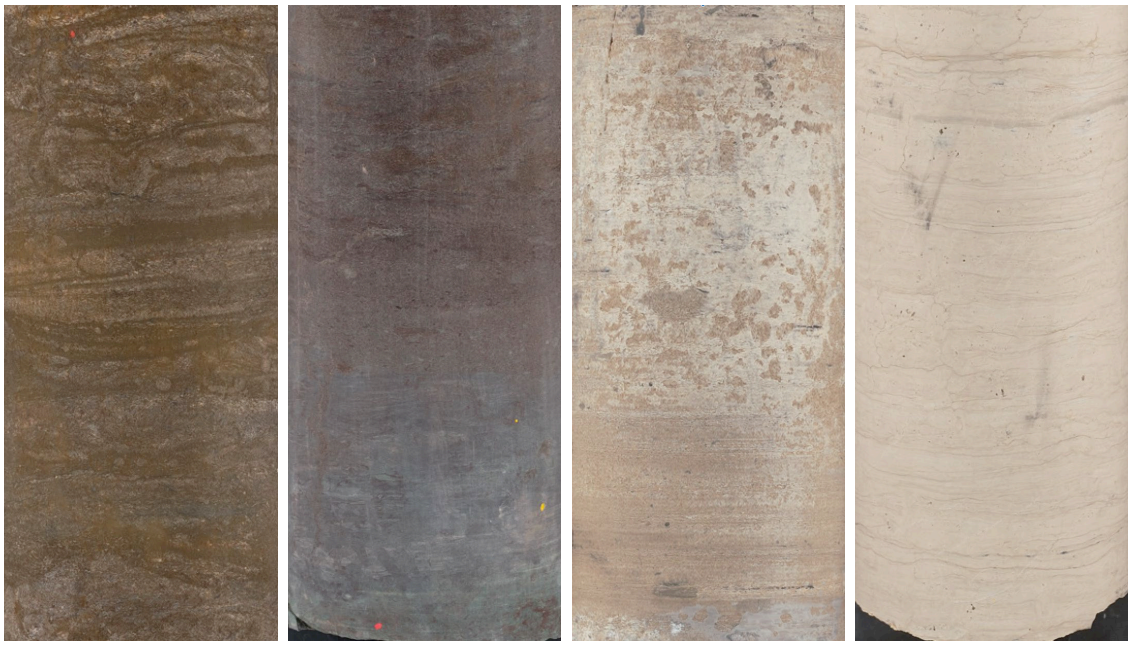

798.61 m («Murch.-Oolith Fm.») | 971.80 m (Klettgau Fm.) | 1'065.13 m (Schinznach Fm.) | 1'126.88 m (Zeglingen Fm.)

Fig. 4.3-9: Illustrations of heterogeneous samples

798.61 m: Nodular, goethite-rich Fe-oolite; 971.80 m: Transition of clay-rich sandstone (top) to sandy claystone (bottom); 1'065.13 m: Dolostone with heterogeneously distributed macroporosity; 1'126.88 m: Dolostone with macroporosity along discrete horizons. Width of photographs is 10 cm.

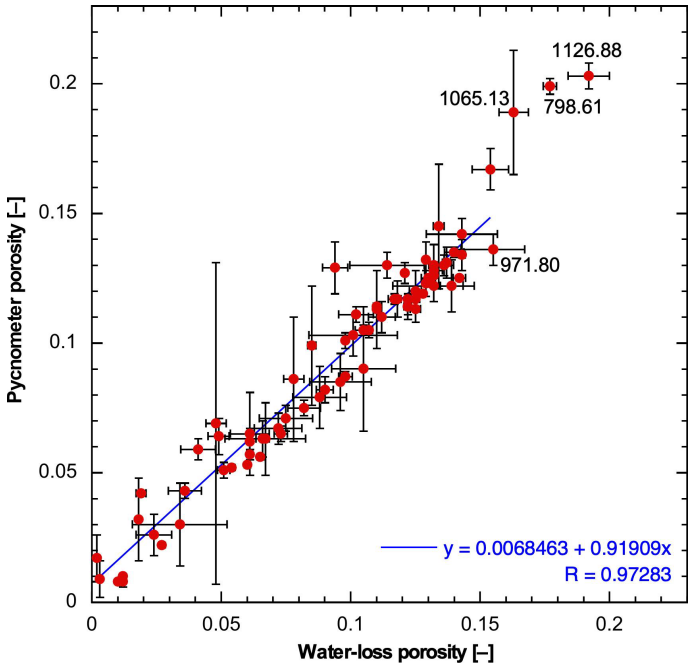

Fig. 4.3-10: Correlation of water-loss and pycnometer porosity

Bars indicate propagated errors. The indicated outliers were excluded from the regression line.

Depth trends

In Fig. 4.3-11, porosity is shown as a function of depth. The shape of the profile is similar to that of water content (Figs. 4.3-1 and 4.3-3), including the systematic trends. The comments made on the distribution of water content with depth (Section 4.3.1) also apply to porosity.

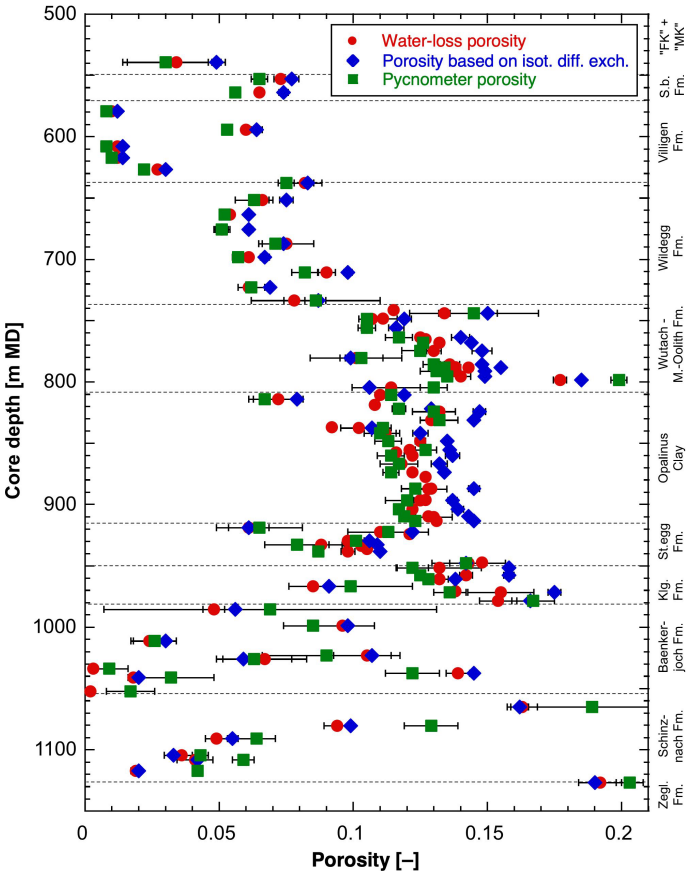

Fig. 4.3-11: Depth trends of porosities obtained by different methods

Porosity as a function of mineralogical composition

The correlation of porosity with clay-mineral content is shown in Fig. 4.3-12. When considering all available data (Fig. 4.3-12a), a general positive correlation can be identified but scatter is substantial. Marked outliers towards high porosity at a low clay-mineral content are dolostones of the Schinznach and Zeglingen Formations (1'080.67 m, 1'126.88 m). These were affected by diagenetic dissolution to some degree, either during the process of dolomitisation or at later stages. Thus, their porosity is not the result of compaction and cementation alone. In the Klettgau Formation, two samples (971.80 m and 978.81 m) contain 45 – 52 wt.-% quartz and feldspars and thus likely have a grain-supported fabric, which limits the compaction of the intergranular space. Three other samples (951.57 m, 957.76 m and 960.88 m) are rich in dolomite (33 – 66 wt.-%).

Four samples from the Bänkerjoch Formation (1'011.38 m, 1'033.99 m, 1'041.28 m, 1'052.63 m) contain 42 – 76 wt.-% anhydrite. The presence of anhydrite tends to reduce porosity for a given clay-mineral content. Fig. 4.3-13 illustrates that porosity tends towards zero in anhydrite-rich samples.

When only samples from the Malm – Dogger – Lias section are considered, i.e. when the mineralogically and texturally more heterogeneous samples from the Triassic are excluded, a more systematic correlation is obtained (Fig. 4.3-12b). Outliers include:

- 710.98 m (Wildegg Formation): Limestone with exceptionally high content of quartz and feldspars (33 wt.-%), thus potentially with a grain-supported fabric.
- 798.61 m, 804.58 m («Murchisonae-Oolith Formation») – Fe-oolitic samples containing goethite, haematite and dolomite. The potential undercompaction of Fe-oolites is discussed in detail in Mazurek et al. (2023).

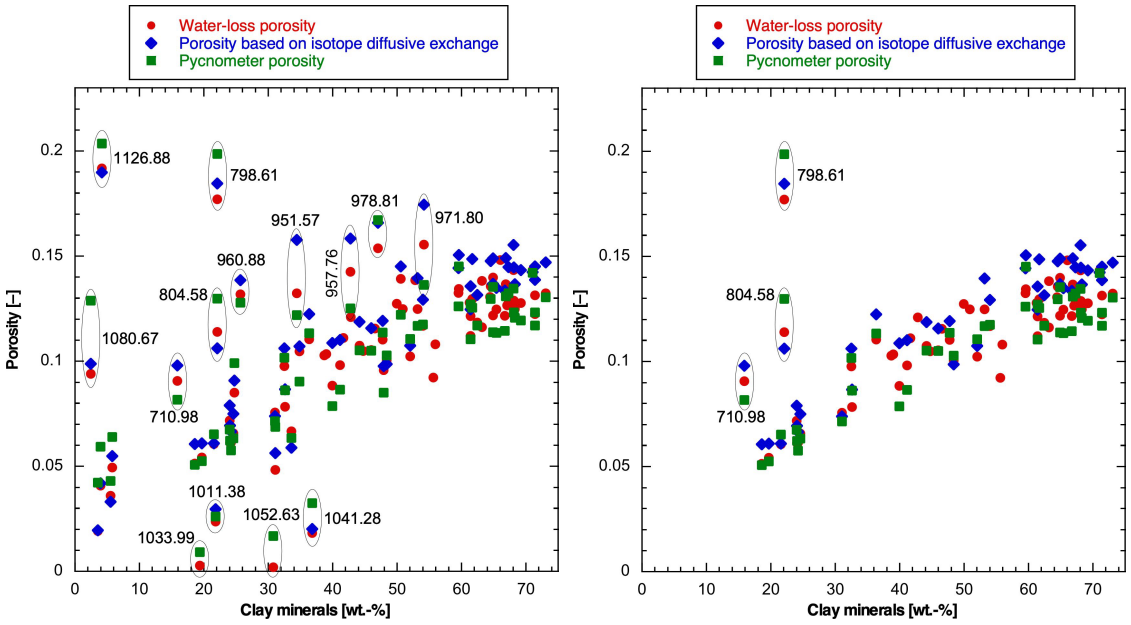

Fig. 4.3-12: Porosity as a function of clay-mineral content

(a) all data, (b) data from the section Malm – Dogger – Lias.

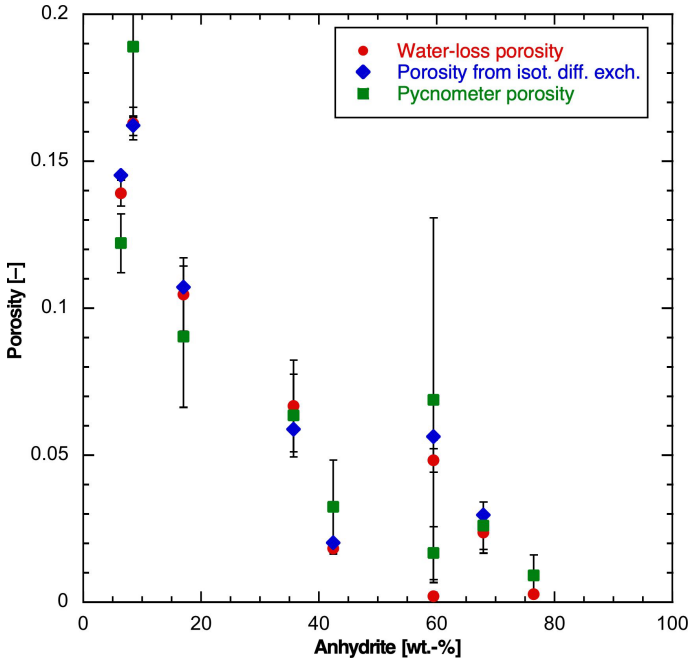

Fig. 4.3-13: Porosity of anhydrite-bearing samples

4.3.5 Specific surface area and pore-size distributions from N_2 ad-/desorption

Thomas Gimmi

Depth trends

Nitrogen adsorption data were obtained for 11 samples from the upper and lower confining units of the Opalinus Clay, comprising very different lithologies (Tab. 4.3-2)[7]. These included 7 samples on which squeezing experiments were performed, 3 samples used for advective displacement experiments, and one regular porewater sample. One sample was from the «Murchisonae-Oolith Formation» (798.61 m), five were from the «Parkinsoni-Württembergica-Schichten» (741.49 m, 748.50 m, 765.33 m, 774.58 m, 788.06 m), four from the Staffelegg Formation (924.21 m from the Rietheim Member, 933.70 m and 936.46 m from the Frick Member, and 947.42 m from the Schambelen Member), and one from the Klettgau Formation (at 970.89 m from the Ergolz Member).

Because of the comparably small number of samples and the lack of data from the Opalinus Clay, the depth trends of the specific surface area S_{BET} are not very clear (Fig. 4.3-14). However, a comparison with the data obtained from the other boreholes from the Nördlich Lägern area (STA2-1, STA3-1 and BUL1-1; right plot in Fig. 4.3-14) shows similar variations with rock formations in all these boreholes, when considering that the samples from BUL1-1 with low S_{BET} values in the upper part of the Wutach Formation to the «Murchisonae-Oolith Formation» all originate from the «Herrenwis Unit». This unit is encountered also in STA3-1 (at a similar position) and in STA2-1 (thinner and located closer to the Opalinus Clay), but no nitrogen adsorption data are available from this unit for these two boreholes. In BAC1-1, the «Herrenwis Unit» was not encountered.

[7] This batch of sample was intentionally focused on the confining units.

As N_2 cannot reach interlayer pores of smectites, S_{BET} represents surfaces of external (non-interlayer) pores. The largest value of about 41 m^2/g was found for the Staffelegg Formation sample from the Schambelen Member (947.42 m). Larger values between about 27 – 34 m^2/g were found for the samples from the Klettgau Formation and from the «Parkinsoni-Württembergica-Schichten» (upper part of the zone denoted as «Wutach Formation – Murchisonae-Oolith Formation»). A low value of ~ 7 m^2/g was found for the sample from the «Murchisonae-Oolith Formation» at the bottom of this zone, which is lower than those found in other boreholes. As observed before, the S_{BET} values in the Staffelegg Formation span a considerable range (~ 14 – 41 m^2/g), due to heterogeneities regarding depositional environment and diagenesis.

The variation of the specific surface area S_{BET} with depth is generally related to trends observed in other physical and mineralogical properties of samples from the BAC1-1 borehole, such as the bulk dry density, the gravimetric water content, the water-loss porosity, or the clay-mineral content.

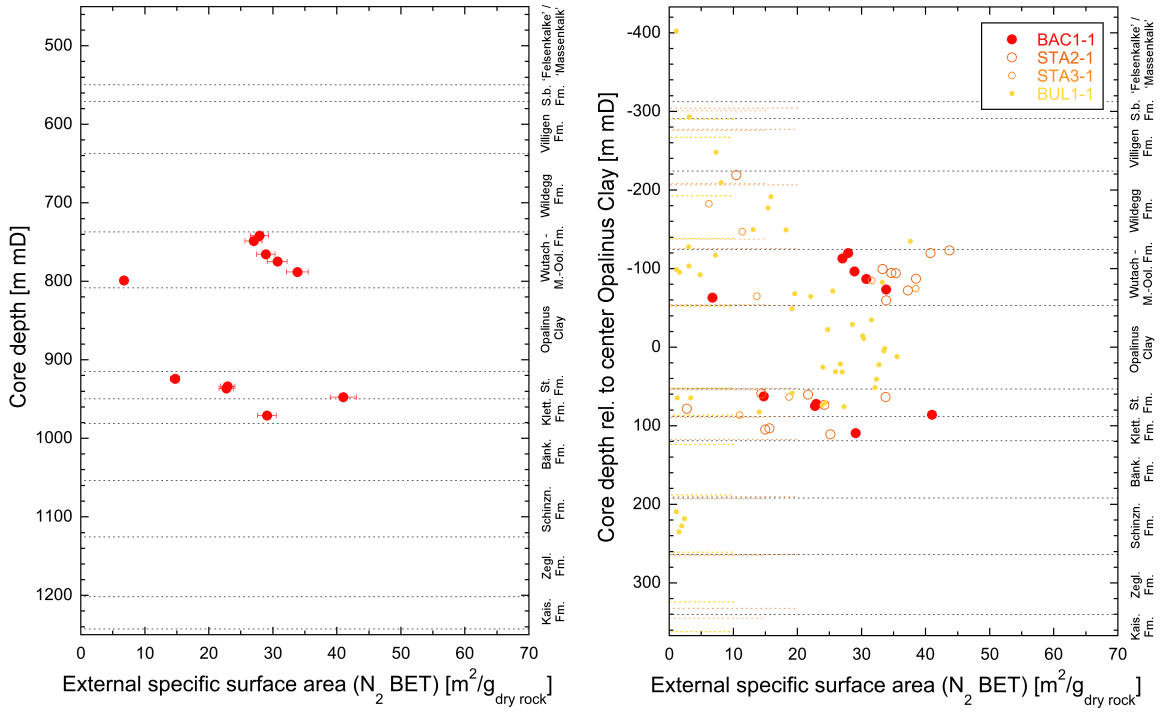

Fig. 4.3-14: Specific surface area (S_{BET}) derived from N_2 adsorption as a function of depth

Left: Data from the BAC1-1 borehole. Right: Comparison of data from the BAC1-1 borehole with those from the STA2-1, STA3-1 and BUL1-1 boreholes, with depth relative to the center of Opalinus Clay.

S_{BET} represents external surfaces only. The total specific surface area, including interlayer surfaces, would be larger depending on the smectite content of the sample. Errors resulting from sample preparation and handling are estimated to be ± 5% in general and ± 10% for $S_{BET} < 2$ m^2 g^{-1}, as given by the error bars. In the right plot, the shorter dashed lines show formation boundaries for the STA2-1, STA3-1 and BUL1-1 boreholes.

Correlation of S_{BET} with water content and clay-mineral content

The specific surface area S_{BET} tends to increase with the gravimetric water content (Fig. 4.3-15). When excluding the samples from the Rietheim Member in the Staffelegg Formation (924.21 m) and from the «Murchisonae-Oolith Formation» (798.61 m), the correlation for the remaining nine samples is similar as that for the samples from the BUL1-1 borehole. One has to keep in mind, though, that for BAC1-1 only samples from the confining units were analysed.

The sample from the «Murchisonae-Oolith Formation» and also that from the Rietheim Member have low specific surface areas compared to their water content. This is certainly related to their specific mineralogical compositions. The former sample contains 52 wt.-% calcite, 22 wt.-% clay minerals, 10 wt.-% dolomite, and 9 wt.-% goethite, while the latter contains 43 wt.-% clay minerals, 25 wt.-% calcite, 11 wt.-% quartz, and 9 wt.-% organic carbon.

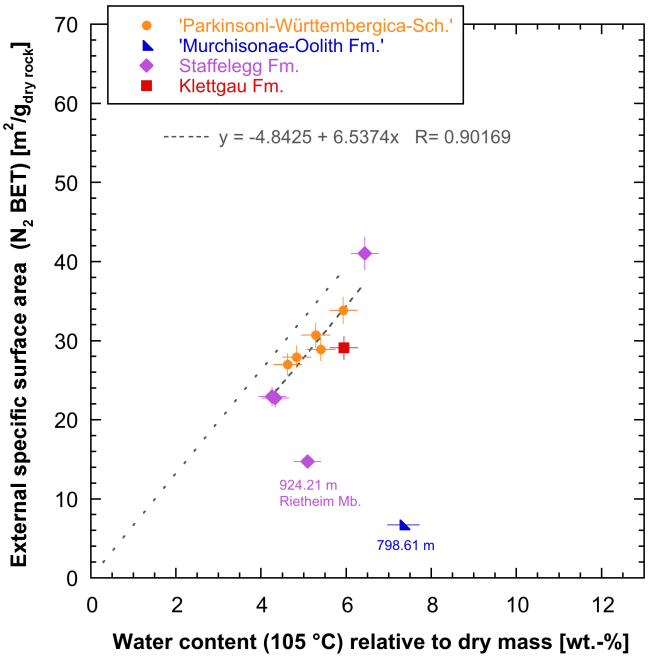

Fig. 4.3-15: Specific surface area (S_{BET}) derived from N_2 adsorption plotted against the gravimetric water content relative to the dry mass of the samples

Error bars show estimated errors for the water content (based on standard deviations of other samples) and estimated errors for S_{BET}. The dotted line shows the regression obtained for the BUL1-1 data set which includes samples from all formations. The slope is similar to the regression for the BAC1-1 data when excluding the samples at 798.61 m and 924.21 m (dashed line).

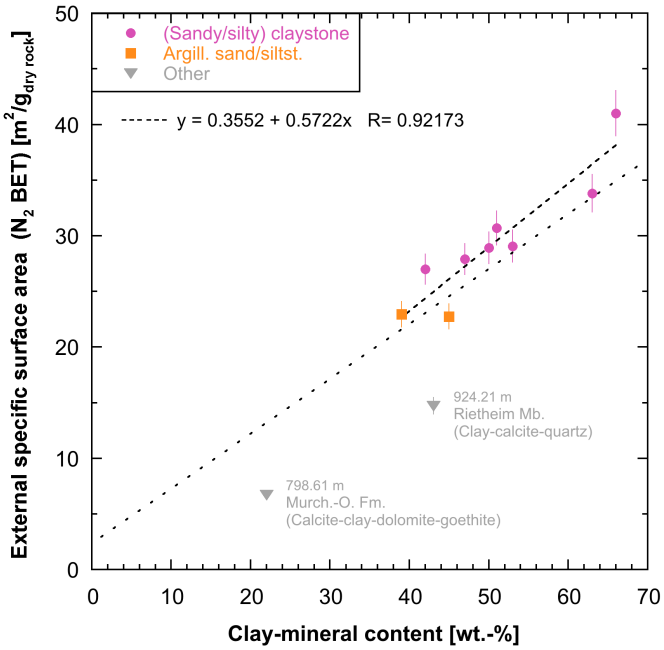

Fig. 4.3-16: Relation between external specific surface area (S_{BET}) derived from N_2 adsorption and content of clay minerals

The samples for which clay mineralogy is available are assigned to classes according to their positions in the Füchtbauer diagram (i.e., according to lithological rock types). The dotted line shows the regression obtained for the BUL1-1 data including samples from all formations, the dashed line is a regression line for the BAC1-1 data excluding the samples at 798.61 m and 924.21 m

The specific surface area S_{BET} also tends to increase with the clay-mineral content (Fig. 4.3-16), with the two samples from the «Murchisonae-Oolith Formation» and from the Rietheim Member plotting below the trend given by the other samples.

When plotting S_{BET} against individual clay end-member contents (Fig. 4.3-17), positive correlations exist with the illite and the smectite end-member contents. While the correlation of the BAC1-1 data with the illite end-member content is similar as that reported for the BUL1-1 data, the correlation with the smectite end-member content for the BAC1-1 data has a lower slope than that of the BUL1-1 data. This is mainly because the BAC1-1 S_{BET} data set is dominated by values from the «Parkinsoni-Württembergica-Schichten», which tend to have comparably high smectite end-member contents but not very large specific surface areas. The samples from the Staffelegg Formation (Rietheim Member, 924.21 m) and partly also from the Klettgau Formation (Ergolz Member, 970.89 m) represent outliers in some of these plots, similar to observations for instance in the STA2-1 data set (no individual clay end-member contents are available for the other previous outlier from the «Murchisonae-Oolith Formation»). Only very vague trends exist between S_{BET} and kaolinite or chlorite end-member contents, like for the BUL1-1 data.

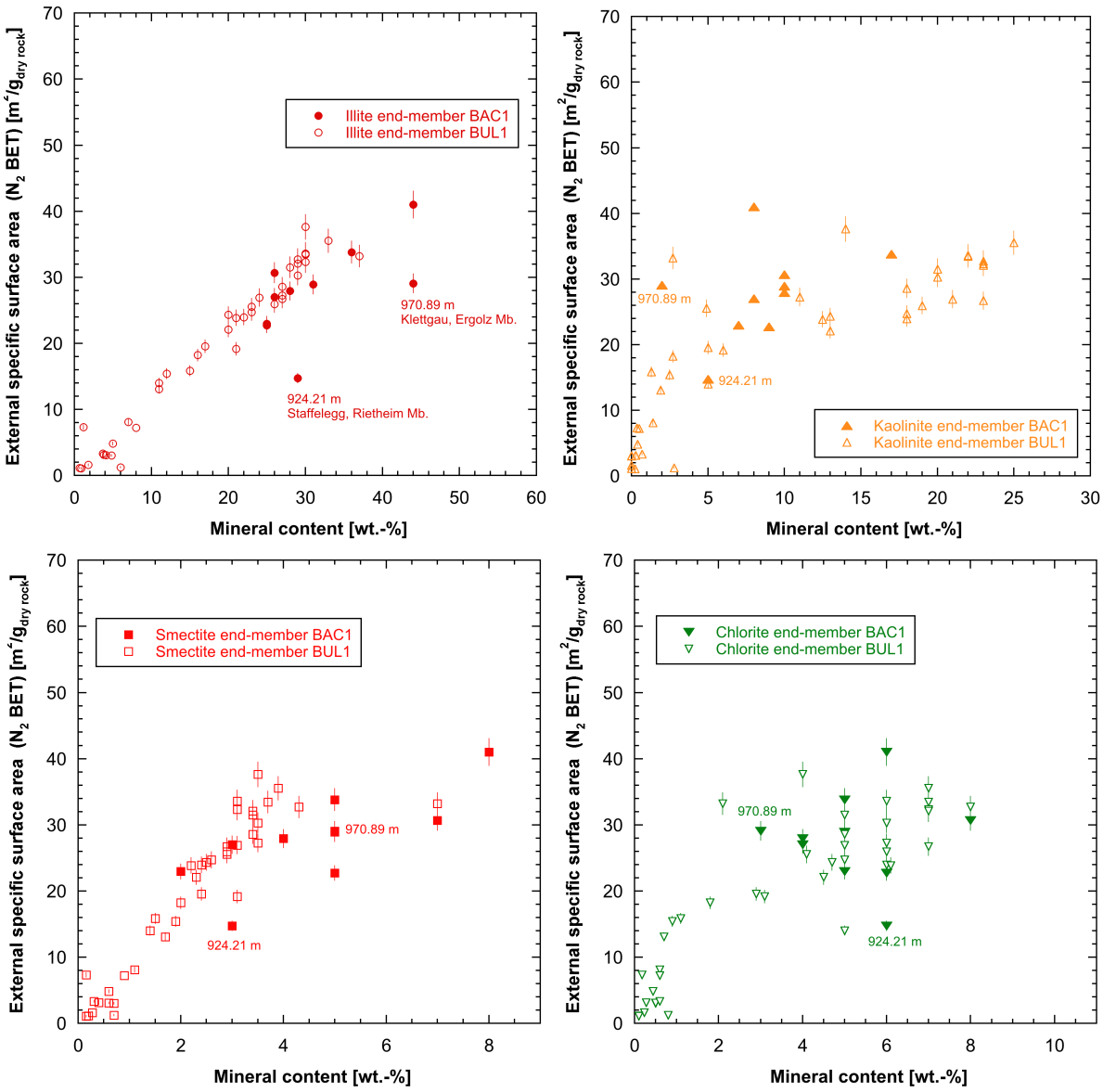

Fig. 4.3-17: Relation between external specific surface area (S_{BET}) derived from N_2 adsorption and contents of specific clay mineral end-members

The solid symbols represent the BAC1-1 data which do not include any samples from the Opalinus Clay; the open symbols show BUL1-1 data including samples from all formations.

Average sizes of external pores derived from S_{BET}

Average sizes of external pores (planar geometry) were estimated from the specific surface area S_{BET} and the water content per dry mass WC_d as:

$$\overline{r_{ext}} = WC_d/(\rho_w\, S_{BET})$$

with ρ_w the water density taken to be 1 g mL^{-1}. This calculation assumes negligible pore volumes in interlayer pores, i.e., it attributes the measured water content to external pores only (which is not appropriate for samples with relevant smectite end-member contents). Also, it assumes a slab (planar) geometry of the pore. Assuming a cylindrical shape of pores, the slab values would have to be multiplied by a factor 2.

The slope of the linear relation in Fig. 4.3-15 represents S_{BET}/WC_d. From the inverse of this slope (6.54 $m^2\ g^{-1}$ wt.-$\%^{-1}$ when excluding the mentioned outliers), we obtain an average layer thickness (or half size) of external pores of 1.5 nm, which corresponds to about 5 to 6 water layers. A similar average value was obtained for the samples from BUL1-1, which included many claystone samples.

Instead of calculating an overall average from the linear regression, it is more interesting to derive an average layer thickness for each sample. Fig. 4.3-18 plots average external pore radii (planar geometry and attributing all water to external surfaces) for each sample as a function of the gravimetric water content per dry solid mass (a) and as a function of the total clay-mineral content (b). The values range between radii of 1.6 and 2.0 nm (diameter of 3.1 – 4.1 nm) for nine samples but attain values of 3.5 nm (diameter 6.9 nm) and 11 nm (diameter 22 nm) for the samples from the Rietheim Member in the Staffelegg Formation (924.21 m) and from the «Murchisonae-Oolith Formation» (798.61 m), respectively, with small S_{BET} values but comparably large water contents.

For the latter sample, no smectite end-member content could be derived. All other samples have 2 – 8 wt.-% smectite end-member contents, so average pore radii considering also interlayer pores would tend to be slightly smaller than the calculated average external pore radii.

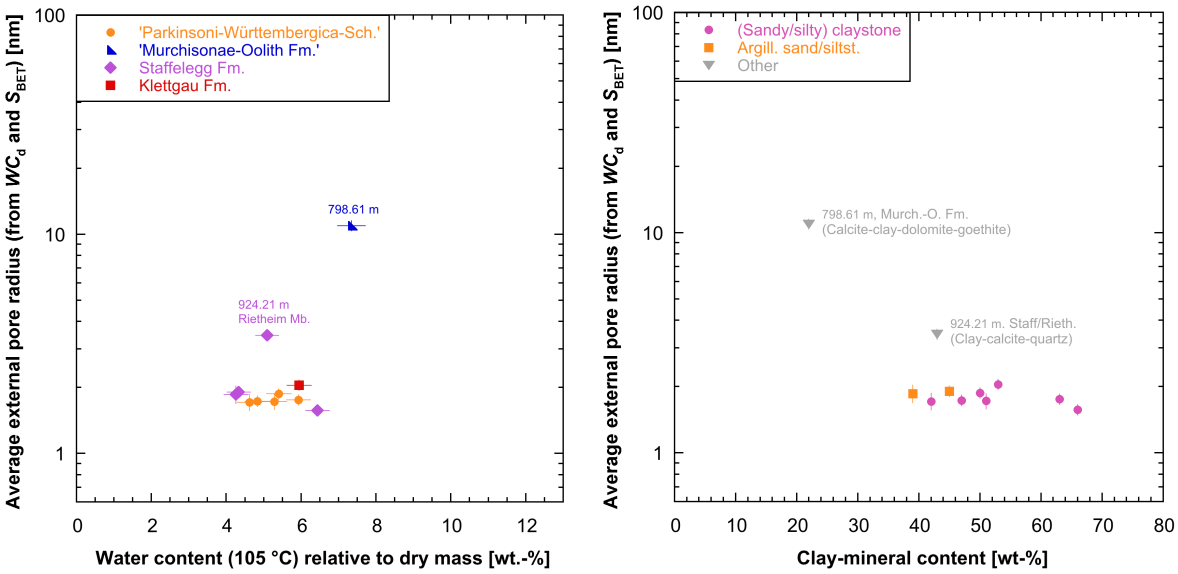

Fig. 4.3-18: Average external pore radius calculated from S_{BET} and the gravimetric water content (assuming planar geometry and insignificant interlayer pore volume) plotted against the gravimetric water content per dry mass of the samples (a) and against the total clay-mineral content (b)

Samples are grouped according to geological units (a) or according to rock lithology (b). Error bars show estimated errors for the water content (based on standard deviations of other samples) and propagated errors for the average external pore radius.

Distribution of external pore sizes derived from N_2 isotherms

Size distributions (diameters) of external pores were derived from N_2 ad- and desorption isotherms (using the standard BJH algorithm, assuming cylindrical geometry). Results from N_2 desorption for all samples are shown in Fig. 4.3-19, grouped according to rock lithology. Most samples show a clear, partly prominent peak at a diameter of about 4 nm in these curves. These peaks are typically related to the closure of the hysteresis of the isotherm and are thus attributed to liquid instabilities (instability of the configuration of liquid nitrogen during desorption) rather than to a distinct pore volume in this size range. The pore volume drained at this point is in reality very likely distributed over a range of (mostly) larger pore sizes. Hysteresis and thus a clear closure peak is generally interpreted as indicating a relatively complex pore architecture (e.g. Thommes et al. 2015), as especially found in clay-rich samples.

The very argillaceous sandstone/siltstone sample at 933.70 m (Staffelegg Formation, Frick Member, clay-mineral content of 39 wt.-%; Fig. 4.3-19a) exhibits a typical distribution for this class of samples, with a clear hysteresis peak besides two comparably weak, but broad (here not very well separated) peaks around ~ 20 nm and ~ 60 nm. The second very argillaceous sandstone/siltstone sample (936.46 m, also Staffelegg Formation, Frick Member, clay-mineral content of 45 wt.-%) shows a less typical size distribution for this class, with a first weak peak (after the hysteresis peak) at ~ 6 – 10 nm and a second, important and relatively sharp peak at ~ 60 nm. This sample has a calcite content of ~ 10 wt.-%, about double the content of that of the overlying sample (5.5 wt.-%), which could be related to the differences.

The very sandy/silty claystone samples (741.49 m, 748.50 m, 970.89 m; Fig. 4.3-19b) and the argillaceous marl (765.33 m) have similar diameter-size distributions, with a peak at ~ 6 – 10 nm and a secondary peak at ~ 60 – 200 nm, in addition to the very strong hysteresis peak. The distributions for the three claystone samples (774.58 m, 788.06 m, 947.42 m) are also similar, with somewhat larger peaks at ~ 6 – 10 nm for the samples at 774.58 m and 788.06 m.

Finally, the diameter-size distributions of the two samples that cannot be classified according to the Füchtbauer scheme are presented in Fig. 4.3-19c. The sample from the «Murchisonae-Oolith Formation» (798.61 m) is characterised by 52 wt.-% calcite, 10 wt.-% dolomite, and 9 wt.-% goethite. It has nearly no hysteresis peak, meaning that the pore network is comparably simple, and then a single broad peak with a maximum at ~ 30 nm. The other sample from the Rietheim Member of the Staffelegg Formation (924.21 m) is characterised by 43 wt.-% clay minerals, 25 wt.-% calcite, 11 wt.-% quartz, and 9 wt.-% organic carbon. It has a clear hysteresis peak and then peaks at ~ 6 nm and ~ 60 nm, similar to other samples falling into the class of very sandy/silty claystones.

The reliability of the pore-size distribution results was tested by comparing maximum adsorbed amounts of N_2 at highest N_2 pressures, expressed as wt.-% H_2O, with the samples' water contents (Fig. 4.3-20). The sample from the «Murchisonae-Oolith Formation» (798.61 m) and five (sandy/silty) claystone or argillaceous marl samples (741.49 m, 765.33 m, 788.06 m, 947.42 m, 970.89 m) have total adsorbed amounts of N_2 lower than their water content. This may indicate incomplete adsorption of N_2 and thus an underestimation of the frequency of some (probably micro-)pores.

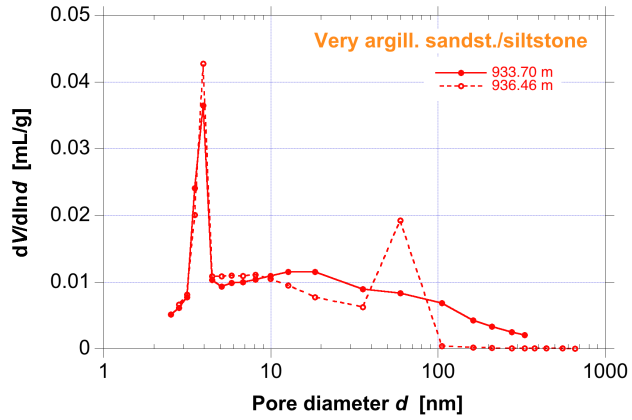

(a)

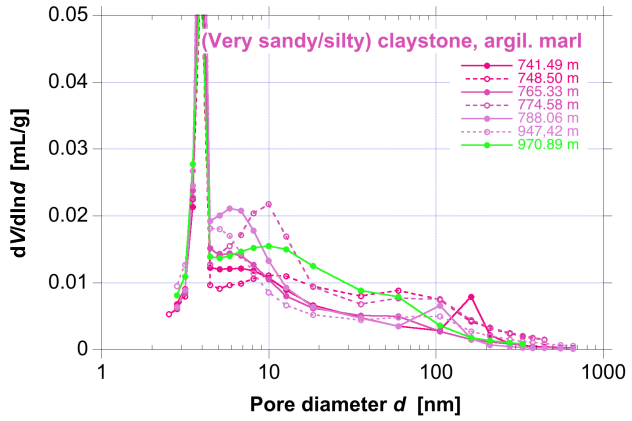

(b)

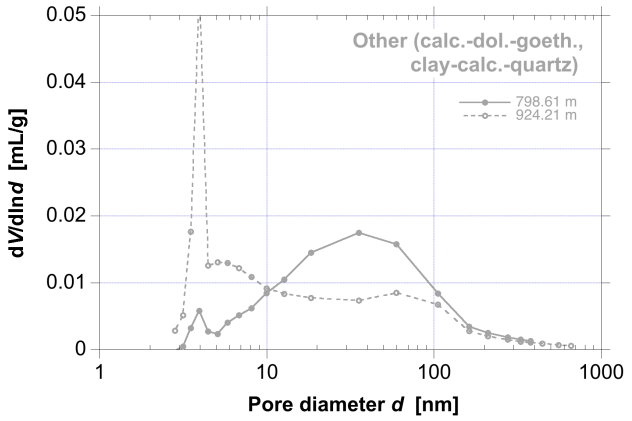

(c)

Fig. 4.3-19: Distribution of (external) pore diameters derived from N_2 desorption

(a) Very argillaceous sandstone/siltstones (933.70 m, 936.46 m), (c) very sandy/silty claystones (741.49 m, 748.50 m, 970.89 m), argillaceous marl (765.33 m) and claystones (774.58 m, 788.06 m, 947.42 m), (c) samples without a Füchtbauer name (789.61 m and 924.21 m).

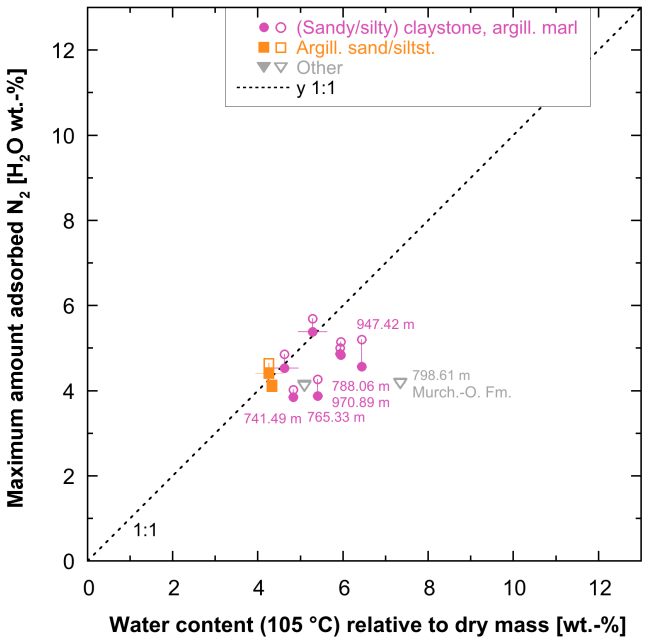

Fig. 4.3-20: Comparison of maximum amount of adsorbed N_2 (recalculated to H_2O wt.-%) with water content per dry sample mass

Open symbols: adsorption, closed symbols: desorption.

Average sizes of external pores based on pore-size distributions calculated from the N_2 isotherms

Average sizes of external pores cannot only be obtained from S_{BET} and the water content as shown above but also from the pore-size distribution derived from N_2 isotherms. In both cases, it is assumed that interlayer pore volumes (which are not probed by N_2 adsorption) are insignificant. Radii directly derived by averaging the BJH pore-size distributions (Fig. 4.3-21) are similar to those estimated from S_{BET} and the gravimetric water content (Fig. 4.3-18) for the sample from the «Murchisonae-Oolith Formation» (798.61 m), and larger by a factor of 1.3 – 2.4 for all other samples. A difference in the order of factor two can be explained by the different geometries assumed in the two cases (radial geometry for the values estimated by averaging the BJH pore-size distributions, planar geometry for the others). The values obtained from the BJH pore-size distributions tend to be small for the (sandy/silty) claystone samples, the argillaceous sandstone/ siltstone sample, and the unclassified clayey sample from the Rietheim Member in the Staffelegg Formation (radii of 2.3 – 4.3 nm and diameter of ~ 5 – 9 nm), while the sample from the «Murchisonae-Oolith Formation» has a comparably large value (radius of ~ 11 nm, diameter of ~ 22 nm). These trends are similar to those observed in the BUL1-1 borehole.

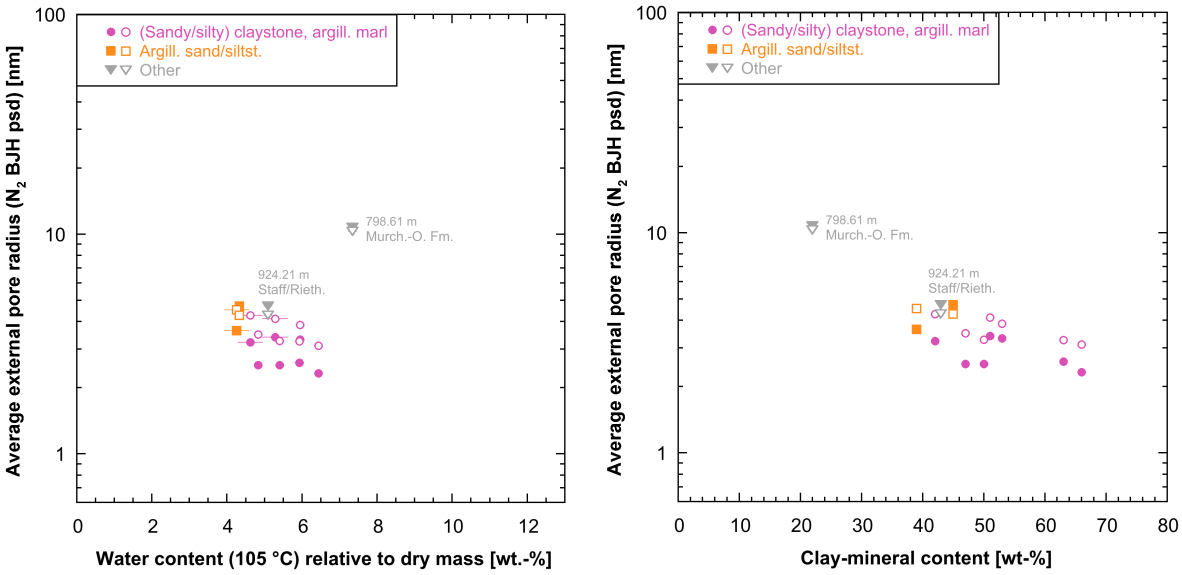

(a) (b)

Fig. 4.3-21: Average external pore radius (assuming insignificant interlayer pore volume) based on the BJH pore-size distribution from the N_2 isotherms (closed symbols: adsorption; open symbols: desorption) plotted against the gravimetric water content per dry mass of the samples (a) and against the total clay-mineral content (b)

Samples are grouped according to rock lithology. Error bars show estimated errors for the water content per dry mass.

4.4 Data from aqueous extraction tests

Carmen Zwahlen

Aqueous extraction (AqEx) tests are a simple but useful method to improve the understanding of the porewater – rock system across a sequence of sedimentary rocks if carried out at regular intervals. In this Section, we present the data from aqueous extraction tests performed at a solid to liquid ratio of approximately 1. The data are discussed further in Chapter 5. The full dataset can be found in Appendix 1, and details about the method are given in Waber (ed.) (2020).

4.4.1 Sample material and overview of analytical work

A total of 93 moisture-preserved drill core samples (PW, AD, SQ) from the Malm to the Zeglingen Formation were subjected to aqueous extraction tests. Additionally, unsqueezed parts of 12 SQ samples were also extracted after drying in order to compare the Cl and Br inventories of wet material ("pre") and dried material ("post").

Additionally, the data of the wet extracted solutions that include analysis of cations were used to model the mineral saturation states and the partial pressure of CO_2. These parameters were calculated with the PHREEQC Version 3.6.2 code (Parkhurst & Appelo 2013) and the PSI/Nagra thermodynamic database (Thoenen et al. 2014) assuming a temperature of 25 °C.

Tab. 4.4-1: Summary of analytical work performed on samples for aqueous extraction tests from the different geological formations (excluding duplicate and post-mortem extracts of AD and SQ experiments; *cf.* Sections 4.7.4 and 4.6.5)

Sample type: PW: porewater sample, AD: advective displacement sample, SQ: squeezing sample, AqEx: aqueous extraction tests, *S/L*: solid to liquid ratio.

Group	**Formation**	**Sample type**	**LAB**	**AqEx at *S/L* 1, pH, Alkalinity, Anions only**	**AqEx at *S/L* 1, pH, Alkalinity, Anions & Cations**
Malm	«Felsenkalke» + «Massenkalk»	PW	RWI		1
Malm	Schwarzbach Fm.	PW	RWI		2
Malm	Villigen Fm.	PW	RWI		5
Malm	Wildegg Fm.	PW	RWI		9
Dogger	«Parkinsoni-Wüttembergica-Sch.»	PW, AD, SQ	RWI	3	11
Dogger	Wedelsandstein Fm.	PW	RWI		1
Dogger	«Murchisonae-Oolith Fm.»	PW	RWI		3
Dogger	Opalinus Clay	PW, AD, SQ	RWI	5	19
Lias	Staffelegg Fm.	PW, AD, SQ	RWI	3	8
Keuper	Klettgau Fm.	PW, SQ	RWI	1	6
Keuper	Bänkerjoch Fm.	PW	RWI		9
Muschelkalk	Schinznach Fm.	PW	RWI		6
Muschelkalk	Zeglingen Fm.	PW	RWI		1
Total		PW, AD, SQ	RWI	12	81

4.4.2 Aqueous extraction tests at a *S/L* of ~ 1

Ion concentrations in aqueous extracts have a limited significance if they are not recalculated to porewater concentrations. For cations possibly involved in reactions (ion exchange/sorption, dissolution/precipitation), this cannot be easily achieved and requires modelling and a set of assumptions. For conservative anions, the recalculation can be based on the measured water content (leading to bulk porewater concentrations) or additionally corrected for anion exclusion (leading to concentrations in the anion-accessible porewater, here called 'free' porewater concentrations). For chemically conservative components, this recalculation is established in Chapter 5. Thus, in this section only ion ratios are presented that are independent of the recalculation formalisms, as well as bulk porewater concentrations for Cl and Br.

4.4.2.1 Anions

The Cl concentrations in the aqueous extracts range from 5 to 860 mg/L or 0.2 to 24 mmol/L reaching a maximum value in the Zeglingen Formation. The Br concentrations vary from 0.08 to 2.8 mg/L or 1×10^{-3} to 3.5×10^{-2} mmol/L with maximum values in the Bänkerjoch Formation (Fig. 4.4-1).

The depth profile of the 1'000*Br/Cl ratio (Fig. 4.4-2) displays values slightly above present-day seawater or at seawater in the Malm. The shift to lower values from the Malm to the «Brauner Dogger» is congruent with a shift in the calcite content. The higher calcite level in the Malm could lead to larger contributions from fluid inclusions which shift the Br/Cl ratio to higher values and

induce more scatter (see report STA2-1 from Zwahlen et al. 2023a). In the «Brauner Dogger» section the Br/Cl ratios are at seawater values except for one SQ sample in the «Parkinsoni-Württembergica-Schichten» that appears to be an outlier with a ratio of 2.0. From the top of the Opalinus Clay section to the bottom of the Klettgau Formation, the Br/Cl ratios decrease to a local minimum close to 1. With increasing depth, the ratios increase in the Bänkerjoch Formation before decreasing in the Schinznach Formation towards a minimum value in the Zeglingen Formation. The low value in the Zeglingen Formation is close to the rock salt measurements from STA2-1 and STA3-1. Two dolomitic samples and one limestone sample in the Schinznach Formation have a higher Br/Cl ratio than expected from the profile shape. Limestone samples of the Schinznach Formation in STA2-1 with a high Br/Cl ratio were explained by a contribution from fluid inclusions, however, this effect was lacking in the dolomitic part of the Schinznach Formation. There is therefore no straightforward explanation for these outliers.

All aqueous extracts from dry material (SQ) have systematically lower ratios compared to extracts on wet material (SQ and others) due to their lower Br concentrations (dry: 0.51 to 1.12 vs. wet: 1.16 to 1.98). In most cases Cl concentrations in extracts from dried material are also lower but less than Br in relative terms. This suggests that Br and to a certain extent Cl are not behaving conservatively after drying and that some Br and to a lower extent Cl are retained during subsequent extraction (e.g. binding to solid organic matter).

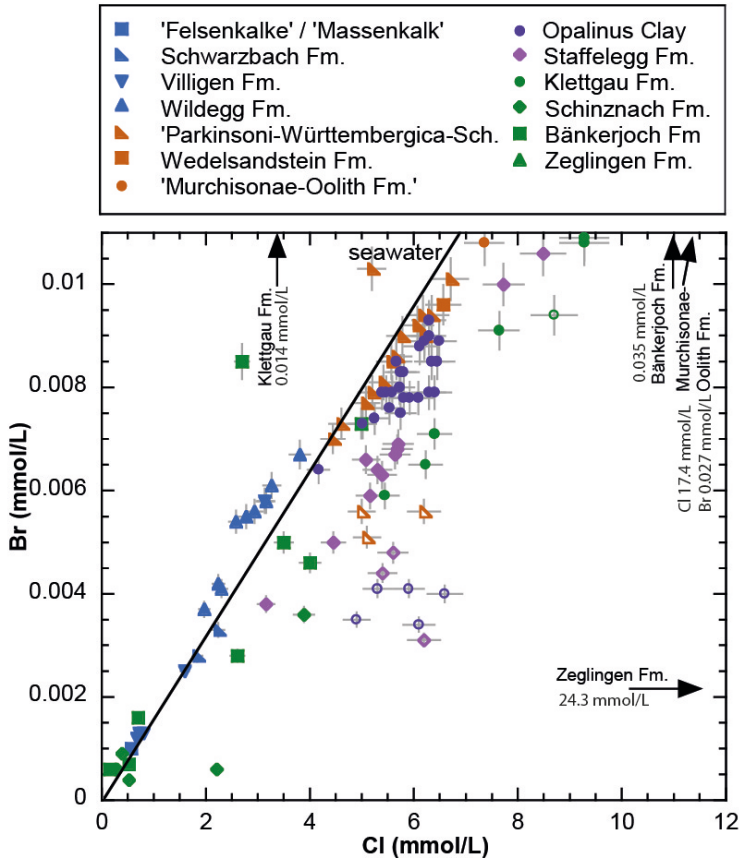

Fig. 4.4-1: Molar Br versus Cl concentrations in aqueous extracts at a *S/L* ratio of about 1

Empty symbols mark aqueous extracts from dry material.

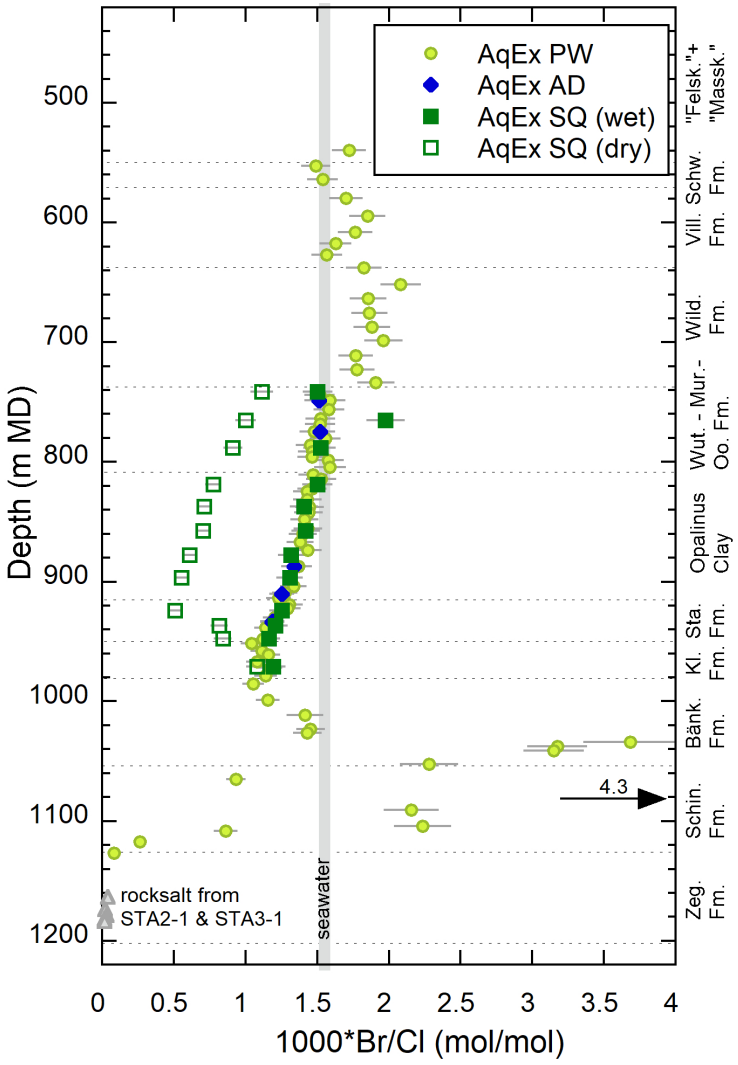

Fig. 4.4-2: Depth profile of the molar Br/Cl ratio in aqueous extracts at a *S/L* ratio of about 1

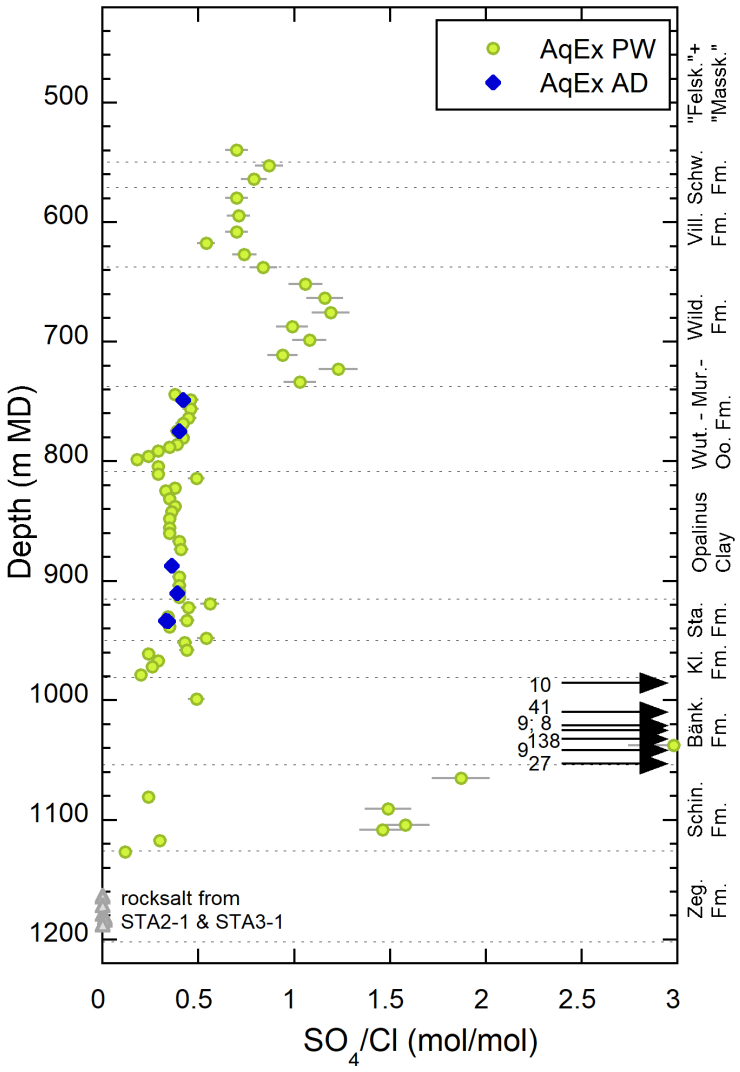

Fig. 4.4-3: Depth profile of SO_4/Cl molar concentration ratio in aqueous extracts at a *S/L* ratio of about 1

The SO_4 concentrations vary between 38 and 345 mg/L with the exception of 9 anhydrite bearing samples in the Bänkerjoch and Schinznach Formations where concentrations of 698 to 3'710 mg/L are reached. The SO_4/Cl ratio in aqueous extract solutions generally does not reflect porewater ratios due to potential dissolution of sulphate-bearing minerals and other processes during the extraction. The ratios are relatively constant in the Malm with a local maximum in the Wildegg Formation. Further below, the SO_4/Cl ratios drop to lower values in the «Brauner Dogger». There is remarkably little scatter in the «Brauner Dogger» to the Klettgau Formation. The aqueous extract samples in the Bänkerjoch Formation show the highest ratios up to a value of 138 related to the dissolution of anhydrite. The ratios decrease in the Schinznach Formation and reach values close to rock salt ratios in the Zeglingen Formation.

The F concentrations in aqueous extracts range between 0.4 and 11 mg/L across the entire depth profile (not shown) with the highest values being in the Schwarzbach and Wildegg Formations. The NO_3 concentrations vary between 0.06 and 1.5 mg/L with the maximum value reached in the Schinznach Formation. The alkalinity varies between 0.4 and 4.6 meq/L. The pH scatters from

the «Felsenkalke» + «Massenkalk» to the Bänkerjoch Formation between 8 and 9.6 with some outliers (Tab. 4.4-2). In the Schinznach and Zeglingen Formations the pH values shift to lower values between 6.5 and 8.0 (Tab. 4.4-2).

4.4.2.2 Cations

The Na concentrations in the aqueous extracts vary between 7 and 1'224 mg/L with maximum values reached in the Bänkerjoch Formation. The Na/Cl ratios of the depth profile show little variability from the Malm to the top of the Bänkerjoch Formation except for a sharp drop in values at the base of the Wildegg Formation (Fig. 4.4-4). The ratios reach a maximum in the middle of the Bänkerjoch Formation before dropping down to ratios around 1 in the Schinznach Formation, which is in agreement with the presence of rock salt in the lower Zeglingen Formation.

The K concentrations range from 1.2 mg/L up to maximum values of 60.3 mg/L in the Bänkerjoch Formation. The Na/K ratios as shown in Fig. 4.4-5 increase steadily from the Malm to the Klettgau Formation with some outliers in the Villigen Formation and the lower part of the «Brauner Dogger». The Na/K ratios reach minimum values in the Schinznach Formation. The lower most sample in the Schinznach Formation and the sample in the Zeglingen Formation displays a higher ratio in agreement with high ratios expected in rocksalt.

The Sr concentrations range from 0.06 to 14.4 mg/L with maximum values reached in the Bänkerjoch Formation. The Sr/Cl ratios have low values in the Malm and Dogger except for a few outliers in the Villigen Formation, «Brauner Dogger» and Opalinus Clay. Much higher values are reached in the Bänkerjoch Formation and the upper part of the Schinznach Formation (Fig. 4.4-6). These high values can be explained by the release of Sr from the dissolution of anhydrite, celestite or carbonates during aqueous extraction. Celestite was not detected by XRD in any of the anhydrite-bearing samples in the Bänkjoch Formation, which could mean (1) that some celestite dissolved (in agreement with the saturation indices of 0, see below), (2) that all Sr is derived from anhydrite or carbonate dissolution, or (3) that the detection limit of XRD is too high to detect small amounts of celestite. Further research is needed to discern the source of the Sr.

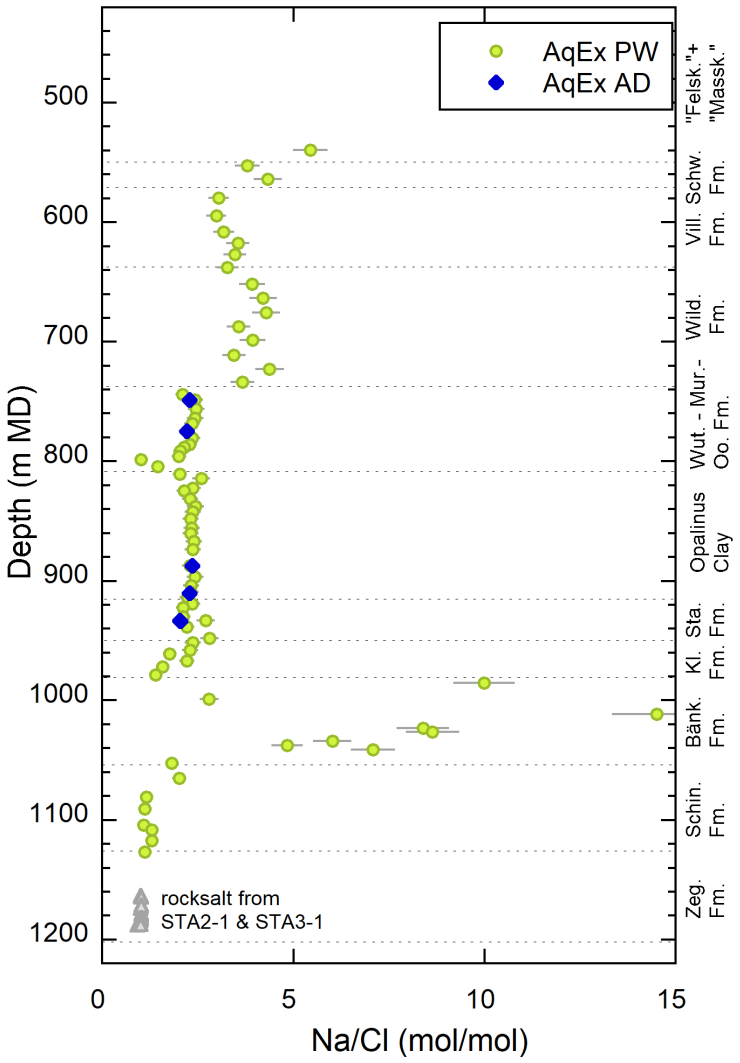

Fig. 4.4-4: Depth profile of the Na/Cl molar concentration ratio in aqueous extracts at a *S/L* ratio of about 1

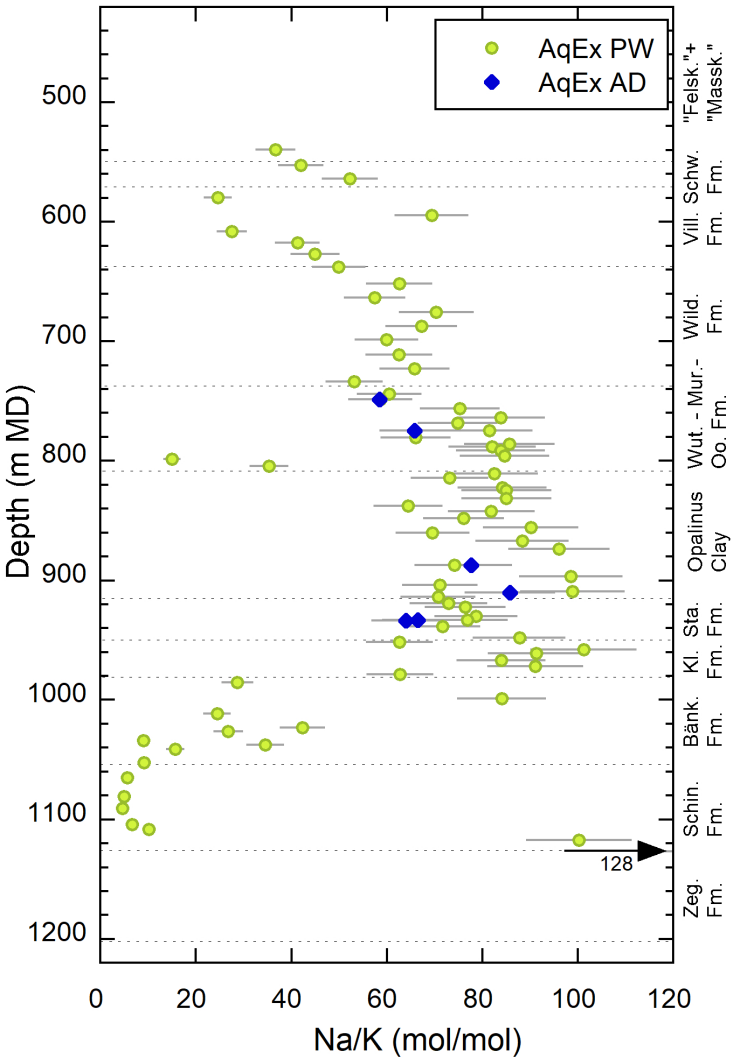

Fig. 4.4-5: Depth profile of the Na/K molar concentration ratio in aqueous extracts at a *S/L* ratio of about 1

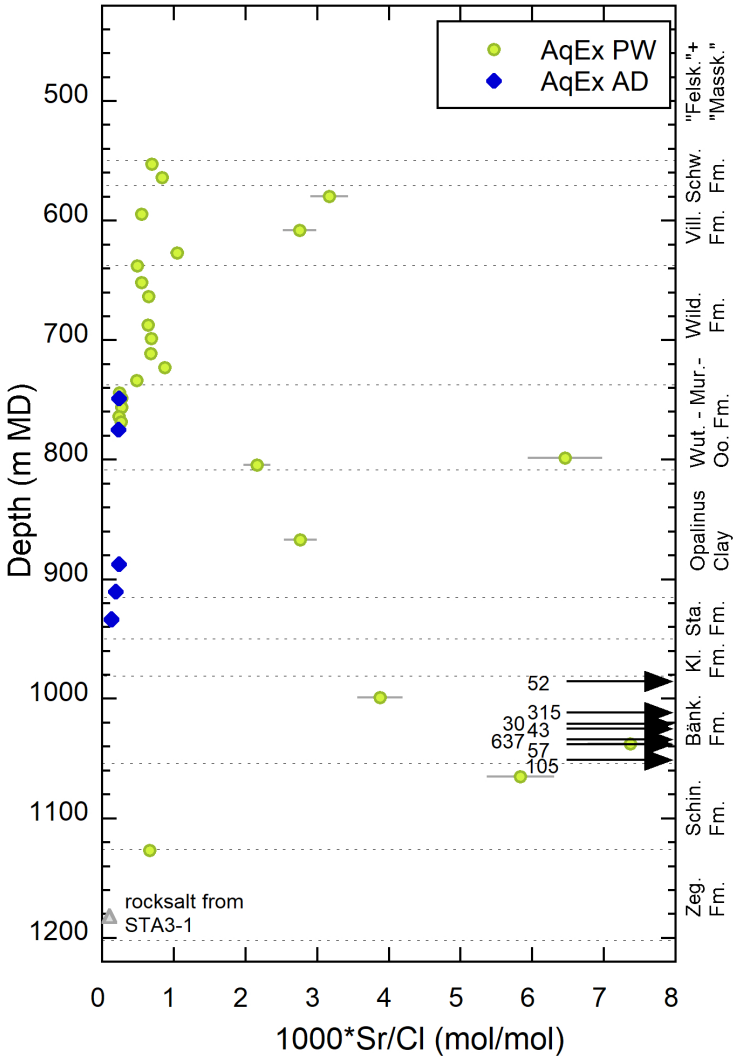

Fig. 4.4-6: Depth profile of the Sr/Cl molar concentration ratio in aqueous extracts at a *S/L* ratio of about 1

4.4.2.3 Saturation indices

The saturation indices of calcite and dolomite of the aqueous extract solutions vary across the different formations (Tab. 4.4-2). From «Felsenkalke» + «Massenkalk» to the top of the Klettgau Formation more than 80% of the solutions are slightly undersaturated with respect to calcite and dolomite despite the presence of calcite in all the samples except for one sample in the Opalinus Clay at 824 m depth. The extraction is conducted under a nitrogen atmosphere and hence the partial pressure CO_2 is much lower than atmospheric pressure. During the subsequent filtration the water is exposed to air and CO_2 may change towards atmospheric pressure which explains the undersaturation with respect to calcite. In a few samples the calculated pCO_2 is substantially above atmospheric pressure which is difficult to explain by a simple process but there might be some uncertainty in the pH measurement.

The samples from the lower part of the Klettgau Formation to Zeglingen Formation are more diverse with half of the samples reaching saturation or oversaturation with respect to calcite (SI -2.0 to 0.9) but only a couple of those are also saturated with respect to dolomite (SI -2.9 to 0.5).

Note that all samples but one from the Schinznach Formation have a low pH of 6.5 to 8.0 and are extremely undersaturated with respect to calcite ($SI_{calcite}$ -2.0 to -0.4) and dolomite ($SI_{dolomite}$ -4.2 to -0.8) despite containing 34 – 96 wt.-% of dolomite (> 92 wt.-% carbonate minerals). This might be related to the extraction time (24 h) that is too short to reach equilibrium with dolomite. The undersaturation with respect to calcite is likely due to the partial equilibration with atmospheric CO_2 as described above. Calcite oversaturation in the anhydrite-bearing samples from the Bänkerjoch and upper Schinznach Formations can be explained by the dissolution of Ca-sulphate producing excess Ca that cannot be precipitated as calcite sufficiently fast.

The sulphate minerals gypsum, anhydrite and celestite are undersaturated by 1 to 3 orders of magnitude in all extract solutions with the exception of 8 samples from the Bänkerjoch Formation. These samples contain 6 to 76 wt.-% anhydrite, remain undersaturated with respect to anhydrite but are saturated or close to saturation with respect to gypsum and celestite, however, no celestite has been detected by XRD (detection limit of 1 wt.-%). Dolomite and celestite saturation indices are missing for some samples because the Mg and Sr concentrations are below the limit of detection, respectively.

Tab. 4.4-2: Saturation indices for calcite, dolomite (disordered and ordered), gypsum, anhydrite and celestite at a *S/L* ~ 1, pH and partial pressure of CO_2 including major input parameters

Mineral saturation indices were calculated with the PHREEQC Version 3 code (Parkhurst & Appelo 2013) and the PSI/Nagra thermodynamic database (Thoenen et al. 2014) assuming a temperature of 25° C. Gr stands for Group, Fm for Formation, F/M for «Felsenkalke» + «Massenkalk», Sw for Schwarzbach Formation, Vi for Villigen Formation, Wi for Wildegg Formation, P-W for «Parkinsoni-Württembergica-Schichten», We for Wedelsandstein Formation, M-C for «Murchisonae-Oolith Formation», Opa for Opalinus Clay, St for Staffelegg Formation, Kl for Klettgau Formation, Bä for Bänkerjoch Formation, Sc for Schinznach Formation, *S/L* for solid/liquid, Cc for Calcite, Do for Dolomite ordered or disordered, Gy for Gypsum, An for Anhydrite and Ce for Celestite, Alk for alkalinity. Empty cells in the SI Do and SI Ce columns are due to concentrations below the limit of detection in Mg or Sr, respectively.

See opposite side.

Tab. 4.4-2: continued

Gr	Fm	depth [m]	SI Cc	SI Do	SI Do	SI Gy	SI An	SI Ce	pH	$\log_{10}$ pCO_2 [bar]	Alk	SO_4 mg/L	Ca mg/L	Mg mg/L	Sr mg/L	Na mg/L	Cl mg/L
Malm	F/M	539.5	0.2	-0.3	0.2	-3.5	-3.8		9.6	-4.7	1.9	38	2	0.4	<0.1	71	20
	Sw	552.9	-0.1	-0.9	-0.4	-2.9	-3.1	-2.4	9.1	-4.0	2.4	187	2	0.6	0.14	196	80
	Sw	564.1	0.1	-0.5	0.1	-3.1	-3.3	-2.5	9.2	4.0	3.2	139	2	0.6	0.13	183	65
	Vi	579.5	-0.3	-1.6	-1.0	-2.9	-3.1	-2.6	8.6	-3.9	0.9	46	6	1.1	0.19	48	24
	Vi	594.5	-0.1	-1.1	-0.5	-2.6	-2.9	-2.3	8.8	-3.8	2.1	213	3	0.9	0.15	215	111
	Vi	608.2	0.1	-0.6	-0.1	-2.9	-3.1	-2.6	9.1	-4.4	1.0	48	5	1.4	0.17	52	25
	Vi	617.5	0.2	-0.5	0.0	-3.3	-3.6		9.5	-4.7	1.5	42	2	0.5	<0.1	66	29
	Vi	627.0	-0.3	-1.4	-0.9	-2.8	-3.0	-2.4	8.6	-3.5	1.9	114	4	0.9	0.15	128	57
	Wi	637.8	-0.3	-1.3	-0.7	-2.6	-2.9	-2.3	8.8	-3.7	2.1	256	3	0.9	0.14	238	112
	Wi	651.7	0.1	-0.5	0.1	-2.6	-2.8	-2.3	9.0	-3.9	2.6	264	4	1.1	0.13	233	92
	Wi	663.7	-0.2	-1.1	-0.6	-2.6	-2.8	-2.3	8.7	-3.6	2.5	250	3	1.0	0.13	217	79
	Wi	675.7	-0.2	-1.1	-0.6	-2.7	-2.9		8.8	-3.7	2.4	225	3	0.8	<0.1	194	70
	Wi	687.3	-0.3	-1.3	-0.8	-2.4	-2.6	-2.1	8.5	-3.3	2.6	311	5	1.4	0.18	268	116
	Wi	698.5	-0.2	-1.1	-0.5	-2.4	-2.7	-2.1	8.6	-3.4	2.7	289	5	1.3	0.17	252	99
	Wi	711.0	-0.4	-1.5	-1.0	-2.3	-2.6	-2.0	8.3	-3.1	2.9	345	5	1.4	0.23	302	135
	Wi	723.1	-0.1	-1.0	-0.4	-2.5	-2.8	-2.1	8.8	-3.6	2.8	271	4	1.0	0.18	231	81
	Wi	733.8	-0.1	-1.0	-0.5	-2.5	-2.8	-2.3	8.8	-3.6	2.7	289	4	0.9	0.13	248	104
'Brauner Dogger'	P-W	744.0	-0.1	-0.9	-0.3	-2.7	-2.9	-2.4	8.8	-3.7	2.7	221	4	1.0	0.13	294	215
	P-W	748.5	0.0	-0.9	-0.4	-2.7	-2.9	-2.5	8.9	-3.8	2.5	210	3	0.7	0.11	273	185
	P-W	748.7	-0.2	-1.2	-0.7	-2.7	-2.9	-2.5	8.7	-3.4	3.0	202	3	0.7	0.11	256	163
	P-W	756.2	0.0	-0.9	-0.3	-2.8	-3.0	-2.5	8.9	-3.6	3.2	195	3	0.7	0.11	252	158
	P-W	763.7	-0.3	-1.4	-0.8	-2.7	-2.9	-2.5	8.5	-3.2	3.6	222	3	0.8	0.1	284	180
	P-W	768.2	-0.1	-1.0	-0.5	-2.6	-2.8	-2.4	8.6	-3.3	3.5	227	4	1.0	0.13	301	198
	P-W	774.6	-0.3	-1.6	-1.0	-2.5	-2.7	-2.4	8.4	-3.1	2.9	235	5	0.9	0.12	315	219
	P-W	774.8	0.2	-0.5	0.1	-2.5	-2.8		8.9	-3.6	3.3	235	5	1.2	<1	324	225
	P-W	780.7	-0.1	-1.1	-0.6	-2.4	-2.7		8.4	-3.2	3.3	235	6	1.4	<1	314	205
	P-W	785.9	-0.2	-1.3	-0.7	-2.6	-2.8		8.5	-3.2	3.5	231	4	1.0	<1	325	220
	P-W	788.3	-0.3	-1.4	-0.8	-2.5	-2.8		8.3	-3.0	3.7	224	5	1.1	<1	331	238
	We	791.3	-0.2			-2.7	-2.9		8.5	-3.2	3.4	186	4	<1	<1	310	233
	M-C	795.9	-0.3	-1.5	-0.9	-2.6	-2.9		8.2	-2.9	3.9	169	5	1.2	<1	341	261
	M-C	798.6	-0.1	-1.2	-0.6	-1.2	-1.4	-0.6	7.2	-2.0	3.0	302	121	20.7	9.83	409	616
	M-C	804.6	0.2	-0.4	0.1	-1.5	-1.7	-1.1	8.0	-2.9	2.4	308	44	11.3	2.13	374	399
Opalinus Clay (Dogger)	OPA	810.9	-0.4	-1.7	-1.1	-2.6	-2.8		8.3	-3.0	3.1	177	5	1.0	<1	294	223
	OPA	814.3	-0.1	-1.1	-0.5	-2.6	-2.8		8.6	-3.4	2.9	195	4	1.1	<1	249	148
	OPA	822.2	-0.2			-2.6	-2.8		8.4	-3.1	3.5	196	4	<1	<1	293	191
	OPA	824.4	-0.3	-1.4	-0.8	-2.6	-2.8		8.4	-3.0	3.6	196	4	1.0	<1	305	220
	OPA	831.4	0.1	-0.5	0.1	-2.7	-2.9		8.8	-3.5	3.9	203	4	1.2	<1	323	217
	OPA	837.6	-0.1	-0.5	0.0	-2.7	-2.9		8.6	-3.2	3.8	183	4	3.0	<1	282	178
	OPA	842.2	-0.3			-2.7	-2.9		8.3	-3.0	3.9	189	4	<1	<1	298	194
	OPA	848.4	-0.2			-2.6	-2.9		8.5	-3.2	3.8	189	4	<1	<1	297	198
	OPA	855.8	-0.2			-2.5	-2.8		8.3	-3.0	3.9	196	5	<1	<1	309	204

Tab. 4.4-2: continued

Gr	Fm	depth [m]	SI Cc	SI Do	SI Do	SI Gy	SI An	SI Ce	pH	$\log_{10}$ pCO_2 [bar]	Alk	SO_4 mg/L	Ca mg/L	Mg mg/L	Sr mg/L	Na mg/L	Cl mg/L
Opalinus Clay (Dogger)	OPA	860.1	-0.3			-2.6	-2.8		8.3	-2.9	4.0	194	4	<1	<1	304	203
	OPA	867.0	-0.3			-2.6	-2.8	-1.4	8.4	-3.1	3.6	210	4	<1	1.3	305	196
	OPA	873.7	-0.4	-1.7	-1.1	-2.5	-2.7		8.2	-2.9	3.6	246	5	1.1	<1	343	223
	OPA	887.2	-0.2	-1.4	-0.9	-2.4	-2.6		8.2	-2.8	4.4	223	6	1.2	<1	343	230
	OPA	887.4	-0.1	-1.3	-0.7	-2.4	-2.6	-2.4	8.2	-2.8	4.6	218	7	1.0	0.1	345	225
	OPA	896.7	-0.2			-2.6	-2.8		8.4	-3.0	4.1	220	4	<1	<1	321	204
	OPA	903.8	-0.2			-2.5	-2.8		8.4	-3.1	3.5	224	5	<1	<1	311	206
	OPA	909.6	-0.3			-2.5	-2.7		8.3	-3.0	3.6	233	5	<1	<1	325	216
	OPA	910.2	-0.3	-1.6	-1.0	-2.5	-2.7	-2.5	8.3	-3.0	3.5	233	5	0.8	0.1	332	223
	OPA	913.6	-0.5			-2.5	-2.7		8.1	-2.8	3.3	245	5	<1	<1	329	227
Lias	St	919.0	-0.2	-1.3	-0.8	-2.3	-2.5		8.6	-3.6	1.9	272	7	1.1	<1	276	180
	St	922.5	-0.4	-1.7	-1.2	-2.1	-2.3		8.1	-3.0	2.4	331	10	1.8	<1	376	274
	St	929.8	-0.1			-2.7	-3.0		8.8	-3.6	2.6	174	3	<1	<1	259	188
	St	933.0	-0.2			-3.1	-3.3		8.8	-3.6	3.0	132	2	<1	<1	197	112
	St	933.3	0.0	-1.1	-0.5	-2.8	-3.0	-2.7	9.0	-3.9	2.4	179	3	0.4	0.1	267	202
	St	933.7	-0.1	-1.2	-0.6	-2.8	-3.0	-2.7	9.0	-4.0	2.2	185	3	0.4	0.1	266	200
	St	938.4	-0.2			-2.8	-3.0		8.7	-3.5	2.9	175	3	<1	<1	263	183
	St	947.9	-0.2			-2.7	-2.9		8.6	-3.3	3.5	232	3	<1	<1	288	158
Trias	Kl	951.6	0.1	-0.3	0.2	-2.6	-2.8		8.9	-3.7	3.3	255	4	1.5	<1	340	221
	Kl	957.8	-0.1	-0.9	-0.4	-2.6	-2.8		8.8	-3.6	2.8	273	4	1.2	<1	338	227
	Kl	960.9	0.4	0.0	0.6	-2.5	-2.7		9.0	-3.8	3.0	211	7	2.0	<1	378	329
	Kl	966.9	0.5	0.5	1.0	-2.8	-3.0		9.3	-4.0	4.0	150	4	1.7	<1	278	193
	Kl	971.8	-1.9	-4.6	-4.0	-2.7	-2.9		7.7	-3.2	0.5	233	3	1.0	<1	338	329
	Kl	978.8	-1.1	-3.1	-2.5	-2.4	-2.6		8.0	-3.4	0.7	249	7	1.6	<1	417	459
	Bä	985.5	0.3	-0.7	-0.2	0.1	-0.2	0.1	8.0	-3.6	0.6	2597	616	43.8	11.9	599	93
	Bä	999.0	0.5	0.3	0.8	-2.8	-3.0	-1.4	9.4	-4.3	3.5	189	4	1.1	1.4	258	142
	Bä	1011.4	0.4	-1.0	-0.5	0.1	-0.1	0.1	8.1	-3.9	0.4	2039	771	17.7	14.4	174	19
	Bä	1023.1	0.7	0.1	0.7	0.1	-0.2	0.2	8.3	-3.6	1.0	3710	555	55.0	13.3	963	177
	Bä	1026.2	0.9	0.3	0.9	0.1	-0.1	0.1	8.3	-3.7	0.9	3007	739	49.5	13.1	695	124
	Bä	1034.0	0.3	-1.8	-1.3	0.1	-0.1	-0.1	7.8	-3.5	0.4	1975	824	6.3	8.3	21	5
	Bä	1037.7	0.4	-0.4	0.1	-0.1	-0.3	-0.1	8.0	-3.2	1.3	3143	403	42.2	7.1	1224	390
	Bä	1041.3	0.7	-0.1	0.5	0.0	-0.2	0.1	8.3	-3.8	0.7	2384	597	40.5	13.5	440	96
	Bä	1052.6	0.5	-0.9	-0.4	0.1	-0.1	-0.3	8.0	-3.5	0.6	1793	843	15.3	6.43	29	25
	Sc	1065.1	0.4	-0.4	0.2	-0.6	-0.8	-0.9	7.5	-2.3	2.9	698	220	24.9	2.0	181	138
	Sc	1080.7	-0.4	-1.3	-0.8	-1.9	-2.2		7.2	-2.0	3.2	76	44	17.5	<1	88	118
	Sc	1091.0	-0.4	-1.4	-0.9	-2.3	-2.6		8.0	-3.4	0.8	42	21	6.9	<1	7	10
	Sc	1104.5	-1.8	-4.2	-3.7	-2.2	-2.4		6.9	-2.4	0.5	60	22	7.0	<1	10	14
	Sc	1108.3	-2.0	-4.8	-4.2	-2.0	-2.3		6.5	-2.0	0.5	73	27	7.0	<1	16	18
	Sc	1117.4	-1.6	-3.9	-3.4	-2.4	-2.6		7.2	-2.7	0.5	64	15	4.1	<1	66	78
	Ze	1126.9	-1.4	-3.5	-2.9	-1.5	-1.7	-1.4	7.0	-2.5	0.6	291	66	17.3	1.4	622	860

4.4.3 Chloride and bromide concentrations in bulk porewater

The formalisms to recalculate Cl and Br concentrations in aqueous extracts to concentrations in bulk porewater are given in Waber (ed.) (2020). In clay-free rocks, this recalculation to bulk water content delivers the transport relevant porewater concentrations of Cl and Br directly. In clay-bearing rocks, the anion-exclusion effect has to be considered in order to arrive at 'free' porewater concentrations. The derivation of the Cl and Br accessible porosity proportion and calculation of 'free' porewater concentrations is established in Chapter 5.

The recalculation of Cl and Br concentrations in aqueous extracts to concentrations in bulk porewater (Figs. 4.4-7 and 4.4-8) requires the knowledge of the water content of the rocks, which is obtained by calculating the average of three gravimetric water contents (one regular sample and two subsamples used for diffusive-exchange experiments). Additional aqueous extraction tests were carried out on 12 dried water content subsamples from the «Brauner Dogger» to the Klettgau Formation in order to compare the concentrations between extracts from dry and wet material.

The depth profiles of Cl and Br concentrations in bulk porewater cover large ranges of 585 to 3'7251 mg/L and 2.1 to 192 mg/L, respectively (Figs. 4.4-7 and 4.4-8). In the Br profile, the 12 aqueous extracts conducted on dried rock material show lower concentrations compared to the extracts from wet material (Fig. 4.4-9). Such differences between extracts from dry and wet material are also seen in the Cl data, even though less strongly (Fig. 4.4-9). These differences may be related to the drying process (e.g., attachment to organic matter), but this issue is not yet resolved. The large organic carbon content of the Rietheim Member sample combined with the pronounced difference in Br and even Cl concentrations illustrates the role of organic matter.

Both, the Cl and Br concentrations, show an increase from the «Felsenkalke» + «Massenkalk» to the Villigen Formation. The profile forms a sharp positive excursion between the trend outlined by the Schwarzbach and Wildegg Formation. There is a general increasing trend in the Cl concentration throughout the Wildegg Formation and «Brauner Dogger» with some scatter in the latter («Murchisonae-Oolith Formation» with iron oxides). The Cl concentrations remain nearly constant throughout the Opalinus Clay. In contrast, the Br concentrations follow a general decreasing trend from the Wildegg Formation to the base of the Opalinus Clay with the same outliers at the base of the «Brauner Dogger» as observed in the Cl profile. In the Staffelegg Formation, both anions show a sharp jump to higher concentrations and a subsequent decrease to values slightly lower than at the base of the Opalinus Clay (Figs. 4.4-7 and 4.4-8).

In the Klettgau Formation, the Br and Cl concentrations increase with some scatter before they decrease again at the top of the Bänkerjoch Formation. The highest values are reached in the lower part of the Bänkerjoch Formation before dropping to much lower values in the Schinznach Formation. At the base of the Schinznach Formation and the Zeglingen Formation, the Cl concentrations form a sharp increase to high concentrations whereas the Br concentrations remain at a low level.

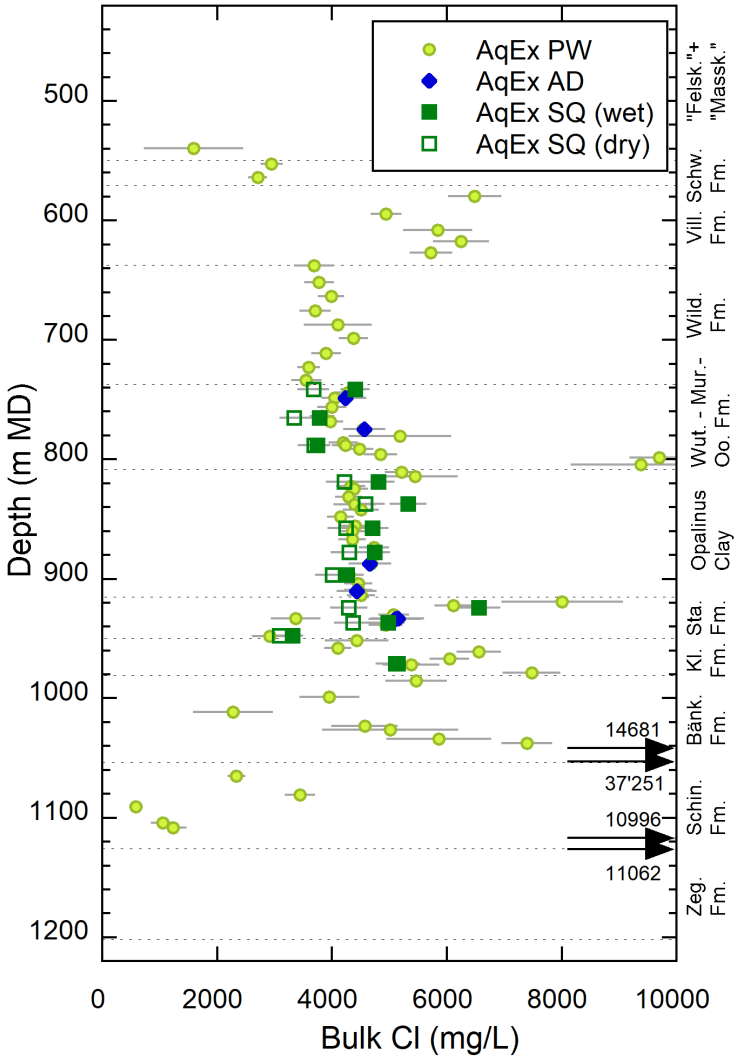

Fig. 4.4-7: Bulk porewater Cl concentrations versus depth from aqueous extracts of PW, AD and SQ samples

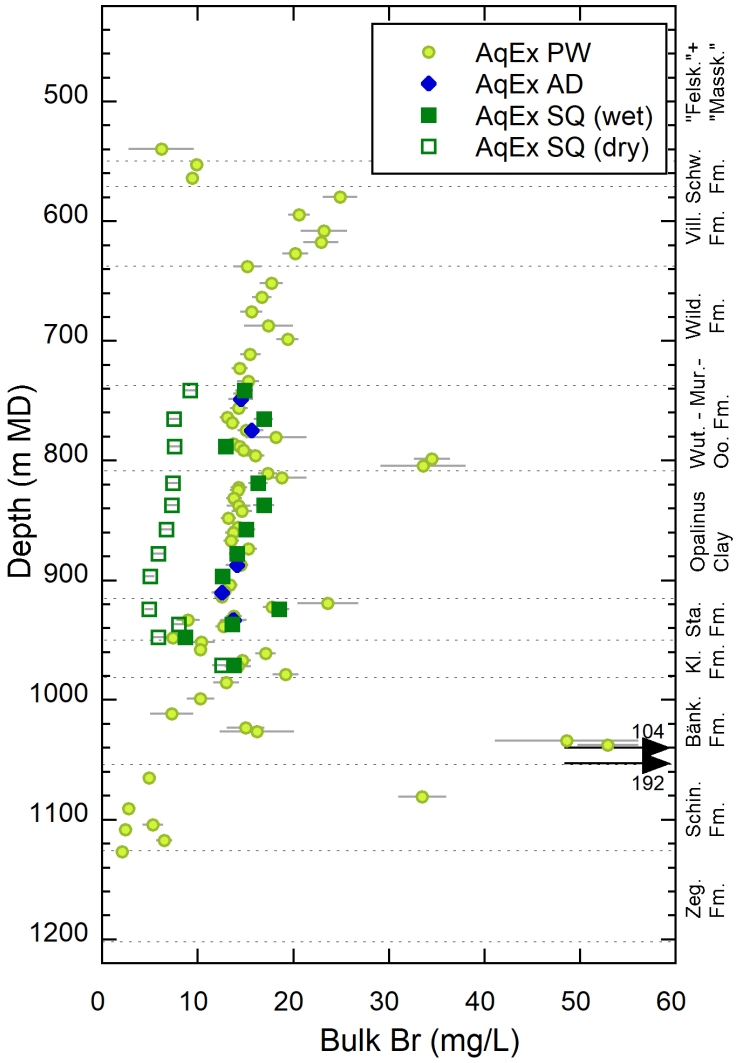

Fig. 4.4-8: Bulk porewater Br concentrations versus depth from aqueous extracts of PW, AD and SQ samples

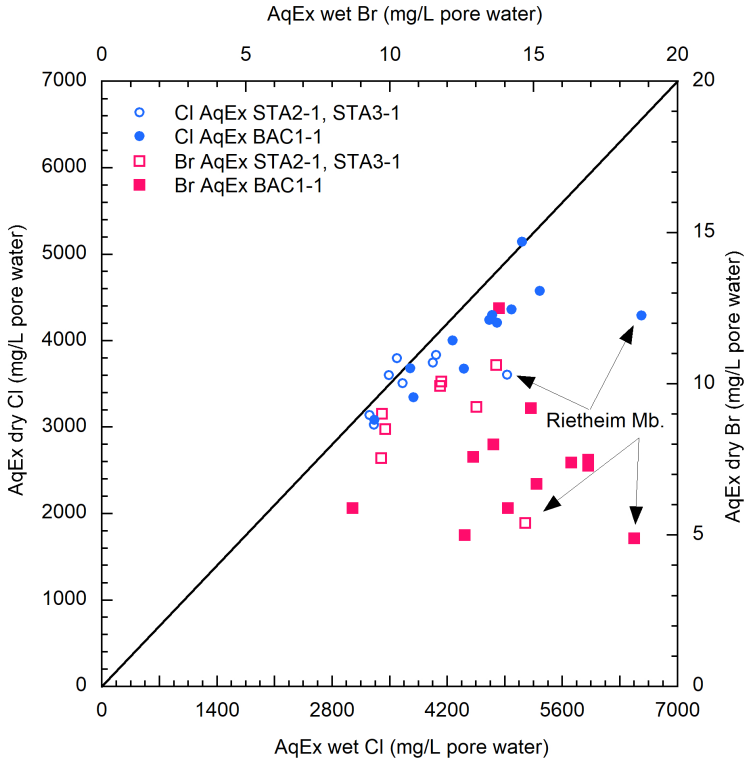

Fig. 4.4-9: Bulk porewater Br and Cl concentrations in aqueous extracts on wet versus dry material of SQ samples from STA2-1, STA3-1 and BAC1-1

Note that the samples from the Rietheim Member (Staffelegg Formation) are exceptionally low in Br and Cl concentrations in the aqueous extract conducted on dry material.

4.5 Cation-exchange extraction data

Paul Wersin

Six samples used for advective displacement experiments (AD) and four porewater (PW) samples were analysed at Uni Bern with the nickel ethylenediamine (Ni-en) extraction method to determine the cation exchange capacity (CEC) and the composition of the clay exchanger (for methodology see Waber ed. 2020). Material from end pieces above and below the AD core was mixed to obtain a representative sample for Ni-en extraction.

The CEC can be derived in two ways: (1) From the consumption of the index cation (Ni in this case) during extraction and (2) from the sum of extracted cations (ΣCAT). Note that the latter includes (i) the exchangeable cations, (ii) cations dissolved in the porewater and (iii) cations released from potentially dissolving minerals (e.g. carbonates, sulphates) during extraction. Thus, in principle, the CEC derived from the sum of cations requires correction from contributions of (ii) and (iii). Corrected CEC and exchangeable cation data are discussed in Section 5.6. The measurements do not include ammonium, NH_4^+, known to be present in small but usually measurable amounts (1 – 1.5 mg/L in aqueous extracts, at $S/L \approx 1$, Appendix B).

Tab. 4.5-1 shows the Ni consumption and extracted cation data (Na, K, Ca, Mg, Sr, Ba) for solid/liquid ratios (*S/L*) around 1[8]. The analyses are reported in meq per kg dry rock. Anion data (F, Cl, Br, SO_4, NO_3) is depicted in Tab. 4.5-2. Note that Ni nitrate was added to the samples, which explains the high NO_3 contents. Three samples from the Bänkerjoch Formation display high levels of SO_4 in the extracts, which is explained by dissolution of anhydrite that is present in these samples.

Tab. 4.5-1: Cation data (in meq/kg_{dry_rock}) from Ni-en extracts at a *S/L* ratio around 1

Fe content in extract: < 0.001 mg/kg.

Type	Depth	Formation	*S/L*	Na	K	Ca	Mg	Sr	Ba	ΣCAT	Ni cons.
	[m]		[g/g]	meq/kg	meq/kg	meq/kg	meq/kg	meq/kg	meq/kg	meq/kg	meq/kg
AD	748.50	«Park-Württ.-Sch.»	0.90	47.5	5.0	27.9	12.3	0.6	0.009	93.3	94.9
AD	774.58	«Park-Württ.-Sch.»	0.88	45.6	4.5	26.3	11.6	0.5	0.003	88.6	107.3
AD	887.40	Opalinus Clay	0.90	53.2	3.9	28.8	10.2	0.4	0.008	97.0	81.0
AD	910.21	Opalinus Clay	0.89	56.3	4.4	33.9	10.7	0.5	0.005	105.7	75.6
AD	933.25	Staffelegg Fm.	0.92	37.5	3.4	20.4	6.3	0.3	0.006	67.9	58.0
AD	933.70	Staffelegg Fm.	0.91	38.1	3.7	21.7	6.7	0.3	0.006	70.6	59.6
PW	999.02	Bänkerjoch Fm.	0.91	41.0	2.2	19.7	8.0	0.2	0.004	71.2	80.8
PW	1'026.21	Bänkerjoch Fm.	0.94	23.3	2.2	90.2	5.9	0.6	< 0.002	122.2	55.1
PW	1'033.99	Bänkerjoch Fm.	0.99	0.8	0.2	82.7	0.5	0.2	< 0.002	84.0	11.0
PW	1'037.67	Bänkerjoch Fm.	0.90	76.5	6.9	70.8	11.0	0.5	0.002	166.0	115.8

Tab. 4.5-2: Anion data (in meq/kg_{dry_rock}) from Ni-en extracts at a *S/L* ratio around 1

Nitrate is part of the added Ni-en stock solution.

Type	Depth	Formation	*S/L*	F	Cl	Br	NO_3	SO_4
	[m]		[g/g]	meq/kg	meq/kg	meq/kg	meq/kg	meq/kg
AD	748.50	«Park-Württ.-Sch.»	0.90	< 0.009	5.2	0.008	225.5	3.0
AD	774.58	«Park-Württ.-Sch.»	0.88	< 0.009	6.3	0.009	229.9	3.4
AD	887.40	Opalinus Clay	0.90	< 0.009	6.7	0.009	231.9	3.3
AD	910.21	Opalinus Clay	0.89	< 0.009	6.5	0.008	235.1	3.5
AD	933.25	Staffelegg Fm.	0.92	< 0.009	5.7	0.007	226.4	2.8
AD	933.70	Staffelegg Fm.	0.91	< 0.009	5.8	0.007	224.6	2.8
PW	999.02	Bänkerjoch Fm.	0.91	< 0.009	4.1	0.005	238.8	3.0
PW	1'026.21	Bänkerjoch Fm.	0.94	< 0.009	2.7	0.004	235.3	81.9
PW	1'033.99	Bänkerjoch Fm.	0.99	< 0.009	0.2	< 0.002	232.1	85.2
PW	1'037.67	Bänkerjoch Fm.	0.90	< 0.009	12.2	0.037	238.2	51.7

[8] A solution mass equal to the mass of the wet rock was added, leading to *S/L* (mass of dry rock / [mass of added solution + porewater]) slightly below 1.

The CEC derived from Ni consumption lies in the range of 11 – 116 meq/kg_{rock} and is lower than the uncorrected sum of cations (71 – 166 meq/kg_{rock}).

The depth profiles of Ni consumption and ΣCAT data (Fig. 4.5-1) show similar values for the «Brauner Dogger» and Opalinus Clay samples (≈ 80 – 100 meq/kg) and slightly lower ones for the two samples from the Staffelegg Formation. Conversely, the four samples from the Bänkerjoch Formation indicate a large spread in both datasets. Note that for three of these four samples the difference between the Ni consumption and ΣCAT data is much larger than for the samples from the overlying sequence, especially regarding the two samples at 1'026.21 and 1'033.99 m depth, both of which contain notable amounts of anhydrite.

The CEC derived from Ni consumption correlates rather well with the clay-mineral content (Fig. 4.5-2 left) whereas no clear correlation between the (uncorrected) sum of cations and the clay-mineral content is seen (Fig. 4.5-2 right). This suggests that extracted cations are affected by side-reactions, such as mineral dissolution, during extraction. This point is further discussed in Section 5.6.

Na is the main extracted cation, followed by Ca, Mg and K in the sampled sequence «Brauner Dogger»- Staffelegg Formation, whereas Ca dominates in the Bänkerjoch Formation (Tab. 4.5-1). Note that at this point the extractable cations have not been corrected for the contribution of dissolved cations and mineral dissolution (see Section 5.6). The molar Ca/Na and Ca+Mg/Na ratios show a constant trend with depth in the sampled Jurassic sequence but increase in the Bänkerjoch Formation where they show a large scatter (Fig. 4.5-3). This again is explained by the presence of anhydrite in this formation.

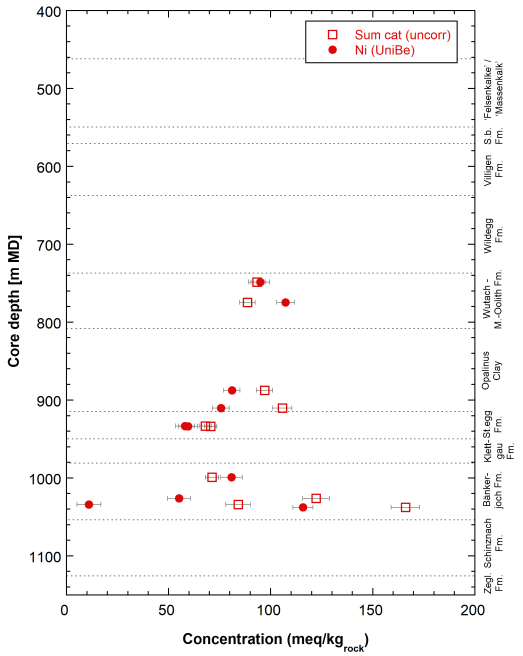

Fig. 4.5-1: Depth profile of Ni consumption and sum of cations (uncorrected, Uni Bern data)

Errors reflect propagated analytical uncertainties.

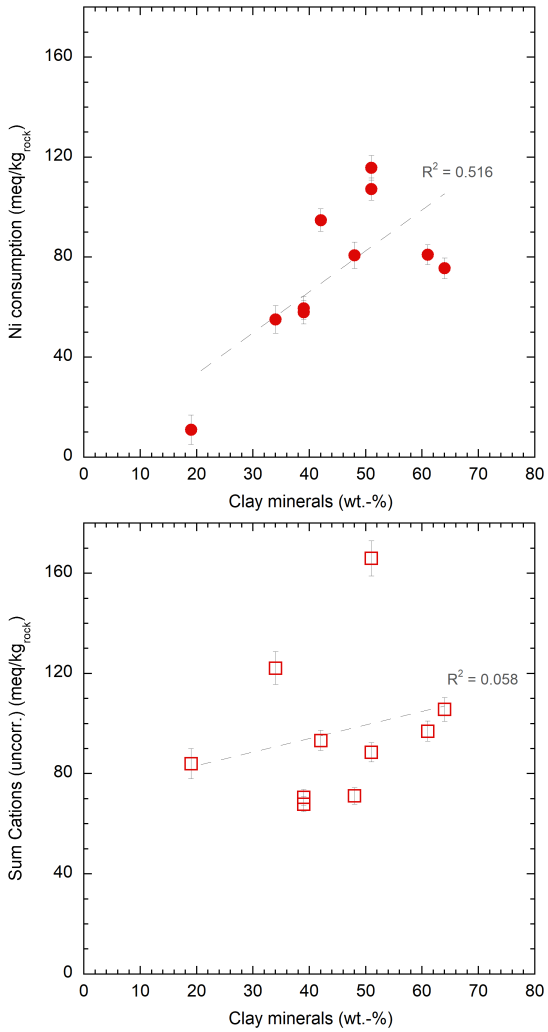

Fig. 4.5-2: Ni consumption (left) and sum cations (uncorrected) (right) vs. clay-mineral content

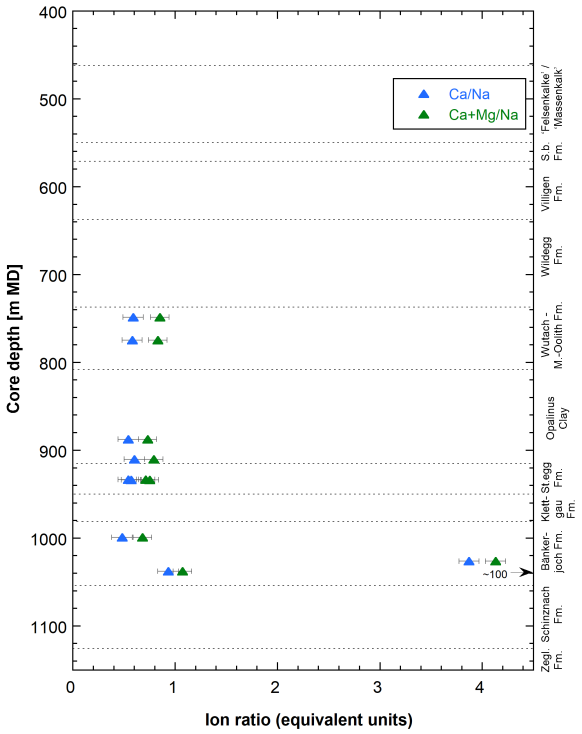

Fig. 4.5-3: Depth profiles of Ca/Na and (Ca+Mg)/Na ratios in Ni-en extracts (Uni Bern data)
Errors reflect propagated analytical uncertainties.

Speciation calculations on the Ni-en extracts were carried out with the PHREEQC Version 3 code (Parkhurst & Appelo 2013) and the PSI/Nagra thermodynamic database (Thoenen et al. 2014) assuming a temperature of 25 °C. The ethylene diamine complexes were taken from the MINTEC database (Allison et al. 1991) and included in the calculations. The concentration of ethylene diamine in the extracts, which was not analysed, was constrained by charge balance. The dissolved carbonate concentration (not measured) was constrained by assuming calcite equilibrium. The calculated TIC values are low, in the range of 0.05 – 0.18 mM (Tab. 4.5-3). The calculated partial pressures of CO_2 (pCO_2) and saturation indices for selected minerals are depicted in Tab. 4.5-3. The Ni-en extracts are clearly undersaturated with regard to the carbonate minerals dolomite and strontianite. They are also undersaturated with regard to the sulphate minerals gypsum and celestite but are either close to saturation or oversaturated with regard to barite. The three lowermost samples (which all contain anhydrite) are close to saturation with regard to anhydrite and celestite and oversaturated or close to saturation with regard to gypsum.

Tab. 4.5-3: Calculated saturation indices of selected minerals, TIC, and log(pCO_2) for Ni-en extract solutions

Calcite saturation was enforced in the calculations.

Type	**Depth** [m]	**Formation**	**Log(pCO_2)** [bar]	**TIC** [mol/kg_w]	**Anhydrite**	**Gypsum**	**Celestite**	**Barite**	**Dolomite (ord)**	**Dolomite (dis)**	**Strontianite**
AD	748.50	«Park.-Württ.-Sch.»	-4.74	1.18E-04	-1.61	-1.39	-1.00	0.45	-0.23	-0.78	-0.88
AD	774.58	«Park.-Württ.-Sch.»	-4.65	1.34E-04	-1.59	-1.37	-1.01	0.11	-0.23	-0.78	-0.90
AD	887.40	Opalinus Clay	-4.49	1.51E-04	-1.56	-1.34	-1.09	0.49	-0.32	-0.87	-1.02
AD	910.21	Opalinus Clay	-4.69	1.14E-04	-1.49	-1.27	-1.06	0.28	-0.37	-0.92	-1.06
AD	933.25	Staffelegg Fm.	-4.45	1.81E-04	-1.73	-1.51	-1.26	0.37	-0.39	-0.94	-1.01
AD	933.70	Staffelegg Fm.	-4.55	1.58E-04	-1.70	-1.49	-1.24	0.37	-0.38	-0.93	-1.02
PW	999.02	Bänkerjoch Fm.	-4.67	1.48E-04	-1.71	-1.50	-1.36	0.10	-0.26	-0.81	-1.13
PW	1'026.21	Bänkerjoch Fm.	-5.27	4.64E-05	0.17	0.38	0.26	0.86	-1.08	-1.63	-1.39
PW	1'033.99	Bänkerjoch Fm.	-5.12	5.46E-05	0.20	0.42	-0.07	0.89	-2.11	-2.66	-1.75
PW	1'037.67	Bänkerjoch Fm.	-5.19	5.50E-05	-0.14	0.08	-0.04	0.73	-0.69	-1.24	-1.39

4.6 Data from squeezing experiments

Martin Mazurek

A set of 12 samples from the interval «Parkinsoni-Württembergica-Schichten» – Klettgau Formation were subjected to porewater squeezing. Photographs of the core samples are shown in Fig. 4.6-1. The mineralogical composition of the samples is listed in Tab. 4.6-1. Clay-mineral contents are ≥ 43 wt.-% for all samples.

Tab. 4.6-1: Mineralogical composition of samples subjected to squeezing experiments

"b.d." = below detection.

Depth [m]	**Formation**	**Member**	**S** [wt.-%]	**C(inorg)** [wt.-%]	**C(org)** [wt.-%]	**Quartz** [wt.-%]	**K-feldspar** [wt.-%]	**Plagioclase** [wt.-%]	**Calcite** [wt.-%]	**Dolomite / Ank.** [wt.-%]	**Siderite** [wt.-%]	**Pyrite** [wt.-%]	**Clay minerals** [wt.-%]
741.49	«Parkinsoni-Württembergica-Sch.»		0.40	2.89	0.46	24	2	2	20	4	b.d.	0.7	47
765.33	«Parkinsoni-Württembergica-Sch.»		1.42	3.02	0.64	18	2	2	23	2	b.d.	2.7	50
788.06	«Parkinsoni-Württembergica-Sch.»		0.40	2.09	0.88	14	2	2	17	b.d.	b.d.	0.7	63
818.92	Opalinus Clay	'Sub-unit with silty calcareous beds'	0.99	1.78	1.00	23	2	2	14	b.d.	1	1.8	56
837.16	Opalinus Clay	'Upper silty sub-unit'	< 0.05	1.55	0.92	26	2	2	11	b.d.	2	< 0.1	56
857.72	Opalinus Clay	'Upper silty sub-unit'	< 0.05	1.11	0.83	22	2	3	7	b.d.	3	< 0.1	63
877.64	Opalinus Clay	'Mixed clay-silt-carbonate sub-unit'	< 0.05	0.92	1.00	20	2	2	6	b.d.	1	< 0.1	67
896.50	Opalinus Clay	'Clay-rich sub-unit'	< 0.05	1.24	1.02	15	2	3	8	b.d.	3	< 0.1	68
924.21	Staffelegg Fm.	Rietheim Mb.	3.29	3.41	8.60	11	1	2	25	3	b.d.	6.2	43
936.46	Staffelegg Fm.	Frick Mb.	< 0.05	1.15	0.64	40	2	2	10	b.d.	b.d.	< 0.1	45
947.42	Staffelegg Fm.	Schambelen Mb.	< 0.05	1.65	0.39	17	2	2	14	b.d.	b.d.	< 0.1	66
970.89	Klettgau Fm.	Ergolz Mb.	< 0.05	0.44	0.07	26	6	8	2	1	b.d.	< 0.1	53

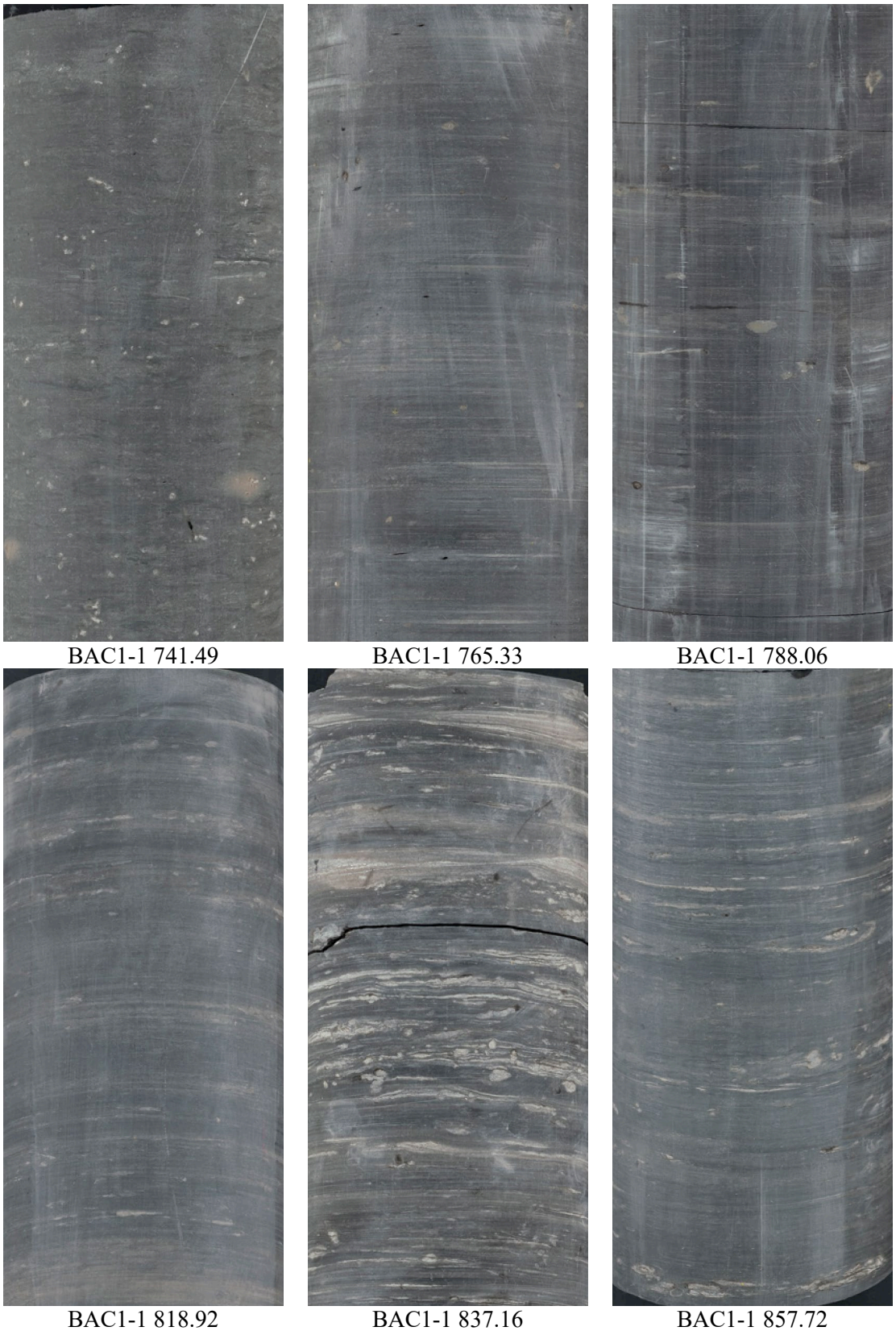

Fig. 4.6-1: Photographs of core samples subjected to squeezing
Width of photographs = 9.5 cm.

BAC1-1 877.64

BAC1-1 896.50

BAC1-1 924.21

BAC1-1 936.46

BAC1-1 947.42

BAC1-1 970.89

Fig. 4.6-1: continued

4.6.1 Mass recovery

The water masses obtained by squeezing are listed in Tab. 4.6-2 and shown graphically in Fig. 4.6-2 as a function of the squeezing pressure. Only a moderate correlation between the initial water content of the sample and the total mass recovery can be identified (Fig. 4.6-3). The majority of the samples yielded first water aliquots at 200 MPa, some at 300 MPa.

Tab. 4.6-2: Water masses squeezed at different pressure steps

The initial water content was reconstructed on the basis of the measured water content of the squeezed sample and the squeezed water mass (see Section 4.6.5), and this value was then used to calculate the initial mass of porewater in the sample. "-": pressure step not applied.

					Mass squeezed at P =					
Depth [m]	**Formation**	**Initial sample mass (CRIEPI)** [g]	**Initial water content (wet)** [wt.-%]	**Mass of porewater prior to squeezing** [g]	**100 MPa** [g]	**200 MPa** [g]	**300 MPa** [g]	**400 MPa** [g]	**500 MPa** [g]	**Total mass squeezed** [g]
741.49	«Parkinsoni-Württembergica-Sch.»	429.41	3.88	16.64	0	0	0.69	0.44	-	1.13
765.33	«Parkinsoni-Württembergica-Sch.»	408.11	4.50	18.38	0	1.04	1.73	0.87	-	3.64
788.06	«Parkinsoni-Württembergica-Sch.»	413.35	5.18	21.43	0	1.35	1.30	0.90	-	3.55
818.92	Opalinus Clay	403.96	4.36	17.62	0	0.71	1.25	1.35	-	3.31
837.16	Opalinus Clay	396.88	4.17	16.54	0	0.78	1.33	1.18	-	3.29
857.72	Opalinus Clay	337.10	4.64	15.65	0	1.55	1.35	-	-	2.90
877.64	Opalinus Clay	355.54	4.91	17.45	0	2.18	1.32	-	-	3.50
896.50	Opalinus Clay	373.46	4.72	17.62	0	1.51	1.30	1.01	-	3.82
924.21	Staffelegg Fm.	336.50	3.88	13.06	0	0.60	1.41	1.45	-	3.46
936.46	Staffelegg Fm.	342.24	3.75	12.83	0	0	0.27	0.84	0.74	1.85
947.42	Staffelegg Fm.	338.04	5.30	17.92	0	1.59	1.68	-	-	3.27
970.89	Klettgau Fm.	372.62	4.61	17.16	0	0	0.95	0.95	-	1.90

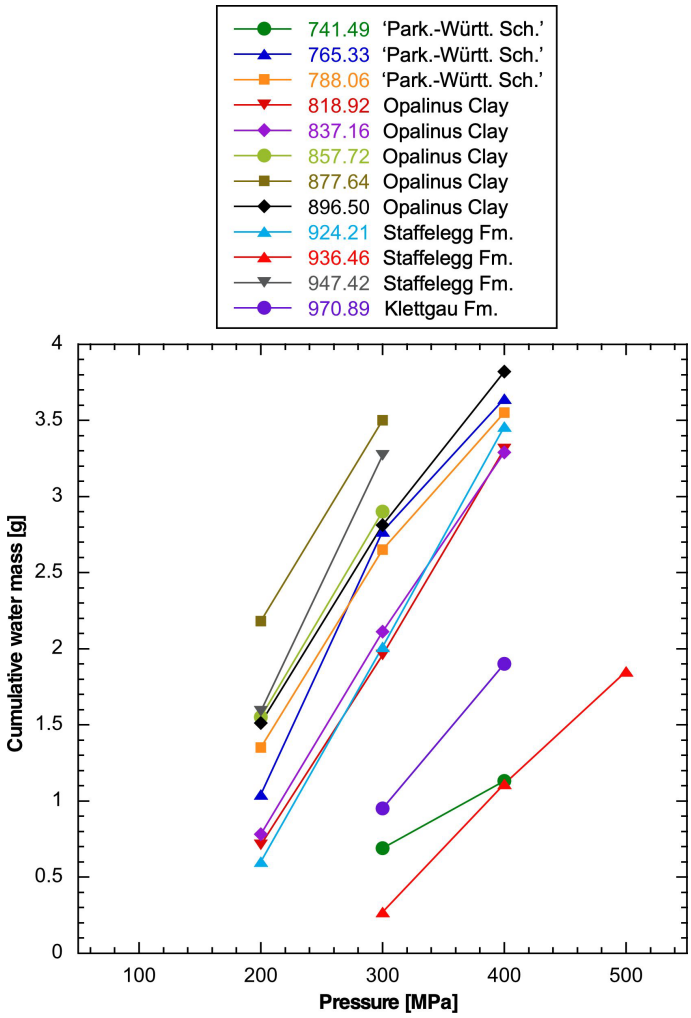

Fig. 4.6-2: Cumulative water masses obtained by squeezing as a function of the squeezing pressure

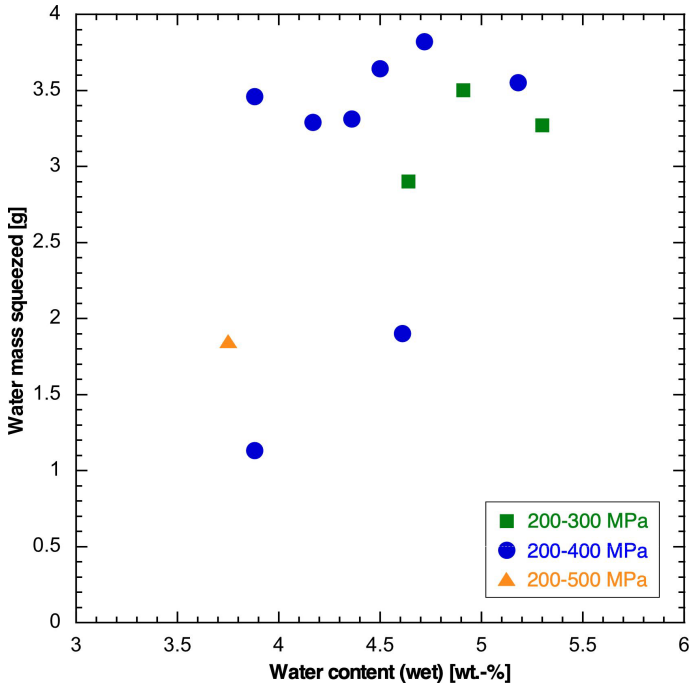

Fig. 4.6-3: Correlation of the original water content and the cumulative water mass obtained by squeeezing

4.6.2 Chemical composition of squeezed waters

With one exception, the first squeezed aliquots yielded ≥ 0.6 g water, from which a complete dataset (major-ion composition, TIC/TOC, pH, water isotopes) could be obtained. The chemical compositions of squeezed waters are listed in Tab. 4.6-3 and are shown graphically as a function of squeezing pressure in Fig. 4.6-4. Na is by far the most abundant cation, and Cl dominates the anions, followed by SO_4.

The concentrations of the monovalent ions Na, K, Cl and Br decrease with squeezing pressure, likely due to ion-filtration effects that become important at higher pressures (Mazurek et al. 2015). Ca and Mg evolve slightly towards higher concentrations. As discussed in Mazurek et al. (2015) and Rufer & Mazurek (2018), the composition of the first water aliquot recovered from a sample is considered to be closest to that of the porewater, and these analyses are highlighted by bold print in Tab. 4.6-3. F concentrations, in particular in the first squeezed aliquots, are contaminated by F leached from the fiberglass filters and so are not representative of the porewater. For clarity, the subset of the data that is considered useful for further interpretation is summarised in Tab. 4.6-4.

For sample 947.42, the squeezing process was initially disturbed, as the pressure was initially unstable and reached 300 MPa for 2 h before coming down to 200 MPa, at which pressure the first water aliquot was taken. The resulting consolidation behaviour, recorded by the piston movement, was anomalous and differed from that of the other samples. Even though the details of the pertinent processes are not well known at this stage, this anomaly affected the chemical and isotopic data of the squeezed waters, yielding results that are at odds with those obtained from nearby samples. Therefore, all results for this sample are considered uncertain and are highlighted as such below in tables and graphics.

Tab. 4.6-3: Chemical composition of squeezed waters: full dataset

Bold print indicates the selected ("best") aliquots. F concentrations, in particular in the first squeezed aliquots, are contaminated by F leached from the fiberglass filters and so are not representative of the porewater. Data for sample 947.42 are uncertain and shown in italics.

Depth [m]	**Pressure** [MPa]	**Squeezing time** [d]	**Mass squeezed** [g]	**Na** [mg/L]	**NH_4** [mg/L]	**K** [mg/L]	**Ca** [mg/L]	**Mg** [mg/L]	**Sr** [mg/L]	**F** [mg/L]	**Cl** [mg/L]	**Br** [mg/L]	**NO_3** [mg/L]	**SO_4** [mg/L]	**pH**	**TIC** [mg/L]	**TOC** [mg/L]	**TDS** [mg/L]	**Charge balance** [%]
741.49	**300**	**3**	**0.69**	**4'750**	**< 10**	**91.3**	**934**	**202**	**20.0**	**9.6**	**7'513**	**25.1**	**8.47**	**2'290**	**7.97**	**18.0**	**167.0**	**16'102**	**2.0**
	400	2	0.44	4'072	< 10	53.8	1'006	220	18.7	5.7	6'780	22.1	5.00	2'523				14'708	0.6
765.33	**200**	**3**	**1.04**	**5'122**	**< 10**	**96.2**	**875**	**221**	**19.2**	**10.6**	**8'059**	**26.8**	**8.81**	**2'108**	**8.69**	**16.5**	**169.3**	**16'801**	**2.5**
	300	3	1.73	4'347	< 10	50.8	875	223	22.5	5.3	6'850	23.0	3.44	2'122	8.81	12.8	103.9	14'691	2.8
	400	2	0.87	3'544	< 10	28.5	867	222	19.0	4.2	5'958	19.4	3.68	2'022	8.76	11.0	90.4	12'836	1.2
788.06	**200**	**3**	**1.35**	**5'088**	**< 10**	**82.5**	**883**	**264**	**19.0**	**7.3**	**8'016**	**27.4**	**6.03**	**2'118**	**8.44**	**17.7**	**103.8**	**16'707**	**3.1**
	300	3	1.30	4'050	< 10	42.9	868	252	17.8	4.9	6'576	22.1	5.74	2'073	8.49	16.2	84.7	14'080	2.4
	400	2	0.90	3'526	< 10	29.1	896	266	20.9	4.0	5'883	19.2	4.87	2'072	8.44	16.9	81.0	12'885	2.3
818.92	**200**	**3**	**0.71**	**5'503**	**< 10**	**96.0**	**849**	**267**	**13.6**	**13.4**	**8'647**	**28.4**	**9.59**	**2'244**	**8.53**	**20.9**	**157.4**	**17'934**	**2.1**
	300	3	1.25	4'886	< 10	70.4	903	270	15.2	7.0	7'757	25.4	5.93	2'215	8.51	18.5	125.1	16'374	2.7
	400	2	1.35	4'081	< 10	46.5	901	271	15.4	4.9	6'515	21.8	4.36	2'134	8.50	18.9	107.9	14'199	3.4
837.16	**200**	**3**	**0.78**	**5'233**	**< 10**	**103.4**	**870**	**158**	**17.5**	**10.7**	**8'123**	**26.3**	**7.52**	**1'966**	**8.99**	**10.8**	**151.3**	**16'723**	**2.7**
	300	3	1.33	4'643	< 10	61.2	937	211	16.7	5.5	7'484	24.6	4.35	2'060	8.76	10.0	122.9	15'621	2.4
	400	2	1.18	3'792	< 10	38.6	984	230	15.6	4.2	6'565	21.0	3.87	1'980	8.77	13.5	97.0	13'799	1.3
857.72	**200**	**3**	**1.55**	**4'659**	**< 10**	**73.2**	**969**	**202**	**20.1**	**7.5**	**7'619**	**24.2**	**7.12**	**1'939**	**8.77**	**10.1**	**145.4**	**15'720**	**2.5**
	300	2	1.35	3'711	< 10	37.9	1'001	227	19.8	4.2	6'354	19.8	3.17	1'914	8.83	15.5	102.9	13'474	2.3
877.64	**200**	**3**	**2.18**	**4'673**	**< 10**	**67.0**	**971**	**227**	**19.9**	**7.7**	**7'362**	**22.3**	**6.38**	**2'072**	**8.67**	**13.1**	**131.7**	**15'626**	**3.8**
	300	2	1.32	3'384	< 10	34.7	1'054	253	19.6	4.1	5'961	18.2	2.67	2'006	8.75	8.6	99.8	12'882	2.5
896.50	**200**	**3**	**1.51**	**4'732**	**< 10**	**71.9**	**1'057**	**233**	**17.8**	**6.3**	**7'599**	**21.9**	**6.81**	**2'329**	**8.60**	**13.5**	**139.4**	**16'284**	**2.8**
	300	3	1.30	3'680	< 10	45.0	1'103	238	16.3	6.3	6'320	18.0	4.40	2'203	8.61	15.4	108.6	13'822	2.2
	400	2	1.01	3'137	< 10	32.3	1'197	264	16.3	4.8	5'548	16.3	2.57	2'111	8.50	15.5	97.5	12'503	4.0
924.21	**200**	**3**	**0.60**	**6'403**	**< 10**	**131.4**	**925**	**257**	**15.3**	**10.2**	**9'417**	**26.4**	**8.67**	**3'303**	**8.36**	**21.6**	**152.3**	**20'762**	**1.8**
	300	3	1.41	5'655	< 10	83.8	1'060	282	21.8	5.3	8'617	24.8	2.55	3'163	8.52	19.1	113.5	19'128	2.2
	400	2	1.45	5'061	< 10	63.2	1'138	300	16.8	4.8	8'407	22.5	2.26	3'123	8.39	20.6	103.5	18'347	-0.1
936.46	**300**	**4**	**0.27**	**6'004**	**< 10**	**96.0**	**938**	**145**	**11.4**	**14.0**	**8'844**	**23.4**	**16.41**	**2'408**	**8.52**			**18'502**	**3.5**
	400	3	0.84	5'781	< 10	83.8	922	133	13.0	8.9	8'599	22.5	9.94	2'807	8.61	13.7	91.6	18'545	1.3
	500	3	0.74	5'492	< 10	71.2	923	153	13.4	6.3	8'179	22.0	4.83	2'816	8.57	15.3	80.1	17'840	1.4
947.42	**200**	**3**	**1.59**	***4'168***	***< 10***	***74.5***	***630***	***85***	***11.5***	***10.6***	***5'721***	***13.8***	***15.43***	***2'088***	***8.96***	***12.2***	***73.8***	***12'956***	***3.5***
	300	4	1.68	*3'176*	*< 10*	*36.4*	*813*	*110*	*13.4*	*4.6*	*4'830*	*11.8*	*4.16*	*2'090*	*8.72*	*12.2*	*43.9*	*11'196*	*2.1*
970.89	**300**	**3**	**0.95**	**6'093**	**< 10**	**115.7**	**950**	**143**	**15.9**	**10.3**	**9'069**	**23.0**	**8.38**	**3'043**	**8.74**	**15.9**	**109.0**	**19'666**	**1.0**
	400	2	0.95	5'895	< 10	96.9	916	146	16.9	6.6	8'665	22.8	5.42	2'854	8.69	17.8	87.4	18'806	1.8

Tab. 4.6-4: Chemical composition of squeezed waters: summary of selected analyses to be used for interpretation

Data for sample 947.42 are uncertain and shown in italics.

Depth [m]	**Formation**	**Pressure** [MPa]	**Squeezing time** [d]	**Mass squeezed** [g]	**Na** [mg/L]	**K** [mg/L]	**Ca** [mg/L]	**Mg** [mg/L]	**Sr** [mg/L]	**Cl** [mg/L]	**Br** [mg/L]	**NO_3** [mg/L]	**SO_4** [mg/L]	**pH**	**TIC** [mg/L]	**TOC** [mg/L]
741.49	«Park.-W.-Sch.»	300	3	0.69	4'750	91.3	934	202	20.0	7'513	25.1	8.47	2'290	7.97	18.0	167.0
765.33	«Park.-W.-Sch.»	200	3	1.04	5'122	96.2	875	221	19.2	8'059	26.8	8.81	2'108	8.69	16.5	169.3
788.06	«Park.-W.-Sch.»	200	3	1.35	5'088	82.5	883	264	19.0	8'016	27.4	6.03	2'118	8.44	17.7	103.8
818.92	Opalinus Clay	200	3	0.71	5'503	96.0	849	267	13.6	8'647	28.4	9.59	2'244	8.53	20.9	157.4
837.16	Opalinus Clay	200	3	0.78	5'233	103.4	870	158	17.5	8'123	26.3	7.52	1'966	8.99	10.8	151.3
857.72	Opalinus Clay	200	3	1.55	4'659	73.2	969	202	20.1	7'619	24.2	7.12	1'939	8.77	10.1	145.4
877.64	Opalinus Clay	200	3	2.18	4'673	67.0	971	227	19.9	7'362	22.3	6.38	2'072	8.67	13.1	131.7
896.50	Opalinus Clay	200	3	1.51	4'732	71.9	1'057	233	17.8	7'599	21.9	6.81	2'329	8.60	13.5	139.4
924.21	Staffelegg Fm.	200	3	0.60	6'403	131.4	925	257	15.3	9'417	26.4	8.67	3'303	8.36	21.6	152.3
936.46	Staffelegg Fm.	300	4	0.27	6'004	96.0	938	145	11.4	8'844	23.4	16.41	2'408	8.52		
947.42	Staffelegg Fm.	200	3	1.59	*4'168*	*74.5*	*630*	*85*	*11.5*	*5'721*	*13.8*	*15.43*	*2'088*	*8.96*	*12.2*	*73.8*
970.89	Klettgau Fm.	300	3	0.95	6'093	115.7	950	143	15.9	9'069	23.0	8.38	3'043	8.74	15.9	109.0

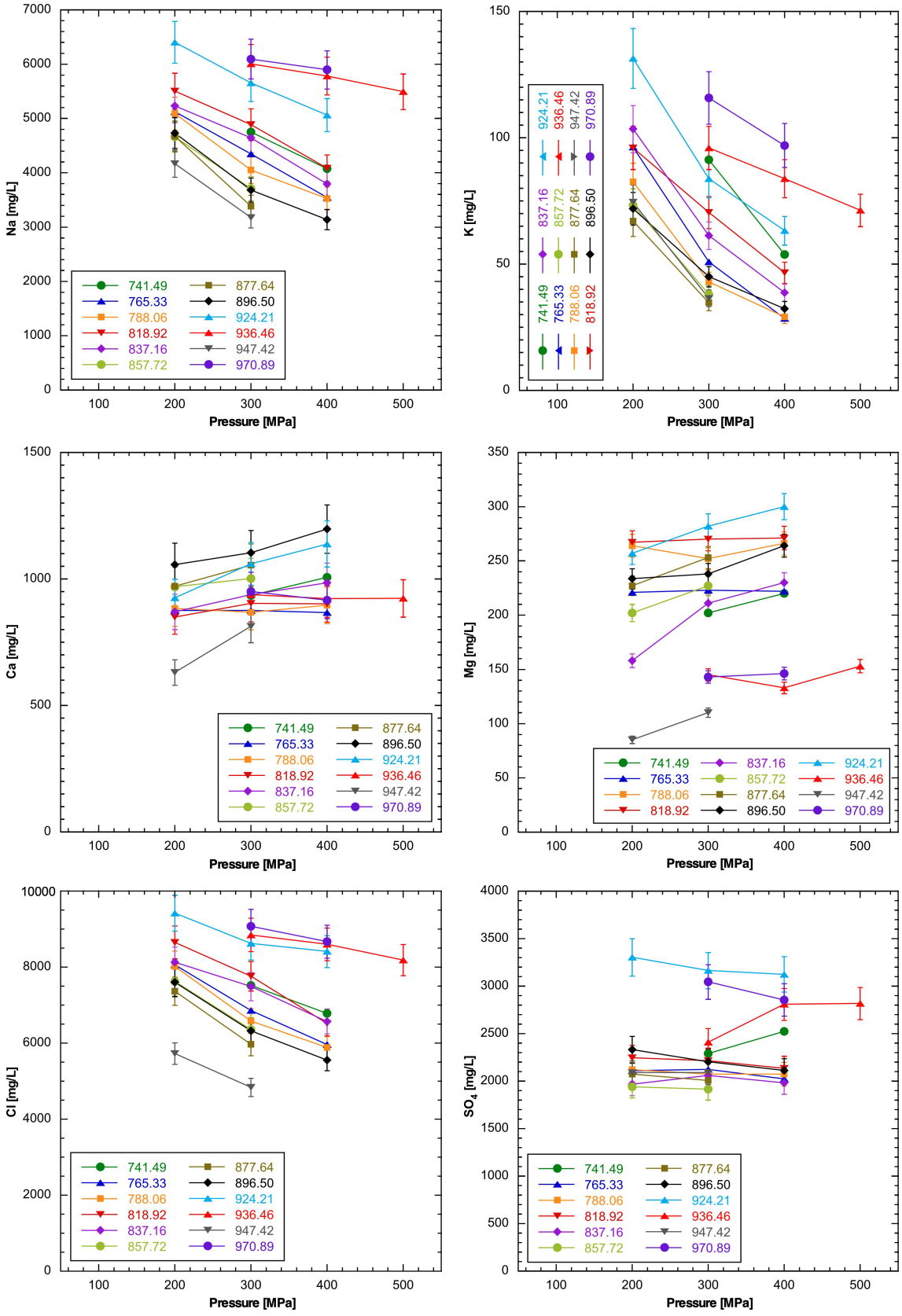

Fig. 4.6-4: Ion concentrations in squeezed waters as a function of squeezing pressure

Bars indicate analytical errors of ion-chromatography analysis.

4.6.3 Depth trends

Profiles with depth for various pore-water constituents are shown in Fig. 4.6-5. The following observations can be made:

- Na and Cl show distinct relative maxima near the top of the Opalinus Clay. This feature has not been observed in any of the other boreholes. The concentrations decrease markedly with depth within the Opalinus Clay.
- SO_4 contents are constant in the upper part of the profile but tend to increase in the lower Opalinus Clay.
- In comparison to the Opalinus Clay, Na, Cl and SO_4 concentrations are higher in the Staffelegg and Klettgau Formations.
- The Br/Cl ratio is only slightly below the marine value in the Dogger above the Opalinus Clay. Within and below the latter, a marked decrease can be seen towards the uppermost Triassic.
- The SO_4/Cl ratio is near constant in the upper part of the profile but increases with depth below about 820 m (upper part of the Opalinus Clay).

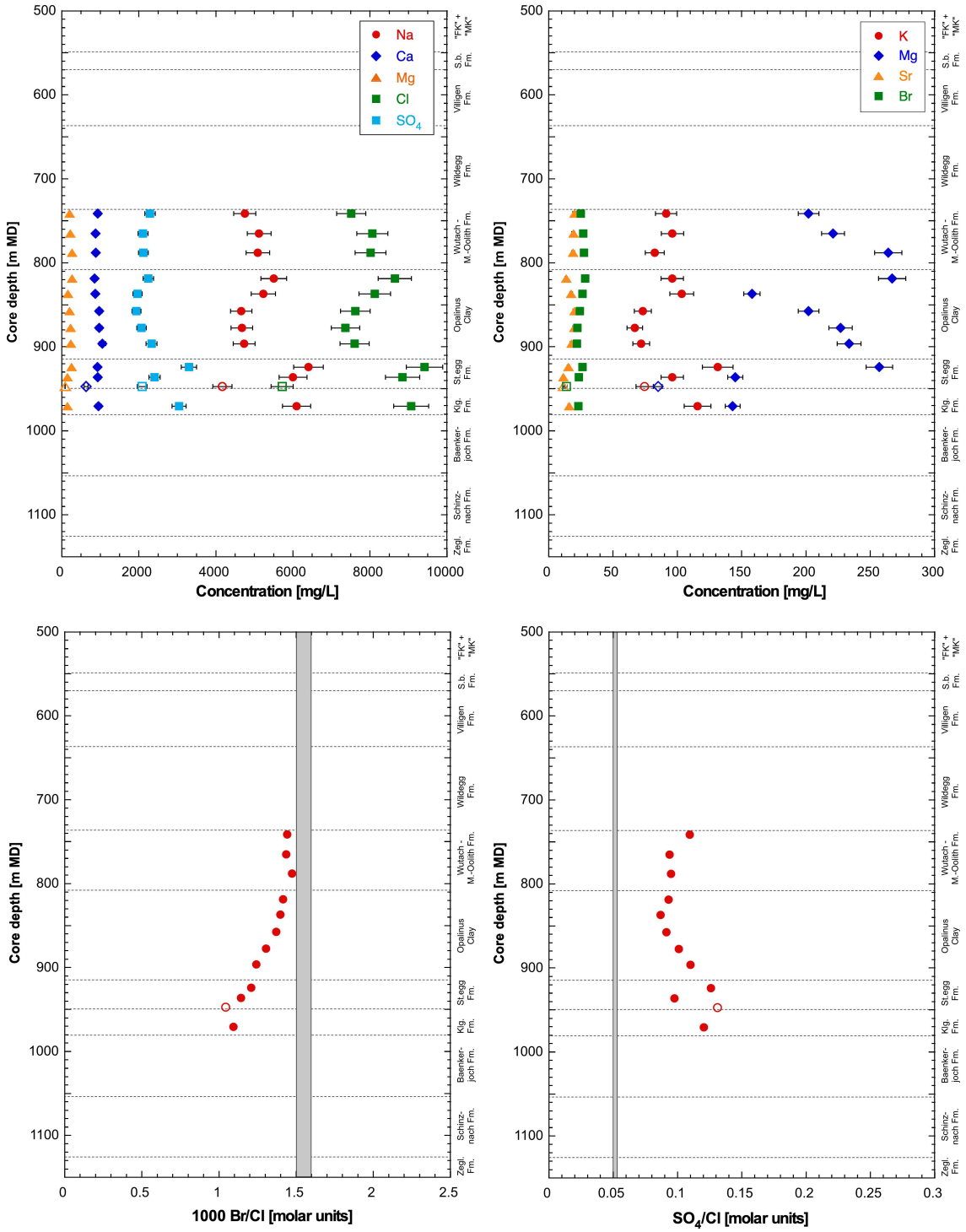

Fig. 4.6-5: Depth trends of ion concentrations and ion ratios in squeezed waters

Only the selected aliquots are shown for each sample. Bars indicate analytical errors of ion-chromatography analysis. Grey bars represent current seawater ratios. Data for sample 947.42 are uncertain and shown by open symbols.

4.6.4 Geochemical modelling and mineral saturation states

Mineral saturation indices for squeezed waters were calculated using PHREEQC V3 and the PSI/Nagra thermodynamic database at 25 °C (Thoenen et al. 2014) and are shown in Tab. 4.6-5.

- Squeezed waters are strongly oversaturated with respect to calcite, aragonite, dolomite and magnesite, a feature already known from previous studies (e.g. Mazurek et al. 2015). The oversaturation is possibly due to the fact that carbonate mineral solubility at high pressures during squeezing is higher than at atmospheric pressure. Further, outgassing of CO_2 during the squeezing process increases the pH and the saturation indices of calcite and dolomite (Tournassat et al. 2015). Further outgassing may take place in the headspace of the sample vials during sample storage, but this effect is considered marginal at best. The comparatively low calculated pCO_2 suggests that some outgassing may have taken place, which also affects pH. However, this does not markedly affect the obtained major-ion composition due to the large buffering capacity of the rock – water system in clay-rich lithologies. Last, lattice defects in carbonate minerals induced by deformation during squeezing might increase the solubility of these minerals. On the other hand, outgassing into the external atmosphere during sample storage in glass vessels is not considered to contribute to the low pCO_2. Such a process should also be seen by higher δ values of water isotopes, which is not the case (see Section 4.8), but this depends on the mode of water loss (via a gas phase, or via a liquid film). In Section 5.5 below, an attempt is made to restore the outgassing by model calculations assuming equilibrium with calcite.
- Saturation indices for strontianite vary in the range of -0.40 to +0.30, and many are close to 0. However, given the observed outgassing, this does not mean that strontianite is close to equilibrium under in situ conditions (undersaturation would be expected).
- Waters in the upper part of the studied profile are weakly undersaturated with respect to gypsum but close to saturation for sample 895.50 m and deeper. All waters are undersaturated with respect to anhydrite. Note that the in situ temperature in the studied depth interval is within the range of the gypsum-anhydrite transformation.
- Waters are close to saturation with respect to celestite.
- Using the data from Tab. 4.6-3, squeezed waters are strongly oversaturated with respect to fluorite, which is a consequence of the contamination of F concentrations by the filter material. Therefore, no F data are listed in Tab. 4.6-4.

It needs to be stated that both the measured chemical compositions as well as the calculated saturation indices refer to laboratory conditions, and the transfer of these data to in situ conditions requires modelling based on several assumptions. Cooling and pressure release since core recovery affected porewater chemistry to some degree, leading to new equilibria or to transient states if equilibrium was not attained. Model calculations to transfer laboratory results to in situ conditions were undertaken by Mäder & Wersin (2022) and Kiczka et al. (2023). While the temperature effect was found to be limited for most major ions, it is considerable for pH/pCO_2 conditions. Pertinent calculations for the squeezing samples from BAC1-1 are beyond the scope of this report.

Tab. 4.6-5: Mineral saturation indices for squeezed waters

Bold print indicates the selected ("best") aliquots. Data for sample 947.42 are uncertain and shown in italics.

Depth [m]	**Formation**	**Pressure** [MPa]	**pH**	**TIC** [M]	**Log (pCO_2)** [bar]	**SI Calcite**	**SI Aragonite**	**SI Dolomite (ord.)**	**SI Dolomite (disord.)**	**SI Strontianite**	**SI Magnesite**	**SI Gypsum**	**SI Anhydrite**	**SI Celestite**	**SI Fluorite**
741.49	«Parkinsoni-Württ.-Sch.»	**300**	**7.97**	**1.52E-03**	**-3.19**	**0.82**	**0.68**	**1.31**	**0.76**	**-0.39**	**0.17**	**-0.08**	**-0.30**	**-0.03**	**1.31**
		400										-0.01	-0.22	-0.02	0.89
765.33	«Parkinsoni-Württembergica-Sch.»	**200**	**8.69**	**1.40E-03**	**-4.02**	**1.40**	**1.26**	**2.54**	**1.99**	**0.20**	**0.82**	**-0.15**	**-0.36**	**-0.08**	**1.36**
		300	8.81	1.08E-03	-4.28	1.39	1.25	2.53	1.98	0.26	0.81	-0.13	-0.34	0.01	0.77
		400	8.76	9.27E-04	-4.27	1.30	1.16	2.34	1.79	0.09	0.72	-0.13	-0.34	-0.07	0.57
788.06	«Parkinsoni-Württembergica-Sch.»	**200**	**8.44**	**1.50E-03**	**-3.71**	**1.23**	**1.08**	**2.26**	**1.71**	**0.01**	**0.71**	**-0.15**	**-0.36**	**-0.09**	**1.02**
		300	8.49	1.36E-03	-3.79	1.24	1.09	2.27	1.72	0.00	0.71	-0.13	-0.35	-0.10	0.68
		400	8.44	1.43E-03	-3.72	1.23	1.09	2.27	1.72	0.05	0.71	-0.11	-0.33	-0.03	0.52
818.92	Opalinus Clay	**200**	**8.53**	**1.77E-03**	**-3.74**	**1.35**	**1.21**	**2.53**	**1.98**	**0.01**	**0.86**	**-0.15**	**-0.36**	**-0.22**	**1.52**
		300	8.51	1.57E-03	-3.77	1.31	1.17	2.43	1.88	-0.01	0.80	-0.12	-0.33	-0.17	1.00
		400	8.50	1.59E-03	-3.74	1.32	1.18	2.46	1.91	0.01	0.81	-0.11	-0.33	-0.16	0.70
837.16	Opalinus Clay	**200**	**8.99**	**9.16E-04**	**-4.59**	**1.44**	**1.30**	**2.48**	**1.93**	**0.20**	**0.72**	**-0.17**	**-0.38**	**-0.14**	**1.39**
		300	8.76	8.42E-04	-4.33	1.27	1.13	2.23	1.68	-0.02	0.64	-0.12	-0.33	-0.15	0.84
		400	8.77	1.14E-03	-4.21	1.44	1.30	2.58	2.03	0.09	0.82	-0.10	-0.32	-0.18	0.61
857.72	Opalinus Clay	**200**	**8.77**	**8.50E-04**	**-4.34**	**1.30**	**1.16**	**2.25**	**1.70**	**0.07**	**0.63**	**-0.13**	**-0.34**	**-0.09**	**1.12**
		300	8.83	1.31E-03	-4.23	1.55	1.41	2.80	2.25	0.30	0.92	-0.10	-0.32	-0.09	0.62
877.64	Opalinus Clay	**200**	**8.67**	**1.11E-03**	**-4.11**	**1.33**	**1.19**	**2.36**	**1.81**	**0.10**	**0.71**	**-0.11**	**-0.32**	**-0.07**	**1.12**
		300	8.75	7.29E-04	-4.38	1.26	1.12	2.23	1.68	-0.02	0.65	-0.06	-0.28	-0.07	0.64
896.50	Opalinus Clay	**200**	**8.60**	**1.14E-03**	**-4.01**	**1.31**	**1.17**	**2.30**	**1.75**	**-0.01**	**0.67**	**-0.03**	**-0.25**	**-0.09**	**0.98**
		300	8.61	1.30E-03	-3.96	1.41	1.26	2.48	1.93	0.03	0.75	-0.02	-0.24	-0.13	1.01
		400	8.50	1.31E-03	-3.84	1.36	1.21	2.39	1.84	-0.05	0.71	0.00	-0.21	-0.14	0.81
924.21	Staffelegg Fm.	**200**	**8.36**	**1.83E-03**	**-3.53**	**1.22**	**1.08**	**2.21**	**1.66**	**-0.11**	**0.67**	**0.01**	**-0.20**	**-0.05**	**1.30**
		300	8.52	1.62E-03	-3.77	1.36	1.22	2.48	1.93	0.13	0.80	0.06	-0.16	0.09	0.78
		400	8.39	1.74E-03	-3.59	1.32	1.17	2.39	1.84	-0.06	0.75	0.08	-0.13	-0.02	0.73
936.46	Staffelegg Fm.	**300**	**8.52**									**-0.08**	**-0.29**	**-0.27**	**1.65**
		400	8.61	1.16E-03	-4.01	1.26	1.11	2.00	1.45	-0.14	0.42	-0.02	-0.24	-0.15	1.24
		500	8.57	1.30E-03	-3.91	1.27	1.13	2.10	1.55	-0.11	0.50	-0.02	-0.23	-0.13	0.94
947.42	Staffelegg Fm.	**200**	***8.96***	***1.03E-03***	***-4.45***	***1.38***	***1.23***	***2.22***	***1.67***	***0.09***	***0.52***	***-0.22***	***-0.44***	***-0.24***	***1.30***
		300	*8.72*	*1.02E-03*	*-4.16*	*1.30*	*1.16*	*2.07*	*1.52*	*-0.03*	*0.45*	*-0.10*	*-0.32*	*-0.16*	*0.68*
970.89	Klettgau Fm.	**300**	**8.74**	**1.35E-03**	**-4.10**	**1.43**	**1.28**	**2.36**	**1.81**	**0.11**	**0.61**	**0.01**	**-0.20**	**-0.04**	**1.37**
		400	8.69	1.51E-03	-3.99	1.43	1.29	2.40	1.85	0.15	0.64	-0.02	-0.24	-0.03	0.97

4.6.5 Water content and aqueous extraction of squeezed and adjacent unsqueezed core material

For the calculation of the Cl-accessible porosity fraction f_{Cl} (see below), the inventories of water and Cl in the rock prior to squeezing must be known. These data can be obtained by two alternative methods:

1. Measure the water content (by drying) and then the Cl content (by aqueous extraction) of the squeezed material (so-called POST data). From these data, the masses of water and Cl remaining in the sample after squeezing can be calculated. By adding the masses of squeezed water and Cl to these data, the respective contents prior to squeezing can be reconstructed.
2. Measure the water content (by drying) and Cl content (by aqueous extraction of wet material) of adjacent unsqueezed material some 10 cm away (so-called PRE data).

Both approaches have advantages and disadvantages:

- Method 1 has the advantage that all measurements are performed on the same material, so potential heterogeneity is not an issue. On the other hand, the reconstruction of the water and Cl inventories is less direct and assumes that the dead volume of the system is negligible (which is likely the case[9]). The results are listed in Tab. 4.6-6.
- Method 2 directly yields the desired data – no addition of two measurements is needed – but relies on the assumption that the measurement performed on adjacent material is also representative for the squeezed material itself. The assumption of homogeneity incurs some degree of uncertainty. Moreover, the material used for the PRE measurements (typically a 8 – 10 cm long piece of core) has been exposed to the atmosphere for a few minutes during sample preparation (dry sawing) prior to being re-sealed again. While this was the case for the squeezed material as well, the exposed surface area of the adjacent cut-off material is much larger. Results are shown in Tab. 4.6-7.

[9] A sensitivity calculation was performed on the impact of dead volume. Assuming a dead volume of 1 mL results is an anion-accessible porosity fraction that is 0.01 – 0.04 higher than the value without consideration of a dead volume. The most strongly expressed shift is found in samples where only a small water volume was squeezed, while it becomes insignificant for samples with a good water yield.

Tab. 4.6-6: Water contents and results of aqueous-extraction tests on previously squeezed samples (method 1, POST data)

Depth [m]	**Formation**	**Water content (wet) of squeezed sample** [wt.-%]	**Mass of porewater in squeezed sample** [g]	**Aqueous extraction of squeezed sample**				
				Mass of dry rock [g]	**Mass of added water** [g]	***S/L*** [g/g]	**Cl** [mg/$L_{extract\ solution}$]	**Br** [mg/$L_{extract\ solution}$]
741.49	«Park.-W.-Sch.»	3.622	15.51	30.00	30.12	0.996	133	0.28
765.33	«Park.-W.-Sch.»	3.645	14.74	30.06	30.01	1.002	104	0.23
788.06	«Park.-W.-Sch.»	4.362	17.88	29.95	30.02	0.998	141	0.31
818.92	Opalinus Clay	3.571	14.31	30.03	30.03	1.000	138	0.24
837.16	Opalinus Clay	3.365	13.25	30.00	30.05	0.998	133	0.24
857.72	Opalinus Clay	3.816	12.75	29.98	29.96	1.001	152	0.26
877.64	Opalinus Clay	3.964	13.95	29.96	29.94	1.000	148	0.24
896.50	Opalinus Clay	3.733	13.80	30.03	29.89	1.005	128	0.20
924.21	Staffelegg Fm.	2.882	9.60	29.94	29.94	1.000	141	< 0.16
936.46	Staffelegg Fm.	3.227	10.98	29.94	29.93	1.000	154	0.29
947.42	Staffelegg Fm.	4.377	14.65	29.97	29.96	1.000	128	0.23
970.89	Klettgau Fm.	4.116	15.26	30.01	29.96	1.002	216	0.45

Tab. 4.6-7: Water contents and results of aqueous-extraction tests on material adjacent to squeezed samples (method 2, PRE data)

Depth [m]	**Formation**	**Water content (wet)** [wt.-%]	**Aqueous extraction of virgin material adjacent to squeezed sample**				
			Mass of dry rock [g]	**Mass of added water** [g]	***S/L*** [g/g]	**Cl** [mg/$L_{extract\ solution}$]	**Br** [mg/$L_{extract\ solution}$]
741.49	«Park.-W.-Sch.»	4.612	28.67	30.41	0.902	192.2	0.65
765.33	«Park.-W.-Sch.»	5.129	28.70	30.37	0.899	184.3	0.82
788.06	«Park.-W.-Sch.»	5.601	28.91	30.28	0.904	201.5	0.69
818.92	Opalinus Clay	4.286	29.66	30.43	0.934	201.4	0.68
837.16	Opalinus Clay	3.622	29.36	30.46	0.930	186.1	0.59
857.72	Opalinus Clay	4.640	28.64	30.45	0.899	206.3	0.66
877.64	Opalinus Clay	5.092	28.82	30.48	0.900	228.6	0.68
896.50	Opalinus Clay	5.093	29.46	30.52	0.918	209.9	0.62
924.21	Staffelegg Fm.	4.847	28.78	30.48	0.901	301.4	0.85
936.46	Staffelegg Fm.	4.154	29.69	30.42	0.936	202.0	0.55
947.42	Staffelegg Fm.	6.049	28.95	30.46	0.896	191.1	0.50
970.89	Klettgau Fm.	5.614	28.59	30.37	0.892	271.0	0.73

4.6.6 Chloride-accessible porosity

The Cl-accessible porosity fraction f_{Cl} can be estimated from

$$f_{Cl} = \frac{C_{Cl\ in\ bulk\ porewater}}{C_{Cl\ in\ squeezed\ water}}$$

$C_{Cl\ in\ squeezed\ water}$ is taken from Tab. 4.6-4, assuming that these data represent the concentrations in the anion-accessible pore space. $C_{Cl\ in\ bulk\ porewater}$ can be obtained using the two alternative methods described in Section 4.6.5. According to method 1, the masses of Cl and water obtained by squeezing and by drying/aqueous extraction of the squeezed material are added. The formalism is documented in more detail in Mazurek et al. (2021), and the results are listed in Tab. 4.6-8.

Alternatively, applying method 2, $C_{Cl\ in\ bulk\ porewater}$ can be obtained directly by drying/aqueous extraction of adjacent, unsqueezed rock according to

$$C_{Cl\ in\ bulk\ porewater} = \frac{C_{Cl\ in\ extract\ solution}}{S/_L\ w_d}$$

using the data listed in Tab. 4.6-7 (w_d = water content relative to dry rock). The results are shown in Tab. 4.6-9.

The resulting Cl-accessible porosity fractions obtained by the two methods are also listed in Tabs. 4.6-8 and 4.6-9. They are shown as a function of the clay-mineral content in Fig. 4.6-6. The values of f_{Cl} lie in the range of 0.45 – 0.61 (method 1) and 0.47 – 0.70 (method 2). Method 2 yields slightly higher values for the majority of the samples. Overall, method 1 is considered to be the preferred way to calculate f_{Cl}, given the fact that all measurements refer to identical materials and so heterogeneity plays no role.

Tab. 4.6-8: Cl-accessible porosity fractions derived from squeezing and aqueous-extraction experiments using method 1 to obtain $C_{Cl\ in\ bulk\ porewater}$

Data for sample 947.42 are uncertain and shown in italics.

Depth [m]	**Formation**	**Total mass of squeezed Cl** [mg]	**Mass of Cl in aq. extract of squeezed core** [mg]	**Porewater mass squeezed** [g]	**Water mass remaining in squeezed core** [g]	**Cl in bulk porewater** [mg/L]	**Cl-accessible porosity fraction f_{Cl}** [-]
741.49	«Park.-Württ.-Sch.»	8.17	55.04	1.13	15.51	3'797	0.51
765.33	«Park.-Württ.-Sch.»	25.42	40.58	3.64	14.74	3'590	0.45
788.06	«Park.-Württ.-Sch.»	24.67	55.49	3.55	17.88	3'741	0.47
818.92	Opalinus Clay	24.63	53.21	3.31	14.31	4'419	0.51
837.16	Opalinus Clay	24.04	50.73	3.29	13.25	4'522	0.56
857.72	Opalinus Clay	20.39	48.73	2.90	12.75	4'415	0.58
877.64	Opalinus Clay	23.92	49.85	3.50	13.95	4'226	0.57
896.50	Opalinus Clay	25.29	45.41	3.82	13.80	4'013	0.53
924.21	Staffelegg Fm.	29.99	45.57	3.46	9.60	5'786	0.61
936.46	Staffelegg Fm.	15.66	50.76	1.85	10.98	5'176	0.59
947.42	Staffelegg Fm.	*17.21*	*41.04*	*3.27*	*14.65*	*3'250*	*0.57*
970.89	Klettgau Fm.	16.85	76.47	1.90	15.26	5'438	0.60

Tab. 4.6-9: Cl-accessible porosity fractions derived from squeezing and aqueous-extraction experiments, using method 2 to obtain $C_{Cl\ in\ bulk\ porewater}$

Depth [m]	**Formation**	**Cl concentration in bulk porewater (in adjacent unsqueezed rock)** [mg/L]	**Cl-accessible porosity fraction f_{Cl}** [-]
741.49	«Park.-Württ.-Sch.»	4'409	0.59
765.33	«Park.-Württ.-Sch.»	3'791	0.47
788.06	«Park.-Württ.-Sch.»	3'757	0.47
818.92	Opalinus Clay	4'816	0.56
837.16	Opalinus Clay	5'325	0.66
857.72	Opalinus Clay	4'716	0.62
877.64	Opalinus Clay	4'736	0.64
896.50	Opalinus Clay	4'261	0.56
924.21	Staffelegg Fm.	6'569	0.70
936.46	Staffelegg Fm.	4'978	0.56
947.42	Staffelegg Fm.	*3'314*	*0.58*
970.89	Klettgau Fm.	5'111	0.56

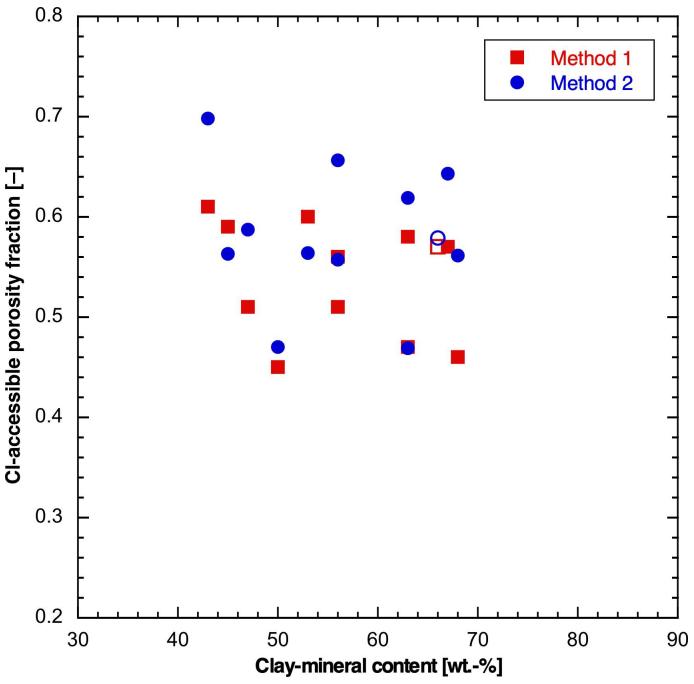

Fig. 4.6-6: Cl-accessible porosity fractions derived from squeezing experiments as a function of the clay-mineral content

See text for explanations regarding the two methods. Data for sample 947.42 are uncertain and shown by open symbols.

4.6.7 Composition of stable isotopes of squeezed water

Results of analyses of stable water isotopes are listed in Tab. 4.6-10 and shown as a function of depth in Fig. 4.6-7. The following observations can be made:

- Within any sample, the variation of the δ values with squeezing pressure is small. Nevertheless, a tendency towards slightly more negative δ values can be recognised with increasing pressure. The difference between the last and first aliquot lies in the range +0.02 to -0.28 ‰ for $\delta^{18}O$ and -0.09 to -1.25 for $\delta^{2}H$.
- Both $\delta^{18}O$ and $\delta^{2}H$ show distinct and regular trends towards decreasing values with depth.
- In a plot $\delta^{18}O$ vs. $\delta^{2}H$ (Fig. 4.6-8), the shallower samples are located far on the right side of the global ($\delta^{2}H = 8 \times \delta^{18}O + 10$; Craig 1961) and the local ($\delta^{2}H = 7.55 \times \delta^{18}O + 4.8$; Kullin & Schmassmann 1991) meteoric water lines. The deeper samples come closer to these lines.
- The same information is illustrated in Fig. 4.6-9 by the depth trend of deuterium excess ($\delta^{18}O - 8 \times \delta^{2}H$), which increases systematically with depth.

Tab. 4.6-10: Composition of stable isotopes of squeezed waters

The aliquots selected for interpretation are shown in bold. Data for sample 947.42 are uncertain and shown in italics.

Depth [m]	**Formation**	**Pressure** [MPa]	**$\delta^{18}O$** [‰ VSMOW]	**$\delta^{2}H$** [‰ VSMOW]	**D excess** [‰]
741.49	«Parkinsoni-Württ.-Sch.»	**300**	**-2.97**	**-37.6**	**-13.8**
		400	-3.11	-38.2	-13.3
765.33	«Parkinsoni-Württ.-Sch.»	**200**	**-3.22**	**-37.8**	**-12.0**
		300	-3.35	-38.3	-11.5
		400	-3.50	-39.0	-11.0
788.06	«Parkinsoni-Württ.-Sch.»	**200**	**-3.72**	**-39.5**	**-9.8**
		300	-3.81	-40.0	-9.6
		400	-3.90	-40.0	-8.8
818.92	Opalinus Clay	**200**	**-3.64**	**-39.2**	**-10.1**
		300	-3.77	-39.8	-9.6
		400	-3.91	-40.2	-8.9
837.16	Opalinus Clay	**200**	**-3.86**	**-40.0**	**-9.1**
		300	-3.89	-40.1	-9.0
		400	-4.09	-40.8	-8.0
857.72	Opalinus Clay	**200**	**-4.40**	**-41.0**	**-5.8**
		300	-4.48	-41.5	-5.6
877.64	Opalinus Clay	**200**	**-4.65**	**-41.5**	**-4.3**
		300	-4.83	-42.5	-3.9
896.50	Opalinus Clay	**200**	**-4.80**	**-42.0**	**-3.6**
		300	-4.89	-42.4	-3.3
		400	-5.04	-43.2	-2.9
924.21	Staffelegg Fm.	**200**	**-4.86**	**-42.5**	**-3.7**
		300	-4.95	-42.9	-3.3
		400	-5.13	-43.5	-2.5
936.46	Staffelegg Fm.	300	no data	no data	no data
		400	**-4.99**	**-42.3**	**-2.4**
		500	-4.97	-42.5	-2.7
947.42	Staffelegg Fm.	**200**	***-5.67***	***-44.4***	***1.0***
		300	*-5.72*	*-44.8*	*0.9*
970.89	Klettgau Fm.	**300**	**-5.11**	**-43.7**	**-2.9**
		400	-5.17	-43.8	-2.4

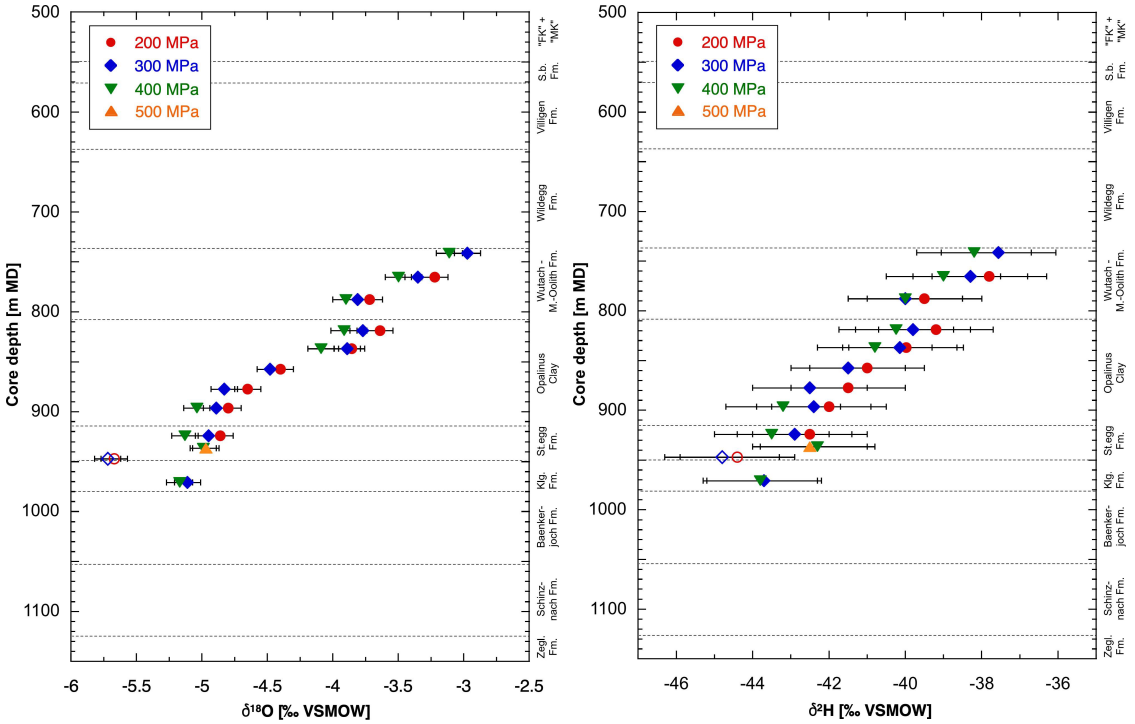

Fig. 4.6-7: Depth trends of $\delta^{18}O$ and $\delta^{2}H$ in squeezed waters

Data for sample 947.42 are uncertain and shown by open symbols.

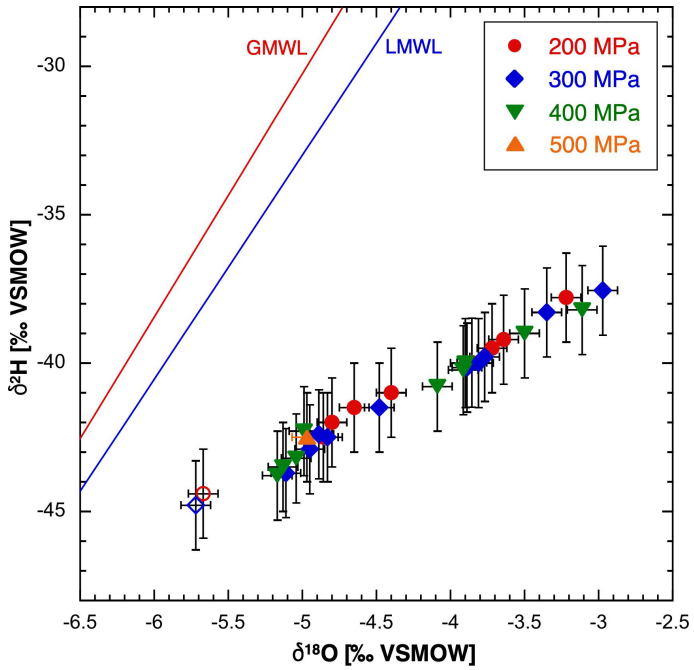

Fig. 4.6-8: Plot of $\delta^{18}O$ vs. $\delta^{2}H$ for squeezed waters

GMWL = Global Meteoric Water Line, LMWL = Local Meteoric Water Line. Data for sample 947.42 are uncertain and shown by open symbols.

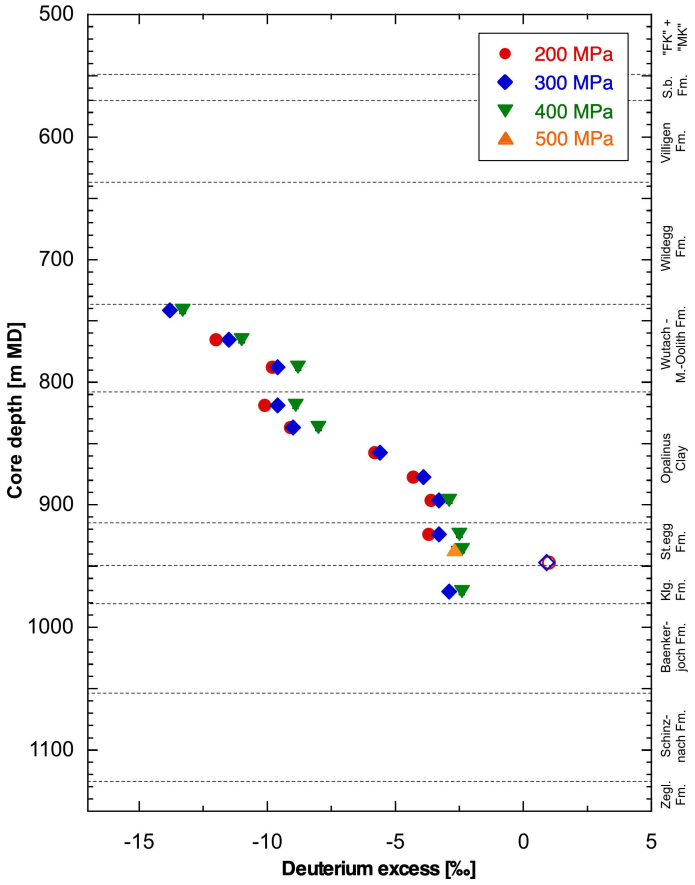

Fig. 4.6-9: Depth trend of deuterium excess in squeezed waters

Data for sample 947.42 are uncertain and shown by open symbols.

4.6.8 Comparison of squeezing and advective-displacement data for sample 933.70

Rationale and procedure

Sample 933.70, an argillaceous siltstone from the Frick Member of the Staffelegg Formation (51 wt.-% quartz + feldspars, 9 % carbonates, 39 % clay minerals), was subjected to an extended analytical programme, with the objective to compare results from different extraction methods. First, the virgin sample was cut to 3 slices, and the peripheral slices were subjected to aqueous extraction. The central slice was subjected to an advective-displacement experiment, and 35 pore-water aliquots from an extended time series were sampled, of which 17 were analysed (sample characterisation and data see Section 4.7). Early aliquots are considered to closely represent the composition of the porewater, while the late aliquots are dominated by the artificial porewater (APW) that was used for the experiment. When the experiment was terminated, the total amount of sample collected at the outflow corresponded to 3.81 pore volumes, and the chemical and isotopic compositions of the late eluates evolved only marginally over time. After the dismantling of the experiment, the core was dry-cut normal to its axis into 2 slices, a base slice (inlet side) 1.3 cm thick and a remaining main sample 7 cm thick. From the main sample a slab alongside the core axis was cut. This slab and the base slice were subjected to aqueous extraction and water content measurements, while the main slice was re-sealed and subjected to a squeezing experiment. The experimental workflow is illustrated in Fig. 4.6-10.

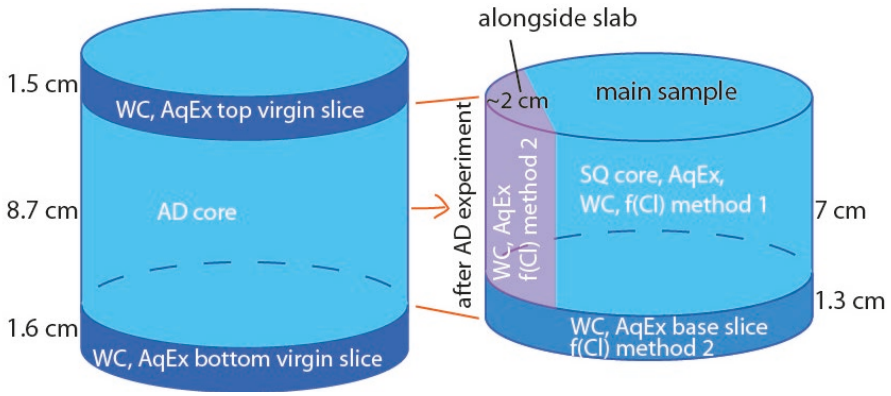

Fig. 4.6-10: Sketch of the experimental workflow and the location of different sample materials and analyses of core BAC1-1-933.70-AD

Analyses and experiments include aqueous extraction (AqEx), water content (WC) and advective displacement (AD) on the virgin rock sample (left), and AD post-mortem analysis and squeezing (SQ) including SQ post-mortem analyses on the AD core (right).

Composition of squeezed and advectively displaced waters

The composition of the early aliquots obtained by advective displacement (AD) is given in Tab. 4.6-11. The composition of the last aliquot, taken well after the breakthrough of the artificial porewater (APW), is similar but not identical to that of the APW. Assuming a homogeneous, piston-like displacement of the in situ porewater by the infiltrating APW, the concentrations of conservative components in the porewater after termination of the experiment should lie between that of the APW and that of the last aliquot. Note that the APW was prepared using water with an extremely high δ^2H, which served as a tracer to quantify the fraction of APW in the sampled aliquots. For cations, the evolution is complicated by cation exchange equilibria, which may lead to cation concentrations temporarily evolving away from the APW concentration during the AD experiment. This phenomenon was observed during the present AD experiment for Mg and K, whereas Na, Ca and Sr concentrations evolved smoothly towards the APW concentration (Section 4.7).

The water masses obtained by subsequent squeezing (SQ) are listed in Tab. 4.6-12 as a function of the squeezing pressure. After 3 days at 300 MPa, 0.7 g water were squeezed. Over the following 2 days, another 0.11 g were obtained at the same pressure. Then, pressure was increased to 400 MPa for 2 days and yielded 0.7 g water. Chemical and isotopic compositions of these aliquots are listed in Tab. 4.6-11. Data pertaining to the second aliquot obtained at 300 MPa are considered uncertain due to the small water mass. Thus, focussing on aliquots 300 (1) and 400 shows the usual drop of the contents of monovalent ions (Na, K, Cl), whereas the contents of bivalent ions (Ca, Mg, SO_4) remain near-constant. As argued above, the first aliquot is considered to be the closest representation of the porewater, so the following discussion focusses on aliquot 300 (1).

A substantial number of AD and SQ experiments were conducted in the frame of the TBO campaign, and in general, ion concentrations obtained from squeezing were slightly below those from advective displacement. This issue is discussed in more detail by Kiczka et al. (2023), and the main point is that, given the different experimental set-ups, the two methods likely sample somewhat different parts of the nanometric pore space where ion concentrations vary as a function of

the distance from the negatively charged clay-mineral surfaces. In this context, it is remarkable that in case of sample 933.70, the first squeezed aliquot has distinctly higher concentrations of all solutes in comparison to the last AD aliquot and the APW, except for Mg and TIC.

A potential explanation of this observation is a heterogeneous distribution of porewater composition during the advective-displacement experiment. While 3.8 pore volumes of APW finally entered the sample, flow may have been focussed to fast pathways, whereas the original in situ porewater may not have been fully displaced in less permeable parts of the sample. Incomplete displacement can indeed explain the observations, given the fact that the in situ porewater, represented by the early AD aliquot, has a higher salinity than the APW. Considering Cl, an admixture of 12% in situ porewater to the last aliquot or 10% to the APW would explain the Cl content obtained from the squeezing experiment (Tab. 4.6-11). Similar fractions are found for $\delta^{18}O$, while in the case of $\delta^{2}H$ a smaller admixture results. Regarding the discrepancy between the $\delta^{18}O$ and the $\delta^{2}H$ results, a pertinent observation was made for diffusive exchange experiments performed on post-mortem AD cores (Section 4.7) where a good match of the $\delta^{2}H$ values was obtained, whereas $\delta^{18}O$ values were slightly higher than those from the last aliquot and the APW. The reason for this is not yet understood.

It is concluded that the original objective of the experimental sequence, namely the squeezing of a sample with a known porewater composition (as explored by advective displacement) and direct comparison of the results, was not feasible. The likely explanation is that advective displacement occurred along preferential pathways in the studied core, whereas the displacement of the in situ porewater from less permeable regions of the core remained incomplete. As the rock fabric is pervasively deformed during squeezing, squeezed waters average over the compositions of preferential pathways and more stagnant regions within the core.

The advective-displacement experiment yields Peclet numbers for transport of H_2O in the range 5 to 15, i.e. advection and, to a lesser extent, diffusion are relevant transport mechanisms. Incomplete chemical equilibration between preferential pathways and stagnant parts of the core is therefore possible. Runtimes substantially longer than in this study (150 – 270 d, 1.2 – 3.8 pore volumes percolated) are expected for the equilibration of the entire core volumes.

Tab. 4.6-11: Chemical composition of squeezed and advectively displaced waters from sample 933.70

F concentrations in squeezed waters, in particular in the first aliquots, are contaminated by F leached from the fiberglass filters and so are not representative of the porewater. "n.d." = no data.

Type	Na [mg/L]	NH_4 [mg/L]	K [mg/L]	Ca [mg/L]	Mg [mg/L]	Sr [mg/L]	F [mg/L]	Cl [mg/L]	Br [mg/L]	NO_3 [mg/L]	SO_4 [mg/L]	pH	TIC [mg/L]	TOC [mg/L]	$\delta^{18}O$ [‰ VSMOW]	$\delta^{2}H$ [‰ VSMOW]
AD early aliquot	6582	< 10	62.1	1037	217	29.7	< 1.6	9816	24.4	50.2	2834	7.42	23.5	591.0	-4.94	-43.1
AD last aliquot	4249	< 10	57.1	502	106	13.6	< 1.6	5840	< 1.6	< 1.6	2165	7.39	31.9	38.9	-11.33	109.9
APW	4009	< 10	78.4	488	206	0.5	< 1.6	5908	< 1.6	1.94	2146	7.43	33.9	< 5	-11.24	113.3
SQ 300 MPa (1)	4678	< 10	80.2	531	96	< 10	14.4	6311	< 1.6	9.97	2661	8.66	14.0	98.3	-10.37	105.2
SQ 300 MPa (2)	4947	< 10	84.8	447	77	< 10	13.3	6247	< 1.6	7.54	2680	n.d.	n.d.	n.d.	n.d.	n.d.
SQ 400 MPa	4349	< 10	59.8	562	102	< 10	8.8	5676	< 1.6	6.53	2588	8.92	10.8	77.4	-10.44	105.7
Admixture of in situ pore-water to last aliquot [%]								12							12	3
Admixture of in situ pore-water to APW [%]								10							14	5

Tab. 4.6-12: Water masses squeezed from AD sample 933.70 at different pressure steps

The initial water content was reconstructed on the basis of the measured water content of the squeezed sample and the squeezed water mass (see Section 4.6.5), and this value was then used to calculate the initial mass of porewater in the sample. "-": pressure step not applied.

					Mass squeezed at P =					
Sample	Initial sample mass (CRIEPI) [g]	Initial water content (wet) [wt.-%]	Mass of porewater prior to squeezing [g]	100 MPa [g]	200 MPa [g]	300 MPa (1) [g]	300 MPa (2) [g]	400 MPa [g]	500 MPa [g]	Total mass squeezed [g]
AD post-mortem	301.96	3.05	9.20	0	0	0.70	0.11	0.70	-	1.51

Aqueous extraction and anion accessibility

The following materials were subjected to aqueous extraction (see also Fig. 4.6-10):

- Virgin slices below and above the AD core; the wet material was extracted, and water content was measured on fragments obtained from the slices.
- Main sample of the core subjected to advective displacement and then to squeezing; the squeezed core was first dried and then extracted.

- Slice cut from the base (= inflow side) of the core subjected to advective displacement (not squeezed); the wet material was extracted, and water content was measured on fragments obtained from the slice.
- Slab cut alongside the main part of the core prior to squeezing; the wet material was extracted, and water content was measured on fragments obtained from the same slab.

Results are listed in Tabs. 4.6-13 and 4.6-14 (data for the virgin slices are given in Section 4.7). Following the formalism detailed in Section 4.6.5, anion accessibility can be obtained from these data, in combination with the Cl contents in the squeezed water, and results are given in Tab. 4.6-15. The anion accessible porosity fractions obtained by method 2 compare well with the accessibilities derived by the AD method considering either the first water aliquots and aqueous-extraction data from a virgin slice (0.51 – 0.52), or the AD post-mortem data (last water aliquot and aqueous-extraction data from the base slice; 0.54). Details are given in Section 4.7.

Tab. 4.6-13: Water contents and results of aqueous-extraction tests on previously squeezed sample 933.70

Sample	**Water content (wet) of squeezed sample** [wt.-%]	**Mass of porewater in squeezed sample** [g]	**Aqueous extraction of dried squeezed sample**				
			Mass of dry rock [g]	**Mass of added water** [g]	***S/L*** [g/g]	**Cl** [$mg/L_{extract\ solution}$]	**Br** [$mg/L_{extract\ solution}$]
AD post-mortem	3.01	9.04	30.07	29.82	1.008	103	< 0.16

Tab. 4.6-14: Water contents and results of aqueous-extraction tests on unsqueezed material adjacent to squeezed sample 933.70

Sample	**Water content (wet)** [wt.-%]	**Aqueous extraction of unsqueezed wet material adjacent to squeezed sample**				
		Mass of wet rock [g]	**Mass of added water** [g]	***S/L*** [g/g]	**Cl** [$mg/L_{extract\ solution}$]	**Br** [$mg/L_{extract\ solution}$]
Alongside slab, AD post-mortem	4.230	30.41	30.29	0.922	141	< 0.16
Base slice, AD post-mortem	4.601	30.51	30.38	0.916	141	< 0.16

Tab. 4.6-15: Cl-accessible porosity fractions derived from squeezing and aqueous-extraction experiments on sample 933.70

Method	**Total mass of squeezed Cl** [mg]	**Mass of Cl in aq. extract of squeezed core** [mg]	**Porewater mass squeezed** [g]	**Water mass remaining in squeezed core** [g]	**Cl in bulk porewater** [mg/L]	**Cl-accessible porosity fraction f_{Cl}** [-]
Using data from aqueous extraction of squeezed core (method 1 in Section 4.6.5)	9.08	29.84	1.51	10.55	3'688	0.58
Using data from aqueous extraction of unsqueezed adjacent material, alongside slab (method 2 in Section 4.6-5)					3'461	0.55
Using data from aqueous extraction of unsqueezed adjacent material, base slice (method 2 in Section 4.6-5)					3'193	0.51

Conclusions

- The original objective, namely the direct comparison of porewater data obtained by advective displacement and squeezing, could not be achieved.
- The available data point towards a heterogeneous distribution of porewater chemistry after the completion of the advective-displacement experiment, i.e. to the existence of preferential pathways and more stagnant regions within the sample.
- This finding has no direct consequences on the interpretation of early aliquots from AD as good representations of the porewater because initially the composition is homogeneous in the whole sample due to long-term diffusive equilibration, i.e. fast pathways and stagnant regions are expected to yield comparable results for the free porewater.
- The comparison indicates that the AD and SQ methods sample different regions of the core. While the AD technique preferentially mobilises the porewater in the better connected and possibly larger pores representing the preferential pathways, the squeezing process is related to a major brittle rock deformation and so likely taps water not only from fast pathways but also from the stagnant regions that may be richer in clay and so dominated by smaller pores. Because the original porewater was not completely exchanged during the AD experiment, the salinity of the squeezed water exceeds that of the last aliquot and the APW.
- This hypothesis potentially offers an explanation for the slightly lower salinity obtained from squeezed waters in comparison to AD waters, as observed throughout the TBO campaign. A lower average salinity in the stagnant regions, which are sampled by SQ but not AD, can be envisioned due to a higher degree of anion exclusion (smaller pores, more clay surfaces). Hence, despite not fulfilling the initial objectives, the results of this method comparison exercise support the present understanding of the origin of the different salinities obtained by the two methods.

4.7 Data from advective-displacement experiments

Mirjam Kiczka, Carmen Zwahlen, Andreas Jenni, Urs Mäder

Advective-displacement (AD) experiments are a methodology for a comprehensive physico-chemical characterisation, including porewater chemistry and certain transport properties (details in method report, Waber ed. 2020). This section presents a data summary, more details where important, and short discussions where appropriate. The full datasets are provided in Appendix B. Integration of the data into context and depth profiles are included in Chapter 5.

Six samples from the Opalinus Clay and the clay-rich confining units were processed. These experiments were successful from a technical point of view, subjected to a similar analytical programme, with differences mainly related to the duration of each experiment (numbers of sampled fluid aliquots). Problems in earlier experiments from other boreholes of the TBO programme (i.e. BOZ1-1, BOZ2-1, STA3-1, STA2-1), which were related to high nitrate concentrations and gas production, were successfully eliminated in the experiments for BAC1-1 due to improvements in the experimental set-up as detailed in Section 4.7.2. Two experiments were initiated for each of the clay-rich stratigraphic sections (Dogger above the Opalinus Clay, Opalinus Clay and Lias) in order to ensure a successful experiment for each of the sections, as it was not known a priori, if the nitrate issues were successfully resolved. Once all experiments have proved successful, a limited analytical programme was subjected to one of the two cores from the same unit. Overall, the programme fulfilled the planned work, but provided partly longer durations of advective displacement than requested. The duration of the percolation period was 149 – 269 days, transporting 1.2 – 3.8 pore volumes of fluid. Doubling the number of experiments, in particular the two samples from the lower confining units, which differ just by 0.5 m in depth, provides an added value as a control on the consistency of the obtained porewater compositions.

The extent of pre- and post-mortem characterisation of core material was optimised based on gained experience from former boreholes BUL1-1, TRU1-1, MAR1-1, BOZ1-1, BOZ2-1, STA3-1 and STA2-1 investigations. Furthermore, the duplicate experiments provided the opportunity for an extensive additional post-mortem programme aimed at an inter-method comparison with the isotope diffusive exchange, squeezing and through-diffusion techniques. The results of the isotope diffusive exchange experiments are included in this section, whereas the results of the post-mortem squeezing tests are presented in Section 4.6. The results of the through-diffusion experiments were not available at the time of preparing this report and therefore could not be compared with AD results at this time.

The salinity observed in Opalinus Clay and adjacent units in this borehole is intermediate compared to those of other boreholes from the Nördlich Lägern area, i.e., lower than in BUL1-1 but higher than in STA2-1 and STA3-1.

4.7.1 Sample material and overview of analytical work

The six sample cores (Fig. 4.7-1) span 186 m of clay-rich confining and host rock units (748 m – 934 m depth), from the «Parkinsoni-Württembergica-Schichten» – («Brauner Dogger») to the Staffelegg Formation including two samples from the Opalinus Clay.

X-ray computed tomography (CT) was performed on a medical scanner (Waber ed. 2020) for sample selection (Fig. 4.7-2) and detection of disturbing features (fractures, pyrite accumulations, macro-fossils, etc.). Dry cutting with a mitre saw was used for obtaining a central core segment for AD experiments (yellow in Fig. 4.7-2), and adjacent 2 discs for ancillary characterisation (green in Fig. 4.7-2). The central core segment was machined on a lathe from 95 mm to 80 mm in diameter. Tab. 4.7-1 lists all analytical work performed on the six samples.

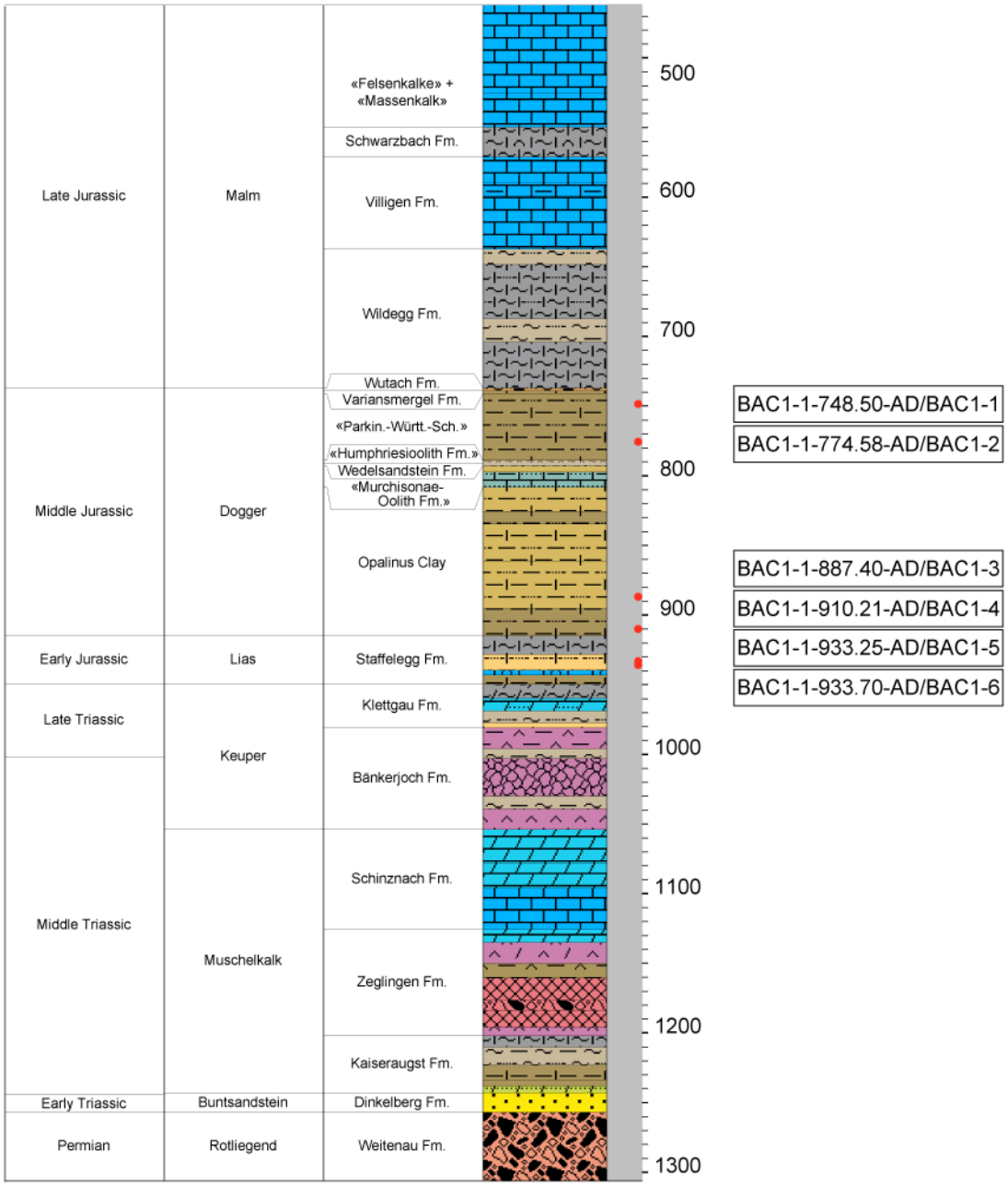

Fig. 4.7-1: Location of samples used for advective-displacement experiments (red dots)
Short labels are consecutively numbered laboratory abbreviations.

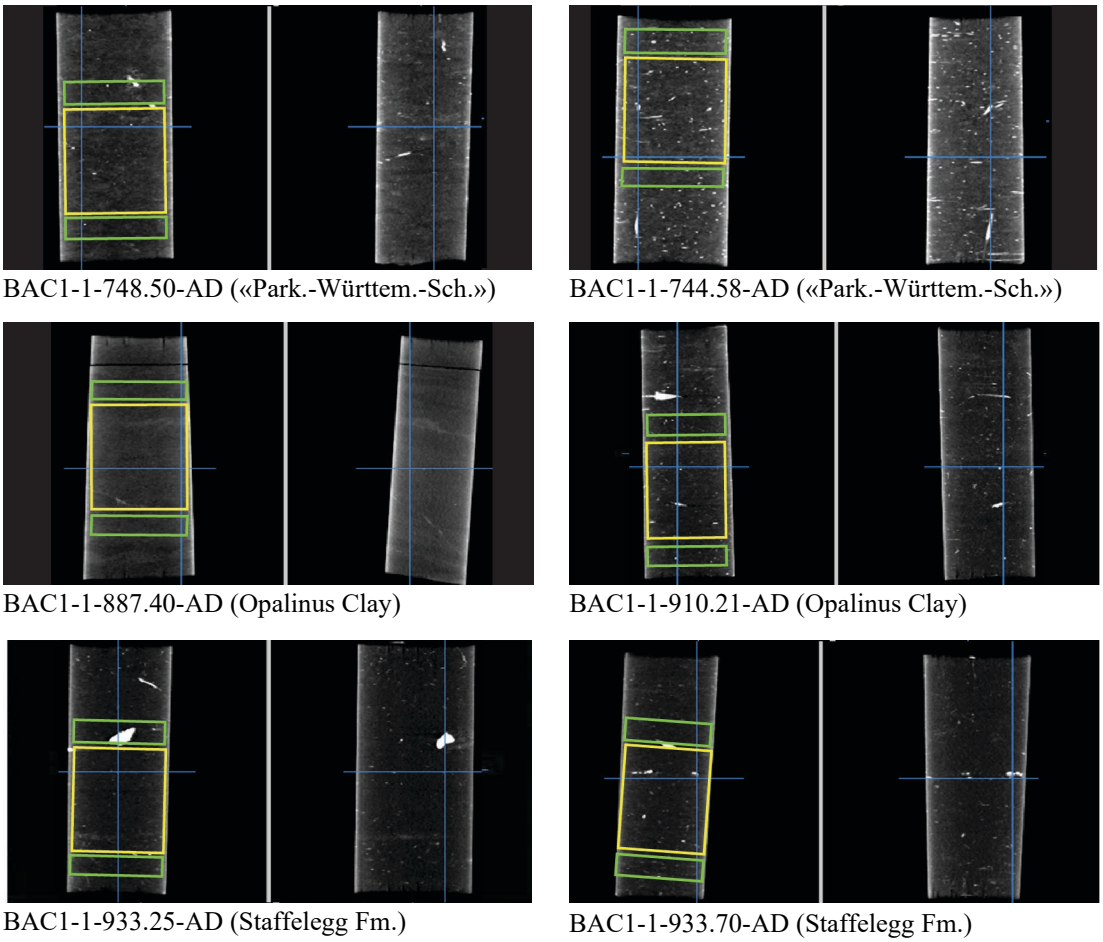

BAC1-1-748.50-AD («Park.-Württem.-Sch.»)

BAC1-1-744.58-AD («Park.-Württem.-Sch.»)

BAC1-1-887.40-AD (Opalinus Clay)

BAC1-1-910.21-AD (Opalinus Clay)

BAC1-1-933.25-AD (Staffelegg Fm.)

BAC1-1-933.70-AD (Staffelegg Fm.)

Fig. 4.7-2: X-ray CT images of AD samples

Core diameter is 95 mm. Central sections parallel to core axis at right angle. Grey scale range setting is 1700-2500 HU. Yellow segments are used for advective displacement, green segments for pre-characterisation. Low X-ray absorbance represents clay/quartz-rich sections (darker grey), slightly lighter grey indicates carbonate-richer parts, siderite is brighter, and pyrite is white (strongest absorbance). Black lines/gaps represent fractures. Image base is downhole direction.

Tab. 4.7-1: Summary of analytical work performed on samples for advective-displacement experiments

y = yes = done; n = no = not done; integer numbers refer to the number of samples processed; +: samples from above (left number) and below (right number) the core were processed, or the sum of both samples (ave); 'above' and 'below' refer to the orientation in the infiltration apparatus, which is rotated by 180° in case of BAC1-4 and BAC1-5 in Fig. 4.7-2 (see section below); xx: placeholder for analysis specific Lab sample ID; Pre: sample pre-characterisation; Post: post-mortem characterisation; WC: water content; M: mass; V,A,L: core volume, sectional area and length; Min: mineralogy; Clay: clay mineralogy; AqEx: aqueous extracts; Ni-en: cation selectivity with Ni-en method; Post_WC: post-mortem water content determined along a profile with n segments; AD_exp: complete analysis of fluid sample aliquots collected during advective displacement; Post_experiment: Experiments on core material; IDE: Isotope diffusive exchange experiment; Diffusion experiment: core material prepared for tracer diffusion at PSI

Parameter	**BAC1-1**	**BAC1-2**	**BAC1-3**	**BAC1-4**	**BAC1-5**	**BAC1-6**
Sample ID RWI	BAC1-1-748.50-AD	BAC1-1-774.58-AD	BAC1-1-887.40-AD	BAC1-1-910.21-AD	BAC1-1-933.25-AD	BAC1-1-933.70-AD
Lab sample ID	BAC1-1xx-AD	BAC1-2xx-AD	BAC1-3xx-AD	BAC1-4xx-AD	BAC1-5xx-AD	BAC1-6xx-AD
Depth [m]	748.50	774.58	887.40	910.21	933.25	933.70
Geol. unit	«Park.-Württem.-Sch.»	«Park.-Württem.-Sch.»	Opalinus Clay	Opalinus Clay	Staffelegg Fm.	Staffelegg Fm.
Member					Frick Mb.	Frick Mb.
AD_exp	y	y	y	y	y	y
Pre_WC	1+1	1+1	1+1	1+1	1+1	1+1
Pre_M	y	y	y	y	y	y
Pre_V,A,L	y	y	y	y	y	y
Pre_Min	1	1	1	1	1	1
Pre_Clay	1	1	1	1	1	1
Pre_AqEx	1+1	1+1	1+1	1+1	1+1	1+1
Pre_Ni-en	ave	ave	ave	ave	ave	ave
Post_WC	3	4	3	4	2	2
Post_M	y	y	y	y	y	y
Post_V,A,L	y	y	y	y	y	y
Post_AqEx	2	2	2	2	2	2
Post_Ni-en	2	n	2	n	n	n
Abras_Drilling_Fl	n	n	n	n	n	n
Post_experiment	2 IDE	2 IDE	2 IDE	2 IDE	(Diffusion-experiment)	Squeezing

4.7.2 Conditions of advective-displacement experiments

Sample preparation was performed according to Waber (ed.) (2020). In addition to the description therein, the cores were fully wrapped with electric tape on top of the latex sleeves (it was only applied to the ends of the latex rubber sleeves in sample preparations for previous boreholes). Then, a cold-shrink tube (3M Kaltschrumpfschlauch 8430.9, EPDM, 93.7/42.6/229) was applied, overlapping the edges of the Ti adapters. The ends were sealed with clear silicone sealant, as done with the latex rubber sleeves. These two additional layers, in particularly the new cold-shrink tube are considered to be responsible for the successful elimination of the earlier nitrate issue.

Cores were infiltrated from the base upwards (Fig. 4.7-2), i.e., against downhole direction, except BAC1-4 and BAC1-5: these cores were flipped by 180° and were infiltrated parallel to the downhole direction. The aqueous extract from the top of the core segment as mounted in the apparatus can be compared with the early exfiltrating chemistry to estimate the anion accessible porosity. All figures or sample names refer to the orientation in the infiltration apparatus.

The overview table (Tab. 4.7-2) presents some experiment-specific parameters such as variation in sample preparation, sample processing dates, storage time and other characteristic times like arrival of the first fluid drop and its electric conductivity. Numbers of samples taken and analysed are listed as well as average pressures for confining and injection. The number of percolated pore volumes is based on the water content determined from pre-characterisation. Infiltration pressure of the artificial porewater (APW) was on average 46 bar, pressurised by He. The hydraulic gradients are large, 5'000 – 6'000 m_{H2O}/m (sample dimensions are in Tab. 4.7-4). Experiments were started within 10 days of sample delivery and within 4 weeks after drilling. The time until arrival of a first fluid drop at the electric conductivity cell (outflow, before sampling syringe) was 4 – 9 days after the start of infiltration.

Confining pressure was on average 60 – 63 bar, pressurised by a piston pump that was used to pressurise a diaphragm accumulator (Parker Membranspeicher MBSP 050-210/60 S ST NBR), where a sturdy NBR membrane separates the confining fluid from a pressurised gas compartment (nitrogen). There is no gas – water interface in this set-up, and no gas is expected to dissolve in the confining fluid other than a small amount initially present.

Especially at early stages, gas exfiltrated the core (Tab. 4.7-2), but this decreased rapidly. Detailed studies of samples from previous boreholes BOZ1-1 and MAR1-1 (Wersin et al. 2022a and Mäder et al. 2021), including the determination of the density of the gas by high-precision weighing and gas characterisation indicated that the initial exfiltrating gas mainly consisted of air that is present at the core surface, in filters and in dead-space (entrapped during preparation). In experiments BAC1-3 and BAC1-4, the initial gas volume is higher than would be expected from the dead volumes, but still in the same range of experiments in BOZ1-1 and MAR1-1. Given the supressed gas ingress from the confining fluid in the BAC1-1 experiments, an additional gas source may add to the initial exfiltrating gas, which however is not yet understood.

The EC-cell mounted in experiment BAC1-4 showed different calibration curves before and after the experiment. Depending on the applied correction, the values differ by 4.5 mS/cm at ~ 20 mS/cm. The evolution of EC values in this experiment (Section 4.7.5.3) indicates the presence of an initial coating on the electrode surfaces that dissolved with ongoing percolation.

The drop of the APW level in the infiltration tank below the capillary inlet led to inadvertent He infiltration into core BAC1-1 after 140 days (after 1.3 pore volumes percolated). On 25.03.2022 at ~ 20:00, gas started to exfiltrate the core into the sampling syringe. The gas breakthrough was detected on 28.03.2022 at 8:00, the APW tank was refilled, and the gas injection stopped. Within the following ~ 4 weeks the exfiltrating gas volumes decreased to levels before the gas breakthrough and the hydraulic conductivity increased to values similar as before. Evolutions of tracer

concentrations (^{2}H, ^{18}O) in the exfiltrate were not affected by the breakthrough of the inert gas (Section 4.7.5). These observations indicated that solute transport was only temporarily slowed down during a gas breakthrough across this confined core, and no preferential pathway for advective or diffusive transport persisted.

Tab. 4.7-2: Conditions of advective-displacement experiments

Parameter	**BAC1-1**	**BAC1-2**	**BAC1-3**	**BAC1-4**	**BAC1-5**	**BAC1-6**
Depth [m]	748.50	774.58	887.40	910.21	933.25	933.70
Geol. unit	«Park.-Württem.-Sch.»	«Park.-Württem.-Sch.»	Opalinus Clay	Opalinus Clay	Staffelegg Fm.	Staffelegg Fm.
Drilled	10.10.2021	12.10.2021	21.10.2021	23.10.2021	25.10.2021	25.10.2021
Delivered	01.11.2021	01.11.2021	01.11.2021	01.11.2021	01.11.2021	01.11.2021
Prep_AD	04.11.2021	04.11.2021	08.11.2021	08.11.2021	11.11.2021	11.11.2021
Injection	05.11.2021	05.11.2021	09.11.2021	09.11.2021	12.11.2021	12.11.2021
First drop	12.11.2021	12.11.2021	15.11.2021	18.11.2021	17.11.2021	15.11.2021
Days to first drop	7.0	7.3	5.6	9.0	5.6	3.6
Initial gas [mL]	0.8	0.2	4.0	1.1	0.5	5.1
End_AD	28.06.2022	07.04.2022	28.06.2022	07.04.2022	08.08.2022	28.06.2022
Duration [d]	234.8	152.8	230.8	148.8	269.0	228.0
Pore-volumes	2.4	1.4	2.8	1.2	2.7	3.8
EC_initial (25 °C) [mS/cm]	25.7	29.5	25.7	17.5 (post-cal) 22.0 (pre-cal)	22.5	29.4
Filter	single PEEK					
Core packing	Teflon tape, 2 latex sleeves, electric tape, cold-shrink tube					
Confining pressure	Piston pump on water, diaphragm accumulator					
AD-samples	27	20	32	17	29	35
AD-samp_chem	13	8	16	7	10	17
AD-samp_isotopes	17	12	21	11	15	22
inline pH	9	6	11	5	8	12
P_Conf [bar]	60	60	60	60	60	63
P_Inf [bar]	46	45	46	47	45	46
Gradient [mH_2O/m]	5469	5517	5376	5933	5153	5397

4.7.3 Mineralogy and petrophysical properties

For each core, the mineralogy was determined on the combined subsamples cut adjacent to the core segment used for the AD experiments (Tab. 4.7-1). Results are summarised in Tab. 4.7-3 and plotted in Section 4.2. Samples cover a range of clay-mineral contents of 39 – 64 wt.-%, calcite contents of 5 – 21 wt.-%, and quartz contents of 18 – 45 wt.-%. The clay-mineral fraction is composed of variable amounts of illite (17 – 25 wt.-%), illite/smectite mixed layers (6 – 14 wt.-%), and kaolinite (7 – 20 wt.-%).

Carbon, sulphur and nitrogen analyses are also included. Pyrite contents are in most samples moderately low (0.4 – 2 wt.-%) because pyrite-rich lithologies, in particularly with larger concretions were avoided based on X-ray CT characterisation (Fig. 4.7-2). More details, including end-member clays, are included in Appendix B.

Tab. 4.7-3: Mineralogy of advective-displacement samples, including C, S and N analyses

b.d.: below detection.

Parameter	**Unit**	**BAC1-1**	**BAC1-2**	**BAC1-3**	**BAC1-4**	**BAC1-5**	**BAC1-6**
Depth	[m]	748.50	774.58	887.40	910.21	933.25	933.70
Geological unit		«Park.-Württem.-Sch.»	«Park.-Württem.-Sch.»	Opalinus Clay	Opalinus Clay	Staffelegg Fm.	Staffelegg Fm.
S	[wt.-%]	0.5	1.0	0.2	0.5	0.4	0.3
C(inorg)	[wt.-%]	2.5	2.8	1.3	1.2	1.0	1.1
C(org)	[wt.-%]	0.5	0.6	1.1	0.8	0.7	0.5
N	[wt.-%]	0.0	0.0	0.1	0.1	b.d.	b.d.
Quartz	[wt.-%]	28	18	21	19	45	45
K-feldspar	[wt.-%]	5	4	3	3	5	4
Plagioclase	[wt.-%]	3	2	2	2	2	2
Calcite	[wt.-%]	17	21	6	7	5	6
Dolomite / Ankerite	[wt.-%]	4	2	b.d.	b.d.	3	3
Siderite	[wt.-%]	b.d.	b.d.	5	3	b.d.	b.d.
Anhydrite	[wt.-%]	b.d.	b.d.	b.d.	b.d.	b.d.	b.d.
Celestite	[wt.-%]	b.d.	b.d.	b.d.	b.d.	b.d.	b.d.
Pyrite	[wt.-%]	0.9	1.8	0.4	1.0	0.8	0.5
Clay minerals	**[wt.-%]**	**42**	**51**	**61**	**64**	**39**	**39**
Illite	[wt.-%]	17	16	22	25	19	19
Illite/smectite ML (85-90)	[wt.-%]	b.d.	7	b.d.	b.d.	b.d.	b.d.
Illite/smectite ML (75-80)	[wt.-%]	11	b.d.	1	13	7	8
Illite/smectite ML (50-70)	[wt.-%]	b.d.	7	9	b.d.	b.d.	b.d.
Illite/smectite ML (20-40)	[wt.-%]	b.d.	b.d.	1.0	b.d.	b.d.	b.d.
Smectite	[wt.-%]	0.3	2.2	b.d.	b.d.	0.1	0.1
Kaolinite	[wt.-%]	7.9	10.1	19.9	17.8	7.1	7.1
Chlorite	[wt.-%]	0.6	1.2	0.9	1.3	0.8	0.9
Chl/Sm ML (85-95)	[wt.-%]	4.1	7.6	8.5	7.6	4.6	4.5
Total illite/smectite	[wt.-%]	11.4	14.1	10.2	12.6	6.6	7.7
(tot_ill/sm+sm)/ (total_clay)		0.28	0.32	0.17	0.20	0.17	0.20
(tot_ill+ill/sm+sm)/ (total_clay)		0.70	0.63	0.52	0.59	0.68	0.68

A plethora of petrophysical parameters can be derived from sample dimensions, mass, water content, and changes in these parameters determined before and after an AD experiment (Tab. 4.7-4). These quantities include porosity, bulk density, grain density, water uptake during the experiments, and unsaturated porosity (saturation ratio). The relationships are given in Waber (ed.) (2020). Note that the water content determined for pre-characterisation is based on 2 sub-samples adjacent to the AD core segment, if sufficient material was available.

The corrected initial water content as well as any unsaturated (gas-filled) porosity fraction of the core used in the AD experiment can be derived from the post-mortem water content and the usually observed slight core volume expansion during the experiment. The core volume increases by 0.4 – 1.7% (Tab. 4.7-4), accompanied by a water uptake of 4.4 – 5.6 g. Accounting for volume expansion, there remains a small net water uptake of 0.2 – 3.2 g that must reflect an initially small volume of unsaturated porosity, corresponding to a saturation ratio in the range 0.94 – 0.99. This analysis is valid if significant drying of a sample core is avoided by minimising exposure times, as was done for AD experiments (Waber ed. 2020). For samples BAC1-3 and BAC1-6, the measured core expansion was slightly larger than the mass increase, resulting in negative values for the initially unsaturated pore volume, thus saturation ratios of > 1. The largest measurement uncertainty is associated with the measurement of the core dimensions using callipers. Although reading precision is in the order of 0.05 mm, using callipers on slightly uneven cores adds to the uncertainty, as do any small breakouts along edges. Assuming a practical accuracy of ± 0.1 mm for diameter and length, results in a typical error of approximately ± 1 mL in core volume (or ± 1 g in terms of porewater mass) for the core dimensions commonly used. Such an error would translate to an error in saturation ratio of approximately ± 0.045 at porewater contents of 40 – 50 g. Thus, the initial state can be assumed saturated for all samples with saturation ratios > 0.955.

There are significant differences in water content measured in adjacent samples (pre-characterisation) and in the core itself (post-mortem), the latter showing 4 – 8%$_{rel.}$ higher values. This reduces to 1 – 2.5%$_{rel.}$ lower values (6.7% and 5.4% in case of BAC1-1 and BAC1-6, respectively) when accounting for core expansion (Fig. 4.7-3). This leads to different values of bulk wet density, water-loss porosity and grain density (assuming saturated conditions) derived from pre-characterisation and post-mortem data. This spread is larger than measurement uncertainties and illustrates that the largest contribution to uncertainty is sample heterogeneity for parameters that depend on water content. Differences in water content commonly correlate with differences in clay-mineral content, such that this heterogeneity is mainly an issue of lamination in fine-grained sediments. For post-mortem material from experiments BAC1-1 to BAC1-4, two additional gravimetric water contents were measured on the subsamples of the isotope diffusive exchange experiments (IDE) after the diffusive equilibration. The average of those two measurements matches well the values of the direct WC measurement. Note, that WC back-calculated from the isotopic compositions determined in the IDE (not shown here) are systematically higher than the corresponding gravimetric WC. This is further discussed in Section 4.3.1.

Tab. 4.7-4: Core dimensions and derived petrophysical parameters

_L = length; _A = area; _V = volume; _M = mass; WD = wet density; GD = grain density; WCw = water content rel. to wet mass; _WL = water loss

Parameter	**Unit**	**BAC1-1**	**BAC1-2**	**BAC1-3**	**BAC1-4**	**BAC1-5**	**BAC1-6**
Depth	[m]	748.50	774.58	887.40	910.21	933.25	933.70
Geological unit		«Park.-Württem.-Sch.»	«Park.-Württem.-Sch.»	Opalinus Clay	Opalinus Clay	Staffelegg Fm.	Staffelegg Fm.
Pre_Core_M	[g]	**1'077.06**	**1'061.43**	**1'081.23**	**973.58**	**1'103.91**	**1'088.77**
Pre_Core_DM	[cm]	8.00	8.00	7.99	7.99	8.01	8.00
Pre_Core_L	[cm]	8.46	8.40	8.59	7.82	8.70	8.57
Pre_Core_A	[cm^2]	50.27	50.26	50.20	50.19	50.36	50.28
Pre_Core_V	[cm^3]	425.19	422.17	431.33	392.69	438.04	431.12
Post_Core_M	[g]	**1'082.50**	**1'066.78**	**1'086.78**	**978.28**	**1'108.28**	**1'093.51**
Post_Core_DM	[cm]	8.02	8.02	8.02	8.01	8.03	8.02
Post_Core_L	[cm]	8.52	8.43	8.68	7.83	8.73	8.64
Post_Core_A	[cm^2]	50.54	50.47	50.52	50.35	50.60	50.47
Post_Core_V	[cm^3]	430.36	425.49	438.39	394.23	441.69	436.23
Delta_M	[g]	**5.44**	**5.35**	**5.55**	**4.69**	**4.37**	**4.74**
Delta_Core_DM	[cm]	0.021	0.016	0.026	0.012	0.019	0.015
Delta_Core_L	[cm]	0.059	0.032	0.085	0.007	0.030	0.068
Delta_Core_A	[cm^2]	0.261	0.204	0.321	0.154	0.246	0.192
Delta_Core_V	[cm^3]	**5.177**	**3.319**	**7.063**	**1.544**	**3.654**	**5.102**
Delta_Core_V-%	[%]	1.218	0.786	1.637	0.393	0.834	1.184
Pre_Bulk_WD	[g/cm^3]	**2.533**	**2.514**	**2.507**	**2.479**	**2.520**	**2.525**
Post_Bulk_WD	[g/cm^3]	**2.515**	**2.507**	**2.479**	**2.481**	**2.509**	**2.507**
Delta_Bulk_WD	[g/cm^3]	-0.018	-0.007	-0.028	0.002	-0.011	-0.019
Delta_Bulk_WD-%	[%]	-0.704	-0.280	-1.106	0.088	-0.435	-0.739
Pre_GD	[g/cm^3]	**2.726**	**2.733**	**2.730**	**2.701**	**2.694**	**2.701**
Post_GD	[g/cm^3]	**2.714**	**2.742**	**2.717**	**2.722**	**2.695**	**2.688**
Delta_GD	[g/cm^3]	-0.013	0.009	-0.013	0.020	0.001	-0.013
Corr_Pre_GD	[g/cm^3]	**2.712**	**2.727**	**2.727**	**2.696**	**2.690**	**2.691**
Pre_WCw		**0.0442**	**0.0502**	**0.0515**	**0.0526**	**0.0407**	**0.0409**
Post_WCw		**0.0460**	**0.0537**	**0.0558**	**0.0562**	**0.0437**	**0.0429**
Delta_WCw		0.0019	0.0035	0.0043	0.0035	0.0030	0.0020
Corr_Pre_WCw		**0.0412**	**0.0489**	**0.0510**	**0.0516**	**0.0399**	**0.0387**
Pre_H_2O_Core	[g]	**47.59**	**53.26**	**55.64**	**51.25**	**44.89**	**44.54**
Post_H_2O_Core	[g]	**49.84**	**57.30**	**60.65**	**54.97**	**48.40**	**46.89**
Delta_H_2O_Core	[g]	2.25	4.04	5.01	3.71	3.51	2.35
Corr_Pre_H_2O_Core	[g] or [mL]	**44.40**	**51.95**	**55.11**	**50.28**	**44.03**	**42.15**
Unsat_Vol	[g] or [mL]	0.26	2.03	-1.52	3.15	0.71	-0.36
Pore_Vol_tot	[mL]	44.66	53.98	53.59	53.42	44.74	41.79
Sat_ratio		**0.99**	**0.96**	**1.03**	**0.94**	**0.98**	**1.01**
Pre_Poro_WL		**0.1119**	**0.1262**	**0.1290**	**0.1305**	**0.1025**	**0.1033**
Post_Poro_WL		**0.1158**	**0.1347**	**0.1384**	**0.1394**	**0.1096**	**0.1075**
Delta_Poro_WL		0.0039	0.0085	0.0094	0.0089	0.0071	0.0042
Delta_Poro_WL-%	[%]	3.4616	6.7458	7.2507	6.8261	6.9311	4.0408
Corr_Pre_Poro_WL		**0.1044**	**0.1230**	**0.1278**	**0.1280**	**0.1005**	**0.0978**
Corr_Pre_Poro_tot		**0.1050**	**0.1279**	**0.1242**	**0.1360**	**0.1021**	**0.0969**
Delta_Corr_Poro_WL-%	[%]	**0.1119**	**0.1262**	**0.1290**	**0.1305**	**0.1025**	**0.1033**

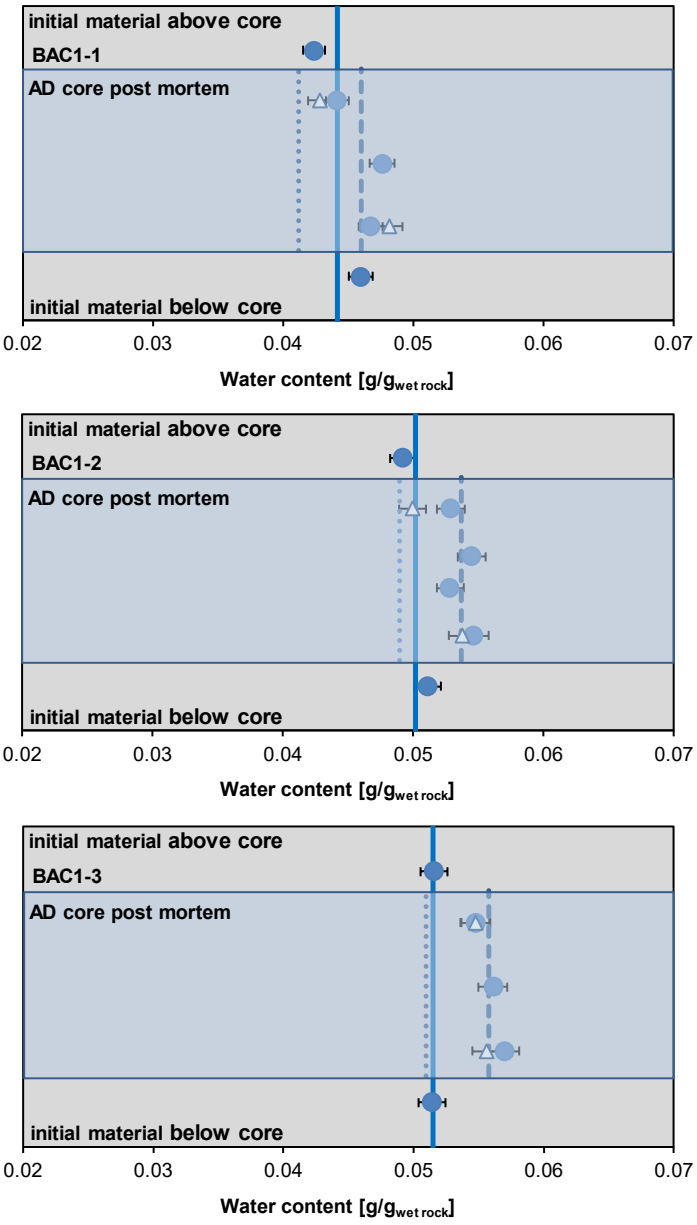

Fig. 4.7-3: Details of water content measurements before and after AD experiments

BAC1-1 = BAC1-1-748.50-AD («Parkinsoni-Württembergica-Schichten»); BAC1-2 = BAC1-1-774.58-AD («Parkinsoni-Württembergica-Schichten»); BAC1-3 = BAC1-1-887.40-AD (Opalinus Clay); BAC1-4 = BAC1-1-910.21-AD (Opalinus Clay); BAC1-5 = BAC1-1-933.25-AD (Staffelegg Formation); BAC1-6 = BAC1-1-933.70-AD (Staffelegg Formation). Vertical lines indicate the average value for pre-characterisation (solid line), average of post-mortem characterisation (dashed line) and the calculated corrected initial water content (dotted line). Triangles in BAC1-1 to BAC1-4 indicate average gravimetric WC measured after the IDE experiments. Error bars refer to measurement uncertainty of 2%.

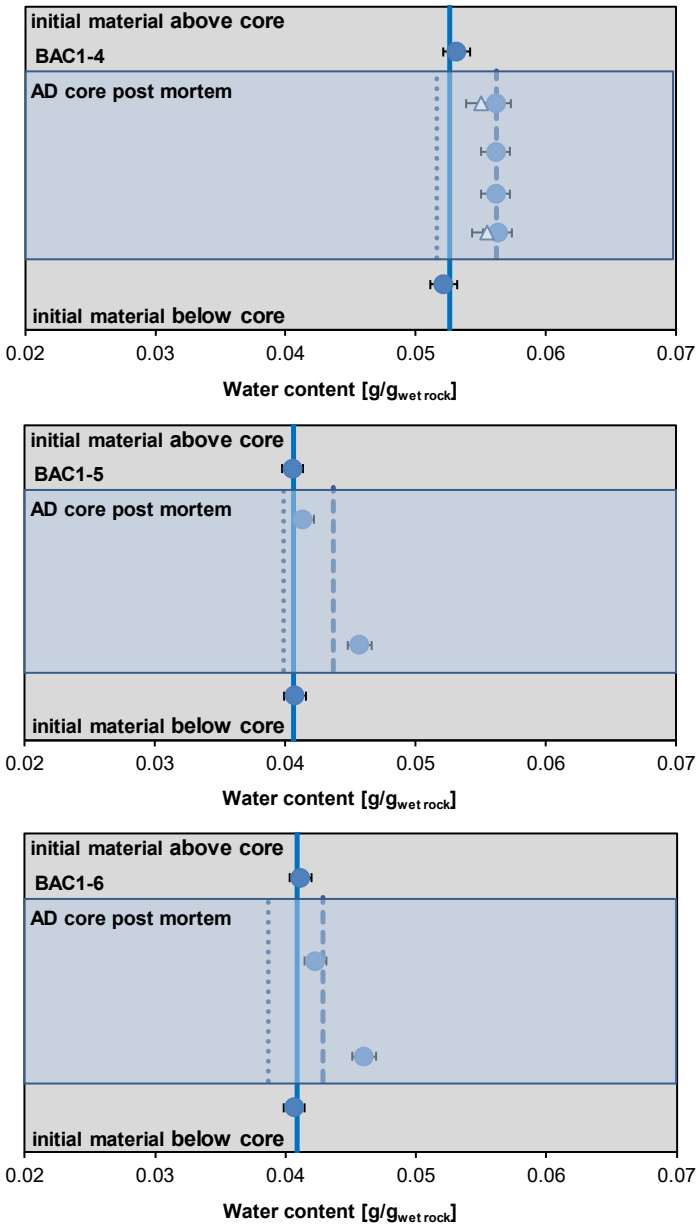

Fig. 4.7-3: continued

4.7.4 Aqueous extracts, CEC and cation selectivity of AD samples

Aqueous extracts, CEC and cation selectivity determinations were carried out within the pre-characterisation and post-mortem analysis. Detailed analyses are provided in Appendix B. Methods are the same as used for other core samples (Waber ed. 2020), with the exception of sample masses for water content that may have been smaller than used for regular core sample analysis. Averaged data – also used for integrative data plots – are presented in this section. Averaging refers to aqueous extraction measurements of pieces above and below the segment used for the AD experiments (indicated in Fig. 4.7-2 and Tab. 4.7-5). For CEC and cation selectivity, the pieces were combined in equal proportions and analysed as a single sample.

All averaged aqueous extract solutions (Tab. 4.7-5) from pre-characterisation processed at $S/L \approx 1$ contain low concentrations of NH_4 (up to 2.1 mg/L). NO_3 remained with the exception of BAC1-3 below the detection limit of 0.16 mg/L. $S/L\ (S_d/(L+PW))$ refers to the exact S/L of the aqueous extract accounting for the initial porewater of the wet solid sample. The factor $(1/WC_w \cdot L/S_w)$ refers to the scaling factor required to scale aqueous concentrations for conservative components to porewater concentrations (i.e., at water content).

Characteristic molar anion ratios (Tab. 4.7-6) follow a distinct trend with depth, with Br/Cl and SO_4/Cl ratios decreasing with depth. Cation ratios do not show a systematic depth trend but show a high degree of consistency for samples originating from the same Formation. Tab. 4.7-7 shows that the aqueous extract solutions are slightly below or very close to calcite saturation. Extracts are distinctly undersaturated with respect to sulphates and strontianite, and slightly less but still clearly undersaturated with respect to dolomite (ordered). TIC was used as input for the carbon system because the titrated alkalinity would also include acetate. However, the calculated alkalinity agrees well with the measured one due to low relative acetate concentrations in samples from this borehole.

Aqueous extracts of all cores were also produced after termination of the experiments. A thin disc (13 – 24 mm) from the top and base of each core was processed according to the protocols used for pre-characterisation. The base of the core represents the inlet of the artificial porewater (APW), whereas the top represents the outflow to the sampling syringe. The two may yield different results depending on the overall progress of fluid percolation (different concentrations in inlet sample compared to outlet), and averaging is therefore meaningless, unless a full break-through was achieved, including equilibration with the exchanger.

Results (Tab. 4.7-8) show that Br (not present in the APW) was effectively flushed out of each core, whereas other minor anionic components were buffered to some extent (e.g. F, NO_3).

The initially observed elevated TOC were flushed out at the APW inlet side but remained at a similar level at the outflow side. The core of BAC1-3 being an exception due to the long runtime, and there also the top was depleted in TOC. Acetate initially present in the samples from the «Parkinsoni-Württembergica-Schichten» and Opalinus Clay was fully flushed out. Ion-exchange processes must be considered to fully understand the changes in cation ratios. A more in-depth analysis will be required to reconcile differences between extracts from pre-characterisation and post-mortem analysis.

Calculation of post-mortem speciation and saturation indices (Tab. 4.7-9) of the aqueous extract solutions from Tab. 4.7-8 indicated no significant change compared to calculations based on core material before the experiment: post-mortem extracts are also close to calcite saturation and distinctly undersaturated with respect to sulphates and strontianite. Note, that Mg and Sr partly dropped below the detection limits. TIC was used as input for the carbon system.

Tab. 4.7-5: Composition of aqueous extract solutions from pre-characterisation

Parameter	**Unit**	**BAC1-1**	**BAC1-2**	**BAC1-3**	**BAC1-4**	**BAC1-5**	**BAC1-6**
Depth	[m]	748.50	774.58	887.40	910.21	933.25	933.70
Geological unit		«Park.-Württem.-Sch.»	«Park.-Württem.-Sch.»	Opalinus Clay	Opalinus Clay	Staffelegg Fm.	Staffelegg Fm.
averaging		top+base (1+1)	top+base (1+1)	top+base (1+1)	top+base (1+1)	top+base (1+1)	top+base (1+1)
$1/WC_w*L/S_w$		22.96	20.85	20.71	19.88	25.52	25.50
Rock wet	[g]	30.30	30.54	30.12	30.41	30.34	30.30
Water	[g]	29.40	30.41	30.55	30.22	30.26	30.37
WC_w	[g/g_{wet}]	0.044	0.050	0.051	0.053	0.041	0.041
S/L ($S_d/(L+PW)$)		0.944	0.908	0.890	0.905	0.924	0.920
pH at titration		8.94	8.36	8.21	8.31	9.00	9.00
Na	[mg/L]	273	315	345	332	267	266
NH_4	[mg/L]	2.07	1.78	1.57	1.56	1.76	2.06
K	[mg/L]	7.93	8.13	7.54	6.57	6.82	7.07
Ca	[mg/L]	3.44	4.93	7.22	4.70	3.03	2.82
Mg	[mg/L]	0.664	0.924	1.012	0.841	0.420	0.414
Sr (OES)	[mg/L]	0.105	0.122	0.130	0.104	0.064	0.063
Ba (OES)	[mg/L]	< 0.025	< 0.025	< 0.025	< 0.025	< 0.025	< 0.025
F	[mg/L]	3.60	2.60	1.58	2.94	4.13	4.14
Cl	[mg/L]	185	219	225	223	202	200
Br	[mg/L]	0.63	0.75	0.68	0.63	0.54	0.54
NO_3	[mg/L]	< 0.16	< 0.16	0.16	< 0.16	< 0.16	< 0.16
SO_4	[mg/L]	210	235	218	233	179	185
Alk (tit)	[meq/L]	2.54	2.95	4.57	3.49	2.40	2.23
Alk as HCO_3	[mg/L]	154.9	179.9	278.8	213.1	147.3	137.0
TOC	[mg/L]	3.53	3.66	3.28	4.04	3.20	4.13
TIC	[mg/L]	27.1	34.6	54.5	40.5	25.0	22.6
lactate	[mg/L]	< 2	< 2	< 2	< 2	< 2	< 2
acetate	[mg/L]	3.45	3.89	5.27	4.44	< 2	< 2
propionate	[mg/L]	< 2	< 2	< 2	< 2	< 2	< 2
formate	[mg/L]	< 2	< 2	< 2	< 2	< 2	< 2

Tab. 4.7-6: Cation ratios and details of carbon system in aqueous extract solutions from pre-characterisation

Parameter	**Unit**	**BAC1-1**	**BAC1-2**	**BAC1-3**	**BAC1-4**	**BAC1-5**	**BAC1-6**
Depth	[m]	748.50	774.58	887.40	910.21	933.25	933.70
Geol. unit		«Park.-Württem.-Sch.»	«Park.-Württem.-Sch.»	Opalinus Clay	Opalinus Clay	Staffelegg Fm.	Staffelegg Fm.
Br/Cl*1'000	[mol/mol]	1.52	1.52	1.34	1.25	1.19	1.19
SO_4/Cl	[mol/mol]	0.42	0.40	0.36	0.39	0.33	0.34
Ca/Mg	[mol/mol]	3.14	3.23	4.33	3.39	4.37	4.13
Ca/Sr	[mol/mol]	72	88	121	99	104	99
(Ca+Mg)/(Na+K)	[eq/eq]	0.014	0.018	0.024	0.016	0.013	0.012
Alk (tit)	[meq/L]	2.54	2.95	4.57	3.49	2.40	2.23
TIC	[meq/L]	2.26	2.88	4.53	3.37	2.08	1.88
acetate	[meq/L]	0.058	0.066	0.089	0.075	< 0.03	<0.03
TOC	[mg/L]	3.5	3.7	3.3	4.0	3.2	4.1
acetate (as C)	[mg/L]	1.40	1.58	2.14	1.81	< 0.814	<0.814

Tab. 4.7-7: Saturation indices calculated for aqueous extract solutions from pre-characterisation

PSI/Nagra 2012 thermodynamic database (Thoenen et al. 2014), calculated in PHREEQC for 25 °C, using ordered dolomite; kgw = kg water; charge = Σ(cation charge) – ׀Σ(anion charge)׀; %-error = 100*charge / (Σ(cation charge) + ׀Σ(anion charge)׀).

Parameter	**unit**	**BAC1-1**	**BAC1-2**	**BAC1-3**	**BAC1-4**	**BAC1-5**	**BAC1-6**
Depth	[m]	748.50	774.58	887.40	910.21	933.25	933.70
Geological unit		«Park.-Württem.-Sch.»	«Park.-Württem.-Sch.»	Opalinus Clay	Opalinus Clay	Staffelegg Fm.	Staffelegg Fm.
Charge	[eq/kg_w]	1.9E-04	1.9E-04	2.0E-04	2.9E-04	1.5E-04	2.6E-04
%-Error		0.78	0.69	0.65	0.99	0.64	1.10
Acetate	[eq/kg_w]	5.8E-05	6.6E-05	8.9E-05	7.5E-05	<3.0E-5	<3.0E-5
Ionic strength	[mol/kg_w]	1.45E-02	1.66E-02	1.78E-02	1.72E-02	1.38E-02	1.38E-02
tot_alk	[eq/kg]	2.44E-03	2.93E-03	4.56E-03	3.41E-03	2.27E-03	2.07E-03
pH		8.94	8.36	8.21	8.31	9.00	9.00
Log pCO_2	[bar]	-3.85	-3.15	-2.80	-3.03	-3.95	-3.99
SI(calcite)		-0.02	-0.32	-0.11	-0.323	-0.038	-0.111
SI(dolomite)		-0.40	-1.02	-0.73	-1.05	-0.59	-0.71
SI(gypsum)		-2.68	-2.49	-2.37	-2.52	-2.79	-2.81
SI(celestite)		-2.47	-2.38	-2.40	-2.46	-2.74	-2.73
SI(strontionaite)		-1.06	-1.47	-1.40	-1.52	-1.24	-1.29
SI(anhydrite)		-2.91	-2.71	-2.60	-2.75	-3.02	-3.03

Tab. 4.7-8: Composition of aqueous extract solutions from post-mortem characterisation

n.a.: not analysed

Parameter	**Unit**	**BAC1-1**		**BAC1-2**	
Depth	[m]	748.50		774.58	
Geological unit		«Parkinsoni-Württembergica-Schichten»		«Parkinsoni-Württembergica-Schichten»	
averaging		top post-mortem (outflow side)	base post-mortem (inflow side)	top post-mortem (outflow side)	base post-mortem (inflow side)
$1/WC_w*L/S_w$		23.99	22.22	20.13	19.61
Rock wet	[g]	30.05	30.85	30.19	29.85
Water	[g]	30.52	30.59	30.53	30.37
WC_w	[g/g_{wet}]	0.04	0.05	0.05	0.05
S/L ($S_d/(L+PW)$)		0.90	0.92	0.89	0.88
pH at titration		8.79	8.67	8.80	8.46
Na	[mg/L]	234	240	281	268
NH_4	[mg/L]	1.65	1.30	1.52	1.39
K	[mg/L]	5.74	5.49	7.79	7.68
Ca	[mg/L]	2.45	2.89	3.57	3.49
Mg	[mg/L]	0.54	0.65	< 1	1.00
Sr (OES)	[mg/L]	0.08	0.07	< 1	< 1
Ba (OES)	[mg/L]	< 0.025	< 0.025	< 0.025	< 0.025
F	[mg/L]	3.45	3.35	2.72	2.82
Cl	[mg/L]	112.0	119.0	158	149
Br	[mg/L]	< 0.16	< 0.16	< 0.16	< 0.16
NO_3	[mg/L]	< 0.16	0.2	0.58	0.18
SO_4	[mg/L]	191	184	231	224
Alk (tit)	[meq/L]	3.18	3.38	3.34	3.34
Alk as HCO_3	[mg/L]	194	206	205	208
TOC	[mg/L]	3.8	1.0	4.7	1.7
TIC	[mg/L]	36.3	39.9	40.3	41.0
lactate	[mg/L]	< 2	< 2	< 2	< 2
acetate	[mg/L]	< 2	< 2	< 2	< 2
propionate	[mg/L]	< 2	< 2	< 2	< 2
formate	[mg/L]	< 2	< 2	< 2	< 2

Tab. 4.7-8: (continued)

Parameter	**Unit**	**BAC1-3**		**BAC1-4**	
Depth	[m]	887.40		910.21	
Geological unit		Opalinus Clay		Opalinus Clay	
averaging		top post-mortem (outflow side)	base post-mortem (inflow side)	top post-mortem (outflow side)	base post-mortem (inflow side)
$1/WC_w*L/S_w$		19.17	18.77	18.45	18.69
Rock wet	[g]	30.64	30.18	31.00	30.56
Water	[g]	30.49	30.55	30.40	30.44
WC_w	[g/g_{wet}]	0.05	0.06	0.06	0.06
S/L ($S_d/(L+PW)$)		0.90	0.88	0.91	0.90
pH at titration		8.38	8.36	8.27	8.32
Na	[mg/L]	307	305	298	279
NH_4	[mg/L]	1.28	1.12	1.39	1.29
K	[mg/L]	5.72	6.26	7.09	6.92
Ca	[mg/L]	4.20	4.57	3.82	3.64
Mg	[mg/L]	0.81	1.13	< 1	< 1
Sr (OES)	[mg/L]	0.09	0.08	< 1	< 1
Ba (OES)	[mg/L]	< 0.025	< 0.025	< 0.025	< 0.025
F	[mg/L]	1.69	1.60	3.13	3.21
Cl	[mg/L]	146	148	157	148
Br	[mg/L]	< 0.16	< 0.16	< 0.16	< 0.16
NO_3	[mg/L]	< 0.16	0.31	0.26	0.20
SO_4	[mg/L]	207	203	232	208
Alk (tit)	[meq/L]	5.17	5.12	3.84	3.92
Alk as HCO_3	[mg/L]	316	313	237	250
TOC	[mg/L]	< 0.5	< 0.5	3.6	1.0
TIC	[mg/L]	72.0	70.8	46.7	49.2
lactate	[mg/L]	< 2	< 2	< 2	< 2
acetate	[mg/L]	< 2	< 2	2.31	< 2
propionate	[mg/L]	< 2	< 2	< 2	< 2
formate	[mg/L]	< 2	< 2	< 2	< 2

Tab. 4.7-8: (continued)

Parameter	**Unit**	**BAC1-5**		**BAC1-6**	
Depth	[m]	933.25		933.70	
Geological unit		Staffelegg Fm.		Staffelegg Fm.	
averaging		top post-mortem (outflow side)	base post-mortem (inflow side)	top post-mortem (outflow side)	base post-mortem (inflow side)
$1/WC_w*L/S_w$		25.17	22.96	24.55	22.64
Rock wet	[g]	30.43	30.42	30.41	30.51
Water	[g]	30.44	30.54	30.29	30.38
WC_w	[g/g_{wet}]	0.04	0.05	0.04	0.05
S/L ($S_d/(L+PW)$)		0.92	0.91	0.92	0.92
pH at titration		8.96	8.98	9.16	8.96
Na	[mg/L]	226	228	228	223
NH_4	[mg/L]	1.50	1.22	1.69	1.36
K	[mg/L]	5.01	5.24	5.50	5.99
Ca	[mg/L]	2.42	2.35	2.32	2.50
Mg	[mg/L]	0.41	0.52	0.37	0.56
Sr (OES)	[mg/L]	0.04	0.04	0.04	0.03
Ba (OES)	[mg/L]	< 0.025	< 0.025	< 0.025	< 0.025
F	[mg/L]	4.24	4.00	4.50	4.02
Cl	[mg/L]	137	144	141	141
Br	[mg/L]	< 0.16	< 0.16	< 0.16	< 0.16
NO_3	[mg/L]	0.17	< 0.16	1.33	0.39
SO_4	[mg/L]	158	160	159	164
Alk (tit)	[meq/L]	2.71	2.58	2.58	2.44
Alk as HCO_3	[mg/L]	165	157	157.5	149.0
TOC	[mg/L]	6.6	< 0.5	3.6	< 0.5
TIC	[mg/L]	30.4	30.1	28.8	26.2
lactate	[mg/L]	< 2	< 2	< 2	< 2
acetate	[mg/L]	< 2	< 2	< 2	< 2
propionate	[mg/L]	< 2	< 2	< 2	< 2
formate	[mg/L]	< 2	< 2	< 2	< 2

Tab. 4.7-9: Saturation indices calculated for aqueous extract solutions obtained post-mortem

PSI/Nagra 2012 thermodynamic database (Thoenen et al. 2014), calculated in PHREEQC for 25 °C, using ordered dolomite; kg_w = kg water; charge = Σ(cation charge) – ׀Σ(anion charge % ;׀-error = 100*charge / (Σ(cation charge) + ׀Σ(anion charge),(׀ < d.l. : below detection limit.

Parameter	**Unit**	**BAC1-1**		**BAC1-2**	
Depth	[m]	748.50		774.58	
Geological unit		«Park.-Württem.-Sch.»		«Park.-Württem.-Sch.»	
Position		top post-mortem (outflow side)	base post-mortem (inflow side)	top post-mortem (outflow side)	base post-mortem (inflow side)
Charge	[eq/kg_w]	8.36E-05	3.48E-05	-2.77E-04	-3.15E-04
%-Error		0.40	0.16	-1.09	-1.29
Acetate	[eq/kg_w]	< 3.0E-05	< 3.0E-05	< 3.0E-05	< 3.0E-05
Ionic strength	[mol/kg_w]	1.25E-02	1.27E-02	1.52E-02	1.46E-02
tot_alk	[eq/kg]	3.19E-03	3.45E-03	3.54E-03	3.49E-03
pH		8.79	8.67	8.80	8.46
log$P(CO_2)$	[bar]	-3.56	-3.40	-3.53	-3.17
SI(calcite)		-0.16	-0.16	0.03	-0.29
SI(dolomite)		-0.63	-0.62	Mg < d.l.	-0.77
SI(gypsum)		-2.84	-2.79	-2.64	-2.64
SI(celestite)		-2.62	-2.67	Sr < d.l.	Sr < d.l.
SI(strontianite)		-1.20	-1.30	Sr < d.l.	Sr < d.l.
SI(anhydrite)		-3.07	-3.01	-2.87	-2.87
Parameter	**Unit**	**BAC1-3**		**BAC1-4**	
Depth	[m]	887.40		910.21	
Geological unit		Opalinus Clay		Opalinus Clay	
Position		top post-mortem (outflow side)	base post-mortem (inflow side)	top post-mortem (outflow side)	base post-mortem (inflow side)
Charge	[eq/kg_w]	-7.44E-04	-6.45E-04	6.68E-05	-2.49E-04
%-Error		-2.65	-2.31	0.25	-0.99
Acetate	[eq/kg_w]	< 3.0E-05	< 3.0E-05	3.9E-05	< 3.0E-05
Ionic strength	[mol/kg_w]	1.63E-02	1.62E-02	1.57E-02	1.48E-02
tot_alk	[eq/kg]	6.08E-03	5.97E-03	3.92E-03	4.14E-03
pH		8.38	8.36	8.27	8.32
log$P(CO_2)$	[bar]	-2.85	-2.84	-2.93	-2.95
SI(calcite)		-0.06	-0.05	-0.38	-0.32
SI(dolomite)		-0.49	-0.35	Mg < d.l.	Mg < d.l.
SI(gypsum)		-2.63	-2.59	-2.63	-2.59
SI(celestite)		-2.55	-2.61	-2.55	-2.61
SI(strontianite)		-1.25	-1.32	-1.25	-1.32
SI(anhydrite)		-2.85	-2.82	-2.85	-2.82

Tab. 4.7-9: (continued)

Parameter	**Unit**	**BAC1-5**		**BAC1-6**	
Depth	[m]	933.25		933.70	
Geological unit		Staffelegg Fm.		Staffelegg Fm.	
Position		top post-mortem (outflow side)	base post-mortem (inflow side)	top post-mortem (outflow side)	base post-mortem (inflow side)
Charge	[eq/kg_w]	7.67E-05	-3.67E-05	5.21E-05	1.30E-04
%-Error		0.38	-0.18	0.26	0.66
Acetate	[eq/kg_w]	< 3.0E-05	< 3.0E-05	< 3.0E-05	< 3.0E-05
Ionic strength	[mol/kg_w]	1.18E-02	1.20E-02	1.20E-02	1.17E-02
tot_alk	[eq/kg]	2.74E-03	2.71E-03	2.70E-03	2.36E-03
pH		8.96	8.98	9.16	8.96
log$P(CO_2)$	[bar]	-3.82	-3.84	-4.06	-3.88
SI(calcite)		-0.07	-0.07	0.05	-0.12
SI(dolomite)		-0.57	-0.45	-0.33	-0.54
SI(gypsum)		-2.92	-2.93	-2.95	-2.88
SI(celestite)		-2.93	-2.99	-2.95	-3.05
SI(strontianite)		-1.34	-1.39	-1.21	-1.54
SI(anhydrite)		-3.14	-3.15	-3.17	-3.11

Cation exchange capacities and cation selectivities determined by the Ni-en method (Waber ed. 2020) for pre-characterisation were performed on a single combined sample for each core from the two samples used for aqueous extracts. The results are also presented and interpreted in Section 4.5. Tab. 4.7-10 shows uncorrected (for porewater contribution and mineral dissolution/ precipitation) capacities of 68 – 106 meq/kg (dry rock) with errors of up to ~ ± 5%. Ni consumptions (Ni_cons) are 17 – 20% lower in the case of samples from BAC1-3, BAC1-5 and BAC1-6, but even 40% less in BAC1-4. For the two samples from the «Parkinsoni-Württembergica-Schichten» Ni consumption agree well (BAC1-1) or are even higher than the sum of cations (SumCat, BAC1-2). Ammonium was not measured but is expected to be present on the exchanger judged by the presence of up to 2 mg/L of NH_4 in the aqueous extracts performed at the same *S/L* ratio (Tab. 4.7-5). The high nitrate concentrations derive from the Ni-en solution. The negative charge balance arises from the lack of incorporating ethylendiamine complexes from the Ni-en solution into the calculation (Tab. 4.7-10). The low Br concentrations agree with the Br concentrations in the aqueous extracts, as well as the Br/Cl ratios, whereas the SO_4/Cl ratios tend to be slightly lower than in the aqueous extracts. The cation occupancies (selectivities) derived from Ni-en extracts and the applied correction for the porewater contribution are presented in Section 4.5.

Tab. 4.7-11 shows the results of post-mortem cation occupancy measurements performed on BAC1-1 and BAC1-3 AD cores using slices from the top (outflow) and the base (inflow) of the core. The Ni consumptions of the top and base samples for each core overlap within the analytical error, whereas the sum of cations is larger in the base than in the top samples, exceeding the analytical error, but remain below the Ni consumption values. Cation occupancies in the top and bottom samples of each core are almost identical. A slight shift towards higher Ca and lower Na fractional occupancies in the bottom slice compared with the top slice are observed however, after correcting for mineral dissolution (correction of Ca by SO_4 and Na by Cl). Lower Sr fractional occupancies in the bottom slice reflect the absence of Sr in the APW. Compared to the initial material (Section 5.6), differences in the corrected fractional occupancies in the post-mortem top and bottom slices are ≤ 0.05. This illustrates that the cation exchanger is not yet at full equilibrium with the APW in the entire core, but differences between the equilibrium with the in situ porewater and APW are rather minor.

Tab. 4.7-10: Composition of Ni-en extract solutions and related parameters from pre-characterisation

kg_d = kg dry rock

Parameter	**Unit**	**BAC1-1**	**BAC1-2**	**BAC1-3**	**BAC1-4**	**BAC1-5**	**BAC1-6**
Depth	[m]	748.50	774.58	887.40	910.21	933.25	933.70
Geological unit		«Park.-Württem.-Sch.»	«Park.-Württem.-Sch.»	Opalinus Clay	Opalinus Clay	Staffelegg Fm.	Staffelegg Fm.
averaging		1 averaged	1 averaged	1 averaged	1 averaged	1 averaged	1 averaged
$1/WC_w*L/S_w$		24.03	21.41	20.49	20.32	25.67	25.76
Rock wet	[g]	30.34	30.16	30.84	30.43	30.61	30.40
Solution	[g]	30.87	30.88	30.93	30.95	30.71	30.79
WC_w	[g/g_{wet}]	0.04	0.05	0.05	0.05	0.04	0.04
S/L ($S_d/(L+PW)$)		0.90	0.88	0.90	0.89	0.92	0.91
pH (initial)		8.25	8.25	8.25	8.25	8.25	8.25
Ni (initial)	[mg/L]	5457	5'457	4'846	4'846	5'288	5'288
pH (final)		8.42	8.39	8.29	8.36	8.34	8.38
Na	[mg/L]	983	928	1100	1147	791	798
K	[mg/L]	177	156	136	151	121	132
Mg	[mg/L]	134	124	112	115	70	74
Ca	[mg/L]	503	467	520	601	377	397
Sr	[mg/L]	23.7	20.8	17.7	18.7	12.9	13.5
Ba	[mg/L]	0.549	0.191	0.470	0.300	0.378	0.372
Fe	[mg/L]	< 0.05	< 0.05	< 0.05	< 0.05	< 0.05	< 0.05
Ni	[mg/L]	2'722	2'417	2'470	2'643	3'518	3'489
F	[mg/L]	< 0.16	< 0.16	< 0.16	< 0.16	< 0.16	0.16
Cl	[mg/L]	165	197	213	203	187	186
Br	[mg/L]	0.56	0.67	0.65	0.58	0.51	0.49
NO_3	[mg/L]	12'586	12'605	12'934	12'909	12'901	12'678
SO_4	[mg/L]	130	144	141	148	122	123
TDS	[mg/L]	17'425	17'060	17'646	17'936	18'101	17'892
Charge %-err	[%]	-8.69	-13.73	-11.97	-8.31	-8.45	-7.37
Na	[meq/kg_d]	47.5	45.6	53.2	56.3	37.5	38.1
K	[meq/kg_d]	5.0	4.5	3.9	4.4	3.4	3.7
Mg	[meq/kg_d]	12.3	11.6	10.2	10.7	6.3	6.7
Ca	[meq/kg_d]	27.9	26.3	28.8	33.9	20.4	21.7
Sr	[meq/kg_d]	0.60	0.54	0.45	0.48	0.32	0.34
Ba	[meq/kg_d]	0.009	0.003	0.008	0.005	0.006	0.006
Fe	[meq/kg_d]	< 0.002	< 0.002	< 0.002	< 0.002	< 0.002	< 0.002
SumCat	[meq/kg_d]	93.3	88.6	97.0	105.7	67.9	70.6
SumCat_err	[meq/kg_d]	4.00	3.80	4.00	4.70	3.00	3.10
Ni_cons	[meq/kg_d]	94.9	107.3	81.0	75.6	58.0	59.6
Ni_cons_err	[meq/kg_d]	4.50	4.40	4.00	4.10	4.60	4.60
Br/Cl	[mol/mol*1000]	1.51	1.51	1.35	1.27	1.21	1.17
SO_4/Cl	[mol/mol]	0.29	0.27	0.24	0.27	0.24	0.24

Tab. 4.7-11: Composition of Ni-en extract solutions and related parameters from post-characterisation

kg_d = kg dry rock

Parameter	**Unit**	**BAC1-1**		**BAC1-3**	
Depth	[m]	748.50		887.40	
Geological unit		«Park.-Württem.-Sch.»		Opalinus Clay	
averaging		top post-mortem (outflow side)	base post-mortem (inflow side)	top post-mortem (outflow side)	base post-mortem (inflow side)
$1/WC_w*L/S_w$		24.02	22.75	19.27	18.80
Rock wet	[g]	30.42	30.44	30.95	30.53
Solution	[g]	30.93	30.93	30.96	30.96
WC_w	[g/g_{wet}]	0.04	0.05	0.05	0.06
S/L ($S_d/(L+PW)$)		0.90	0.90	0.90	0.88
pH (initial)		8.29	8.29	8.29	8.29
Ni (initial)	[mg/L]	5'649	5'649	5'649	5'649
pH (final)		8.35	8.36	8.23	8.26
Na	[mg/L]	861	878	1'073	1'049
K	[mg/L]	190	195	156	173
Mg	[mg/L]	131	150	121	157
Ca	[mg/L]	400	530	516	593
Sr	[mg/L]	23.4	21.4	18.3	16.9
Ba	[mg/L]	0.556	0.619	0.477	0.513
Fe	[mg/L]	< 0.1	< 0.1	< 0.1	< 0.1
Ni	[mg/L]	2'703	2'770	2'493	2'527
F	[mg/L]	< 0.16	< 0.16	< 0.16	< 0.16
Cl	[mg/L]	108	110	139	138
Br	[mg/L]	< 0.16	< 0.16	< 0.16	< 0.16
NO_3	[mg/L]	12'209	11'926	12'413	12'186
SO_4	[mg/L]	136	143	136	138
TDS	[mg/L]	16'764	16'726	17'067	16'980
Charge %-error	[%]	-10.07	-5.75	-9.31	-6.32
Na	[meq/kg_d]	38.1	38.9	46.7	46.8
K	[meq/kg_d]	5.0	5.1	4.0	4.5
Mg	[meq/kg_d]	11.0	12.5	9.9	13.3
Ca	[meq/kg_d]	20.3	26.9	25.8	30.3
Sr	[meq/kg_d]	0.54	0.50	0.42	0.40
Ba	[meq/kg_d]	0.008	0.009	0.007	0.008
Fe	[meq/kg_d]	< 0.004	< 0.004	< 0.004	< 0.004
SumCat	[meq/kg_d]	74.9	83.9	86.9	95.3
SumCat_err	[meq/kg_d]	3.19	3.50	3.85	4.09
Ni_cons	[meq/kg_d]	102.1	99.7	107.6	108.8
Ni_cons_err	[meq/kg_d]	4.30	4.40	4.20	4.30
Br/Cl	[mol/mol*1'000]	-	-	-	-
SO_4/Cl	[mol/mol]	0.46	0.48	0.36	0.37

4.7.5 Chemical and isotopic evolution of displaced porewater aliquots

An artificial porewater (APW) was injected to force advective displacement. The outflow of each experiment was continuously sampled in small syringes (Waber ed. 2020). These syringe aliquots were analysed for chemical and water stable isotope composition. Hydraulic conductivity was evaluated for each sampled aliquot (Darcy's law), and any expelled gas was also recorded, although gas-tightness is commonly good, but cannot be ensured for a syringe sampling system. Most data for each experiment are included in tables and graphs in this section, and more details are provided in Appendix B.

According to the method of advective displacement (Mäder 2018), it is expected that the first few sampled aliquots are of similar composition and represent the displaced porewater from the sample core. After this, a gradual breakthrough of the injected APW should be observed, until full breakthrough of conservative components (e.g. Cl, Br), given enough time.

4.7.5.1 Artificial porewater used for advective displacement

An artificial porewater (APW) composition (Tab. 4.7-12, details in text below) was chosen that was based on work performed for the deep geothermal well Schlattingen-1 (advective-displacement experiments detailed in Mäder & Waber 2017). The composition was calculated with PHREEQC for 25 °C, to be saturated with respect to calcite and dolomite, and a partial pressure of CO_2 of $10^{-2.2}$ bar. This partial pressure was imposed by bubbling with an Ar/CO_2 gas mixture during mixing and again when the fluid reservoir was filled before the experiments started. A recipe with the appropriate amounts of PA-grade chemicals is given in Tab. 4.7-13.

Deuterium was added as a water tracer for advective-diffusive transport, aiming for a δ^2H of approximately +100 ‰ (VSMOW). There is no Br contained in the APW and therefore bromide-breakout can be used as an anionic tracer in the case of significant Br concentrations in the porewater. If the Cl concentration in the APW is significantly different from the displaced early aliquots, Cl breakthrough forms an additional anionic tracer for transport.

All experiments from the BAC1-1 borehole were fed with the same batch of APW, but from three separate PFA-coated fluid tanks. Some tanks had to be topped up once over the course of the experiment with the same batch of APW. After every tank opening, the headspace was filled with He after bubbling with the Ar/CO_2 gas mixture mentioned above. The water isotope composition of the APW prior to the experiments, and as sampled afterwards from one tank agreed well within analytical uncertainties.

Tab. 4.7-12: Composition and recipe for the artificial porewater

* calculated from the weighed-in chemical compounds; pH measured; CO_2-Ar bubbling not taken into account; n.a.: not analysed.; § APW in the infiltration tank after the experiment.

Parameter	**Unit**	**Recipe**	**Calculated ***	**Measured**	**Compounds**
pH		7.19		7.43	
Na	[mg/L]	3'989	3'988	4'009	NaCl; $NaHCO_3$; Na_2SO_4
NH_4	[mg/L]			< 10	
K	[mg/L]	79.4	79.4	78.4	KCl
Ca	[mg/L]	503	503	488	$CaCl_2 \cdot 2H_2O$
Mg	[mg/L]	226	226	206	$MgCl_2 \cdot 6H2O$
Sr (OES)	[mg/L]			< 0.5	
Ba	[mg/L]			< 0.5	
Si	[mg/L]			0.937	
Al	[mg/L]			< 50	
F	[mg/L]			< 1.6	
Cl	[mg/L]	5'992	5'985	5'908	$CaCl_2 \cdot 2H_2O$; KCl; $MgCl_2 \cdot 6H_2O$
Br	[mg/L]			< 1.6	
NO_3	[mg/L]			1.94	
SO_4	[mg/L]	2'305	2'304	2'146	Na_2SO_4
I	[mg/L]			n.m	
TOC	[mg/L]			< 5	
TIC	[mg/L]	29.3	29.32	33.9	$NaHCO_3$
lactate	[mg/L]			< 20	
acetate	[mg/L]			< 20	
propionate	[mg/L]			< 20	
formate	[mg/L]			< 20	
$\delta^{18}O$	[‰ VSMOW]		-11.43	-11.24 -11.23 § -11.20§	
$\delta^{2}H$	[‰ VSMOW]	100	110.9	113.3 112.7 § 113.2§	D_2O

Tab. 4.7-13: Recipe for the artificial porewater for a 2-litre batch

Chemical	**Manufacturer**	**Grade**	**Recipe**		**Batch2 BAC1**
			[g/kg$_w$]	[g/2kg$_w$]	weighted in [g/2 L]
$NaHCO_3$	Merck	p.a.	0.2051	0.4101	0.4103
$CaCl_2 \cdot 2H_2O$	Merck	p.a.	1.8465	3.6930	3.6922
KCl	Merck	p.a.	0.1514	0.3029	0.3027
$MgCl_2 \cdot 6H_2O$	Merck	p.a.	1.8907	3.7814	3.7812
NaCl	Merck	p.a.	7.1916	14.3831	14.3837
Na_2SO4	AnalaR NORMAPUR	Ph.Eur.	3.4089	6.8177	6.8121
D_2O (100%)	Roth	> 99.8% D	0.0318	0.0635	0.0673

4.7.5.2 Physical conditions, hydraulic conductivity, sampling and pore volume equivalents

All core samples were subjected to 60 – 63 bar hydraulic confining pressure, and an infiltration pressure of initially around 48 bar set by a He headspace. The infiltration pressure was gradually decreasing with time (displaced APW, and any small He leak), and was replenished repeatedly until the end of the last experiment. The pressure range covered 44 – 49 bar.

Temperature conditions were stable without diurnal fluctuations, ranging seasonally from 21.5 to 25.5 °C. Critical temperature-sensitive measurements, such as electric conductivity, pH and hydraulic conductivity, were temperature-compensated, either intrinsically or explicitly (details in Waber ed. 2020).

Hydraulic conductivity referenced to 25 °C was evaluated for all sampled aliquots based on sample mass and Darcy's law (detailed data in Appendix B, method in Waber ed. 2020; Fig. 4.7-4). Observations in all AD experiments performed so far show initially lower apparent hydraulic conductivities due to the expulsion of gas from the dead volume in the outflow, and any small unsaturated volume in the sample core itself. Then, hydraulic conductivities increase, followed by a slight decrease to a steady-state value, if sufficient run-time was provided. The graph in logarithmic scale better illustrates the differences between the early gas expulsion period and the period with the expected gradual conductivity increase.

The early conductivities (after approximately 0.2 pore volumes, when gas exfiltration decreased, and conductivity increased linearly) and those measured towards the end of the experiments (Tab. 4.7-14) span a narrow range from 1.4 – 3.6 × 10^{-13} m/s. This conductivity refers to a direction perpendicular to bedding and a sample length of 8 – 9 cm, measured at very large hydraulic gradients (Tab. 4.7-2). The latter values are most representative for in situ conditions, although the confining stress of 60 bar (6 MPa) in the experiments is still considerably less than the lithostatic stresses at 748 – 934 m depth.

The APW level in the tank inadvertently dropped below the level of the top end of the capillary that infiltrates the BAC1-1 core after a percolation duration of 1.3 pore volumes (25.03.2022 3am ± 6 h: acceleration of the of infiltration pressure decrease with time from linear to exponential due to increasing conductivity caused by pore space desaturation). Subsequently, pressurised helium entered the core, which led to an exponentially increasing fluid outflow, followed by a gas breakthrough at 28.3.2022 8:44am (infiltration pressure drop to zero, helium outflow into the

sampling syringe). Quantitative investigation of the infiltration pressure vs. time using the ideal gas law allows for the quantification of the desaturated volume in the core of 5.9 ± 0.7 ml. This represents 12% of the pore volume, or 1.4% of the core. After topping up the tank (Section 4.7.5.1) and re-establishment of the hydraulic head, helium gas contained in the sample core, exfiltrated along with the porewater. This led to the visibly low apparent hydraulic conductivity shortly after 1.3 pore volumes (Fig. 4.7-4). The exponential decrease of the infiltration pressure during desaturation of the core lasted for more than 3d. In contrast, during re-saturation, the infiltration pressure decreased exponentially for only 15 min, followed by a linear decrease characteristic for advective flow under saturated conditions, at rates similar to before the gas infiltration. Thereafter, the evolution of the hydraulic conductivity continued as before the gas breakthrough. This suggests the closure of any potential preferential pathways after the gas breakthrough. The influence of the gas breakthrough on the evolution of the outflow chemistry is discussed in Section 4.7.5.4.

In experiment BAC1-5 the infiltration valve was accidentally closed from day 165 (26.04.2022) to 185 (16.05.2022). Due to the missing infiltration pressure, apparent hydraulic conductivities dropped and only slowly recovered after re-starting the infiltration, without quite reaching the values from before the closure.

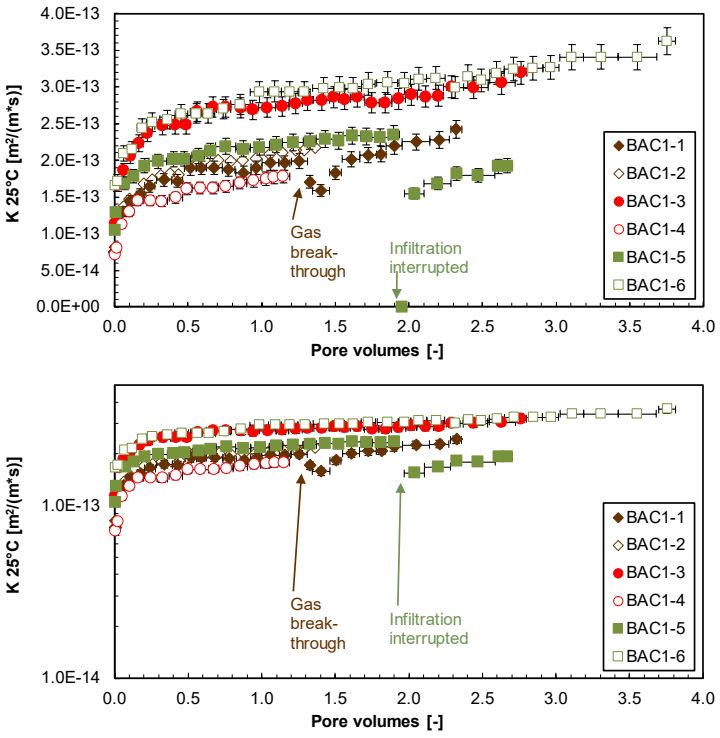

Fig. 4.7-4: Evolution of hydraulic conductivity during advective-displacement experiments

Linear scale (top) and logarithmic scale (bottom). BAC1-1 = BAC1-1-748.50-AD («Parkinsoni-Württembergica-Schichten»); BAC1-2 = BAC1-1-774.58-AD («Parkinsoni-Württembergica-Schichten»); BAC1-3 = BAC1-1-887.40-AD (Opalinus Clay); BAC1-4 = BAC1-1-910.21-AD (Opalinus Clay); BAC1-5 = BAC1-1-933.25-AD (Staffelegg Formation); BAC1-6 = BAC1-1-933.70-AD (Staffelegg Formation). Pore volume fractions relate to transport time based on water content. Experiment duration is 149 – 269 days. Horizontal length of symbol bar covers the sampling duration. Vertical bars are an estimate of combined uncertainties.

Tab. 4.7-14: Hydraulic conductivity of AD samples

Parameter	**Unit**	**BAC1-1**	**BAC1-2**	**BAC1-3**	**BAC1-4**	**BAC1-5**	**BAC1-6**
Depth	[m]	748.50	774.58	887.40	910.21	933.25	933.70
Geol. unit		«Park.-Württem.-Sch.»	«Park.-Württem.-Sch.»	Opalinus Clay	Opalinus Clay	Staffelegg Fm.	Staffelegg Fm.
Early_K (25 °C)	[m/s]	1.54×10^{-13}	1.68×10^{-13}	2.23×10^{-13}	1.45×10^{-13}	1.78×10^{-13}	2.44×10^{-13}
Late_K (25 °C)	[m/s]	2.42×10^{-13}	2.17×10^{-13}	3.19×10^{-13}	1.78×10^{-13}	1.92×10^{-13}	3.63×10^{-13}

The time axis for all data representations of sequential fluid aliquots is converted to pore volume fractions by dividing the cumulative sample mass (volume) by the water content of the core. In this way, experiments with very different hydraulic conductivities or different water contents can be represented in a meaningful way for transport. There may be some minor ambiguities in case where water contents from pre-characterisation deviate from the true water content of a sample core, or if a significant initial unsaturated porosity fraction would be present. The chosen approximation is sufficient for a visual presentation of data.

Sampled aliquots (mass) plotted versus pore volume fraction (time) provide an overview of all syringe samples taken for all six AD experiments (Fig. 4.7-5). For each experiment, 17 to 35 samples were collected, although not all were analysed.

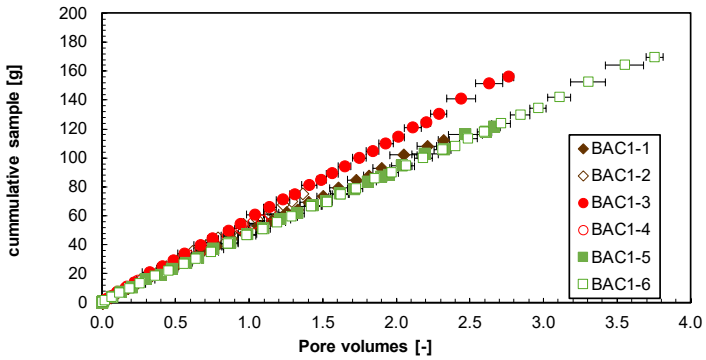

Fig. 4.7-5: Sampling schedule and sample volumes taken

BAC1-2 = BAC1-1-774.58-AD («Parkinsoni-Württembergica-Schichten»); BAC1-3 = BAC1-1-887.40-AD (Opalinus Clay); BAC1-4 = BAC1-1-910.21-AD (Opalinus Clay); BAC1-5 = BAC1-1-933.25-AD (Staffelegg Formation); BAC1-6 = BAC1-1-933.70-AD (Staffelegg Formation). Each data point represents a syringe aliquot taken, with the horizontal bar indicating the duration for sampling, here converted to pore volume fraction percolated. Different slopes reflect different volumetric flow rates scaled by porosity.

4.7.5.3 Inline measurement of electric conductivity and pH

Electric conductivity (EC) was continuously monitored in all experiments (Fig. 4.7-6, Waber ed. 2020, for method). Conductivity cells were initially calibrated but may show a drift to varying extent over time due to electrode corrosion, commonly resulting in low apparent readings. Therefore, electric conductivity values are only meant to provide an indication of salinity but are not used quantitatively.

The electric conductivities in all experiments, except BAC1-4, show a similar evolution and follow in principle the major components. After a short plateau or early increase, values decrease asymptotically and approximate the APW value. In BAC1-6, values remain somewhat above the APW, whereas in BAC1-5, the interrupted infiltration pressure at 2 pore volumes is also reflected in a drop in the electric conductivities. In both experiments, the porewater chemistry does not indicate any deviations from the approach to APW values and the shift in the EC readings is presumably related to aging of the EC cells. In BAC1-5, corrosion of the EC-cell by the stagnant and presumably higher concentrated porewater (slow evaporation in EC via fittings) can be envisioned during the period of the closed infiltration valve. BAC1-4 shows a very distinct increase of the electric conductivity in the early phase, which is not reflected in the major ion evolution. A distinctly difference in pre-calibration to post-calibration of this specific EC cell, which would account for a difference of 4 – 5 mS/cm indicates some initial coating on the electrode surfaces that redissolved during the experiment.

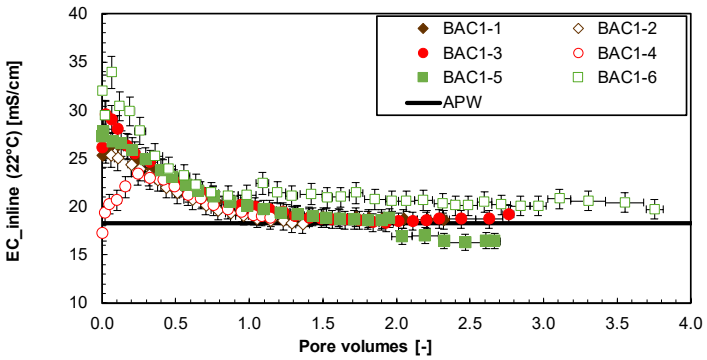

Fig. 4.7-6: Evolution of electric conductivity (22 °C) during advective-displacement experiments

BAC1-1 = BAC1-1-748.50-AD («Parkinsoni-Württembergica-Schichten»); BAC1-2 = BAC1-1-774.58-AD («Parkinsoni-Württembergica-Schichten»); BAC1-3 = BAC1-1-887.40-AD (Opalinus Clay); BAC1-4 = BAC1-1-910.21-AD (Opalinus Clay); BAC1-5 = BAC1-1-933.25-AD (Staffelegg Formation); BAC1-6 = BAC1-1-933.70-AD (Staffelegg Formation). Pore volume fractions relate to transport time based on water content. Experiment duration is 149 – 269 days. Horizontal length of symbol bar covers the sampling duration; vertical bars are an estimate of combined uncertainties.

The aim was to measure pH inline three times before/after sampling of the first four aliquots, and less frequently at later stages (method in Waber ed. 2020). Measurements took 12 – 24 hrs in most cases, to ensure that the dead volume of the very small flow-through pH cell was sufficiently flushed given the very small flow rates of the experiments. The micro-electrode was left installed in the flow-through cell and was tested before and after each pH measurement period with a standard solution. The initial calibration was made at pH 7 and 9, and simple drift tests and corrections were made with a standard solution at pH 7. The electrode slope was tested from time to time and was found to remain remarkably stable. In most cases, drift corrections over 12 – 24 hrs

were ≤ 0.1 pH units. The overall uncertainty is difficult to assess because these small electrodes may respond to manipulations at the flow-through cell (response to small strains), and also small gas bubbles temporarily affect readings. It is estimated that an error of ± 0.2 pH units is appropriate for most measurements. pH values of early aliquots measured in the laboratory are also tabulated below (Tab. 4.7-15).

These inline pH measurements (Fig. 4.7-7) are rather tricky and require careful handling of the equipment. Criteria to accept a value include a small drift and a reasonably well-defined pH-plateau, as well as a stable non-zero electric conductivity (no gas bubbles). It cannot be excluded that for long measurement durations some effect from outgassing or in-gassing of CO_2 may influence the readings. pH measurements on small aliquots taken from the syringes are slightly shifted relative to the inline measurements but show comparable evolutions with progress of percolation. Overall, inline pH values are remarkably constant during the experiments, with only a slight tendency to higher values in the early measurements. All in-line pH values are within a narrow range of 6.9 to 7.5, with the exception of the BAC1-6 initial value.

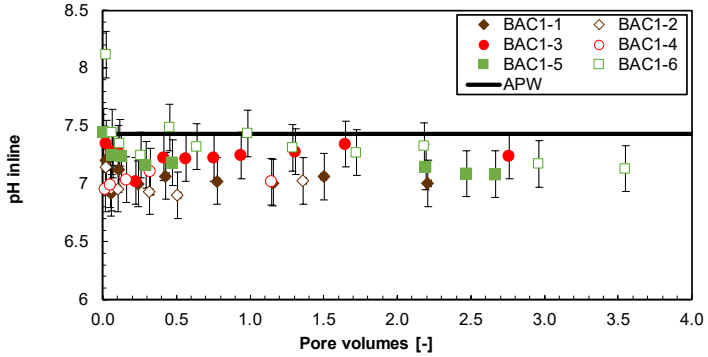

Fig. 4.7-7: Evolution of inline pH during advective-displacement experiments

BAC1-1 = BAC1-1-748.50-AD («Parkinsoni-Württembergica-Schichten»); BAC1-2 = BAC1-1-774.58-AD («Parkinsoni-Württembergica-Schichten»); BAC1-3 = BAC1-1-887.40-AD (Opalinus Clay); BAC1-4 = BAC1-1-910.21-AD (Opalinus Clay); BAC1-5 = BAC1-1-933.25-AD (Staffelegg Formation); BAC1-6 = BAC1-1-933.70-AD (Staffelegg Formation). Pore volume fractions relate to transport time based on water content. Experiment duration is 149 – 269 days. Horizontal length of symbol bar covers the sampling duration; vertical bars are an estimate of combined uncertainties.

4.7.5.4 Evolution of major and minor components

Evolution of concentrations with progress of percolation are shown in Figs. 4.7-8 to 4.7-13. Selected analytical data for the first two aliquots sampled are summarised in Tab. 4.7-15 further below, with full details in Appendix B. The composition of the earliest aliquots displaced from the core samples are the most representative for the pore fluid extracted, and this is highlighted and interpreted in Section 4.7.5.5.

The displaced **major component Cl** presents a small plateau in the first 2 – 3 samples and a subsequent continuous decrease towards the APW. Only in BAC1-4, the plateau is missing and an immediate evolution towards the APW is observed. The major component **SO_4** is only slightly higher in the initial aliquots than in the APW. In all experiments a plateau and subsequent smooth decrease towards the APW value is observed.

The cations Na, Ca are initially more concentrated in the outflow than in the injected APW and decrease steadily towards the latter (Fig. 4.7-8). In the experiments from the «Parkinsoni-Württembergica-Schichten» (BAC1-1, BAC1-2) and the Opalinus Clay (BAC1-3, BAC1-4), Na concentrations tend to match the APW at around 1.5 to 2 percolated pore volumes, whereas Ca concentrations remain at higher concentrations over the entire experiment duration. The experiments from the Staffelegg Formation (BAC1-5, BAC1-6) show a slightly different evolution with Ca concentrations approaching the APW concentration earlier than the Na concentrations. **Mg** is initially slightly more concentrated (BAC1-1 to BAC1-4) or identical in the outflow compared to the APW but shows in all experiments an evolution towards concentrations below the APW. This indicates ongoing cation exchange still after anions reach equilibrium in some cases due to the large cation reservoir on the exchanger compared with the porewater.

In experiment BAC1-1, the gas breakthrough occurred before the sample at 1.5 PV and in experiment BAC1-5, the infiltration was disrupted at 2 PV as detailed in Section 4.7.5.2. The evolutions of major and minor compounds (Fig. 4.7-10) after both events follow the same trend as before. This indicates no substantial change in transport mechanisms due to the gas breakthrough, in agreement with no substantial change in hydraulic conductivity detected (Fig. 4.7-4), or no significant effect on the porewater chemistry during a changing transport regime as in case of the reduced hydraulic conductivity in the BAC1-5 experiment.

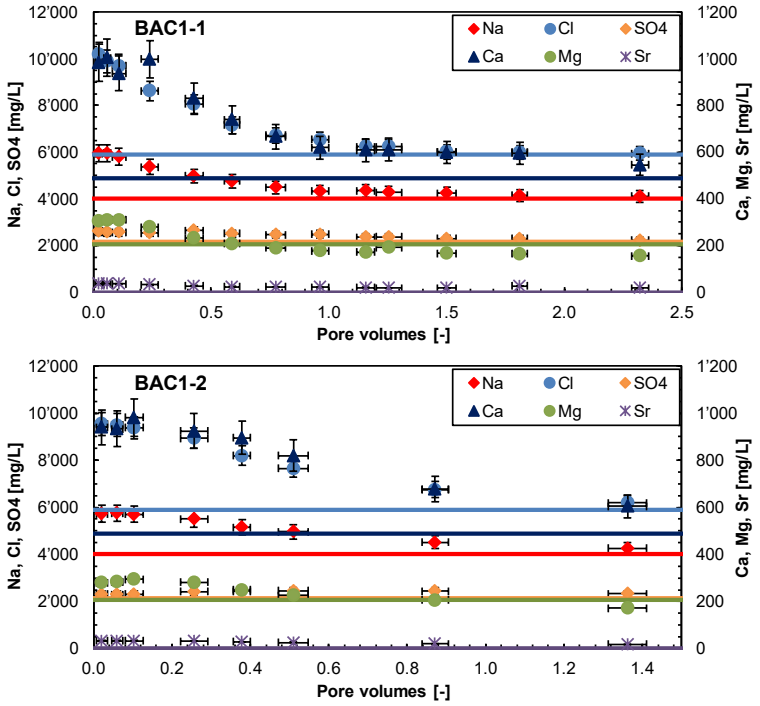

Fig. 4.7-8: Evolution of major components during advective-displacement experiments

BAC1-1 = BAC1-1-748.50-AD («Parkinsoni-Württembergica-Schichten»); BAC1-2 = BAC1-1-774.58-AD («Parkinsoni-Württembergica-Schichten»); BAC1-3 = BAC1-1-887.40-AD (Opalinus Clay); BAC1-4 = BAC1-1-910.21-AD (Opalinus Clay); BAC1-5 = BAC1-1-933.25-AD (Staffelegg Formation); BAC1-6 = BAC1-1-933.70-AD (Staffelegg Formation). Pore volume fractions relate to transport time based on water content. Experiment duration is 149 – 269 days. Horizontal length of symbol bar covers the sampling duration; vertical bars are an estimate of combined uncertainties. Horizontal lines represent the composition of the injected APW.

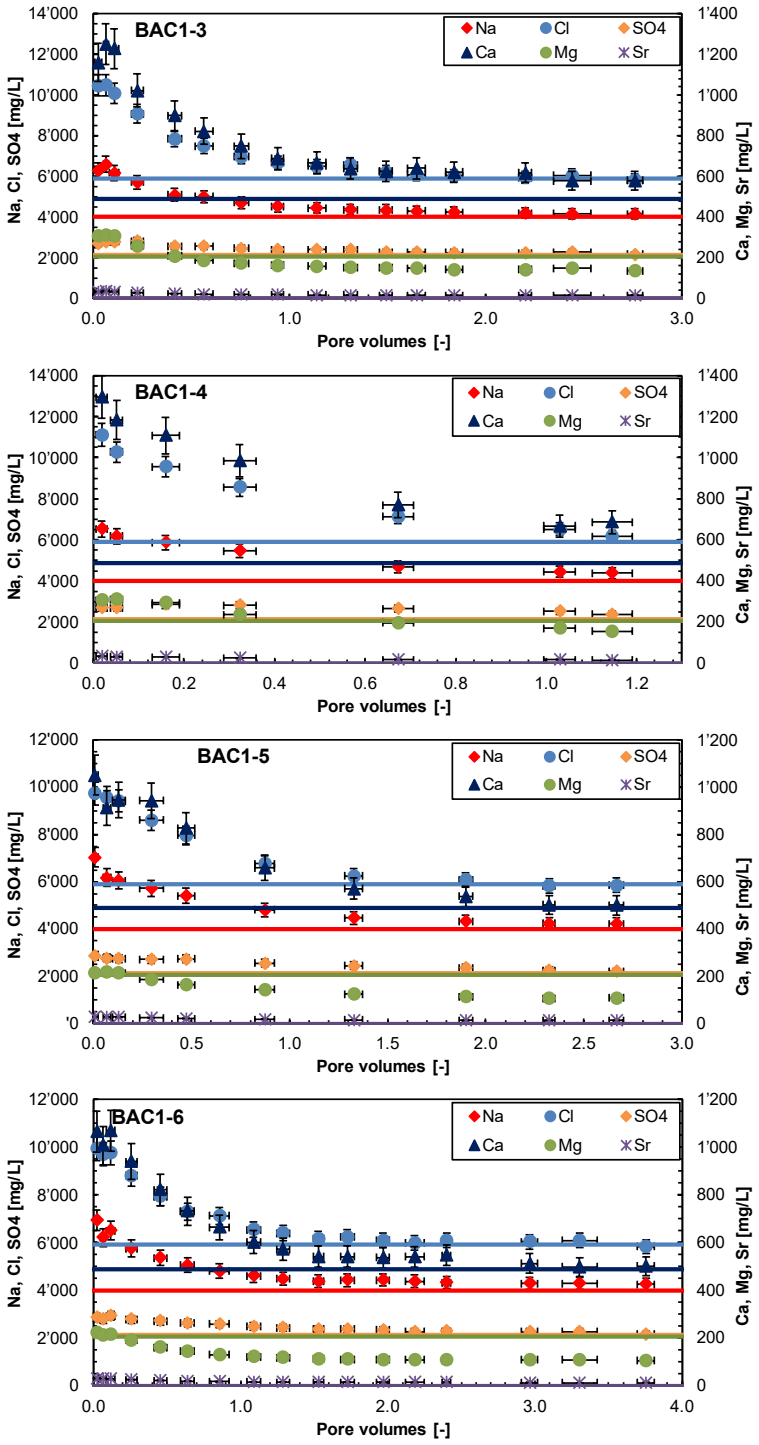

Fig. 4.7-8: continued

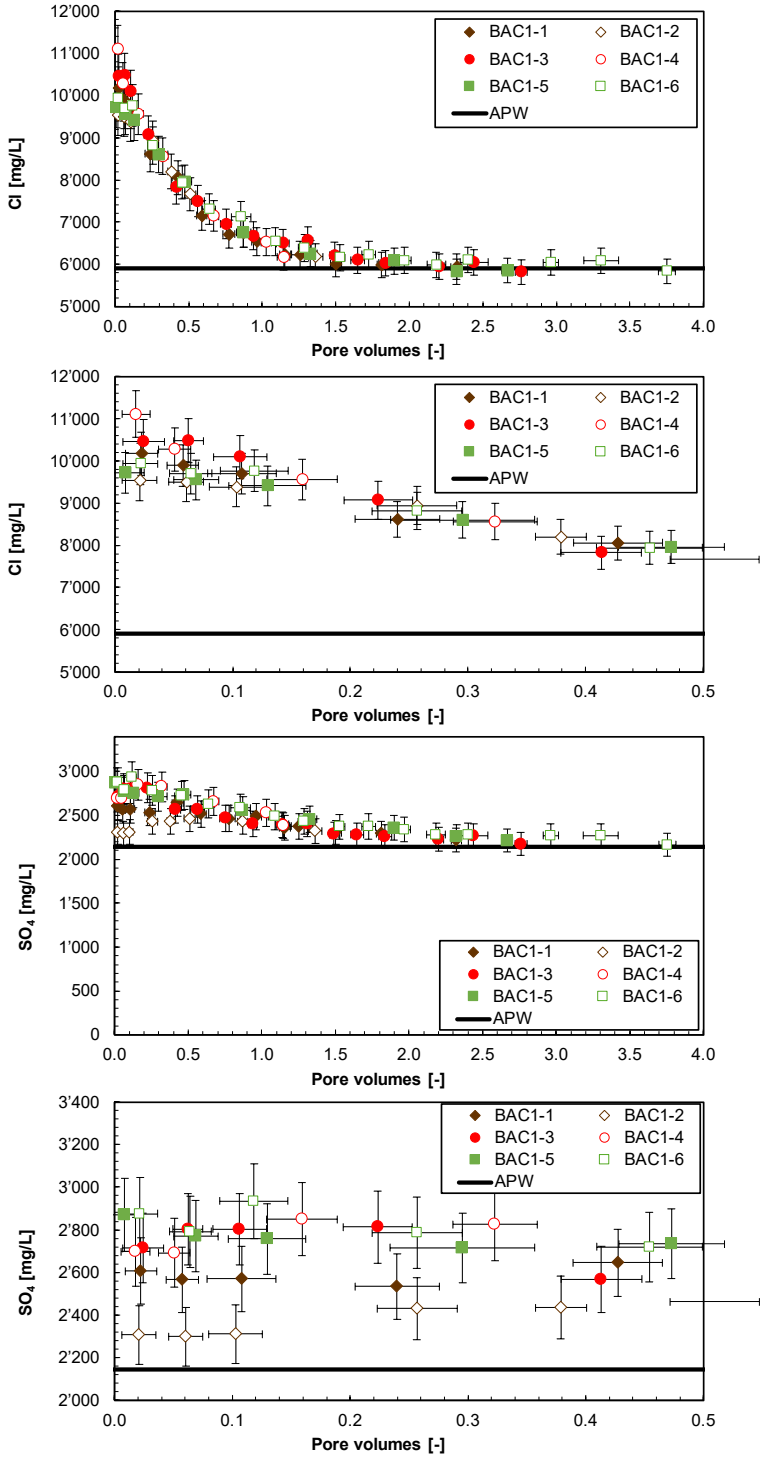

Fig. 4.7-9: Evolution of Cl and SO_4 during advective-displacement experiments: full experiment (top) and early phase (bottom)

BAC1-1 = BAC1-1-748.50-AD («Parkinsoni-Württembergica-Schichten»); BAC1-2 = BAC1-1-774.58-AD («Parkinsoni-Württembergica-Schichten»); BAC1-3 = BAC1-1-887.40-AD (Opalinus Clay); BAC1-4 = BAC1-1-910.21-AD (Opalinus Clay); BAC1-5 = BAC1-1-933.25-AD (Staffelegg Formation); BAC1-6 = BAC1-1-933.70-AD (Staffelegg Formation). Pore volume fractions relate to transport time based on water content. Experiment duration is 149 – 269 days. Horizontal length of symbol bar covers the sampling duration; vertical bars are an estimate of combined uncertainties. Horizontal lines represent the composition of the injected APW.

In all experiments, most major ion concentrations form an early plateau, with the exception of BAC1-4, where the second sample already indicates an evolution towards the APW, although remaining within the uncertainty range of the first sample. A choice was made to use average compositions of the first two analysed aliquots to best represent the porewater composition. The resulting pore fluid compositions are summarised in Tab. 4.7-15 (Section 4.7.5.5) and are also used in the integrative plots in Chapter 5.

Of the **minor components (Br, NO_3, K, Sr, Si)**, only potassium is present in the injected APW. Its concentration evolution is influenced by cation exchange reactions. Potassium concentrations in the early effluent are slightly below the APW concentrations, but in all experiments drop to even lower values until, after more than 2 percolated PV, start to approach the APW again (Fig. 4.7-10). Bromide shows a maximum in the first aliquots, gradually decreasing in all experiments, until flushed out to concentrations < 1 mg/L after 1.5 to 2 PV. This can be used as a reversed break-through of an anionic tracer (see below). Dissolved silica elutes at 3 – 6 mg/L. Sr gradually decreases to a nearly constant value of 12 – 15 mg/L in experiments with sufficient runtime, indicating some sort of buffering. One erratically high value in experiment BAC1-1 at 1.8 PV is not yet understood.

Nitrate initially elutes at concentrations up to 90 mg/L but drops to background levels of < 10 mg/L within the first 0.2 PV. Even the initially elevated values are far below the nitrate concentrations observed in some experiments from BOZ2-1 (Gimmi et al. 2022), STA3-1 (Aschwanden et al. 2022) and in particular STA2-1 (Zwahlen et al. 2023a) in which nitrate concentrations in the range of several g/L were observed. Although the origin of the previously extremely high nitrate concentrations is still not fully understood (likely produced from the kerogeneous solid organic matter), the absence in all six experiments from BAC1-1 and in experiments with the same set-up in STA3-1 and STA2-1 (Aschwanden el al. 2022, Zwahlen et al. 2023a) clearly demonstrate the successful prevention of the nitrate artefact by the additional core wrapping, and using a confining system not affected by dissolved gas (see Section 4.7.2).

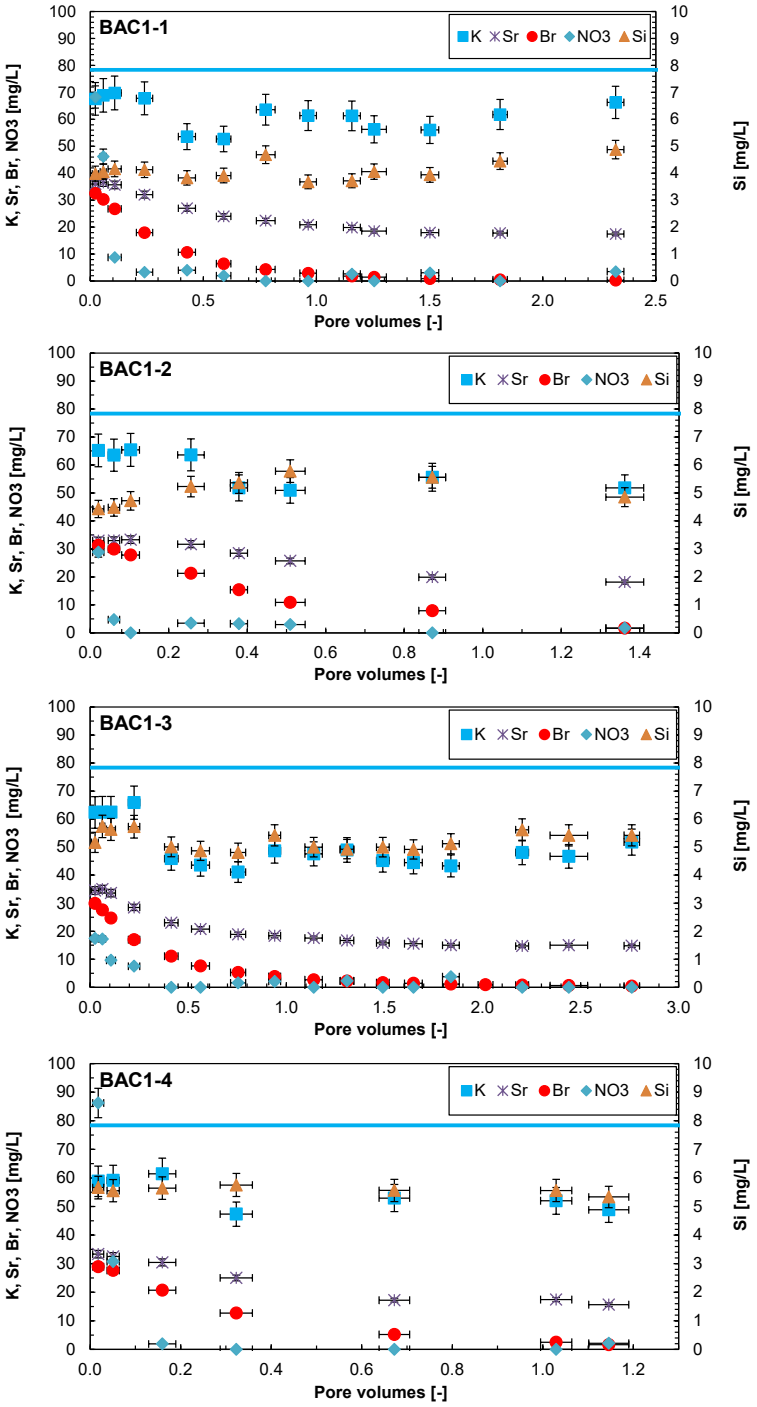

Fig. 4.7-10: Evolution of minor components during advective-displacement experiments

BAC1-1 = BAC1-1-748.50-AD («Parkinsoni-Württembergica-Schichten»); BAC1-2 = BAC1-1-774.58-AD («Parkinsoni-Württembergica-Schichten»); BAC1-3 = BAC1-1-887.40-AD (Opalinus Clay); BAC1-4 = BAC1-1-910.21-AD (Opalinus Clay); BAC1-5 = BAC1-1-933.25-AD (Staffelegg Formation); BAC1-6 = BAC1-1-933.70-AD (Staffelegg Formation). Pore volume fractions relate to transport time based on water content. Experiment duration is 149 – 269 days. Horizontal length of symbol bar covers the sampling duration; vertical bars are an estimate of combined uncertainties. Horizontal line represents the composition of the injected APW for K (0 for others).

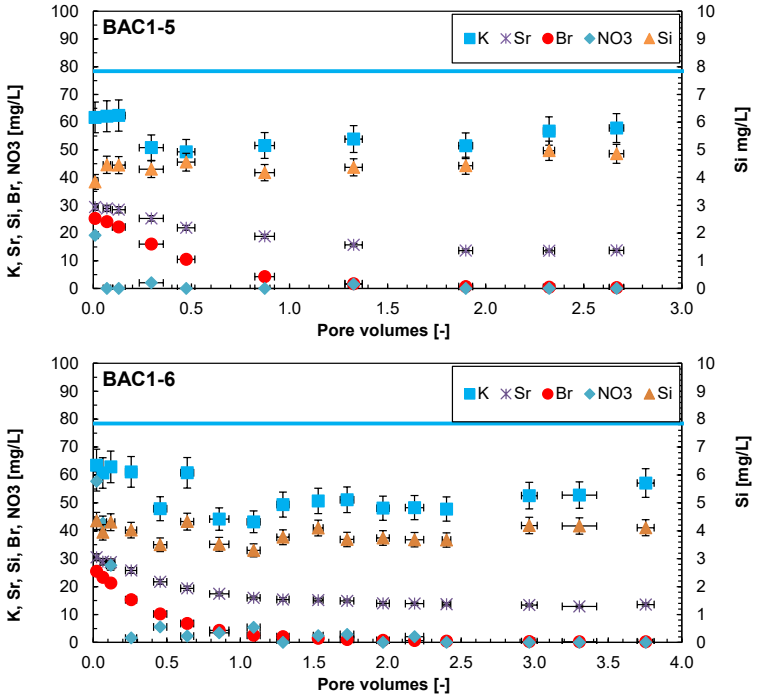

Fig. 4.7-10: continued

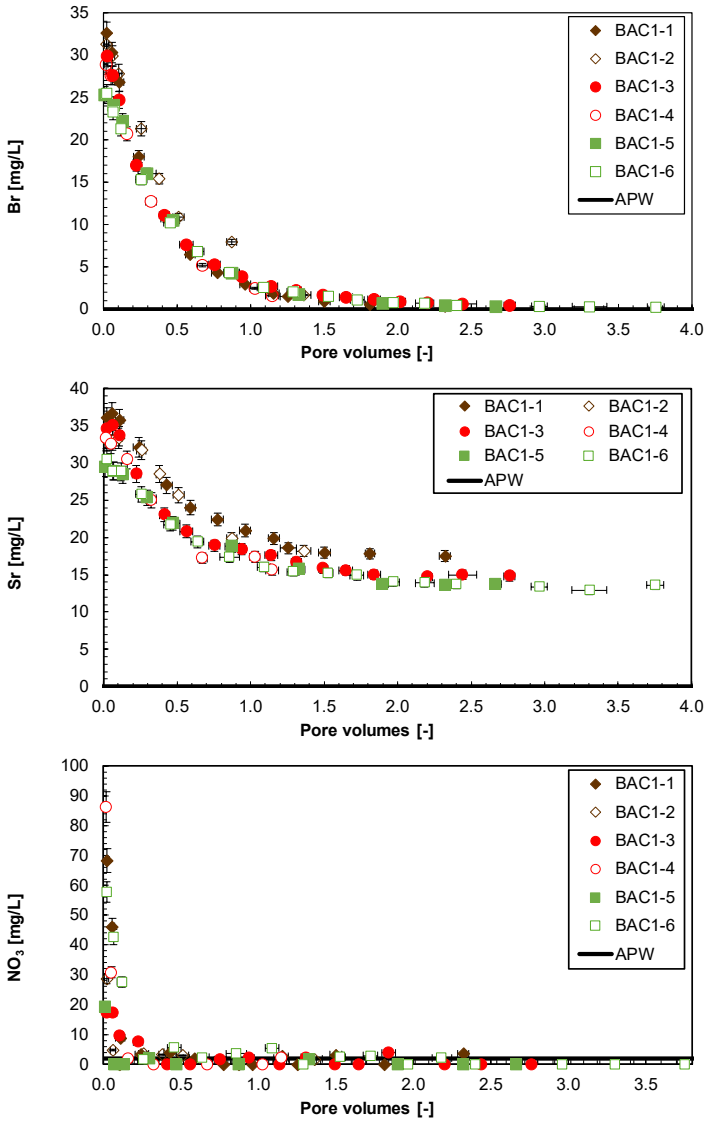

Fig. 4.7-11: Evolution of select minor components during advective-displacement experiments

BAC1-1 = BAC1-1-748.50-AD («Parkinsoni-Württembergica-Schichten»); BAC1-2 = BAC1-1-774.58-AD («Parkinsoni-Württembergica-Schichten»); BAC1-3 = BAC1-1-887.40-AD (Opalinus Clay); BAC1-4 = BAC1-1-910.21-AD (Opalinus Clay); BAC1-5 = BAC1-1-933.25-AD (Staffelegg Formation); BAC1-6 = BAC1-1-933.70-AD (Staffelegg Formation). Pore volume fractions relate to transport time based on water content. Experiment duration is 149 – 269 days. Horizontal length of symbol bar covers the sampling duration; vertical bars are an estimate of combined uncertainties. Br, Sr & NO_3 in the APW are zero. Br and NO_3 concentrations below detection are plotted at zero.

Ba and Al were measured by ICP-OES but remained below or, rarely, close to detection limits. The detection limits depend on dilution factors and were 0.25 – 0.5 mg/L for Ba, and 0.25 – 5 mg/L for Al.

The **carbon system (TIC, TOC, TC, LMWOA)** shares as a common feature that relatively large TOC concentrations are eluted initially (250 – 800 mg/L, but 1'170 mg/L for BAC1-2) that gradually decrease to 30 – 90 mg/L with progressive percolation (Fig. 4.7-12, Tab. 4.7-15 shows averages of first 2 aliquots). TOC clearly dominates the dissolved carbon inventory (TC) at early

times. The TOC can partly be explained by Low-Molecular-Weight Organic Acids (LMWOA), mainly acetate (Fig. 4.7-13). Some later samples show erratically high TOC concentrations, which cannot be explained by similarly increased LMWOA concentrations. A contamination of the samples by remaining lubricant of the syringe or ethanol from cleaning cannot be ruled out.

Aqueous extracts (Tab. 4.7-5) imply TOC values of 50 – 110 mg/L when scaled to porewater content, which is below the range observed in the early aliquots. Aqueous extracts carried out post-mortem (Tab. 4.7-8) show roughly similar TOC concentrations compared to the initial state, but with consistently higher values at the top of the core (outflow) than at the base (inflow; TOC partly flushed out of cores), where TOC levels partly drop below the detection limit. The former observations are similar to previous work, with samples from the Schlattingen-1 geothermal well (Mäder & Waber 2017) and also TBO borehole BUL1-1 (Mazurek et al. 2021), TRU1-1 (Aschwanden et al. 2021), MAR1-1 (Mäder et al. 2021) and BOZ1-1 (Wersin et al. 2022a), where no significant nitrate mobilisation was observed.

TIC elutes initially at lower concentrations than TOC and covers a wide range of concentrations, but generally increases to nearly constant concentrations around 30 – 75 mg/L depending on the core (Figs. 4.7-12 and 4.7-13). In principle, microbial activity might influence TIC/TOC, either in the syringe itself (i.e. during sampling/storage) or at the surface of the core sample, whereby a part of the organic carbon might be oxidised to inorganic carbon, e.g. coupled with microbially mediated sulphate reduction. The rather constant TIC concentrations during each experiment, however, render significant microbial alterations unlikely, as these would imply a more erratic evolution. Furthermore, microbial activity in the syringe was suppressed by regular UV radiation.

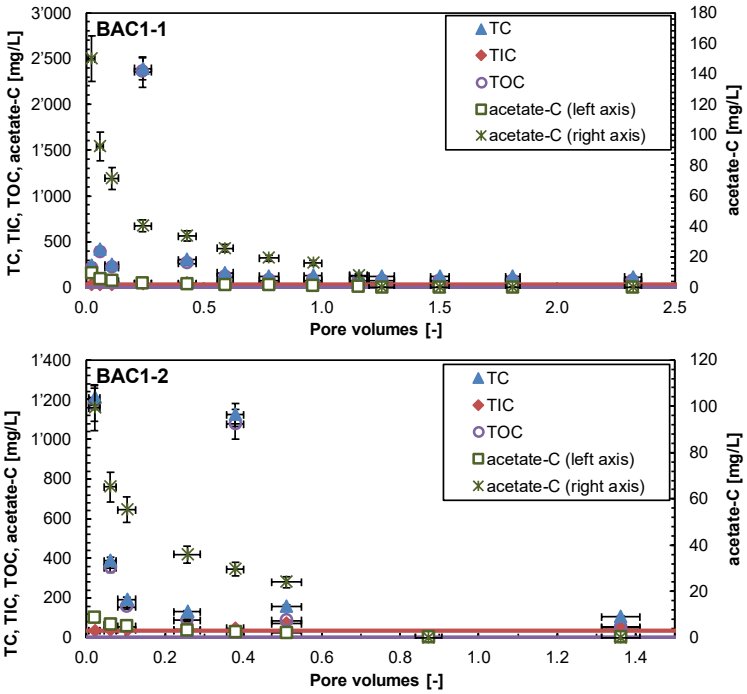

Fig. 4.7-12: Evolution of the carbon system during advective-displacement experiments

BAC1-1 = BAC1-1-748.50-AD («Parkinsoni-Württembergica-Schichten»); BAC1-2 = BAC1-1-774.58-AD («Parkinsoni-Württembergica-Schichten»); BAC1-3 = BAC1-1-887.40-AD (Opalinus Clay); BAC1-4 = BAC1-1-910.21-AD (Opalinus Clay); BAC1-5 = BAC1-1-933.25-AD (Staffelegg Formation); BAC1-6 = BAC1-1-933.70-AD (Staffelegg Formation). Pore volume fractions relate to transport time based on water content. Experiment duration is 149 – 269 days. Horizontal length of symbol bar covers the sampling duration; vertical bars are an estimate of combined uncertainties. Horizontal lines represent the composition of the injected APW.

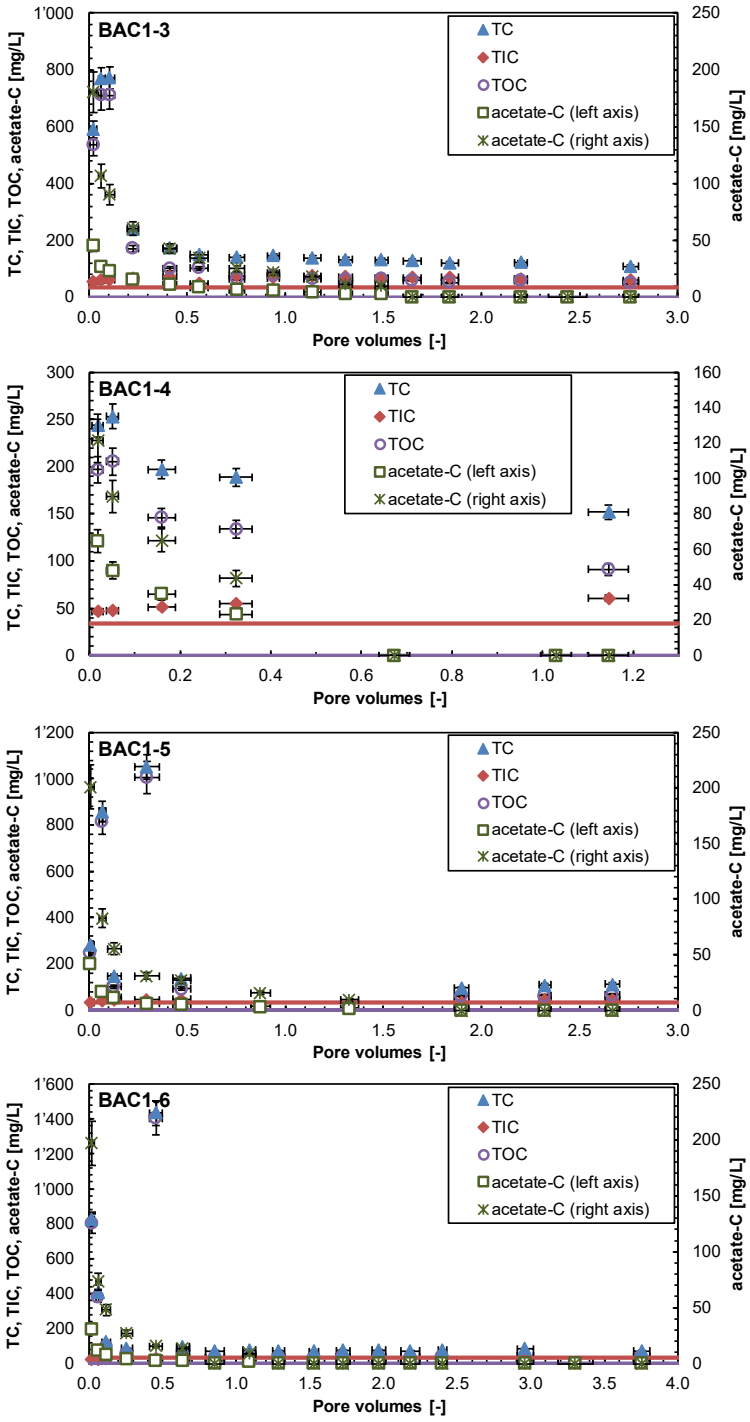

Fig. 4.7-12: continued

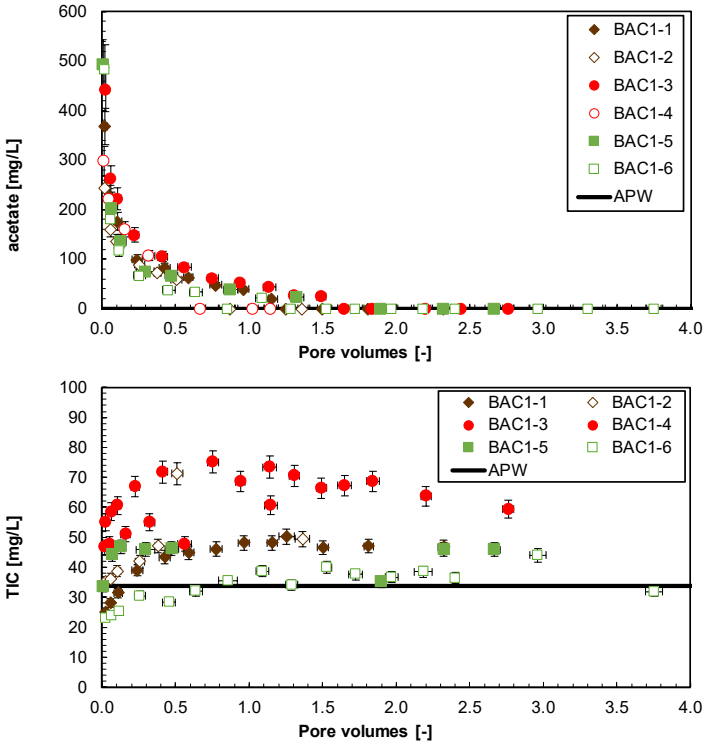

Fig. 4.7-13: Evolution of select carbon components during advective-displacement experiments

BAC1-1 = BAC1-1-748.50-AD («Parkinsoni-Württembergica-Schichten»); BAC1-2 = BAC1-1-774.58-AD («Parkinsoni-Württembergica-Schichten»); BAC1-3 = BAC1-1-887.40-AD (Opalinus Clay); BAC1-4 = BAC1-1-910.21-AD (Opalinus Clay); BAC1-5 = BAC1-1-933.25-AD (Staffelegg Formation); BAC1-6 = BAC1-1-933.70-AD (Staffelegg Formation). Pore volume fractions relate to transport time based on water content. Experiment duration is 149 – 269 days. Horizontal length of symbol bar covers the sampling duration; vertical bars are an estimate of combined uncertainties. Horizontal lines represent the composition of the injected APW. Concentrations below detection (acetate) are plotted at zero.

The **measurement of pH** was performed inline between some of the sampling intervals (Section 4.7.5.3, Fig. 4.7-7, set-up in Waber ed. 2020) and in the laboratory when syringe aliquots were prepared/preserved for analysis. The latter was done in most cases very shortly after sampling (one to a few hours), or after a few days of storage. The total range covered for all samples, inline and laboratory, is 6.9 – 7.9, with one exception (Fig. 4.7-14), both showing similar spreads of 0.6 pH units. Values of both approaches either match within the error, or show a constant offset between the inline and laboratory measured pH (systematically lower for inline pH). This can be explained by outgassing of CO_2 during the laboratory-measured pH leading to higher values.

The pH series define relatively smooth trends with percolation progress, with only small variations within each experiment. The calculated partial pressure of CO_2 is larger than atmospheric in the aliquots, and this bears the potential for outgassing and resultant supersaturation with respect to calcite, and a possibility for some loss of Ca and TIC by calcite precipitation.

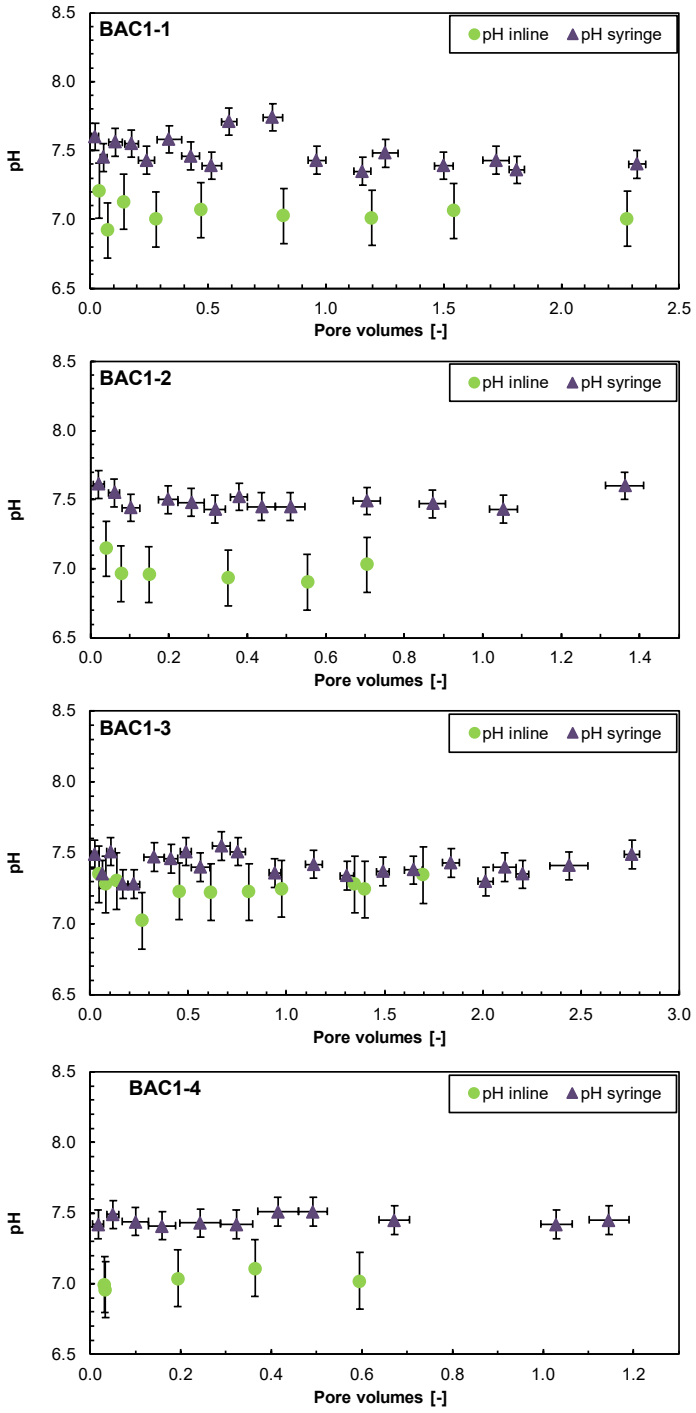

Fig. 4.7-14: Evolution of pH during advective-displacement experiments measured inline and in the outflow collected in syringes

BAC1-1 = BAC1-1-748.50-AD («Parkinsoni-Württembergica-Schichten»); BAC1-2 = BAC1-1-774.58-AD («Parkinsoni-Württembergica-Schichten»); BAC1-3 = BAC1-1-887.40-AD (Opalinus Clay); BAC1-4 = BAC1-1-910.21-AD (Opalinus Clay); BAC1-5 = BAC1-1-933.25-AD (Staffelegg Formation); BAC1-6 = BAC1-1-933.70-AD (Staffelegg Formation). Pore volume fractions relate to transport time based on water content. Experiment duration is 149 – 269 days. Horizontal length of symbol bar covers the sampling duration; vertical bars are an estimate of combined uncertainties.

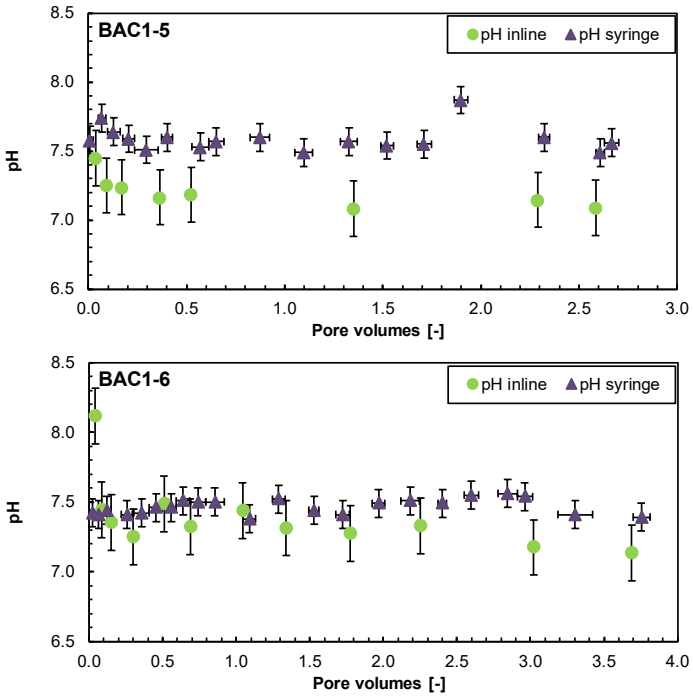

Fig. 4.7-14: continued

4.7.5.5 Early displaced aliquots representing the porewater composition

Early displaced aliquots were generally obtained by averaging the first two measured samples (Tab. 4.7-15). Interpretation of these early-displaced aliquots as being representative of the in situ porewater, contained in the core at the time of the experiment, requires integration and interpretation of the entire dataset supported with geochemical calculations. Comprehensive reactive transport simulations are expected to further constrain the initial porewater compositions, as well as the transport properties of the cores. Speciation calculations of the early compositions are presented in this data report, whereas speciation calculations for all individual syringes are provided in Appendix B. The laboratory pH values were used for the speciation calculations. TIC was used as a constraint for inorganic carbon. A high degree of consistency is observed in the early porewater aliquots obtained from rock samples of a similar depth. This is particularly the case for the close-by samples from BAC1-5 and BAC1-6, for which for most elements the concentrations differed by less than the analytical uncertainty.

The speciation calculations (Tab. 4.7-16) reveal a cation charge surplus (positive 'Charge') that is not large and partially explained by significant TOC concentrations that were not included in the speciation calculation. BAC1-1 is an exception showing a slight anion charge surplus. The aliquots are all significantly oversaturated with respect to calcite and also dolomite, as observed in earlier boreholes. Such oversaturation may result from shifts in pH linked to potential ingassing or outgassing of CO_2 during sampling and storage. Alternatively, the large TOC (and TC) contents pose analytical difficulties to obtain TIC, and associated errors may be larger than commonly assigned to TIC measurements.

Saturation is obtained for gypsum and is slightly exceeded for celestite, similar to the BUL1-1 and STA3-1, STA2-1 boreholes. In contrast, earliest aliquots were generally slightly below gypsum saturation in the boreholes from JO and ZNO. The implication is that the ion-activity products ([Sr]·[SO_4]) and ([Ca]·[SO_4]) are controlling factors, but this does not necessarily mean that these minerals are also present in the core before the experiments. There are larger SO_4, Ca and Sr concentrations in the early aliquots than in the APW. The early aliquots remain under-saturated with respect to strontianite.

Tab. 4.7-15: Composition of earliest aliquots from advective-displacement experiments representing the best estimate of the in situ porewater chemistry

Parameter	**Unit**	**BAC1-1**	**BAC1-2**	**BAC1-3**	**BAC1-4**	**BAC1-5**	**BAC1-6**
Depth	[m]	748.50	774.58	887.40	910.21	933.25	933.70
Geological unit		«Park.-Württem.-Sch.»	«Park.-Württem.-Sch.»	Opalinus Clay	Opalinus Clay	Staffelegg Fm.	Staffelegg Fm.
pH inline	[-]	7.06	7.05	7.32	6.98	7.35	7.78
pH lab	[-]	7.53	7.58	7.42	7.46	7.66	7.42
Na	[mg/L]	5'952	5'744	6'444	6'362	6'606	6'582
NH_4	[mg/L]	10	10	10	10	10	10
K	[mg/L]	68.25	64.35	62.45	58.95	61.90	62.10
Ca	[mg/L]	994	937	1'204	1'239	981	1'037
Mg	[mg/L]	306	282	310	309	217	217
Sr	[mg/L]	36.3	33.0	34.8	32.9	29.2	29.7
Ba	[mg/L]	< 0.5	< 0.5	< 0.5	< 0.25	< 0.25	< 0.5
Si	[mg/L]	4.02	4.45	5.46	5.61	4.15	4.15
Al	[mg/L]	< 50	< 50	< 50	< 25	< 25	< 50
F	[mg/L]	2.2	< 1.6	1.9	< 1.6	< 1.6	< 1.6
Cl	[mg/L]	10'032	9'520	10'468	10'690	9'636	9'816
Br	[mg/L]	31.5	30.6	28.8	28.25	24.7	24.4
NO_3	[mg/L]	57.3	16.8	17.3	58.5	19.2	50.2
SO_4	[mg/L]	2'586	2'302	2'759	2'694	2'820	2'834
TOC	[mg/L]	299	763	623	201	532	591
TIC	[mg/L]	26.7	35.7	56.8	47.2	38.9	23.5
lactate	[mg/L]	< 20	< 20	< 20	< 20	< 20	< 20
acetate	[mg/L]	298	202	353	260	349	332
propionate	[mg/L]	< 20	< 20	< 20	< 20	< 20	< 20
formate	[mg/L]	< 20	< 20	< 20	< 20	< 20	< 20
$\delta^{18}O$	[‰VSMOW]	-3.03	-3.26	-4.48	-4.73	-5.01	-4.94
$\delta^{2}H$	[‰VSMOW]	-38.7	-39.3	-41.7	-42.2	-43.9	-43.1

Tab. 4.7-16: Saturation state of earliest aliquots from advective-displacement experiments

PSI/Nagra 2012 thermodynamic database (Thoenen et al. 2014), calculated in PHREEQC for 25 °C; dolomite-o: ordered dolomite; dolomite-d: disordered dolomite; charge = Σ(cation charge) – ׀Σ(anion charge)׀ ; %-error = 100*charge/ (Σ(cation charge) + ׀Σ(anion charge)׀).

Parameter	**Unit**	**BAC1-1**	**BAC1-2**	**BAC1-3**	**BAC1-4**	**BAC1-5**	**BAC1-6**
Depth	[m]	748.50	774.58	887.40	910.21	933.25	933.70
Geological unit		«Park.-Württem.-Sch.»	«Park.-Württem.-Sch.»	Opalinus Clay	Opalinus Clay	Staffelegg Fm.	Staffelegg Fm.
Charge	[eq/kg_w]	-4.2E-03	2.2E-03	1.1E-02	3.5E-03	2.3E-02	2.0E-02
%-Error		-0.64	0.35	1.52	0.51	3.45	2.95
Acetate	[eq/kg_w]	5.0E-03	3.4E-03	6.0E-03	4.4E-03	5.9E-03	5.6E-03
Ionic strength	[mol/kg_w]	0.37	0.35	0.40	0.40	0.37	0.38
tot_alk	[eq/kg_w]	2.2E-03	3.0E-03	4.7E-03	3.9E-03	3.3E-03	1.9E-03
pH (Lab)		7.53	7.58	7.42	7.46	7.66	7.42
log$P(CO_2)$		-2.59	-2.51	-2.16	-2.28	-2.55	-2.53
SI(calcite)		0.56	0.73	0.85	0.83	0.85	0.41
SI(dolomite-o)		0.95	1.26	1.45	1.38	1.37	0.47
SI(dolomite-d)		0.40	0.71	0.90	0.83	0.82	-0.08
SI(gypsum)		-0.05	-0.11	0.04	0.04	-0.02	0.00
SI(celestite)		0.24	0.16	0.22	0.19	0.18	0.18
SI(strontianite)		-0.42	-0.28	-0.24	-0.30	-0.23	-0.68
SI(anhydrite)		-0.26	-0.32	-0.18	-0.17	-0.23	-0.21

4.7.5.6 Initial values and evolution of the composition of stable water isotopes

In all six experiments (Fig. 4.7-15), δ^2H and $\delta^{18}O$ values show a plateau in the initial ~ 0.15 and ~ 0.2 percolated pore volumes, respectively. This is followed by a smooth sigmoidal evolution towards the composition of the APW. With the exception of the experiments BAC1-2 and BAC1-4, the total percolated pore volumes were large enough to almost reach a full breakthrough of the APW.

For each of the four experiments BAC1-1 to BAC1-4, two post-mortem diffusive isotope exchange (IDE) experiments were conducted on material from the top of the core (AD outflow) and from the bottom of the core (APW inflow). These yielded the isotopic composition of the porewater remaining in the upper and lower third of the core at the end of the AD experiment. Based on the breakthrough of the APW, the remaining gradients within the final core of BAC1-1 and BAC1-3 are expected to be rather small, but still significant in case of the BAC1-2 and BAC1-4 experiments. The isotope signatures from IDE experiments should thus show values between those of the last AD aliquots and the APW, with the values from the inflow side closer to the APW and for the outflow side closer to the last sampled aliquot. This is indeed the case for δ^2H in all 4 experiments, whereas the $\delta^{18}O$ values of the IDE experiments are less consistent. $\delta^{18}O$ values obtained from the outflow side show slightly higher values than both, the last sample aliquot and the APW, whereas for the sample from the inflow side this is less resolved. This may

indicate a remaining non-equilibrated porosity fraction. Assuming a dominant advective transport in some preferential pathways, equal inflow and outflow compositions may be observed, while lateral gradients to a less-well connected porosity fraction still persist (see also Section 4.6 for the comparison with post-mortem squeezing). The observation may however also reflect the tendency of IDE experiments to yield slightly heavier isotopic compositions compared to AD and SQ experiments, in particular for $\delta^{18}O$ (Section 5.7). The reasons for this are still not resolved and require further dedicated studies. Also note that the contrast in $\delta^{2}H$ (traced in APW) is much larger than for $\delta^{18}O$ (laboratory water in APW) and thus small differences in a data series are much better resolved for $\delta^{2}H$.

In the $\delta^{2}H$ – $\delta^{18}O$ diagram, the ratios of stable water isotopes evolve on an almost straight line from the earliest and isotopically lightest ($\delta^{2}H$) or heaviest ($\delta^{18}O$) aliquot towards the APW isotopic composition (Fig. 4.7-16). For the samples from the same lithology, a high consistency is observed for the initial isotopic composition and the evolution towards the APW. It is observed that these water stable isotope ratios from the early aliquots agree well with data from the borehole profile established by the IDE method, in particularly for $\delta^{2}H$. In the $\delta^{18}O$ values a slight shift remains, which not fully understood at the current state (Section 5.7).

The breakthrough behaviour of $\delta^{18}O$ and $\delta^{2}H$ are discussed in more detail in Section 4.7.7 and compared to other data sources in Chapter 5.

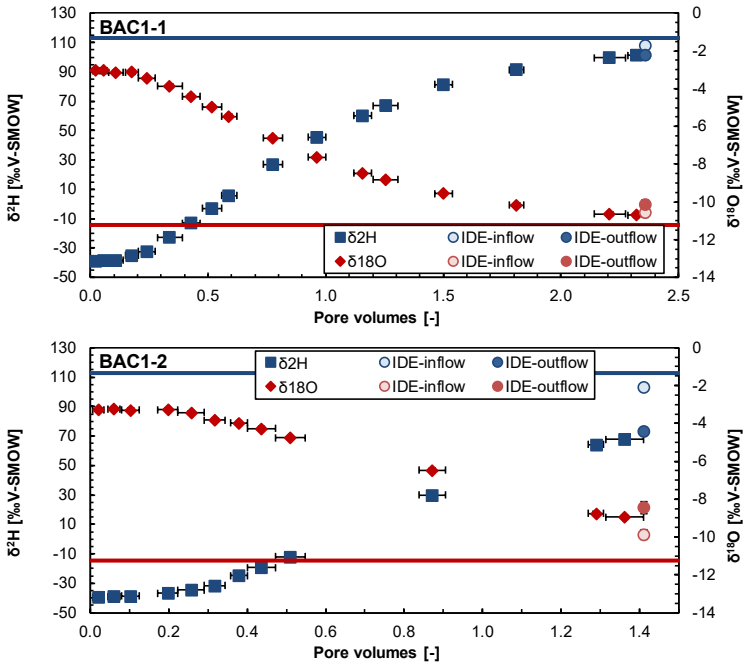

Fig. 4.7-15: Evolution of $\delta^{2}H$ and $\delta^{18}O$ during advective-displacement experiments

Circles on the right in the graphs for BAC1-1 to BAC1-4 indicate the $\delta^{2}H$ and $\delta^{18}O$ obtained in IDE experiments core material adjacent to the APW inflow and sample aliquot.

BAC1-1 = BAC1-1-748.50-AD («Parkinsoni-Württembergica-Schichten»); BAC1-2 = BAC1-1-774.58-AD («Parkinsoni-Württembergica-Schichten»); BAC1-3 = BAC1-1-887.40-AD (Opalinus Clay); BAC1-4 = BAC1-1-910.21-AD (Opalinus Clay); BAC1-5 = BAC1-1-933.25-AD (Staffelegg Formation); BAC1-6 = BAC1-1-933.70-AD (Staffelegg Formation). Pore volume fractions relate to transport time based on water content. Experiment duration is 149 – 269 days. Horizontal length of symbol bar covers the sampling duration. Measurement errors are 1.5 ‰ for $\delta^{2}H$ and 0.1 ‰ for $\delta^{18}O$.

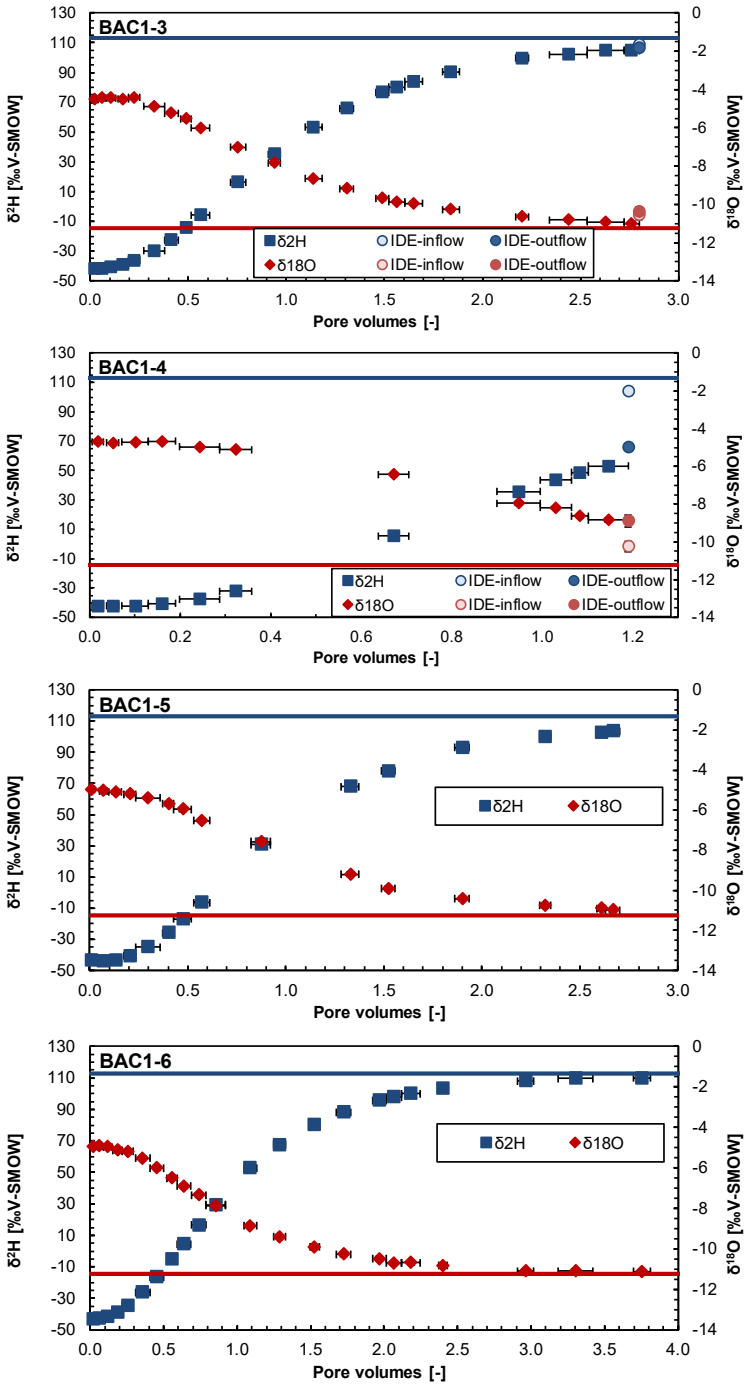

Fig. 4.7-15: continued

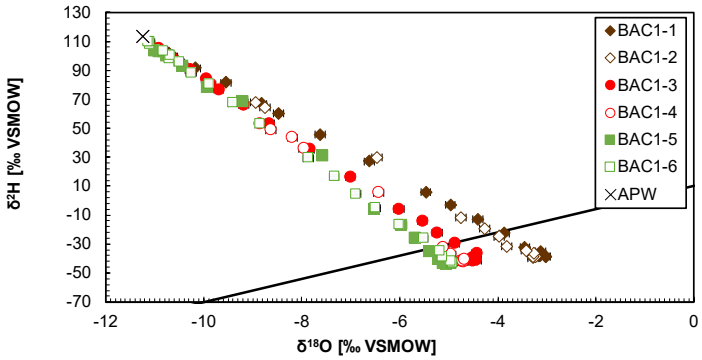

Fig. 4.7-16: Stable isotopes composition of aliquots from advective-displacement experiments

BAC1-1 = BAC1-1-748.50-AD («Parkinsoni-Württembergica-Schichten»); BAC1-2 = BAC1-1-774.58-AD («Parkinsoni-Württembergica-Schichten»); BAC1-3 = BAC1-1-887.40-AD (Opalinus Clay); BAC1-4 = BAC1-1-910.21-AD (Opalinus Clay); BAC1-5 = BAC1-1-933.25-AD (Staffelegg Formation); BAC1-6 = BAC1-1-933.70-AD (Staffelegg Formation). Pore volume fractions relate to transport time based on water content. Experiment duration is 149 – 269 days. Measurement errors are 1.5 ‰ for δ^2H and 0.1 ‰ for $\delta^{18}O$. GMWL is the global meteoric water line. First aliquots are located the furthest to the right and evolve towards the left.

4.7.6 Derivation of anion-accessible porosity

There are several ways by which chloride and bromide accessible porosity fractions may be obtained. The principle is the same: namely, the ratio between the anion concentrations obtained from aqueous extracts up-scaled to porewater content divided by that obtained from earliest aliquots from the advective-displacement experiments (discussion in Waber ed. 2020 and Mäder 2018). There are some variants depending on how water contents were measured and averaged, or how inferred water losses and volume changes may be corrected. In the case where a full or well-advanced breakthrough in chloride is captured, such a ratio may also be obtained by post-mortem aqueous extracts (top and base) and the latest aliquots sampled before the end of the experiments (for the outflow / top), or the injected APW (for the inflow / base). Normally, bromide drops below the limit of detection and only the chloride data can be evaluated for post-mortem datasets. The bromide data commonly is more 'noisy'.

The top two data lines (lines 1 and 2 in Tab. 4.7-17) list the average concentrations (Cl, Br) for the first two displaced aliquots as shown in Tab. 4.7-15. Line 3 lists the concentration of Cl in the last syringe sampled (for post-mortem evaluation). The following three lines list different Cl concentrations in aqueous extracts, up-scaled to water content: for the sample from above the AD core (line 4), for the sample from below (line 5) and a corrected and averaged value (line 6). The correction compensates for a small amount of water loss (unsaturated volume) commonly observed and evaluated from a measured net water uptake. The net water uptake is the measured water uptake (mass gain of the core during the experiment) corrected for a commonly measured small volume increase during the experiment (Section 4.7.3 and Tab. 4.7-4). The correction hinges on the assumption that sample treatment for the AD core and the off-cuts share the same history (core handling, storage, sample preparation) and therefore potentially underwent similar water losses. These corrections are rather small, with small net water uptakes. The following three lines (7 – 9) contain the same data for Br. The observed range in up-scaled concentrations is an indication of heterogeneity, mainly in the clay-mineral content. A homogeneous sample with respect to the degree of anion-exclusion should yield the same up-scaled Cl and Br concentrations,

despite differences in water content. A consistent proportion of anion-accessible porosity would then be evaluated regardless of choosing a sample from the top or from the base as a reference for the early-displaced aliquots. The two data lines for Cl suffixed with _p-m (lines 10 and 11) are the up-scaled chloride concentrations evaluated post-mortem from aqueous extracts from the top of the core (outflow to sampling) and the base of the core (APW inflow).

The final data block (lines 12 – 19 in Tab. 4.7-17) lists the accessible porosity fraction obtained by various combinations and averaging. The first four lines 12 – 15 list values that are derived without knowledge of the net water uptake. The next two lines 16 and 17, including the suffix _corr, indicate values obtained after applying a correction for net water uptake as mentioned above. The last two data lines represent the post-mortem evaluations of the top of the core (outlet, line 18) and the base of the core (inlet, line 19).

Cl accessible porosity fractions calculated for the two Opalinus Clay samples for the initial porewater composition range from 0.41 to 0.44, which is in the range determined previously for Opalinus Clay within the same approach in the TBO boreholes BUL1-1 (Mazurek et al. 2021), MAR1-1 (Mäder et al. 2021) and BOZ1-1 (Wersin et al. 2022a). The Cl accessible porosity fractions in the upper and lower confining units span a slightly larger range with 0.42 – 0.47 and 0.53 – 0.51, respectively. The values obtained for each experiment by the different calculation approaches for the initial state differ by ≤ 0.02. Values calculated for the post-mortem conditions are systematically higher by 0.03 to 0.06. For the post-mortem values for the base (line 19), this could in principle be explained by the small core expansion, which is generally observed at the infiltration side. An expansion is however not observed at the outlet side of the core. Alternatively, this shift could indicate some not yet equilibrated porosity fraction, in which porewater with a higher Cl concentration remained.

Br accessible porosity fractions determined by the different calculation approaches show a slightly larger spread. The values based on the corrected water content (line 16) are 0.02 – 0.03 higher than the respective Cl accessible porosity fractions. This was observed already previously, e.g. in BUL1-1 (Mazurek et al. 2021) and BOZ1-1 (Wersin et al. 2022a), but the reason for this is not yet fully understood. A possible explanation for the higher Br accessible porosity fraction compared to Cl could be a too high Br concentration in the aqueous extract. In contrast to Cl, Br may sorb to organic matter and partly desorb during aqueous extraction.

Tab. 4.7-17: Chloride and bromide-accessible porosity fractions calculated based on AD experiments

Preferred values are shaded in blue. See text for further details.

Line	Parameter	Unit	BAC1-1	BAC1-2	BAC1-3
	Depth	[m]	748.50	774.58	887.40
	Geol. Unit		«Park.-Württem.-Sch.»	«Park.-Württem.-Sch.»	Opalinus Clay
1	Cl-AD_ave (1-2)	[mg/L]	10'032	9'520	10'468
2	Br-AD_ave(1-2) 2nd only (+)	[mg/L]	31.45	30.60	28.75
3	Cl_AD_last	[mg/L]	5'944	6'185	5'823
4	Cl-AqEx-upscaled_top	[mg/L]	4'238	4'593	4'550
5	Cl-AqEx-upscaled_base	[mg/L]	4'234	4'539	4'770
6	Cl-AqEx-upscaled_ave_corr	[mg/L]	**4'169**	**4'494**	**4'586**
7	Br-AqEx-upscaled_top	[mg/L]	14.7	15.9	13.9
8	Br-AqEx-upscaled_base	[mg/L]	14.3	15.4	14.2
9	Br-AqEx-upscaled_ave_corr	[mg/L]	14.2	15.4	13.9
10	Cl-AqEx-upscaled_top_p-m	[mg/L]	2'687	3'172	2'799
11	Cl-AqEx-upscaled_base_p-m	[mg/L]	2'644	2'917	2'778
12	Cl-AqEx_top / Cl-AD_ave		0.42	0.48	0.43
13	Br-AqEx_top / Br-AD_ave		0.47	0.52	0.48
14	Cl-AqEx_ave / Cl-AD_ave		0.42	0.48	0.45
15	Br-AqEx_ave / Br-AD_ave		0.46	0.51	0.49
16	Cl-AqEx_ave_corr / Cl-AD_ave		0.42	0.47	0.44
17	Br-AqEx_ave_corr / Br-AD_ave		0.45	0.50	0.48
18	Cl_AqEx_p-m_top / Cl_last_AD		0.45	0.51	0.48
19	Cl_AqEx_p-m_base / Cl_APW		0.45	0.49	0.47

Tab. 4.7-17: (continued)

Line	Parameter	Unit	BAC1-4	BAC1-5	BAC1-6
	Depth	[m]	910.21	933.25	933.70
	Geol. Unit		Opalinus Clay	Staffelegg Fm.	Staffelegg Fm.
1	Cl-AD_ave (1-2)	[mg/L]	10'690	9'636	9'816
2	Br-AD_ave(1-2) 2nd only (+)	[mg/L]	28.25	24.70	24.40
3	Cl_AD_last	[mg/L]	6'166	5'852	5'840
4	Cl-AqEx-upscaled_top	[mg/L]	4'436	5'202	5'086
5	Cl-AqEx-upscaled_base	[mg/L]	4'429	5'083	5'112
6	Cl-AqEx-upscaled_ave_corr	[mg/L]	**4'362**	**5'061**	**5'018**
7	Br-AqEx-upscaled_top	[mg/L]	12.3	14.2	13.6
8	Br-AqEx-upscaled_base	[mg/L]	12.7	13.3	13.7
9	Br-AqEx-upscaled_ave_corr	[mg/L]	12.3	13.6	13.4
10	Cl-AqEx-upscaled_top_p-m	[mg/L]	2'901	3'449	3'461
11	Cl-AqEx-upscaled_base_p-m	[mg/L]	2'771	3'307	3'193
12	Cl-AqEx_top / Cl-AD_ave		0.41	0.54	0.52
13	Br-AqEx_top / Br-AD_ave		0.44	0.58	0.56
14	Cl-AqEx_ave / Cl-AD_ave		0.41	0.53	0.52
15	Br-AqEx_ave / Br-AD_ave		0.44	0.56	0.56
16	Cl-AqEx_ave_corr / Cl-AD_ave		0.41	0.53	0.51
17	Br-AqEx_ave_corr / Br-AD_ave		0.44	0.55	0.55
18	Cl_AqEx_p-m_top / Cl_last_AD		0.47	0.59	0.59
19	Cl_AqEx_p-m_base / Cl_APW		0.47	0.56	0.54

4.7.7 Transport properties marked by breakthrough of δ^2H, $\delta^{18}O$, Cl and Br

Four components can be used to elucidate transport properties by their breakthrough behaviour, namely Cl, Br, and the water isotope ratios δ^2H and $\delta^{18}O$. Chloride is a good tracer in all six experiments, because the APW has a distinctly lower Cl concentration than the in situ porewater. The resolution towards a full breakthrough is diminished because small differences between large concentrations can no longer be resolved. Bromide is a break-out tracer that is gradually flushed out of the core (no Br in the APW). Water tracers also feature a considerable contrast between the in situ porewater (Tab. 4.7-15) and the APW and are therefore suitable to trace the APW breakthrough.

For comparison (Fig. 4.7-17) all breakthrough data are normalised to 1 and inverted in case of decreasing trends to mimic a breakthrough behaviour. The normalised breakthrough of chloride, for example, is given by $1-(Cl-Cl_{APW})/(Cl_{PW}-Cl_{APW})$, where Cl_{PW} refers to the value of the early aliquots representing the in situ porewater composition (Tab. 4.7-15), which is defined as the average of the first and second measured aliquot. A slightly elevated first value (due to a potential drying of the surface, or an immediate onset of the APW breakthrough) leads to a negative value for the first sample.

In general, Cl and Br breakthroughs behave as expected. However, a small but significant difference between Br and Cl breakthrough behaviour can be observed, with Br showing a faster breakthrough than Cl. This same behaviour was illustrated in earlier work by Mäder (2018). The faster Br breakthrough contradicts the larger calculated Br accessible porosity compared to Cl (Tab. 4.7-16), which indicates that the transport in a clay-rich medium is not yet fully understood, although in this case differences are rather subtle. The gas breakthrough in BAC1-1 has no obvious effect on the breakthrough behaviour of Cl and Br. In contrast, the interrupted infiltration in BAC1-5 is reflected in a slightly retarded Cl and Br breakthrough, in line with a reduced advective transport component as manifested in the reduced apparent hydraulic conductivities. Fig. 4.7-18 compares the Cl breakthrough curves for all six experiments, highlighting the similar transport behaviour in those cores. A slightly retarded breakthrough of Cl in the experiments from the Staffelegg Formation (BAC1-5 and BAC1-6) compared to the other experiments is in line with the larger Cl accessible porosity fraction determined for these two experiments.

Fig. 4.7-19 illustrates the breakthrough behaviour of the Br/Cl molal ratio vs. time (pore volume fraction). Plotting the ratio removes some of the data scatter of the individual data series and illustrates similarities between the different experiments and thus highlights any differences. The six experiments form a set of almost overlapping curves. This further corroborates the similar Cl breakthrough curves and similar trend of Br vs. Cl breakthrough in the individual experiments. The trends of decreasing Br/Cl ratios are mainly caused by the washing out of bromide (no Br in the injected APW), the decrease in Cl concentrations towards the APW and to a minor extent by the observed difference of Br vs. Cl transport properties. The offsets between the Br/Cl ratio in the AqEx and the early aliquot visualise a difference between Cl and Br accessible porosity fractions discussed in Section 4.7.6, which are, however, small when compared with observations made in earlier experiments.

$\delta^{18}O$ and δ^2H break through more slowly compared to the anions Br and Cl, as expected in the presence of any anion-depleted porosity and under advective conditions. In all experiments for the present borehole, as well as earlier experiments with the same improved set-up for the STA3-1 and STA2-1 boreholes (Aschwanden et al. 2022, Zwahlen et al. 2023a), $\delta^{18}O$ and δ^2H breakthroughs match perfectly. Any mismatches observed in earlier AD experiments must be considered as artefacts. Moreover, as visualised in Fig. 4.7-18, the breakthrough behaviour of δ^2H in the six experiments is almost identical, indicating similar transport characteristics.

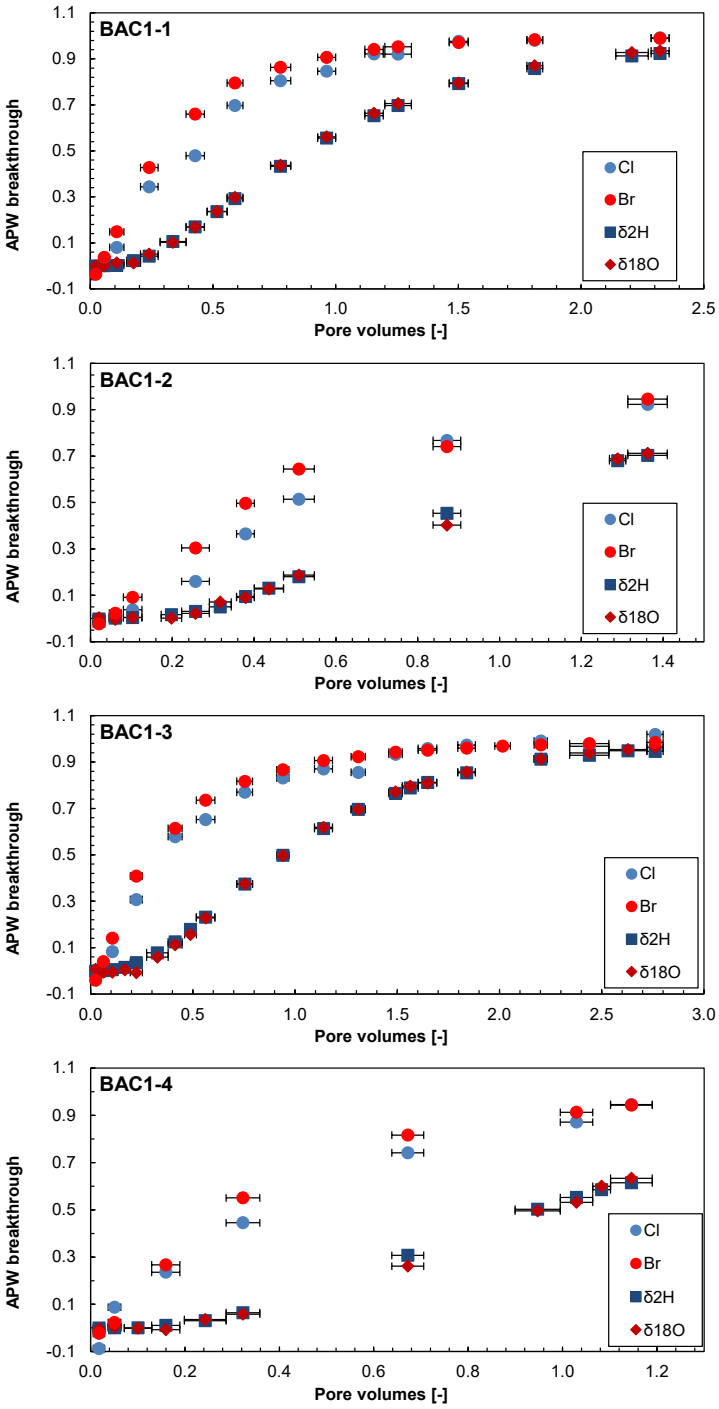

Fig. 4.7-17: Breakthrough of Cl, Br, δ^2H and $\delta^{18}O$ during advective-displacement experiments

BAC1-1 = BAC1-1-748.50-AD («Parkinsoni-Württembergica-Schichte»n); BAC1-2 = BAC1-1-774.58-AD («Parkinsoni-Württembergica-Schichten»); BAC1-3 = BAC1-1-887.40-AD (Opalinus Clay); BAC1-4 = BAC1-1-910.21-AD (Opalinus Clay); BAC1-5 = BAC1-1-933.25-AD (Staffelegg Formation); BAC1-6 = BAC1-1-933.70-AD (Staffelegg Formation). Pore volume fractions relate to transport time based on water content. Experiment duration is 149 – 269 days. Horizontal length of symbol bar covers the sampling duration.

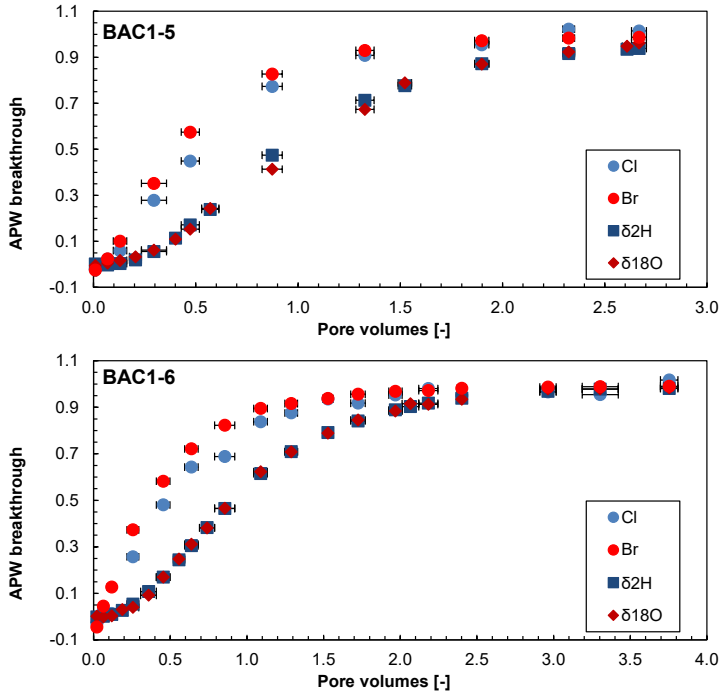

Fig. 4.7-17: continued

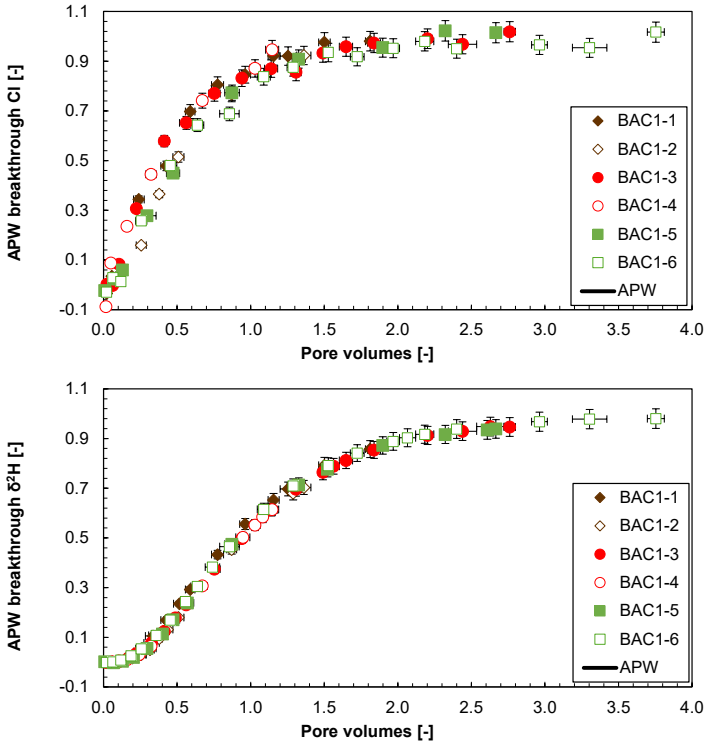

Fig. 4.7-18: Comparison of Cl and δ^2H breakthrough during advective-displacement experiments

BAC1-1 = BAC1-1-748.50-AD («Parkinsoni-Württembergica-Schichten»); BAC1-2 = BAC1-1-774.58-AD («Parkinsoni-Württembergica-Schichten»); BAC1-3 = BAC1-1-887.40-AD (Opalinus Clay); BAC1-4 = BAC1-1-910.21-AD (Opalinus Clay); BAC1-5 = BAC1-1-933.25-AD (Staffelegg Formation); BAC1-6 = BAC1-1-933.70-AD (Staffelegg Formation). Pore volume fractions relate to transport time based on water content. Experiment duration is 149 – 269 days. Horizontal length of symbol bar covers the sampling duration.

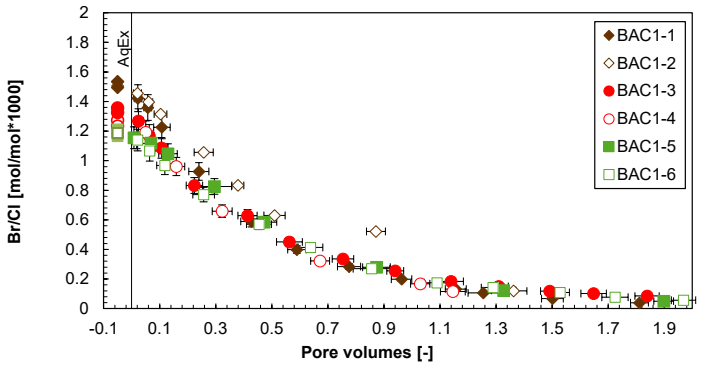

Fig. 4.7-19: Evolution of Br/Cl during advective-displacement experiments

Data on left side (top graph, 'AqEx') are the ratios measured in the aqueous extracts performed for pre-characterisation. Ratios plotted at zero correspond to later aliquots where Br concentration drops below detection. BAC1-1 = BAC1-1-748.50-AD («Parkinsoni-Württembergica-Schichten»); BAC1-2 = BAC1-1-774.58-AD («Parkinsoni-Württembergica-Schichten»); BAC1-3 = BAC1-1-887.40-AD (Opalinus Clay); BAC1-4 = BAC1-1-910.21-AD (Opalinus Clay); BAC1-5 = BAC1-1-933.25-AD (Staffelegg Formation); BAC1-6 = BAC1-1-933.70-AD (Staffelegg Formation). Pore volume fractions relate to transport time based on water content. Experiment duration is 149 – 269 days. Horizontal length of symbol bar covers the sampling duration.

4.7.8 Concluding remarks and open issues

Six advective-displacement experiments were conducted on samples from the clay-rich Dogger units and the Liassic, focussing on the derivation of constraints for a representative porewater composition, anion accessible porosity fractions and transport properties. A systematic and consistent dataset on petrophysical and geochemical properties was obtained not only of value for the specific site characterisation but also for interpretation of porewater chemistry and chloride / bromide accessible porosity fractions across all TBO drilling sites. The duplicate experiments initiated as a backup demonstrated the reproducibility of experimental results and allowed for an inter-method comparison.

Samples cover a clay-mineral content of 39 – 64 wt.-%, with proportions of illite/smectite + smectite compared to the total clay-mineral content ranging from 0.17 to 0.32. The Opalinus Clay samples show Cl-accessible porosity fractions of 0.41 and 0.44, the two samples from the overlying «Parkinsoni-Württembergica-Schichten» of 0.42 and 0.47, and the Staffelegg Formation samples distinctly higher of 0.51 and 0.53. The larger anion-accessible porosity fractions in the latter samples – despite a clay-content of 39 wt.-% – is in line with previous results from the Staffelegg Formation. The hydraulic conductivities are all in the range of $1.4 – 3.6 \times 10^{-13}$ m/s.

An improved experimental set-up, providing an additional sealing layer of the core from the confining fluid and a gas-free confining-pressure system successfully prevented experimental artefacts and disturbing effects encountered in a limited number of previous experiments from some of the TBO boreholes. These include the elevated nitrate concentrations and gas exfiltration exceeding the amount that can be explained by initial dead volumes and initially unsaturated porosity in the core, or He dissolved in the APW during infiltration. Furthermore, the previously observed diverging breakthrough behaviour of the water tracers (immediate apparent breakthrough of $\delta^{18}O$ vs. a delayed "bathtub" shape of the $\delta^{2}H$ curve) is now resolved and both tracers show a perfect match and a conservative behaviour as expected.

Like in all earlier work, there are still unusually high concentrations of TOC mobilised in the earliest aliquots, decreasing gradually to values more in line with aqueous extracts, but still at significant concentrations.

The sulphate system in all early aliquots appears to be controlled by gypsum equilibrium, with celestite showing a slight oversaturation. With ongoing percolation, the sulphate system becomes undersaturated with respect to gypsum and shows an apparent equilibrium with celestite. This has been observed previously in the other boreholes from NL, whereas porewaters from JO and ZNO were generally undersaturated with respect to gypsum.

There had been a 3-days He gas breakthrough event inadvertently provoked in one of the experiments (BAC1-1). The experiment recovered after stopping the gas injection and there was no effect visible on the breakthrough behaviour of the water isotope tracers and Cl and Br. This event attests a remarkably rapid recovery from transporting gas along some preferential pathways to a normal and seemingly undisturbed advective-diffusive fluid transport regime.

The mechanical, hydraulic and electronic / sensor aspects of the experimental set-up reliably performed for the duration of the experiments, and even longer. Likewise, the analytical procedures were already optimised, naturally limited by very small sample volumes in some cases.

4.8 Water-isotope data from diffusive-exchange experiments

Lukas Aschwanden & Thomas Gimmi

The porewater isotope composition ($\delta^{18}O$, $\delta^{2}H$) was derived by isotope diffusive-exchange experiments conducted on core material of 75 samples collected across an interval of 539.4 – 1'126.9 m depth. The obtained highly resolved profiles for $\delta^{18}O$ and $\delta^{2}H$ cover the lithologies from the «Felsenkalke» + «Massenkalk» of the Malm to the Triassic Zeglingen Formation. All experiments were conducted at the University of Bern. The relevant data are summarised in Appendix A.

4.8.1 Data evaluation

4.8.1.1 Experimental and analytical data

All the isotope diffusive-exchange experiments followed the experimental and analytical protocol given in Waber (ed.) (2020). The evaluation of the experimental and analytical data underlying the derivation of the water stable isotope composition of the in situ porewater followed a standardised procedure as detailed below.

In order to qualify for a successful isotope diffusive-exchange experiment the following criteria had to be met (within the propagated analytical uncertainties) by the two experiments (so-called LAB[10] and NGW[11] experiments) conducted for one core sample:

- No severe leakage (evaporation). In most cases, the mass of experiment container including rock and test water before and after experiment remained constant (± 0.04 g). If the loss of mass was > 0.04 g, corrections were applied to the measured isotope value of the equilibrated test water by Rayleigh-distillation calculations before calculating the porewater isotope ratio, assigning the mass loss to evaporation of the initial test water. If the correction of the $\delta^{18}O$ value for evaporation was > 0.5 ‰ VSMOW (typically meaning that the mass loss of test water was > 5% of the initial mass of test water), the porewater isotope value was marked as less reliable.
- Reasonable mass ratio of porewater to test water yielding a change in the isotope signal of the test water after equilibration outside the propagated analytical uncertainty. Porewater to test water ratios as low as 0.1 – 0.2 were accepted but the calculated isotope composition of the porewater was marked as less reliable, whereas ratios < 0.1 lead to unreliable results that were rejected. The mass of porewater in an experiment is defined by the mass of rock and its gravimetric water content. The latter is not known when starting an experiment.
- Limited mass transfer between rock and test water, i.e., 1) limited transfer of test water to rock (< 0.5 $m_{\text{test water}}$) caused either by high salinity of porewater compared to test water or hydrating mineral phases (e.g. anhydrite, halite), or 2) limited transfer of porewater to test water (< 0.02 g) caused by high salinity of test water compared to porewater. Such mass transfer between rock and test water may lead to isotope fractionation processes whose impacts on the experiments are poorly understood. Porewater isotope data not fulfilling these

[10] LAB: Isotope diffusive-exchange experiments with laboratory tap water used as test water.

[11] NGW: Isotope diffusive-exchange experiments using test water depleted in ^{18}O and ^{2}H (melt water of Antarctic ice cores).

criteria are kept but classified as less reliable provided that the experiments do not show any further unconformities and that the calculated porewater isotope data and water contents derived from isotope mass balance agree well with those of neighbouring samples (i.e. within the propagated analytical uncertainty). If this is not the case (i.e. the data constitute outliers), the experiments are considered as failed.

- Stable isotope analyses of test water solutions within the required accuracy.

Of the 75 investigated samples (150 individual experiments) only two experiment couples did not pass these criteria, owing to very low mass ratios of porewater to test water (< 0.1; BAC1-1-1033.99-PW and BAC1-1-1052.63-PW). Porewater isotope compositions calculated from these experiments are unreliable and are not shown in the following graphs.

For 7 samples (Tab. 4.8-1) the experimental data resulted in an elevated uncertainty of the calculated isotope composition of the in situ porewater. Two samples show low porewater to test water ratios of 0.1 – 0.2 and five samples show minor transfer of porewater to test water. Porewater isotope compositions calculated from these experiments are afflicted by somewhat larger uncertainties. These data are shown but marked with open symbols in the following graphs.

Tab. 4.8-1: Summary of samples showing experimental artefacts

Porewater isotope compositions calculated from these experiments are afflicted by somewhat larger uncertainties.

Elevated uncertainty of calculated porewater isotope composition owing to:	**Sample ID**
Low porewater to test water ratios (0.1 – 0.2)	BAC1-1-579.46-PW BAC1-1-617.51-PW
Transfer of porewater to test water (> 0.02 g)	BAC1-1-798.61-PW BAC1-1-1065.13-PW BAC1-1-1080.67-PW BAC1-1-1090.95-PW BAC1-1-1108.32-PW
Relative difference of more than 20% between water contents from isotope mass balance and gravimetry (criterion 2 in Section 4.8.1.2)	BAC1-1-1011.38-PW

4.8.1.2 Calculation of porewater composition and water contents

Porewater $\delta^{18}O$ and $\delta^{2}H$ values were calculated using equation 76 in Appendix A in Waber (ed.) (2020) considering the ratio *q* of the gravimetric water contents of the individual subsamples used in the experiments (for details see Appendix A in Waber ed. 2020). Water contents could then also be calculated by mass balance from the porewater isotope values. The robustness of the calculated porewater $\delta^{18}O$ and $\delta^{2}H$ values was further tested according to the following criteria:

- A relative difference of less than 20% between the water contents calculated from $\delta^{18}O$ and $\delta^{2}H$ data derived from the NGW experiments with test water depleted in ^{18}O and ^{2}H.
- A relative difference of less than 20% between the average water content calculated by isotope mass balance from $\delta^{18}O$ and $\delta^{2}H$ data and the average of the gravimetric water content of the two subsamples used in the experiments.

If the relative difference in the different water contents is larger than 20% the calculated porewater $\delta^{18}O$ and $\delta\ ^{2}H$ values are considered less reliable. Such data may still be used for further interpretation by accepting the larger propagated uncertainty; they are marked with open symbols in the following graphs.

Of the 73 samples that passed the experimental quality criteria (*cf.* Section 4.8.1.1; including samples with elevated experimental uncertainties) only one sample (BAC1-1-1011.38-PW) shows larger discrepancies according to criterion 2 above (Tab. 4.8-1 and Figs. 4.8-1 and 4.8-2). This sample does not show any experimental irregularities but a very low *q* value (0.71). Thus, the difference between the average of the water contents derived by isotope mass balance and the average of the gravimetric water content of the two subsamples reflects lithological heterogeneity. Note that in anhydrite-bearing lithologies hydration of anhydrite during the isotope diffusive-exchange experiments also plays a role, although its extent and effect is unknown at this stage.

All samples that pass the above criterion 2 display a consistent, previously observed relationship between the average water content derived by isotope mass balance and the average of the gravimetric water content of the subsamples used in the experiments, the former being around 9% larger than the latter (Fig. 4.8-2). As the water content is generally well correlated with the clay-mineral content of the rocks (*cf.* Section 4.3), it was postulated that this difference might be associated with minor exchange with water of different isotope composition adsorbed on clay minerals (e.g. Pearson et al. 2003). However, no stringent explanation exists at this stage.

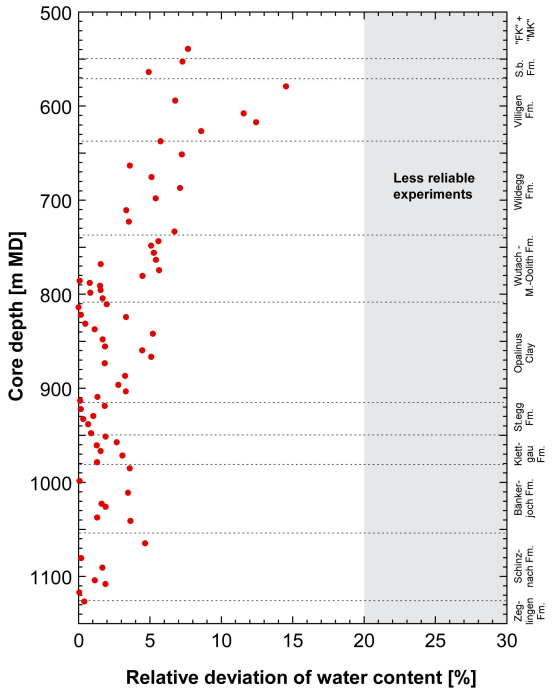

Fig. 4.8-1: Relative deviation of water contents obtained from $\delta^{18}O$ and $\delta^{2}H$ mass balance

The relative deviation is defined as the absolute difference between the water contents calculated from the $\delta^{18}O$ and $\delta^{2}H$ mass balance, divided by the latter (using data from the NGW experiment only; Waber ed. 2020). For all investigated samples the relative deviation of water contents obtained from $\delta^{18}O$ and $\delta^{2}H$ mass balance is < 20% (see text for details).

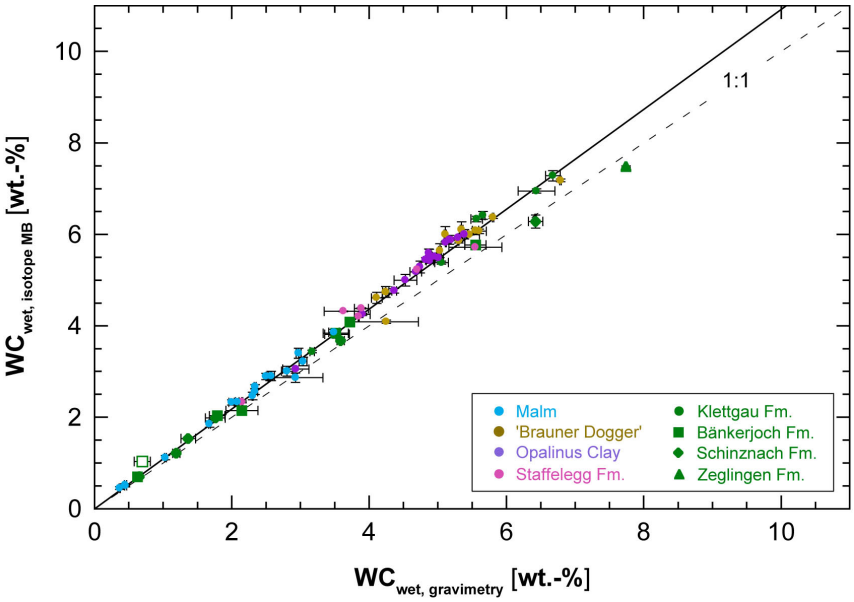

Fig. 4.8-2: Average water content obtained by water-loss at 105 °C ($WC_{wet,\ gravimetry}$) of subsamples LAB and NGW vs. average water content calculated from $\delta^{18}O$ and $\delta^{2}H$ mass balance from NGW diffusive-exchange experiments ($WC_{wet,\ isotope\ MB}$)

Open symbols in this plot refer to samples showing differences larger than 20% between the average water content derived by isotope mass balance and the average gravimetric water content of the two subsamples used in the experiment. These samples are excluded from the linear regression (solid black line), which has a slope of 1.09.

4.8.2 $\delta^{18}O$ and $\delta^{2}H$ values of porewater

4.8.2.1 Depth profiles of porewater isotope composition

All the porewater isotope data that pass the various quality criteria are illustrated in Fig. 4.8-3 as a function of depth. In the uppermost part of the investigated sequence across the interval «Felsenkalke» + «Massenkalk» – Villigen Formation $\delta^{18}O$ and $\delta^{2}H$ values of the porewater generally evolve from –3.6 ‰ VSMOW and –46 ‰ VSMOW, respectively, towards more enriched signatures reaching a general maximum of –1.9 ‰ VSMOW and –33 ‰ VSMOW, respectively, at the base of the Villigen Formation. However, the scatter of the data and uncertainties are large, which is mainly related to experimental difficulties associated with these lithologies, such as, e.g., low water contents. From the base of the Villigen Formation down to the base of the Klettgau Formation, $\delta^{18}O$ and $\delta^{2}H$ values of the porewater show remarkably well-defined, continuous, approximately linear profiles characterised by a steady depletion in heavy isotopes reaching values of –5.3 ‰ VSMOW and –45 ‰ VSMOW, respectively in the water-conducting zone of the Klettgau Formation at around 970 m depth (*cf.* Section 5.7 for further discussion). The main difference between the trends of porewater $\delta^{18}O$ and $\delta^{2}H$ values is that – relatively – the depletion in ^{18}O is distinctly stronger than that in ^{2}H. This slightly different behaviour is also illustrated in Fig. 4.8-4, which shows the depth profile of deuterium excess (defined as $\delta^{2}H - 8 \times \delta^{18}O$; deuterium excess is +10‰ for a sample that lies on the GMWL, lower values of deuterium excess reflect sample positions to the right of the GMWL in a plot of $\delta^{18}O$ vs. $\delta^{2}H$; note that the deuterium excess as used at this stage carries no direct implications about the paleoclimate at the time of infiltration). From the base of the Villigen Formation down to the Klettgau Formation, D-excess linearly increases from –21 ‰ to 0 ‰.

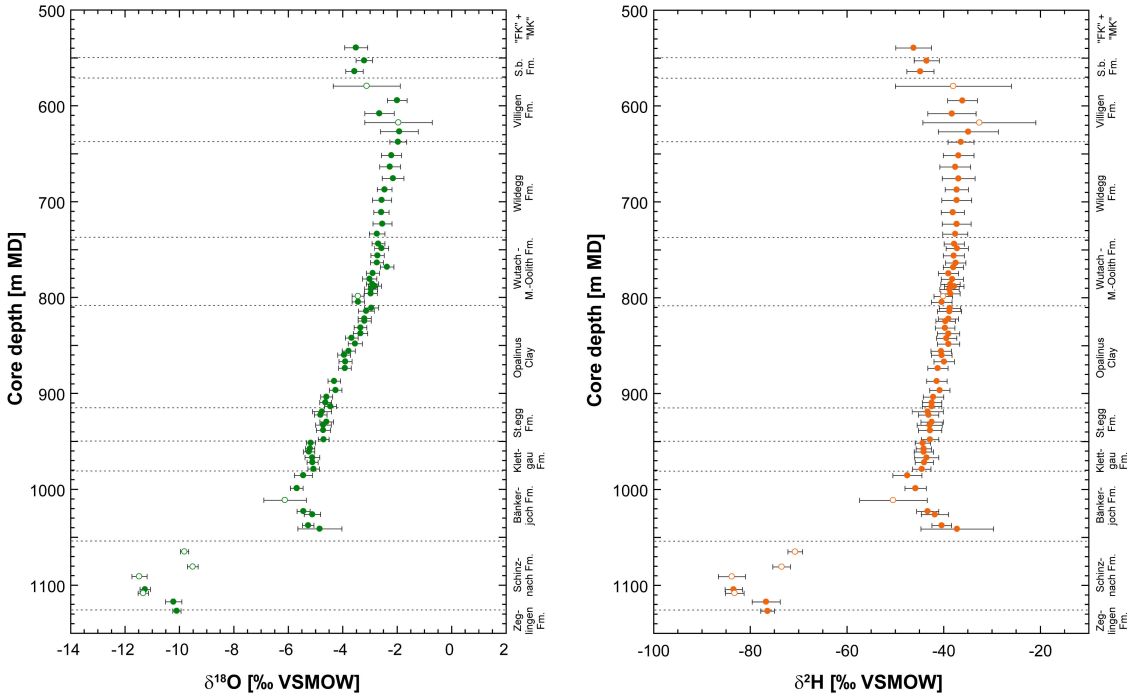

Fig. 4.8-3: Depth distribution of porewater $\delta^{18}O$ and $\delta^{2}H$ values obtained from isotope diffusive-exchange experiments

Open symbols refer to porewater isotope values which are less reliable owing to experimental artefacts as described in Section 4.8.1.1.

In the top of the Bänkerjoch Formation, both $\delta^{18}O$ and $\delta^{2}H$ values start to increase and they reach a local maximum of –4.9 ‰ VSMOW and –37 ‰ VSMOW, respectively, at the base of the Formation before sharply evolving towards most negative values in the water-conducting zone of the Schinznach Formation at around 1'100 m depth (–11.5 ‰ VSMOW and –84 ‰ VSMOW, respectively; *cf.* Section 5.7). Further down towards the Zeglingen Formation, porewater isotope signatures tend to increase again. D-excess generally increases from the top of the Bänkerjoch Formation towards a maximum of around 8.0 ‰ in the water-conducting zone of the Schinznach Formation (*cf.* Section 5.7) before decreasing towards the top of the Zeglingen Formation.

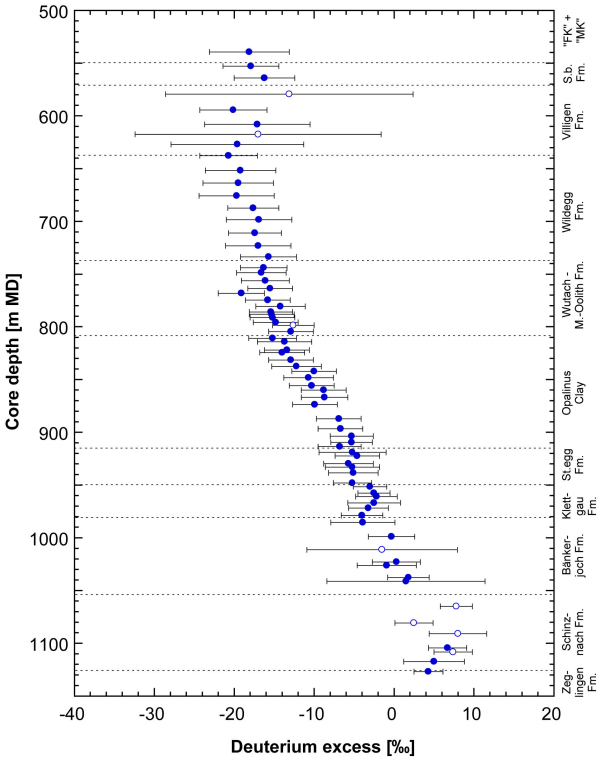

Fig. 4.8-4: Depth trend of deuterium excess in porewater based on the isotope diffusive-exchange technique

Deuterium excess is +10 ‰ for a sample that lies on the GMWL. Lower values of deuterium excess reflect sample positions to the right of the GMWL in a plot of δ^2H vs. $\delta^{18}O$. Note that the deuterium excess as used at this stage carries no genetic implications about the origin of H_2O, e.g. on paleoclimate at the time of infiltration. Open symbols refer to samples which are less reliable owing to experimental artefacts as described in Section 4.8.1.1.

4.8.2.2 δ^2H versus $\delta^{18}O$ and comparison with Global Meteoric Water Line

In the δ^2H - $\delta^{18}O$-diagramm (Fig. 4.8-5), some remarkably regular and partly near-linear trends can be observed. Porewater isotope signatures at the top of the cored section in the «Felsenkalke» + «Massenkalk» and in the Schwarzbach Formation fall to the right of the Global Meteoric Water Line (GMWL) and even more enriched $\delta^{18}O$ and δ^2H values are observed in the underlying Villigen Formation. From the Wildegg Formation down to the top of the Bänkerjoch Formation the porewater isotope composition continuously evolves towards values more depleted in ^{18}O and ^2H and approaching the GMWL, indicating a meteoric component in the latter porewaters. In the remainder of the Bänkerjoch Formation the porewater $\delta^{18}O$ and δ^2H values evolve along a trajectory about parallel to the GMWL towards signatures more enriched in both ^{18}O and ^2H. Finally, they sharply drop to distinctly more negative values in the Muschelkalk located on or slightly to the right of the GMWL.

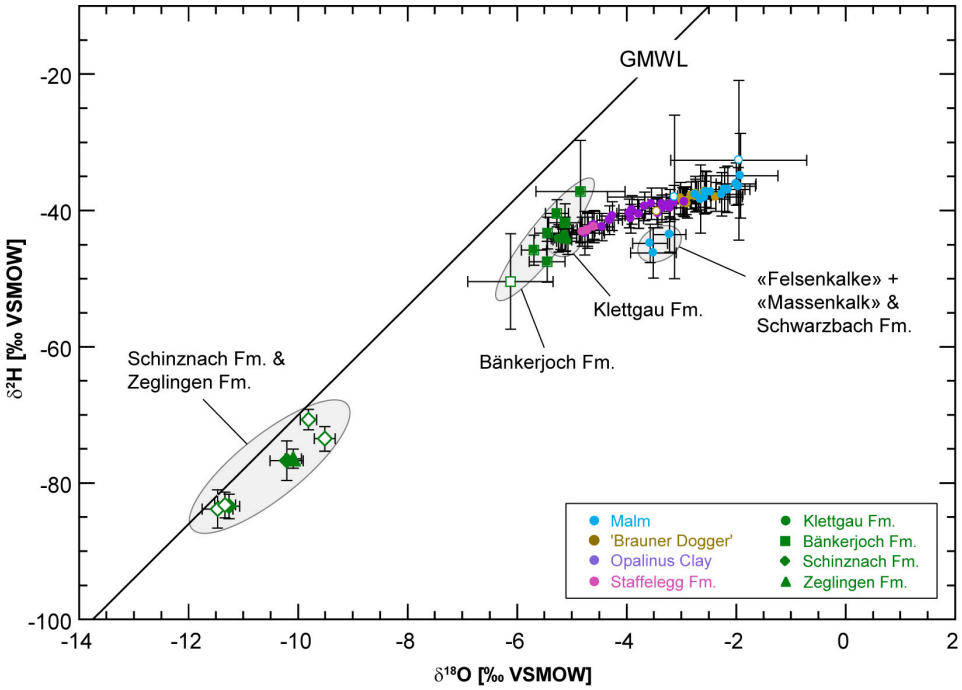

Fig. 4.8-5: δ^2H vs. $\delta^{18}O$ values of porewater obtained from isotope diffusive-exchange experiments

GMWL = Global Meteoric Water Line ($\delta^2H = 8 \times \delta^{18}O + 10$ ‰ VSMOW; Craig 1961), open symbols refer to porewater isotope values which are less reliable owing to experimental artefacts as described in Section 4.8.1.1.

5 Discussion of porewater data

5.1 Chloride data and estimation of Cl- and Br- accessible porosity

Paul Wersin, Carmen Zwahlen, Martin Mazurek, Thomas Gimmi

Chloride, a major component in the porewater, has been determined by squeezing (Section 4.6), advective displacement (Section 4.7) and aqueous extraction (Section 4.4). This anion is considered to behave as a conservative species with no or very limited interaction with the minerals. The same can be said for bromide, which occurs at much lower concentrations in the porewater. In argillaceous rocks, anions are repelled from the negative structural charge of the clay-mineral surfaces and are thus affected by ion exclusion. In other words, they only 'see' part of the total water-filled porosity, the fraction of which is often termed anion-accessible porosity (Pearson 1999, Pearson et al. 2003) or also 'free' porosity. Ion exclusion is not complete according to theory and depends on distance from charged surfaces, but here this simplifying assumption is made for adopting a simplest possible model.

Knowing the concentration of Cl per bulk (total) porewater in a sample from aqueous extraction ($C_{Cl\ in\ bulk\ porewater}$), the Cl-accessible porosity fraction, f_{Cl}, can be estimated from Cl measurements in squeezing ($C_{Cl\ in\ squeezed\ water}$) or advective displacement ($C_{Cl\ in\ adv.\ displaced\ water}$) experiments, assuming that the latter represent the composition of the 'free' porewater:

$$f_{Cl} = \frac{n_{anion-accessible}}{n_{total}} = \frac{C_{Cl\ in\ bulk\ porewater}}{C_{Cl\ in\ squeezed\ or\ adv.displaced\ water}}$$

$C_{Cl\ in\ bulk\ porewater}$ is calculated from:

$$C_{Cl\ in\ bulk\ porewater} = \frac{C_{Cl\ in\ aq.extract}}{WC_{dry}\ {}^{S}/_{L}}$$

with C = concentration [mg/L], n = porosity [–], WC_{dry} = water content relative to dry rock mass [g/g], S/L = solid/liquid ratio of aqueous extraction experiment [g/g]. The Br-accessible porosities are derived in an analogous fashion.

The anion-accessible porosity fractions have been derived according to the above equation for squeezed and advectively displaced porewaters (Tabs. 4.6-8, 4.6-9 and 4.7-17). Both methods enable to mobilise porewater that is thought to be a proxy of the so-called 'free' porewater (not affected by the negatively charged clay surface). It should be noted, however, that the two methods operate by entirely different mechanisms. Whereas porewater is mobilised by mechanical compaction implying a deformation of the porespace in the squeezing method, this is achieved by a strong hydraulic pressure gradient imposed by an artificial porewater in the advective displacement method. Thus, method-specific artefacts may be expected and likely not the same volume of the porespace is sampled by the two methods. In the case of non-reactive Cl, experimental artefacts appear to be minor as suggested from previous studies (e.g. Mazurek et al. 2021). In the case of the squeezed waters, it is generally assumed that the waters squeezed at the lowest pressure best reflect the in situ porewater (Mazurek et al. 2015, Wersin et al. 2016). For the advectively displaced waters, the first two measured aliquots are assumed to be the most representative of the in situ porewater (Section 4.7).

The derived values of the Cl-accessible porosity fraction (f_{Cl}) for the two datasets are shown as a function of the clay-mineral content in Fig. 5.1-1, with the SQ values derived according to the method 1 and method 2 whereby method 1 is deemed to be the preferred method (see Section 4.6,

Tab. 4.6-8). Porosity fractions obtained from AD and SQ experiments (method 1) range between 0.41 and 0.61. The corresponding mean value of all AD and SQ samples is 0.511 ± 0.065. This value is similar as that for the BUL1-1 borehole (0.52 ± 0.06), but somewhat above values for the other previous boreholes TRU1-1 (0.45 ± 0.05, Aschwanden et al. 2021), MAR1-1 (0.46 ± 0.08, Mäder et al. 2022), STA3-1 (0.4 5 ± 0.05, Aschwanden et al. 2022), STA2-1 (0.48 ± 0.06, Zwahlen et al. 2023a), BOZ1-1 (0.42 ± 0.08, Wersin et al. 2022a) and BOZ2-1 (0.42 ± 0.07, Gimmi et al. 2022). It should be noted that the f_{Cl} values derived from AD are below those of SQ, with an average value of 0.46 for AD compared to 0.54 for SQ.

There is no clear trend with clay-mineral content within the range of the AD and SQ samples (39 – 68 wt.-%). There are no data available from BAC1-1 at lower clay-mineral contents where a dependency on this parameter would be expected, as indicated for example for the BUL1-1 data (also depicted in Fig. 5.1-1). It would be important to know the anion accessibility also at lower clay-mineral contents because within the sampled interval the lithologies in the BAC1-1 profile vary substantially. In order to derive a porewater profile for Cl, the anion accessibility in these lithologies must be known or assumed. In BUL1-1, which also lies in the Nördlich Lägern siting region, an increasing trend of f_{Cl} with decreasing clay-mineral content was suggested below a clay-mineral content of 20 wt.-% (even though the precise relationship could not be discerned) (Fig. 5.1-1). In other boreholes, such as TRU1-1, the increasing trend of f_{Cl} seems to start already at 40 wt.-% clay-mineral content, whereas in BOZ1-1 this "threshold" seems to occur at about 25 wt.-%. Given these premises, we consider a uniform f_{Cl} value of 0.51 for clay mineral contents > 20 wt.-% as "reference" for deriving the Cl profile for the entire sequence, but also explore the effect when assuming a "threshold" clay-mineral content of 40 wt.-% (Section 5.2). Below these "threshold" clay-mineral contents, a linear increase of f_{Cl} to a value of 1 at a clay-mineral content of zero is assumed.

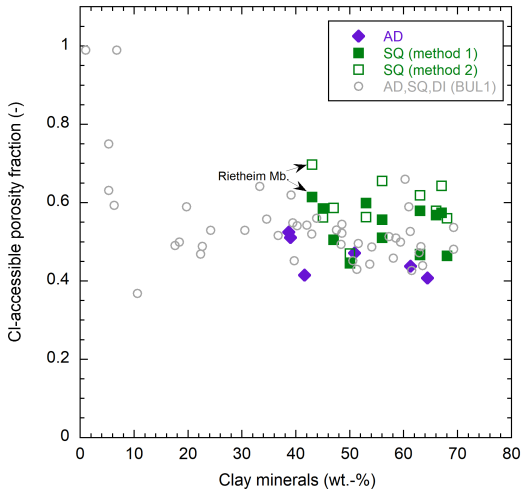

Fig. 5.1-1: Cl-accessible porosity fraction as a function of the clay-mineral content from AD and SQ experiments and comparison to data from the BUL1-1 borehole

BUL1-1 data comprises AD, SQ and through-diffusion data (DI) (Mazurek et al. 2021). The SQ data are derived from method 1 (closed symbols) or method 2 (open symbols) (see Section 4.6).

The fact that f_{Cl} shows considerable scatter when plotted against the clay-mineral content suggests that the latter is not the only parameter that determines the anion accessibility. Mineralogical composition of the clay fraction, mean pore size, grain-size distribution, fabric and other factors are expected to affect the anion accessibility as well. Note that the negative structural charge of the clays is predominately carried by the smectite and illite components. Furthermore, according to theory, the anion accessibility also varies with the salinity and the composition of the porewater, i.e., it is not just a material property. All these partly interdependent effects cannot be properly quantified at this stage, which severely limits the application of theoretical models.

An uncertainty range of ± 20% is considered for f_{Cl}, which is probably sufficient for clay-rich lithologies but may still be an underestimation for clay-poor rocks. This uncertainty propagates into the calculated Cl concentrations in the anion-accessible porewater, i.e., an error of ±20% must be considered in addition to the propagated analytical error.

AD and SQ samples also enable the estimation of the bromide-accessible porosity fraction (f_{Br}) (Fig. 5.1-2). Note that for the SQ data, estimation of Br accessible porosity fractions was only deemed possible with method 2 (based on AqEx data from adjacent cores, see Section 4.6) due methodological reasons. This method tends to yield slightly higher anion-accessible porosity fractions in the case of Cl (see Fig. 5.1-3), the reasons of which are not known at this stage.

The derived f_{Br} values lie between 0.44 and 0.70, with an average value of 0.56 ± 0.07. Note that the highest value of 0.7 originates from a sample with a very high content of C_{org} (9 wt.-%) from the Rietheim Member. A similarly high value for this sample was also obtained for f_{Cl} with method 2 (Fig. 5.1-3) and is consistent with corresponding f_{Cl} data in previous boreholes.

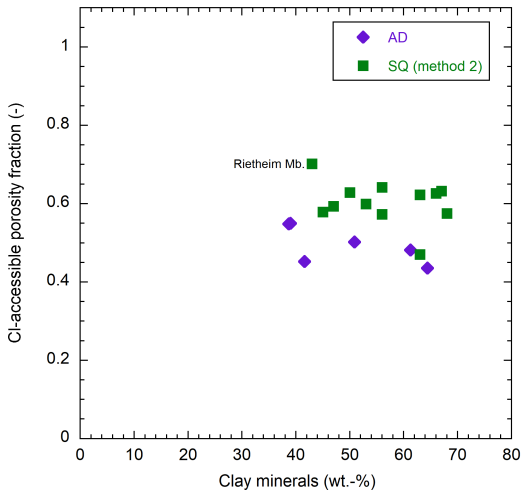

Fig. 5.1-2: Br-accessible porosity fraction as a function of the clay-mineral content derived from SQ (method 2) and AD data

Fig. 5.1-3 illustrates the Cl-accessible porosity fraction as a function of depth. In the upper part of the sequence f_{Cl} values suggest a slightly increasing trend with depth, but further down no clear trend can be discerned. In this figure, also SQ data obtained by method 2 (i.e. Cl concentration in bulk water derived from AqEx of a subsample of the SQ core) are shown. As mentioned above, these illustrate similar but slightly higher values relative to those of method 1.

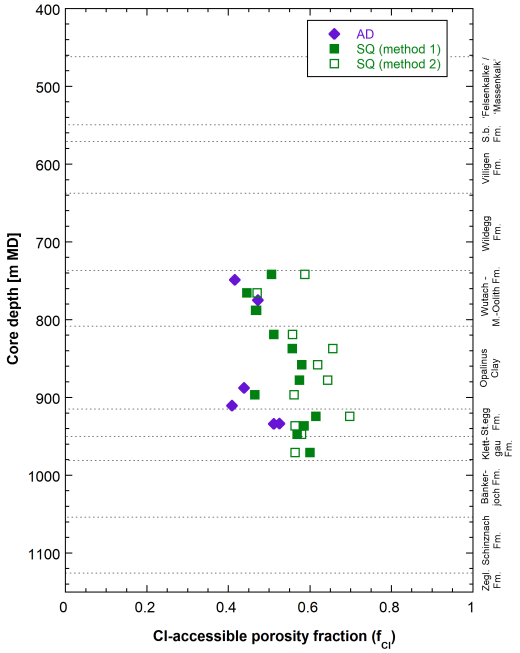

Fig. 5.1-3: Cl-accessible porosity fraction as a function of depth.

Note that f_{Cl} for squeezing sample 947.42 m is uncertain (Section 4.6.6).

5.2 Chloride, bromide and Br/Cl profiles

Paul Wersin, Carmen Zwahlen, Martin Mazurek, Thomas Gimmi

The chloride profile depicted in Fig. 5.2-1 includes aqueous extraction (AqEx) data re-calculated to in situ conditions assuming the relationship between clay-mineral content and f_{Cl} (with clay-mineral content of 20 wt.-% as "threshold" value) as discussed in Section 5.1. The Cl concentrations obtained from squeezing and advective displacement, as well as those for the groundwaters in the Keuper and the Muschelkalk (Table 2.3, Lorenz *in prep.*), are also shown in Fig. 5.2-1. The error bars include the propagated analytical uncertainty and, for aqueous extraction data, an additional 20% that reflects the uncertainty related to f_{Cl} (see Section 5.1, Fig. 5.1-1). It should be pointed out that for samples from the uppermost formations («Felsenkalke» + «Massenkalk», Schwarzbach Formation, Villigen Formation) no mineralogy data were acquired and thus only crude estimates on clay-mineral content could be made.

Data from all three methods (AqEx, AD, SQ) are consistent within the extended error bars. The Cl profile is reasonably well constrained and supported by the dense sampling, in particular in the Opalinus Clay. In some lithologies in the upper and lower confining units, however, Cl concentrations show considerable variations (Fig. 5.2-1) as discussed below. In general, the Cl profile is flat between the Villigen and Klettgau Formations with concentrations of 8 – 11 g/L. Between the Keuper and Muschelkalk aquifers, data suggest a decreasing trend (in spite of the scatter), and porewater concentrations reach low values of ~1g/L in the latter aquifer. Note that Fig. 5.2-1 (left) shows re-calculated AqEx data based on water-loss porosity (Section 4.4). Considering pycnometer porosity instead leads to a similar profile, but with a shift to slightly higher concentrations (Fig. 5.2-1 right). This difference is because of generally slightly lower pycnometer porosities (deduced from grain and bulk wet density measurements). In some cases, however, the opposite can be observed. The reasons for these slight differences in deduced porosities are not known at this stage.

Looking at the Cl profile from the Malm aquifer down to the Muschelkalk aquifer in more detail, one can note:

- In the uppermost part of the sequence («Felsenkalke» + «Massenkalk» and Schwarzbach Formation), a strong increase in Cl levels with depth is evident. Note that no groundwater could be sampled in this section.
- In the lower Malm units (Villigen and Wildegg Formations) the AqEx data based on water-loss porosity indicate a smooth profile, whereas AqEx data based on pycnometer porosity exhibit more scatter. This can be explained by the large error of pycnometer porosity at small porosities where bulk and grain densities differ only marginally.
- From the Villigen Formation down to the base of the Keuper aquifer, chloride concentrations are nearly constant in the range of 8 – 10 g/L. The groundwater concentration in the Keuper is in good agreement with the porewater concentration derived by a squeezing experiment at this depth.
- There are two outliers in the «Murchisonae-Oolith Formation» at about 800 m depth, representing an iron-oolitic horizon. In both samples goethite was identified (1 and 9 wt.-%, respectively). The Cl-accessible porosity fraction is likely underestimated for this type of rock, as indicated from previous boreholes. Pore-size distributions obtained from N_2 adsorption (Section 4.3.5) indicate the predominance of large pores in Fe-oolites, consistent with a high anion accessibility in the pore space. Note that the data based on pycnometer porosity plots closer to the general profile than those based on the water-loss porosity data.
- AD data show a systematic shift to slightly higher concentrations relative to SQ data. This confirms the feature noted in previous boreholes, as discussed in Kiczka et al. (2023).
- There are three outliers in the re-calculated AqEx data at about 920 m depth from the Gross Wolf and Rietheim Members (Staffelegg Formation), in which f_{Cl} values are likely underestimated. The same feature has been observed in previous boreholes (see discussion in Zwahlen et al. 2023b). Here again, pycnometer porosity-based data show less deviation from the general trend compared to water-loss porosity data.
- The scatter in the Bänkerjoch and Schinznach Formations is considerable, but slightly less in the pycnometer porosity-based AqEx data. These data suggest an increasing trend with depth below the Muschelkalk aquifer towards the Zeglingen Formation which may point to the influence of halite dissolution in that formation.

As mentioned above, the Cl-accessible porosity fractions for the samples with low and intermediate clay-mineral content are based on the assumption of a linear relationship with the clay-mineral content < 20 wt.-% (towards a value of 1 for clay-free rock). Fig. 5.2-2 compares the profiles obtained for a "threshold" value of 20 wt.-% (left) with those using a "threshold" value of 40 wt.-%. Both profiles are similar, but the outliers mentioned above deviate less from the overall trend using the latter threshold value. This confirms that the anion-accessible porosity fractions are underestimated for these specific rocks. On the other hand, using 40 wt.-% as threshold leads to a slight shift of the Cl data in the lower Malm relative to the profile below, suggesting that f_{Cl} values are slightly overestimated in this zone by using this threshold value.

In summary, a broadly consistent and well-defined Cl profile for the Opalinus Clay and confining units is obtained from squeezing, advective displacement and aqueous extraction data. The observed scatter is related predominantly to the uncertainty in the anion-accessible porosity (which may not only vary as a function of the clay-mineral content) and, to a lesser extent, to the uncertainty in the water content. In this analysis, a simple relationship of the anion-accessible porosity with the clay-mineral content (as proxy of surface charge) based on squeezing and

advective displacement data was used. Other relationships with the clay-mineral content (e.g., linear extrapolation from clay-mineral content < 40 wt.-%) do not result in a less scattered profile. The lower part of the Cl profile is influenced by the Keuper and Muschelkalk aquifers.

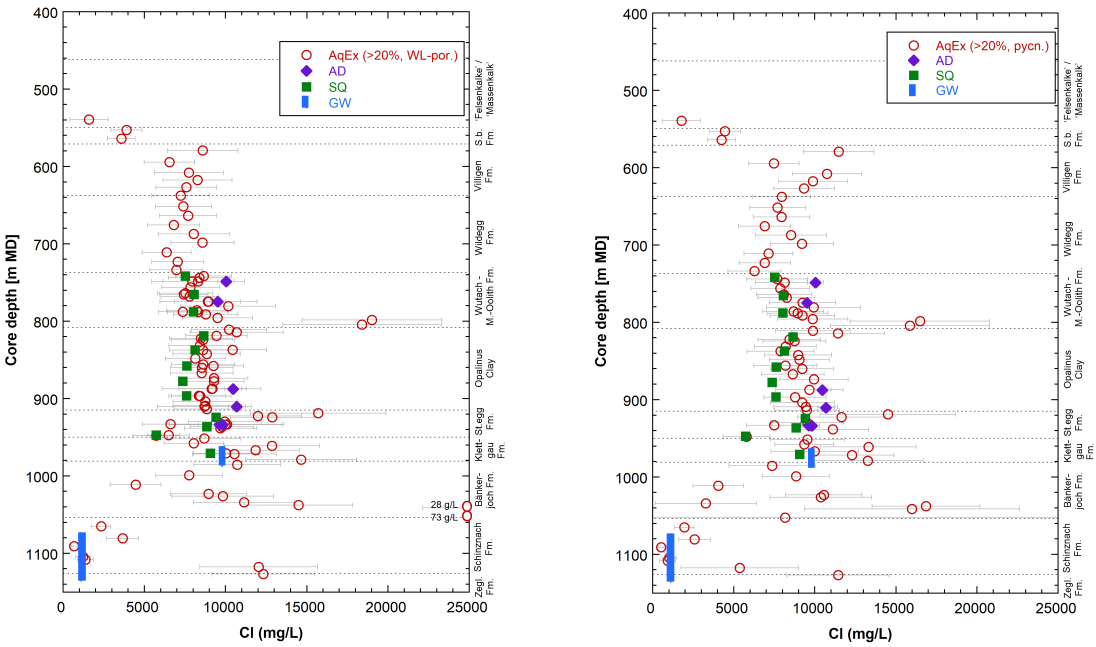

Fig. 5.2-1: Cl profile based on data from squeezing, advective displacement, aqueous extraction, and groundwater samples

AqEx data recalculated from water-loss porosity (left) and pycnometer porosity (right) and assuming 20 wt.-% clay-mineral content as threshold for linear extrapolation of f_{Cl} values (see text).

Aqueous extraction data in the Cl profile re-calculated to Cl-accessible porosity assuming the relationship between accessibility and clay-mineral content for Cl as discussed in Section 5.1. Note that in the upper part of the Malm there are no mineralogical analysis available and clay-mineral contents were roughly estimated as: 0 wt.-% for «Felsenkalke» + «Massenkalk», 10 wt.-% for Schwarzbach and Villigen Formations. Error bars of Cl data from aqueous extraction include propagated analytical uncertainty plus another 20% that reflect the uncertainty related to f_{Cl}. Note that the groundwater data are not corrected for drilling fluid contamination.

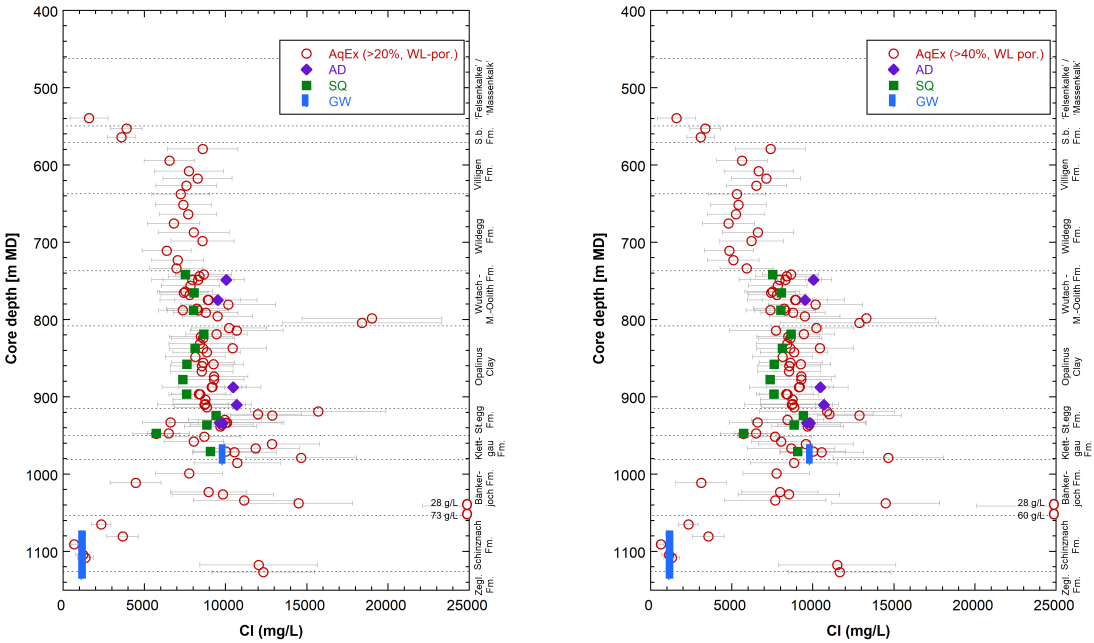

Fig. 5.2-2: Cl profile with data from squeezing, advective displacement, aqueous extraction, and groundwater samples

AqEx data recalculated from water-loss porosity assuming 20 wt.-% clay-mineral content (left) and 40 wt.-% (right) as threshold for linear extrapolation of f_{Cl} values (see text).

Aqueous extraction data re-calculated to Cl-accessible porosity assuming the relationship between accessibility and clay-mineral content as discussed in Section 5.1. Error bars on the data from aqueous extraction include propagated analytical uncertainty plus another 20% that reflect the uncertainty related to f_{Cl}. Note that in the upper part of the Malm there are no mineralogical analysis available and clay-mineral contents were roughly estimated as: 0 wt.-% for «Felsenkalke» + «Massenkalk», 10 wt.-% for Schwarzbach and Villigen Formation. Black encircled points: affected by drilling fluid contamination.

The Br profile (Fig. 5.2-3) reveals a similar shape as the one of Cl, albeit with somewhat more scatter, which is likely related to the larger analytical uncertainty of this minor element. Using the pycnometer porosity (Fig. 5.2-3 right) instead of the water-loss porosity (Fig. 5.2-3 left) to calculate porewater concentrations from aqueous extracts yields a very similar profile, but slightly more scatter and increased concentrations in the centre and the upper part of the sequence.

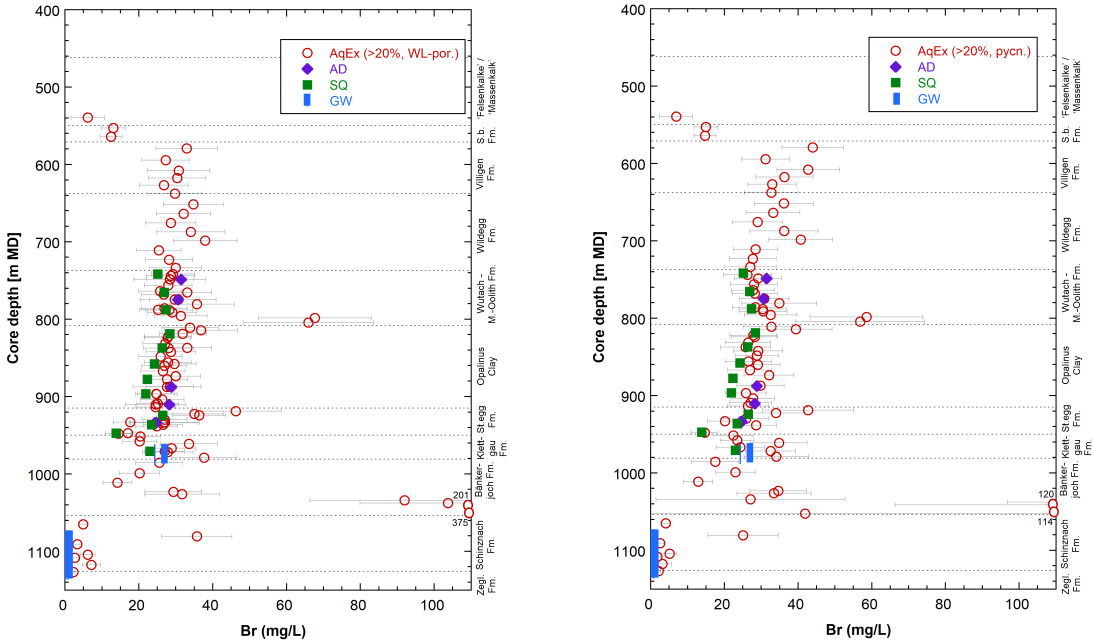

Fig. 5.2-3: Br profile with data from squeezing, advective displacement, aqueous extraction, and groundwater samples

AqEx data recalculated from water-loss porosity (left) and pycnometer porosity (right) and assuming 20 wt.-% clay-mineral content as threshold (see text).

Aqueous extraction data in the Br profile re-calculated to Br-accessible porosity assuming the relationship between accessibility and clay-mineral content for Cl as discussed in Section 5.1. Error bars of Br data from aqueous extraction include propagated analytical uncertainty plus another 20% that reflect the uncertainty related to f_{Br}. Note that in the upper part of the Malm there are no mineralogical analysis available and clay-mineral contents were roughly estimated as: 0 wt.-% for «Felsenkalke» + «Massenkalk», 10 wt.-% for Schwarzbach and Villigen Formations. The groundwater data are not corrected for drilling fluid contamination.

Note that the anionic tracers do not show any irregularities in the fault zone (911.63 – 912.16 m) of the Opalinus Clay or in the fractured interval of the Staffelegg Formation (940.58 – 942.78 m; *cf.* Section 2.2). Thus, based on the porewater isotope profiles there are no indications for recent advective flow in these intervals.

The Br/Cl profile (Fig. 5.2-4) shows less scatter than the individual Cl and Br profiles. This is mainly because uncertainty related to anion-accessibility and water content does not affect the Br/Cl ratio, contrary to the individual concentrations. AqEx, SQ, AD and groundwater data show consistent datasets.

Constant 1000*Br/Cl ratios slightly above seawater with some scatter are depicted in the Malm units. The ratios remain constant in the «Brauner Dogger» but are shifted to slightly lower values (close to seawater) in these units (with one outlier at 765.33 m depth). In the Opalinus Clay – Klettgau Formation section a decrease with depth down to the Keuper aquifer is evident. There is a general increase from the Keuper aquifer towards the base of the Bänkerjoch Formation, reaching very high Br/Cl ratios. Below a strong decrease with an important scatter towards the Muschelkalk aquifer is observed. Such positive excursions at the base of the Bänkerjoch Formation were also observed in the MAR1-1, STA2-1, STA3-1, BOZ1-1, BOZ2-1 boreholes.

They are possibly related to an old signal from highly evolved evaporated seawater in the anhydrite bearing units (see discussion in Wersin et al. 2023). The Br/Cl ratios reach very low levels at the base of Schinznach Formation, even below that of the Muschelkalk groundwater, and are in a similar range as the rocksalt (sampled from STA2-1 and STA3-1) in the underlying Zeglingen Formation.

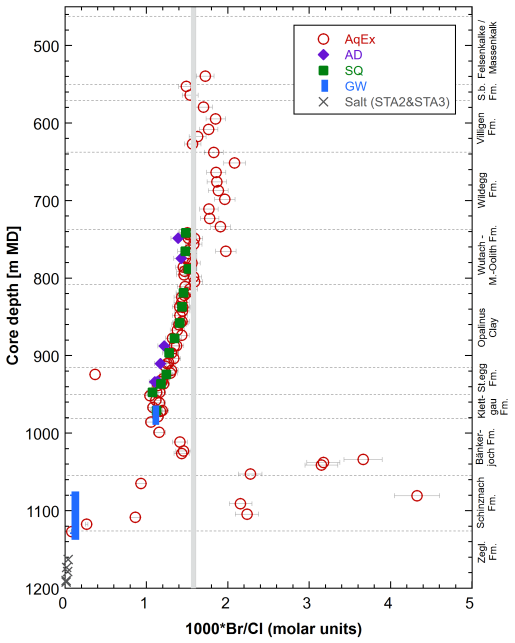

Fig. 5.2-4 1'000*Br/Cl (molar units) profile with data from squeezing, advective displacement, aqueous extraction, groundwater and halite samples

Grey bar: range in modern seawater.

5.3 Sulphate and SO_4/Cl profiles

Paul Wersin, Martin Mazurek, Thomas Gimmi

Sulphate data from squeezing, advective displacement, aqueous extraction and groundwaters are illustrated in Fig. 5.3-1. Data from aqueous extraction were re-calculated to concentrations in bulk porewater (Fig. 5.3-1 left) or to concentrations in anion-accessible porewater (using the same accessibility as for Cl, Fig. 5.3-1 right), assuming conservative behaviour of sulphate. This assumption is not true at least in anhydrite-bearing lithologies in the Bänkerjoch Formation where mineral dissolution contributed to SO_4 concentrations in the extracts, as is evident from the AqEx samples with re-calculated unrealistically high SO_4 concentrations of more than 100 g/L, way above the solubility of gypsum or anhydrite.

SO_4 concentrations based on squeezing and advective displacement yield distinctly lower and consistent values in comparison with the concentrations re-calculated from aqueous extraction. The AD/SQ datasets indicate a constant profile with concentrations of ~ 2 g/L in the «Brauner Dogger» down to the lower part of the Opalinus Clay, from where an increasing trend towards the Keuper aquifer is suggested. The groundwater concentration (3 g/L) is well in line with that of the corresponding squeezed porewater at this depth. Note that the SQ data show a positive

excursion in the Rietheim Member (upper Staffelegg Formation), which has a high content in pyrite and organic carbon. The Muschelkalk groundwater exhibits a lower concentration (~ 1.9 g/L) than the Keuper groundwater.

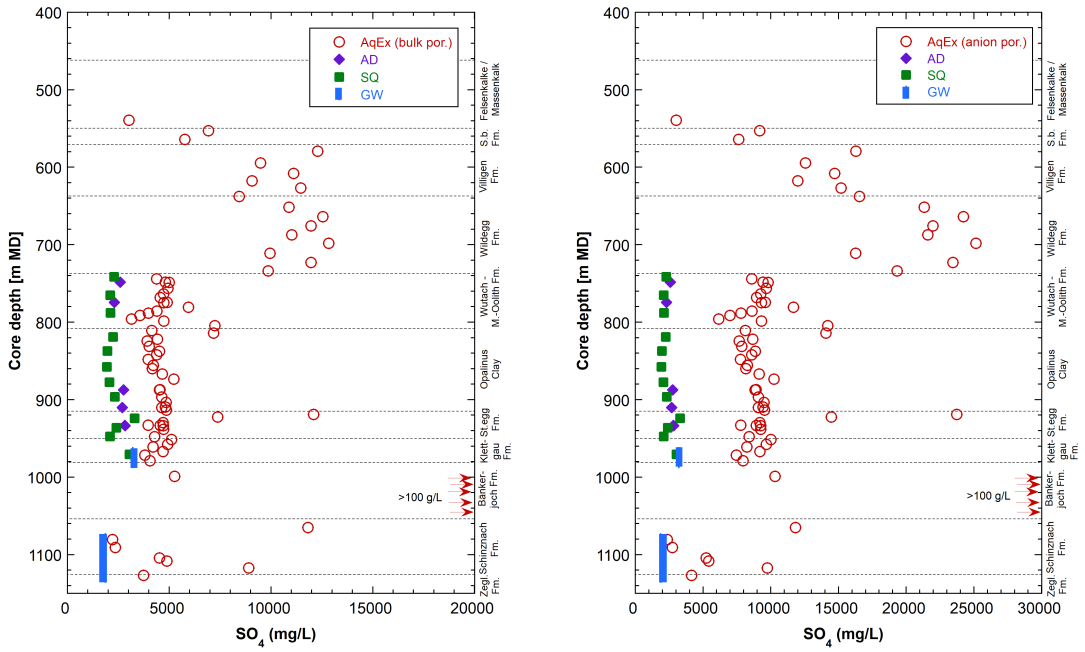

Fig. 5.3-1: SO_4 profiles with data from squeezing, advective displacement, aqueous extraction, and groundwater samples: left: AqEx data re-calculated to bulk porosity, right: AqEx data re-calculated to anion-acessible porosity

Aqueous extraction data re-calculated to contents in bulk porewater using water content. Aqueous data re-calculated to SO_4-accessible porosity assuming the same relationship between accessibility and clay-mineral content as applied above for Cl. Note that in the upper part of the Malm there are no mineralogical analysis available and clay-mineral contents were roughly estimated as: 0 wt.-% for «Felsenkalke» + «Massenkalk», 10 wt.-% for Schwarzbach and Villigen Formation. Note that the groundwater data are not corrected for drilling fluid contamination.

As noted above, the re-calculated aqueous extraction concentrations exhibit systematically higher and more variable concentrations than the SQ and AD data. The discrepancy between aqueous extraction and squeezing/advective displacement data becomes even larger when anion exclusion is considered, e.g. by assuming the same relationship between anion-accessible porosity and clay-mineral content as that applied for Cl (Fig. 5.3-1 right). However, it should be noted that the anion-exclusion effect of SO_4 in the considered rocks is not well known. From double layer theory, the exclusion of SO_4 in clayrocks is predicted to be higher because of its higher charge (Gimmi & Alt-Epping 2018). On the other hand, SO_4 has a larger tendency to form weak complexes, such as with alkaline earths, thus partly compensating the charge effect. Also, data for selenate (which can be regarded as chemical analogue for sulphate) in Opalinus Clay from Mont Terri suggest a similar diffusion regime as for Cl (Gimmi et al. 2014), even though no exact values for anion accessibility are available. A similar discrepancy between squeezing or advective displacement data on the one hand and aqueous extraction data on the other hand has been observed for other boreholes, such as Schlattingen-1 (Wersin et al. 2013), the BUL1-1 borehole (Mazurek et al. 2021), the TRU1-1 borehole (Aschwanden et al. 2021), the MAR1-1 borehole (Mäder et al. 2021), the BOZ1-1 borehole (Wersin et al. 2022a), the BOZ2-1 borehole (Gimmi et al. 2022), the

STA3-1 borehole (Aschwanden et al. 2022) or the STA2-1 borehole (Zwahlen et al. 2023a) as well as in the Mont Terri Rock Laboratory (Wersin et al. 2020). In the latter case, waters sampled from packed-off boreholes exhibited similar sulphate concentrations and SO_4/Cl ratios as waters squeezed from nearby drillcores. The reason for the higher sulphate levels derived from aqueous extraction compared to squeezing or advective displacement data is not understood in detail at this stage, despite recent systematic aqueous extraction studies on Opalinus Clay including Mont Terri and BUL1-1 samples (Debure & Gailhanou 2019, Aschwanden & Wersin 2020, Aschwanden et al. 2023).

The porewaters from AD are slightly oversaturated with regard to celestite (SI +0.16 to +0.24) whereas those from SQ are close to saturation or slightly undersaturated with regard to this phase (SI: -0.27 to -0.04). Celestite could be identified in some samples of the rock matrix of the Opalinus Clay and overlying formation at Mont Terri and Schlattingen-1 by a combined SEM/ microprobe study (Jenni et al. 2019). Moreover, all AD samples are close to saturation with regard to gypsum (SI: -0.11 to +0.04), whereas SQ waters show a larger spread in SI values (-0.22 to +0.01).

The depth profile of SO_4/Cl ratios (Fig. 5.3-2) shows a similar trend as the SO_4 profile. The general discrepancy between AD and SQ data on the one hand and AqEx data on the other is evident and not discussed further. In the «Brauner Dogger» – centre Opalinus Clay sequence, the SO_4/Cl ratios of AD and SQ data are constant, at a value of ~ 0.1, from where they show an increasing trend towards the Keuper aquifer to values of ~ 0.13, consistent with the groundwater value. The underlying Muschelkalk groundwater displays a higher value of 0.63. Note that all SO_4/Cl ratios are higher than that of modern seawater (0.052) (dashed red line in Fig. 5.3-2 right).

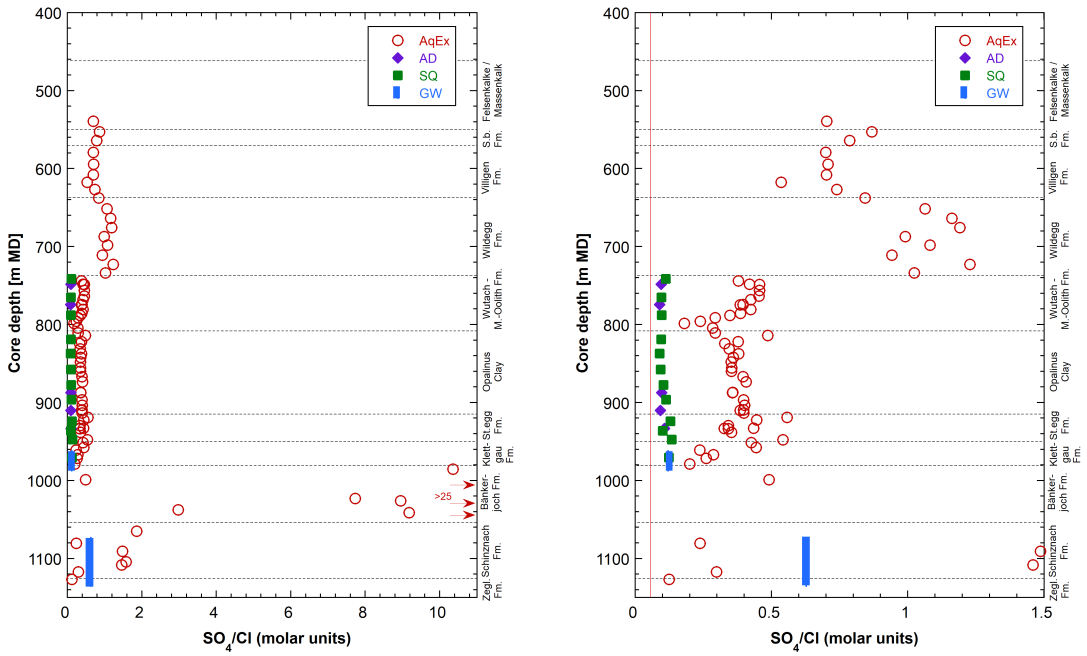

Fig. 5.3-2: Profiles showing molar SO_4/Cl ratios obtained from different methods

Note the different scales of the x axis. Red line: seawater ratio. Note that the groundwater data are not corrected for drilling fluid contamination.

5.4 Cation concentrations in porewaters

Paul Wersin, Eric Gaucher, Thomas Gimmi

Squeezing and advective displacement are the two methods that yield direct information on the cation concentrations in the porewater. Moreover, these can be estimated by simple modelling from the cation exchange data, notably from the cation occupancies on the exchanger. Aqueous extraction data, on the other hand, do not enable straightforward determination of porewater cations because of their modification via cation exchange and mineral reactions during the extraction process.

Both the squeezing and advective displacement methods may potentially induce changes in porewater composition, thus also affecting cation composition and distribution. Data from previous boreholes and the Mont Terri rock laboratory, however, suggest that using not too high squeezing pressures and very early samples in the case of squeezing and advective displacement, respectively, experimental artefacts are relatively minor (e.g. Wersin et al. 2016, Wersin et al. 2020, 2022b), or at least some level of consistency between AD and SQ data is obtained (Mazurek et al. 2021, Aschwanden et al. 2021, Mäder et al. 2021, Wersin et al. 2022a, Gimmi et al. 2022, Kiczka et al. 2023). The processes previously leading to high nitrate concentrations in some AD experiments were successfully prevented by an enhanced sample preparation procedure and experimental set-up in the AD experiments for BAC1-1.

Depth profiles for Na, Ca, Mg and K in porewater samples from SQ and AD are illustrated in Fig. 5.4-1. Na is the main cation, followed by Ca, Mg and K. The Na and, to a lesser extent, the Ca profiles indicate an increasing trend from the «Brauner Dogger» towards the Klettgau Formation. The SQ data, however, suggest a negative excursion of Na in the centre of the Opalinus Clay. There are not sufficient AD data in this zone to confirm or disconfirm this feature. The Ca/Na ratio is constant across the sampled sequence showing values of ~ 0.1 (molar units) (Fig. 5.4-2 right). The Mg profile shows some scatter (reflected by SQ data), suggesting a slightly decreasing trend with depth. The K profile is flat, depicting some scatter in the Staffelegg Formation. The Sr profile indicates a decreasing trend with depth, but AD data are shifted to higher values relative to SQ data (Fig. 5.4-2 left).

Note that SQ sample 947.42 m from the Schambelen Member (lower Staffelegg Formation) represents an outlier with regard to major cations (Na, Ca, Mg), which is related to technical issues during the squeezing experiment (Section 4.6.2).

The cation data are consistent with groundwater data in the Keuper aquifer, except for K. The high K level in the uncorrected groundwater probably indicates the influence of drilling fluid.

The porewater composition in Dogger and Liassic is Na-Cl dominated with little variations as indicated from the available samples. According to the classification of Jäckli (1970)[12] the porewaters are generally of Na-(Ca)-Cl-(SO_4) type, showing slightly increased SO_4 levels in the the Staffelegg Formation and uppermost Klettgau Formation. The relationships of cations and their consistency with exchangeable cation populations are further discussed in Section 5.6.

[12] Ions with > 50 eq.-% are underlined; ions with 20 – 50 eq.-% are not underlined, ions with 10 – 20 eq.-% are put in brackets.

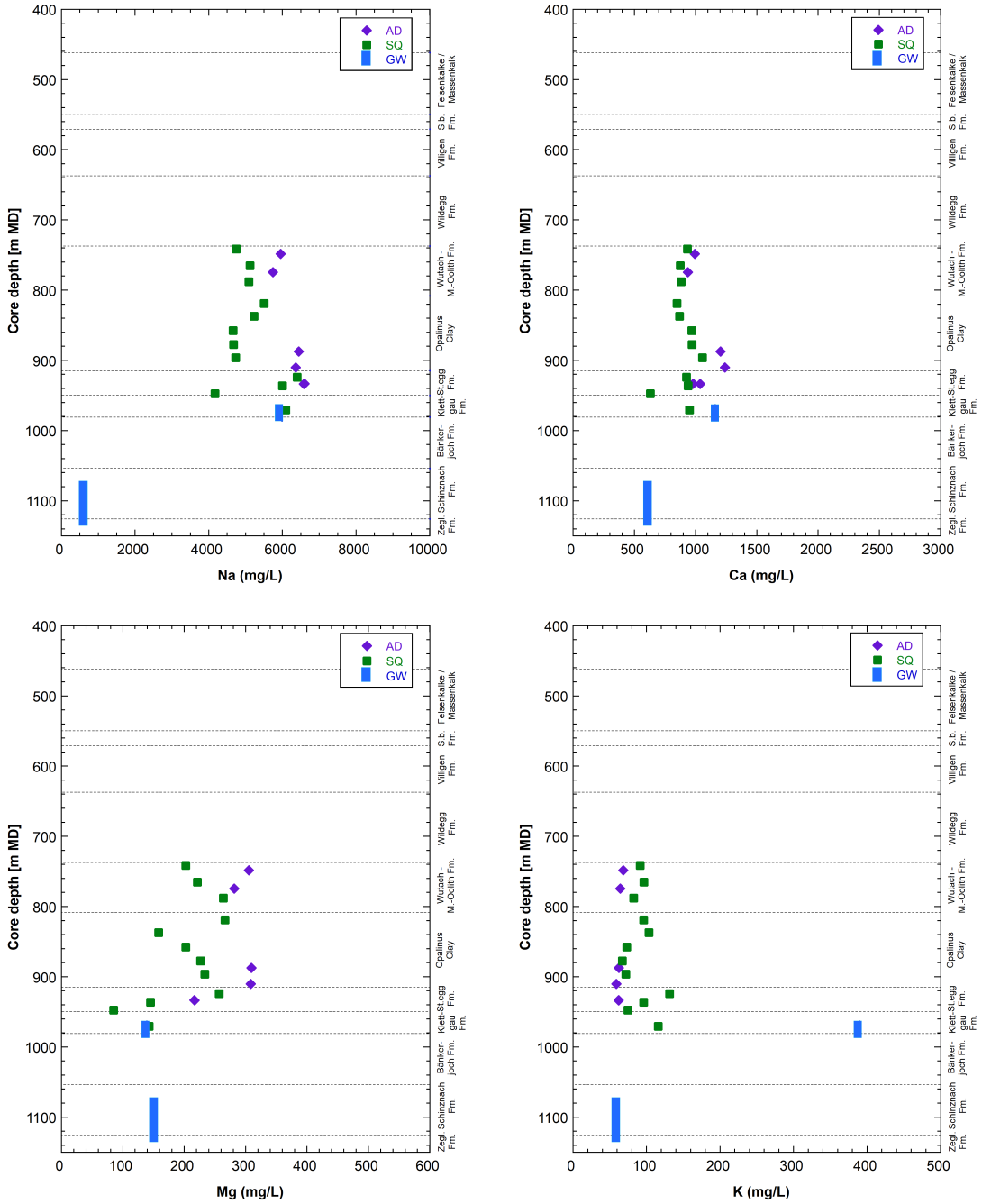

Fig. 5.4-1: Depth profiles for Na, Ca, Mg and K in porewater with data from squeezing, advective displacement and groundwater samples

Note that the groundwater data are not corrected for drilling fluid contamination.

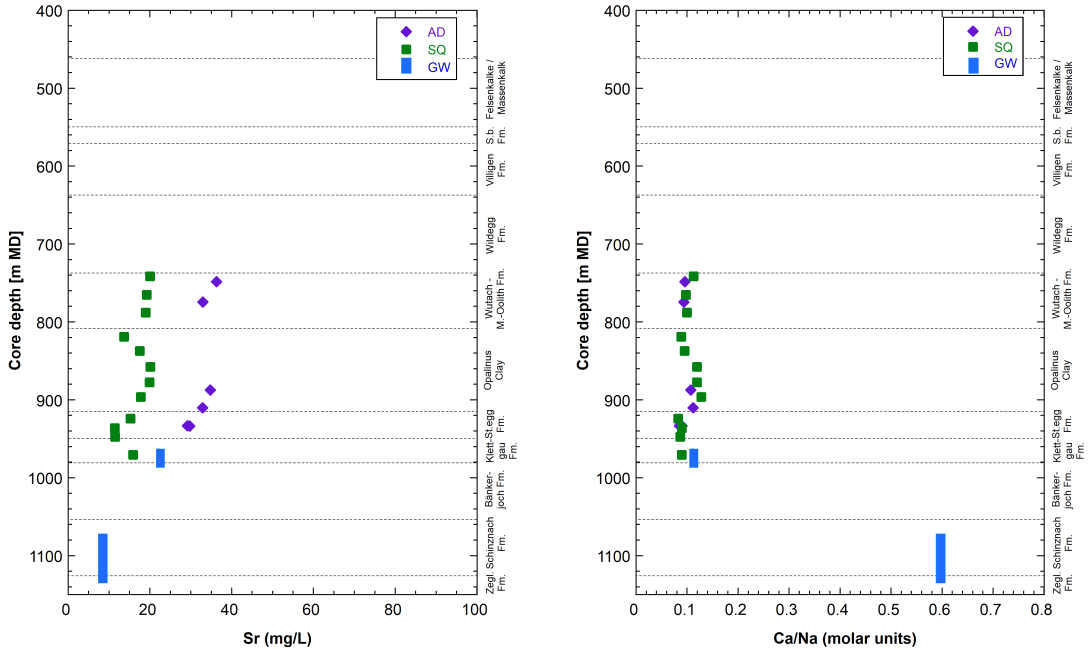

Fig. 5.4-2: Depth profiles for Sr (mg/L) and Ca/Na ratio based on SQ and AD experiments and groundwater analyses

Note that the groundwater data are not corrected for drilling fluid contamination.

5.5 Dissolved carbon species (inorganic, organic), alkalinity, pH and pCO_2

Paul Wersin, Eric Gaucher, Thomas Gimmi

5.5.1 Dissolved inorganic carbon, alkalinity, pH and pCO_2

The two experiments yielding information on the carbonate system of the porewater are squeezing and advective displacement. Notably on samples from these experiments, TIC, alkalinity (determined by titration) and pH can be measured. The alkalinity may include other compounds (e.g. low-molecular organic acids) than the carbonate species (HCO_3^-, CO_3^{2-}) and thus TIC is considered to be a more reliable parameter for constraining the carbonate system of the porewaters (Wersin et al. 2020).

Knowing pH and TIC, the (dissolved) carbonate system is entirely constrained (at constant temperature and pressure) according to Gibbs phase rule and the CO_2 partial pressure can be calculated. It should be noted that it is not straightforward to obtain reliable measurements on these parameters, which are prone to perturbations. For example, degassing of CO_2 during the squeezing process may alter pH and TIC parameters[13] (Tournassat et al. 2015, Wersin et al. 2020).

[13] But alkalinity is not affected by changes in CO_2 partial pressures as long as no dissolution/precipitation reaction occurs.

Equilibrium with calcite, omnipresent in the sedimentary sequence, may help to further constrain on pH/pCO_2. Thus, from the measured Ca, TIC and pH, the saturation state with regard to calcite can be calculated, providing a plausibility test regarding the carbonate system. It is worth noting, however, that calculated saturation indices for calcite close to zero do not a priori confirm that measured parameters, such as pH and TIC, reflect in situ conditions. In fact, perturbations during the experimental procedure might lead to a new equilibrium with calcite at different pH/pCO_2 conditions.

Tab. 5.5-1 shows the measured pH and TIC data together with the derived pCO_2 and saturation index for calcite from speciation calculations with PHREEQC. Note that for the AD samples, pH from in-line measurements (Section 4.7.5.3) are considered here. Measured pH values for the AD samples range from 7.1 to 7.8, whereas those for SQ are higher, in the range of 8.4–9.0, as also illustrated in Fig. 5.5-1 (left, closed symbols). Conversely, for AD samples TIC values tend to be higher (2 – 4.7 mM) compared to the ones of SQ (0.8 – 2.1 mM). Regarding pCO_2, AD data indicate values of -1.8 to -2.9 bar in log units, whereas lower values (-3.2 to -4.6) are derived for SQ data, as also illustrated in Fig. 5.5-1 (right, closed symbols). All samples (except AD 748.55 m) are oversaturated with regard to calcite, but oversaturation is higher in SQ samples.

The pCO_2 data obtained for the AD samples lie within the expected range (about -2 to -3 log(bar) based on earlier pCO_2 measurements and geochemical considerations (see discussion in Wersin et al. 2020), but as noted above, five out of six AD waters are oversaturated with respect to calcite. The oversaturation is more pronounced when considering lab pH which generally display higher values relative to in-line measurements (Section 4.7.5.3), suggesting that the former values are less reliable than the in-line pH value, probably due to CO_2 out-gassing during sampling and storage. Regarding SQ data, pCO_2 appear clearly too low, a feature that has been systematically observed and explained by CO_2 degassing occurring during the squeezing process (Tournassat et al. 2015, Wersin et al. 2020). This process in turn leads to elevated pH and an increase in HCO_3^- and thus CO_3^{2-} activity (leading to calcite oversaturation), schematically represented by the two reactions (where ↑ represents degassing):

$$HCO_3^- \rightarrow CO_2(g)\uparrow + OH^-$$

$$2\ HCO_3^- \rightarrow CO_2(g)\uparrow + CO_3^{2-} + H_2O$$

Tab. 5.5-1: Measured pH and TIC as well as calculated pCO_2, $SI_{calcite}$ from AD and SQ experiments

Calculated pCO_2 and pH assuming calcite equilibrium data (see text).

		Measured		**Calc. from pH, TIC**		**Calc. assuming calcite eq. (see text)**	
Method	**Depth** [m]	**pH**	**TIC** [mmol/L]	**logpCO_2** [bar]	**SI calcite** [-]	**pH** [bar]	**logpCO_2**
AD	748.50	7.06	2.22	-2.14	0.07	7.00	-2.09
AD	774.58	7.05	2.97	-2.01	0.17	6.89	-1.85
AD	887.40	7.32	4.73	-2.06	0.75	6.58	-1.33
AD	910.21	6.98	3.93	-1.83	0.31	6.72	-1.61
AD	933.25	7.35	3.24	-2.25	0.53	6.87	-1.81
AD	933.70	7.78	1.96	-2.89	0.77	7.02	-2.13
SQ	732.74	8.61	2.10	-3.19	0.82	6.98	-1.97
SQ	765.33	8.69	1.38	-4.02	1.40	7.22	-2.49
SQ	788.06	8.44	1.47	-3.71	1.23	7.20	-2.44
SQ	818.92	8.53	1.74	-3.74	1.35	7.05	-2.13
SQ	837.16	8.99	0.90	-4.59	1.44	7.40	-2.84
SQ	857.72	8.77	0.84	-4.34	1.30	7.36	-2.84
SQ	877.64	8.67	1.09	-4.11	1.33	7.26	-2.63
SQ	896.50	8.60	1.12	-4.01	1.31	7.23	-2.59
SQ	924.21	8.36	1.80	-3.53	1.22	7.13	-2.29
SQ	936.46	8.52	1.67	-3.74	1.36	7.12	-2.31
SQ	947.42	8.96	1.02	-4.45	1.38	7.45	-2.82
SQ	970.89	8.74	1.33	-4.10	1.43	7.24	-2.52

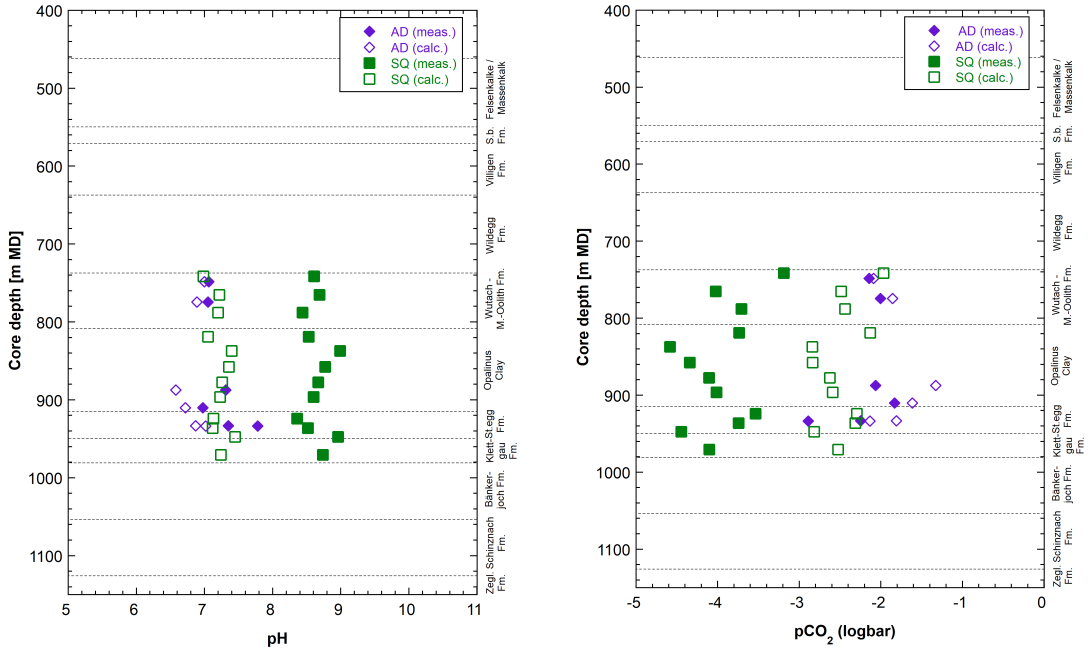

Fig. 5.5-1: pH (left) and pCO_2 values (right) from AD and SQ experiments

Solid symbols: measured pH and pCO_2 calculated from measured pH and TIC ("meas. ")
Open symbols: model calculations based on calcite equilibrium ("calc. ", see text)

The effect of CO_2 degassing during the experimental procedure was evaluated numerically using PHREEQC. Thus, CO_2 gas was added to the experimental solutions until calcite saturation was reached. Looking at the SQ data, this results in lower pH and higher pCO_2 values, depicted as open symbols in Fig. 5.5-1. The calculated pH and pCO_2 for the SQ experiments lie in the range of 7.0 – 7.4 and -2.8 to -2.0 log(bar), respectively. This range appears reasonable and consistent with previous pH and pCO_2 data in Opalinus Clay (Wersin et al. 2020) and supports the hypothesis that the carbonate system was mainly affected by CO_2 degassing and much less by carbonate dissolution during the squeezing procedure.

Regarding the AD data, the shift of the pH and pCO_2 after the correction procedure is less pronounced because the uncorrected data display higher pCO_2 and are closer to calcite saturation compared to SQ data. In fact, adding CO_2 may result in overcorrection, as for example suggested for the AD sample 887.40 m with a low pH (6.6) and high pCO_2 (-1.3 log(bar)). It thus appears that the simple correction procedure is less appropriate for AD data. The observed oversaturation of AD samples with respect to calcite may thus be influenced by some other process than CO_2 degassing during sampling. It should be noted that pH was measured either on a small aliquot in the lab or in a flow-through device on sample aliquots prior or after the sampled aliquot. Degassing can therefore be envisioned for the pH measurement without affecting the TIC values. Correcting for pH uncertainties only suggests pH values in the range of 6.7 – 7.0 and pCO_2 values of -1.5 to -2.2 log(bar). Additional methodological differences between both approaches (storage time and temperature, solution sampling) require further investigations to estimate the influence on measurements.

In summary, correcting SQ data for CO_2 degassing leads to broad consistency with (uncorrected) AD data regarding pH/pCO_2 conditions. AD data on the other hand seem less affected by degassing during sampling but (at least partly) by some other process and/or methodological issues.

5.5.2 Dissolved organic carbon

Information on dissolved organic carbon is available from advective displacement (AD) and squeezing (SQ) data as well as from aqueous extracts of AD cores (AqEx-AD):

- SQ: TOC
- AD: TOC, low molecular-weight organic acids (LMWOA)
- AqEx-AD: low molecular-weight organic acids (LMWOA)

Moreover, the (solid) organic carbon content (C_{org}) from the corresponding SQ and AD samples is available besides those from PW, RP and DI samples.

Before discussing the dissolved organic carbon data it is worth mentioning some general points: The organic carbon in clayrocks such as the Callovo-Oxfordian Formation or the Boom Clay consists of refractory kerogen and only a small fraction is extractable by solvents (< 1%) (Deniau et al. 2008). The water-soluble organic carbon is even smaller, thus for example reaching a few mg C/L in the porewater of Opalinus Clay at Mont Terri or in the Callovo-Oxfordian Formation sampled from seepage boreholes (Courdouan-Merz 2008, Courdouan et al. 2007a & b). Higher concentrations (several tens to hundreds of mg C/L) are generally measured in porewaters expelled from core samples, such as from squeezing or advective displacement (Wersin et al. 2013, Wersin et al. 2020). In the case of the aqueous extracts, also significant amounts of organic carbon are released to the solution. This indicates that a fraction of the "solid" carbon is mobilised during the extraction process.

The TOC porewater concentrations from AD and SQ experiments are illustrated in Fig. 5.5-2 (left). These show a rather narrow range for SQ of 130 – 170 mg/L and higher values with a large spread for AD (200 – 800 mg/L). Two of the AD samples exhibit TOC concentrations of around 200 mg/L, thus not far off from the corresponding SQ concentrations, whereas the remaining four AD samples show much higher concentrations (500 – 800 mg/L). It is interesting to note that the TOC concentrations are not related to (total) organic C profile of the rock (Fig. 5.5-2 right). Regarding the SQ sample from the Rietheim Member (Staffelegg Formation) this becomes particularly evident. This sample contains a high amount of organic carbon but shows no increased TOC concentration relative to the other samples.

A significant share of the TOC in the samples from AD experiments consists of acetate (note that for SQ no LMWOA were measured). Thus, this compound accounts for about 10 – 50% of the TOC. The other measured LWMOAs (lactate, proprionate, formate) are below detection. The nature of the remaining TOC in the AD samples is not known.

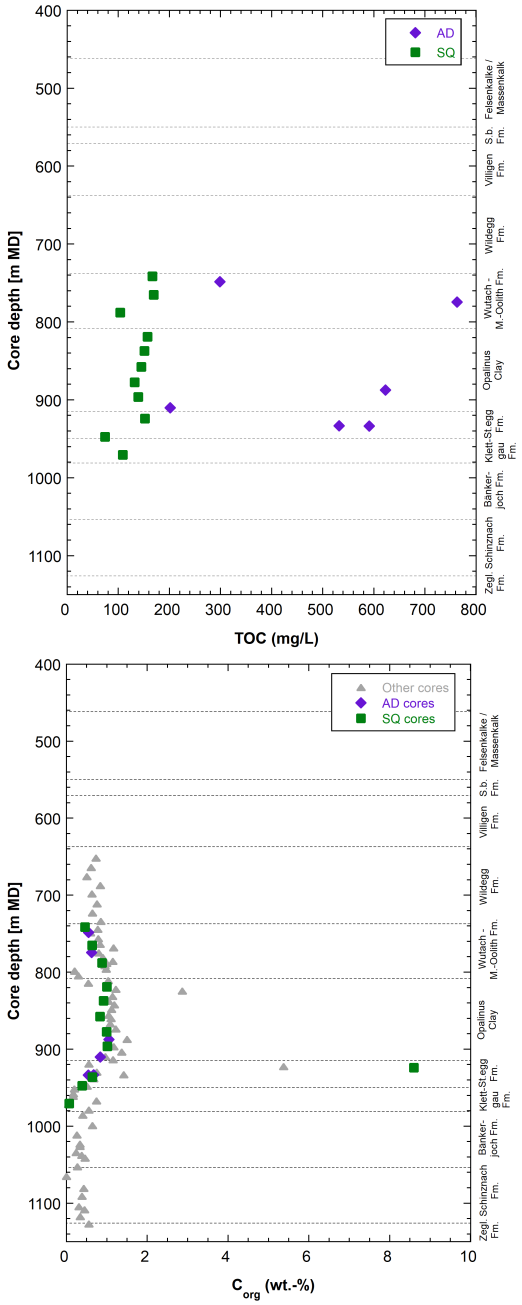

Fig. 5.5-2: TOC concentrations in porewater (left) from AD and SQ experiments and organic carbon content from drillocre samples used for AD, SQ and other purposes

5.6 Cation exchange capacity and exchangeable cation population

Paul Wersin

5.6.1 Corrected exchangeable cation data

As mentioned in Section 4.5, in order to obtain the exchangeable cation concentrations, the extracted cation data need to be corrected for cations dissolved in the porewater and the cations released from (potential) mineral dissolution. As shown from previous work (e.g. Hadi et al. 2019) and also indicated from speciation calculations presented in Section 4.5 (Tab. 4.5-4), carbonate mineral dissolution is minimised with the appropriate *S/L* ratio, extraction time and pH conditions. Such conditions were applied to in the Ni-en extraction tests presented here.

Two correction methods for cations dissolved in the porewater were applied based on the concentrations of the main anions chloride and sulphate (Bradbury & Baeyens 1998, Hadi et al. 2019). The first correction method ($NaCl/Na_2SO_4$) attributes dissolved Cl and SO_4 from the Ni-extracts to Na and leaves the other cations unchanged. The second method ($NaCl/CaSO_4$) attributes Cl to Na and SO_4 to Ca, leaving the other cations unchanged. In both methods, the CEC is calculated from the sum of cations (Σ_{CAT}) minus the concentrations of Cl and SO_4 (normalised to meq/kg_{rock}).

Cation exchange capacity and corrected sum of extracted cations

The cation exchange capacity based on Ni consumption data and Σ_{CAT} is shown in Tab. 5.6-1. Note that for two samples from the Bänkerjoch Formation (1'026.21 m and 1'033.99 m) the correction procedure leads an overcompensation due to the high sulphate concentration in these anhydrite bearing samples, and therefore no meaningful data regarding corrected Σ_{CAT} (sample 1'033.99) and exchangeable cations (samples 1'026.21, 1'033.99) can be derived. Disregarding these two samples, the relative difference between the uncorrected and corrected sums of extracted cations (Σ_{CAT}) is 9 – 38%.

Fig. 5.6-1 (left) shows the CEC parameters as a function of the clay-mineral content. It illustrates the expected increasing trend with clay-mineral content. Both Ni consumption data and (corrected) Σ_{CAT} reveal similar trends as also illustrated in the depth profile (Fig. 5.6-2). Disregarding the above mentioned two samples, the two datasets are broadly consistent, indicating relative differences of -27 to +26%, but most samples lie within 10% difference. Fig. 5.6-1 (right) illustrates the correlation with CEC and illite + 4 × smectite (in wt.-%), which is slightly better than the CEC-clay-mineral content correlation. The parameter illite + 4 × smectite is a proxy of the structural negative charge, which is carried predominately by smectite and illite (e.g. Marques Fernandes & Baeyens *in prep.*). It should be noted that for only part of the samples data on illite and smectite contents are available.

Tab. 5.6-1: Sum of cations and cation occupancies obtained from Ni-en extraction after correction (Uni Bern data)

First line for each sample indicates fractional cation occupancies (in equivalent units) obtained by the $NaCl/Na_2SO_4$ correction method, the second line those obtained by the $NaCl/CaSO_4$ method.

Type	Depth [m]	Formation	Clay-mineral content [wt.-%]	Ni consumption [meq/kg]	ΣCAT raw [meq/kg]	ΣCAT corr. [meq/kg]	Na fr.oc.	K fr.oc.	Ca fr.oc.	Mg fr.oc.	Sr fr.oc.
AD	748.5	«Park.-Württem.-Sch.»	42	94.9	93.3	85.1	0.46 0.50	0.06	0.33 0.29	0.14	0.007
AD	774.58	«Park.-Württem.-Sch.»	51	107.3	88.6	78.9	0.46 0.50	0.06	0.33 0.29	0.15	0.007
AD	887.4	Opalinus Clay	61	81.0	97.0	87.1	0.50 0.53	0.04	0.33 0.29	0.12	0.005
AD	910.21	Opalinus Clay	64	75.6	105.7	95.8	0.48 0.52	0.05	0.35 0.32	0.11	0.005
AD	933.25	Staffelegg Fm.	39	58.0	67.9	59.4	0.49 0.53	0.06	0.34 0.30	0.11	0.005
AD	933.7	Staffelegg Fm.	39	59.6	70.6	62.0	0.48 0.52	0.06	0.35 0.30	0.11	0.005
PW	999.02	Bänkerjoch Fm.	48	80.8	71.2	64.1	0.53 0.58	0.03	0.31 0.26	0.13	0.004
PW	1026.21	Bänkerjoch Fm.	34	55.1	122.2	37.6	a)	a)	a)	a)	a)
PW	1033.99	Bänkerjoch Fm.	19	11.0	84.0	a)	a)	a)	a)	a)	a)
PW	1037.67	Bänkerjoch Fm.	51	115.8	166.0	102.1	0.12 0.63	0.07	0.69 0.19	0.11	0.005

a) Correction procedure leads to erroneous results and is not applicable for these data (see text).

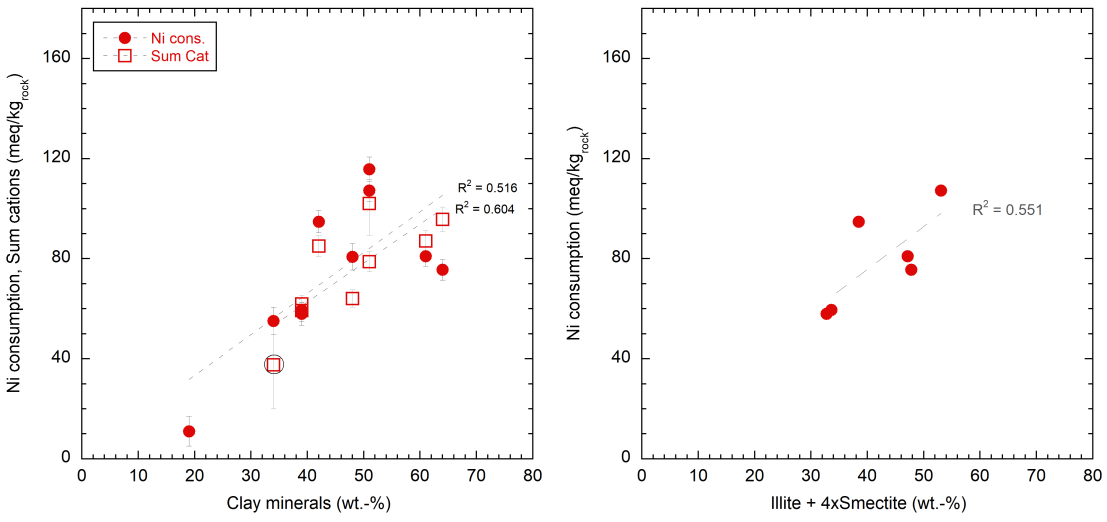

Fig. 5.6-1: Ni consumption and sum of (corrected) cations as a function of the clay-mineral content (left) and Ni consumption as a function of illite + 4 × smectite (right)

Encircled point: Extract affected by anhydrite dissolution (see text).

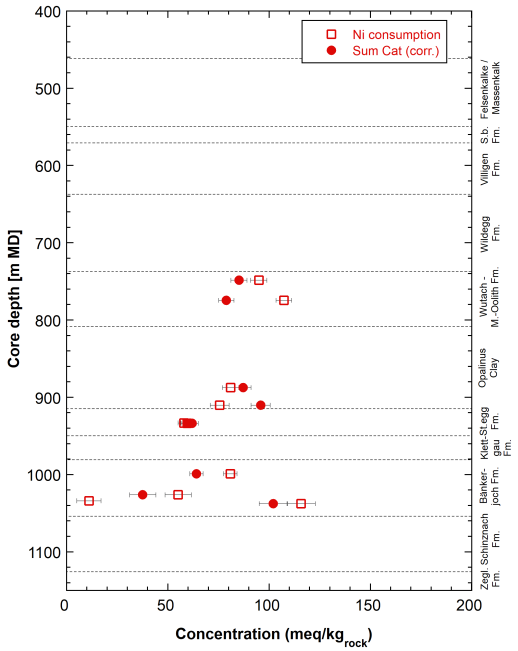

Fig. 5.6-2: Profile of CEC

Figure shows Ni consumption and sum of (corrected) cations.

Only Ni consumption data shown for the two anhydrite-bearing samples from Bänkerjoch Formation (see text).

Exchangeable cation occupancies

The advantage of comparing fractional cation occupancies rather than the extracted cation concentrations is that they are normalised to the sum of cations (as proxy for the CEC) and do not directly depend on the clay-mineral content of the sample.

The fractional occupancies of the main cations are illustrated in Figs. 5.6-3 to 5.6-5. Na and Ca are the main exchangeable cations, followed by Mg and K. The Sr occupancies are considerably lower (0.4 – 0.7% of the CEC).

Fig. 5.6-3 shows the Na and Ca occupancies derived from the two correction methods. Note that in method 1 Cl and SO_4 are attributed to Na, whereas in method 2, SO_4 is attributed to Ca. Thus, the Na fraction is minimised in method 1 and maximised in method 2, while the opposite is true for Ca. The Na and Ca occupancies indicate flat profiles in the «Brauner Dogger» – Staffelegg Formation section. In the underlying Bänkerjoch Formation, strong differences between the two correction methods are evident in the lowest sample. In fact, method 1 (in which extracted Ca is not corrected) results in very high Ca and correspondingly low Na, whereas method 2 (where Ca is corrected by SO_4) yields Na and Ca that seem more in line with the overlying profile. Dissolution of anhydrite (although not detected by XRD) is suspected to have affected the Ca levels in the Ni extract of this sample. Besides the two datasets, the modelled occupancies based on the SQ and AD porewater data are shown. The modelling was done with the PHREEQC simulator and the well-established single-site cation exchange model for Opalinus Clay (Pearson et al. 2011, Wersin et al. 2016). The calculated Na and Ca occupancies are broadly consistent with the data derived from Ni-en extraction, but generally show better agreement with the

Ni-extraction data corrected with method 2. The Ca/Na profile (Fig. 5.6-6 left) shows constant ratios down to the bottom of Staffelegg Formation from where a dereasing trend with depth is suggested (when considering data corrected with method 2).

Mg occupancies from Ni extraction show a slight decrease with depth (Fig. 5.6-4 left). The modelled Mg data based on the porewater analyses are largely consistent with the measured ones but show more scatter. Mg/Ca ratios also exhibit a slight decrease with depth in the upper part of the profile down to the Staffelegg Formation (Fig. 5.6-6 right). Below this formation, data from Ni extraction suggest an increasing trend. Calculated Mg/Ca ratios, however, do not seem to follow the same trend in the lower section, but rather suggest decrease within the Stafelegg Formation. K occupancies from Ni extraction also indicate a slight decrease with depth, in line with the calculated data (Fig. 5.6-4 right). The latter are however shifted to somewhat higher values.

Sr occupancies from Ni extracts, which are well below 0.01 (equiv. fr.), display a similar profile as Mg, but calculated Sr data are consistently lower than the measured ones. Such discrepancy beween calculated and measured data has also been noted in previous boreholes and has been explained by dissolution of Sr-bearing minerals (Wersin et al. 2020).

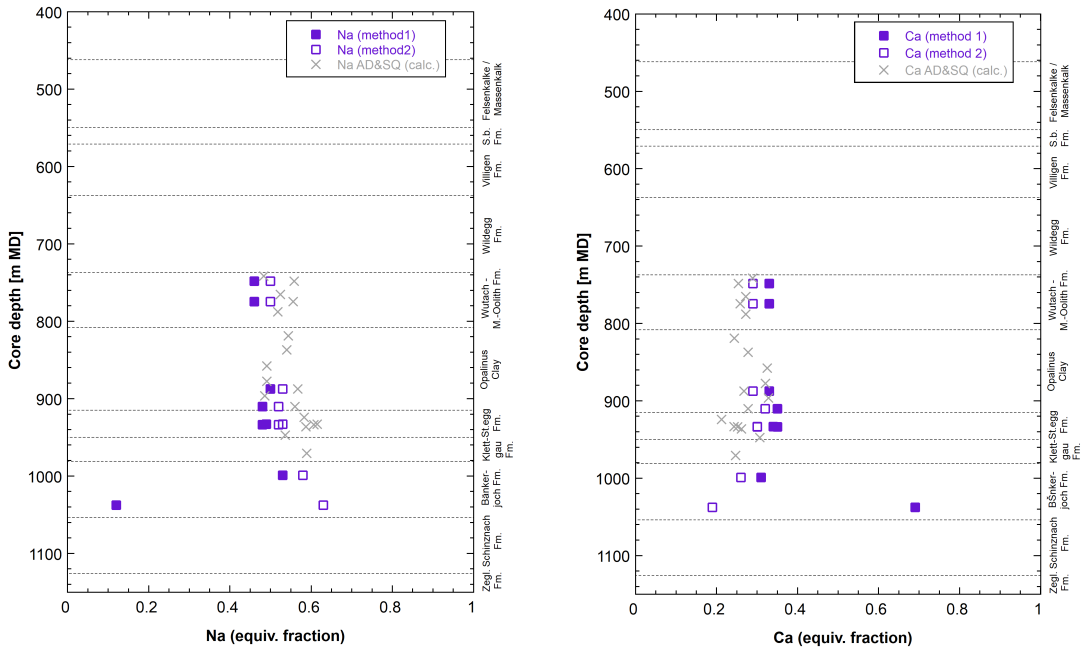

Fig. 5.6-3: Na (left) and Ca (right) occupancies from Ni-en extraction and comparison to values back-calculated from AD and SQ porewater data

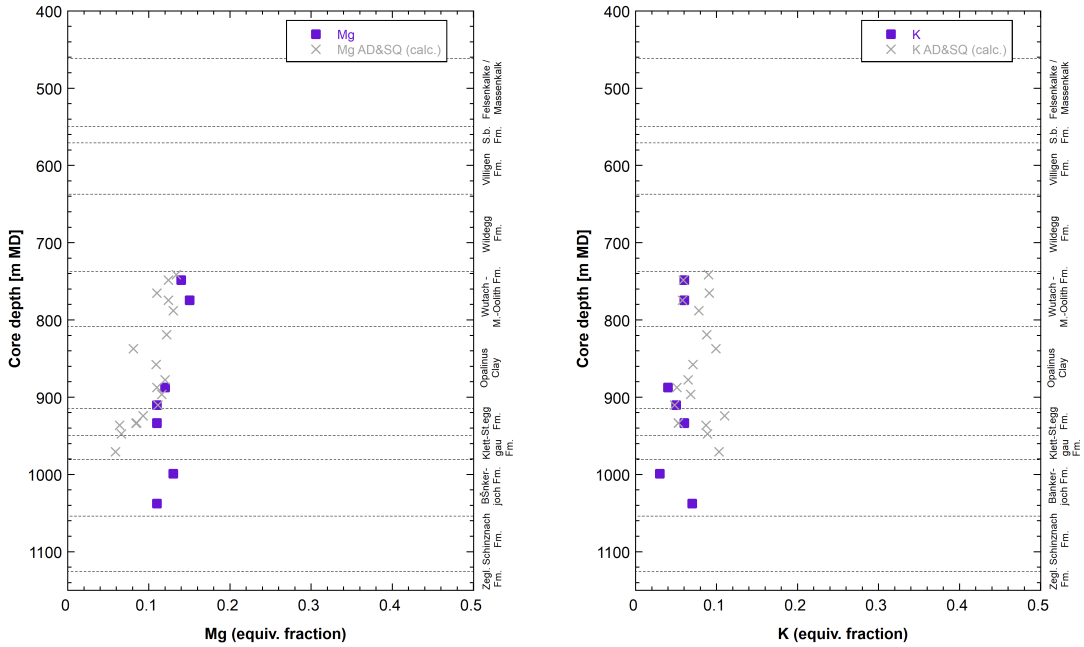

Fig. 5.6-4: Mg (left) and K (right) occupancies from Ni-en extraction and comparison to values back-calculated from AD and SQ porewater data

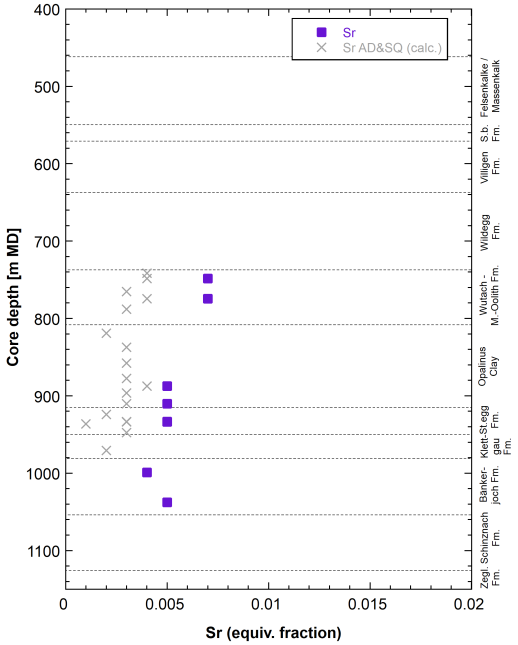

Fig. 5.6-5: Sr occupancies from Ni-en extraction and comparison to values back-calculated from AD and SQ porewater data

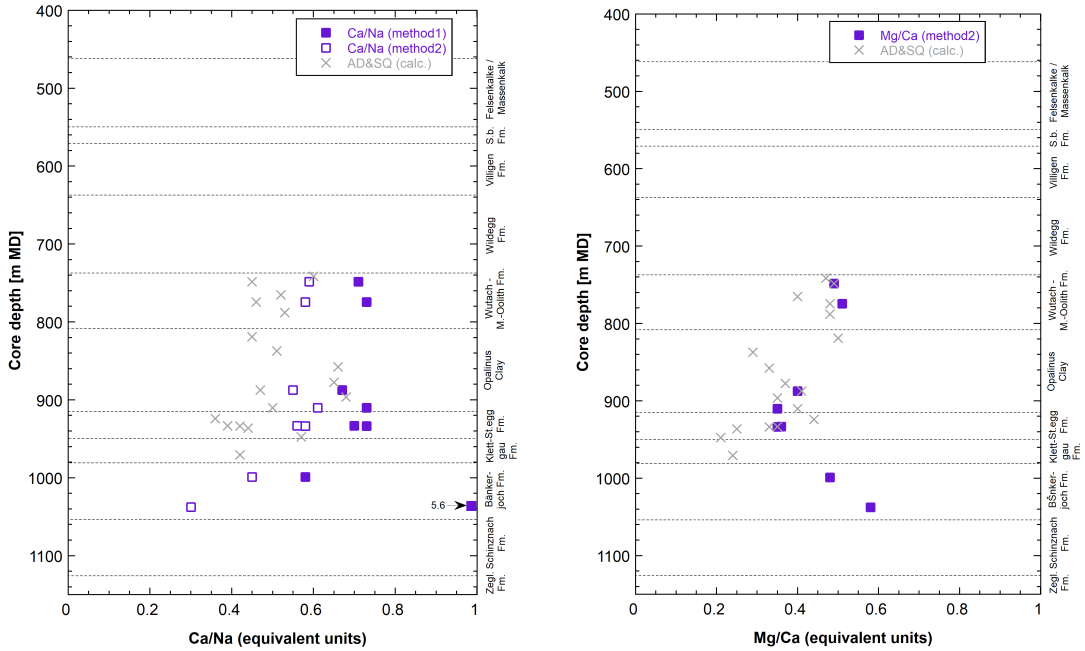

Fig. 5.6-6: Na/Ca ratios (left) and (Mg/Ca) (right) from Ni-en extraction and comparison to values back-calculated from AD and SQ porewater data

Extracted anions

The amounts of extracted Cl and SO_4 (meq/kg_{rock}) are illustrated in Fig. 5.6-7. The Cl concentrations from Ni-en extraction are consistent with the corresponding data from aqueous extraction, indicating a curved profile shape. Regarding SO_4, Ni-exctraction data show lower values than the corresponding AqEx data. A similar feature has been noted in previous boreholes, such as for example in BUL1-1, but the reasons thereof remain unclear at this stage.

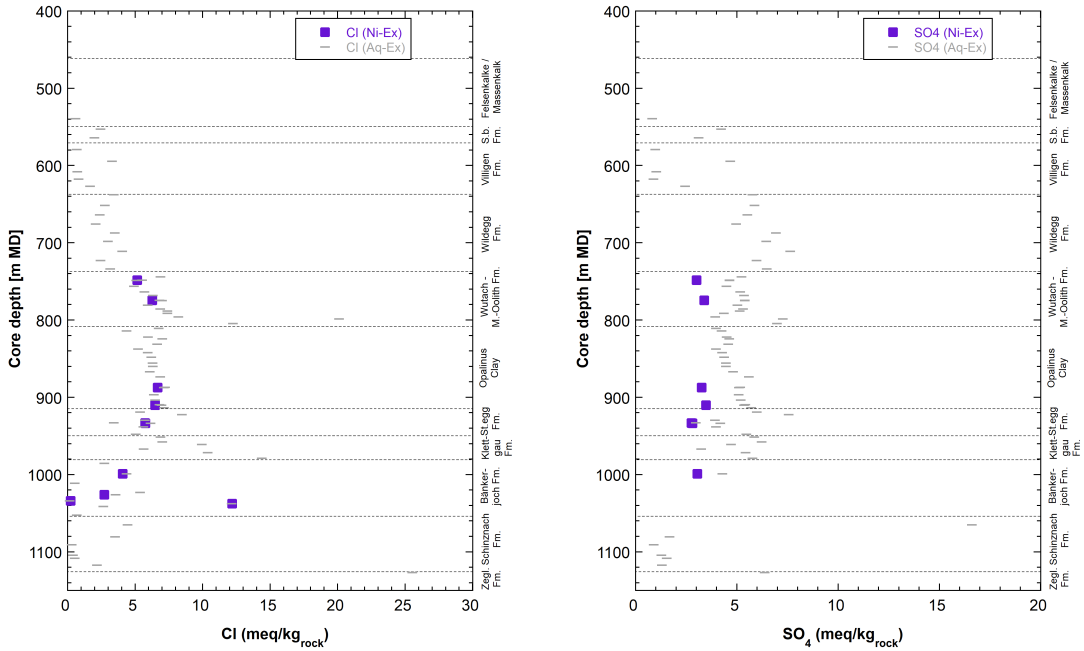

Fig. 5.6-7: Profiles of chloride and sulfate concentrations in CEC extract solutions and comparison to concentrations in standard aqueous extracts (Section 4.4)

5.7 Stable water isotopes

Lukas Aschwanden & Thomas Gimmi

5.7.1 Comparison between different methods for the determination of stable porewater isotope compositions

The porewater oxygen and hydrogen isotope compositions were determined using three different methods including the isotope diffusive-exchange (Section 4.8), advective displacement (Section 4.7) and high-pressure squeezing (Section 4.6) methods. Data of the three techniques are available for the section 737 – 950 m where clay-rich rocks dominate, and all methods can be applied. For the clay-poor rocks of the Malm and the Muschelkalk only data from isotope diffusive-exchange experiments are available. For the advective displacement technique, the average of the first two displaced solution aliquots is considered as being most representative for the in situ porewater. For the squeezed water, the one obtained at the lowest squeezing pressure (200 MPa or 300 MPa) is considered as being most representative for the in situ porewater.

All the porewater isotope data, together with those for the groundwater samples from the aquifers in the Malm, Keuper and the Muschelkalk (*cf.* Section 2.4), are shown in Fig. 5.7-1 as a function of depth. For isotope data from isotope-diffusive exchange experiments the error bars reflect the propagated experimental and analytical uncertainty. For isotope data from advective displacement and high-pressure squeezing experiments only the analytical error is illustrated. In general, for δ^2H, the three methods agree well (within the uncertainty). However, for $\delta^{18}O$ both isotope data from high-pressure squeezing and from advective displacement systematically show slightly lower values compared to the data from isotope diffusive-exchange experiments. The reason for this is currently unknown.

5.7.2 Comparison with groundwater data and depth profiles

Owing to a low hydraulic conductivity (1×10^{-13} m/s) in the tested interval (712.56 to 735.00 m) no groundwater sample could be collected in the cored section of the Malm of BAC1-1. For the Keuper – where a groundwater sample could be collected in the Klettgau Formation – the $\delta^{18}O$ and $\delta^{2}H$ values of the groundwater agree well (i.e. within the propagated uncertainty) with those of the porewater obtained from samples in the packed-off interval. The groundwater in the Klettgau Formation appears to represent the depleted end point of the remarkably linear depth trend of the porewater isotope composition in the overlying interval Wildegg Formation – Klettgau Formation (two samples in the top of the underlying Bänkerjoch Formation show similar isotope compositions, a third one is more depleted but has a large uncertainty and is considered as less reliable based on quality control criteria; *cf.* Section 4.8). This linear depth trend is exceptional compared to all other boreholes of this campaign and Benken (Gimmi & Waber 2004, Gimmi et al. 2007) with an active Keuper aquifer where typically both $\delta^{18}O$ and $\delta^{2}H$ depth profiles are clearly curved. At the same time, the diffusion coefficients in the Dogger – Lias section of BAC1-1 do not differ significantly from those at the nearby STA2-1 borehole (with an active Keuper aquifer; Zwahlen et al. 2023a). Considering the relatively low hydraulic conductivities of the Keuper at BAC1-1 (i.e. compared to other boreholes), the nearly linear trend of the porewater isotope composition likely results from an extended interaction time between groundwater and porewater during comparably slow flow through the aquifer, which leads to a less depleted groundwater signature compared to other sites.

Although both $\delta^{18}O$ and $\delta^{2}H$ values of the porewater indicate a linear decrease from the Wildegg Formation down to the Klettgau Formation, the depletion in ^{18}O is – relatively – stronger than that in ^{2}H. This different behaviour likely reflects inherited trends from the initial porewater isotope profiles (i.e., before the isotope signatures in the adjacent aquifers changed to present-day values). Similar differences, partly less pronounced, were observed in data from other boreholes (Mazurek et al. 2021, Aschwanden et al. 2021, Mäder et al. 2021, Wersin et al. 2022a, Gimmi et al. 2022, Zwahlen et al. 2023a) or even in the older data from Benken (Gimmi & Waber 2004, Gimmi et al. 2007). Note that none of the isotope tracers show any irregularities or excursions in the deformation zone (911.63 – 912.16 m) of the Opalinus Clay and neither in the fractured interval of the Staffelegg Formation (940.58 – 942.78 m; *cf.* Section 2.2). Thus, based on the porewater isotope profiles there are no indications for recent advective flow in these intervals.

Both $\delta^{2}H$ and $\delta^{18}O$ values of the groundwater from the Muschelkalk aquifer are slightly depleted compared to those of the porewater obtained from samples in the packed-off interval. Note that most negative porewater isotope values are observed at around 1100 m depth coinciding with a set of prominent joints at 1'099.40 – 1'103.98 m depth (*cf.* Section 2.2). The Muschelkalk groundwater appears to represent minima of $\delta^{18}O$ and $\delta^{2}H$ and the adjacent porewaters in the Bänkerjoch Formation indicate remarkably steep gradients towards heavier values upwards. Such steep gradients indicate either that the change in the isotope signal of the groundwater towards present-day values is geologically young (as also indicated by the residence time of the groundwater of a few tens of kyrs; Heidinger & Eichinger *in prep.*), and/or the diffusion coefficients in the anhydrite-rich Bänkerjoch Formation are very low. Gimmi et al. (2024) put the BAC1-1 data into context with other boreholes of this campaign.

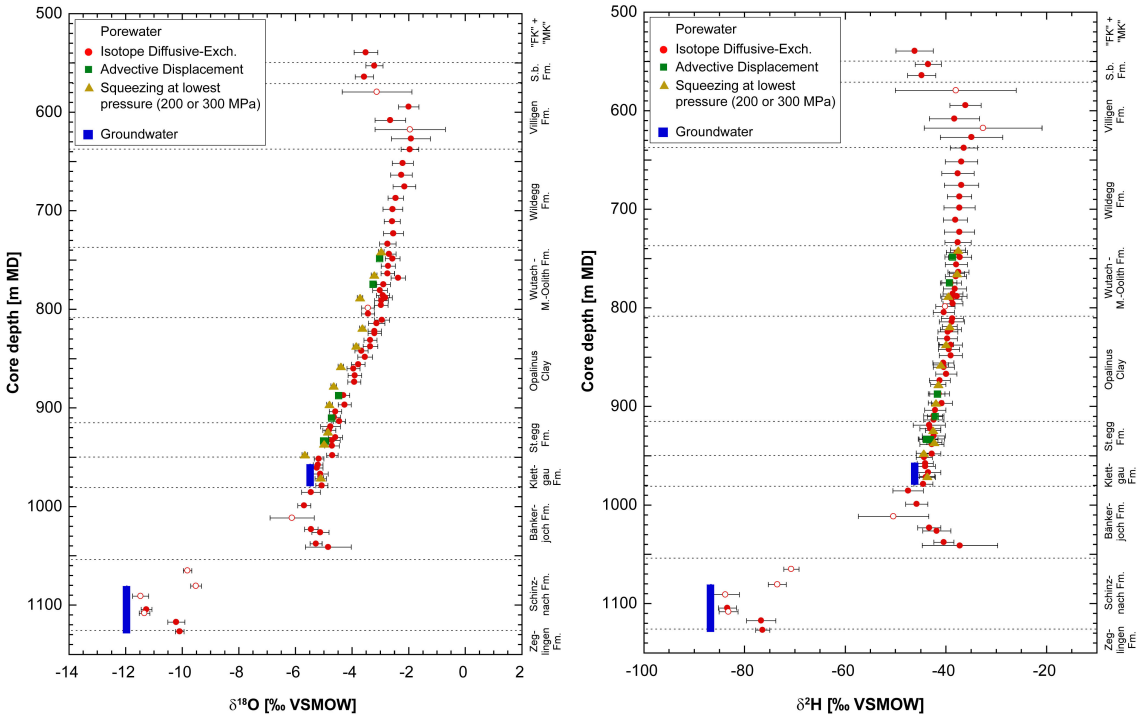

Fig. 5.7-1: Depth trends of $\delta^{18}O$ and $\delta^{2}H$ in groundwater and porewater derived by all techniques

Bars indicate propagated analytical errors (diffusive exchange) or simple analytical errors (squeezing, advective displacement). Groundwater data are from Lorenz (*in prep.*). Open symbols refer to porewater isotope values which are less reliable owing to experimental artefacts (*cf.* Section 4.8).

5.7.3 $\delta^{2}H$ versus $\delta^{18}O$ and comparison with Global Meteoric Water Line

Fig. 5.7-2 illustrates all data in a $\delta^{18}O$ vs. $\delta^{2}H$ diagram. Such diagrams provide information on e.g. climatic conditions during recharge, on water-rock interactions, and/or on mixing of different water components.

Porewater isotope signatures at the top of the cored section in the «Felsenkalke» + «Massenkalk» and in the Schwarzbach Formation plot far to the right of the Global Meteoric Water Line (GMWL) and even more enriched $\delta^{18}O$ and $\delta^{2}H$ values are observed in the underlying Villigen Formation (solid red arrow 1 in Fig. 5.7-2). From the Wildegg Formation down to the water-conducting zone in the Klettgau Formation the porewater isotope composition continuously evolves towards lower $\delta^{18}O$ and $\delta^{2}H$ values approaching the GMWL, indicating a meteoric component in the latter porewaters (solid red arrow 2 in Fig. 5.7-2). The pronounced deviation of the porewater $\delta^{18}O$-$\delta^{2}H$ signatures with respect to the Global Meteoric Water Line at the top of the section in the Malm and the «Brauner Dogger» indicates long residence times of these porewaters, with values affected by exchange with groundwater in the Malm aquifer, and possibly by water-rock interactions. The deviation of the Keuper groundwater from the GMWL is likely due to mixing/diffusive exchange with isotopically different water components (e.g., exchange with adjacent porewater) and/or water-rock interactions. The Bänkerjoch Formation shows somewhat less negative porewater $\delta^{18}O$ and $\delta^{2}H$ values also located slightly to the right of the GMWL (solid red arrow 3 in Fig. 5.7-2). At the base of the Bänkerjoch Formation the porewater isotope

composition sharply evolves to distinctly more negative values in the water-conducting zone of the Muschelkalk located on the GMWL and slightly depleted relative to modern recharge (solid red arrow 4 in Fig. 5.7-2), indicative for infiltration under colder-climate conditions. Note that modern recharge does not only refer to recent or post-glacial recharge but rather recharge under climatic conditions similar to recent conditions (e.g. during an interglacial period in the Quaternary).

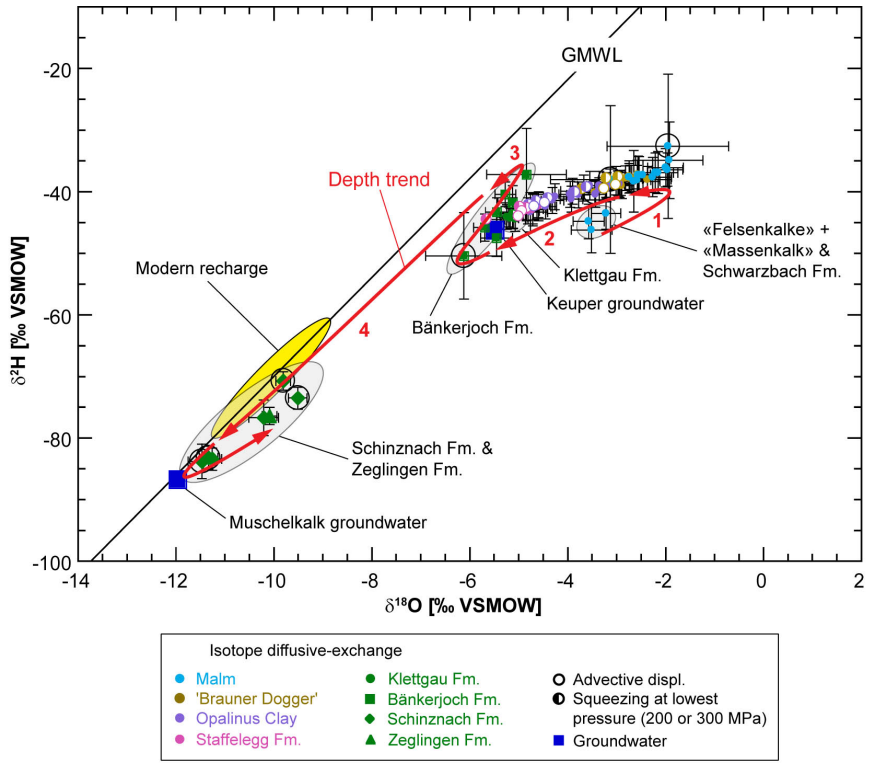

Fig. 5.7-2: δ^2H vs. $\delta^{18}O$ for groundwater and porewater derived by all techniques

Bars indicate propagated analytical errors (diffusive exchange) or simple analytical errors (squeezing, advective displacement). Groundwater data are from Lorenz (*in prep.*). GMWL = Global Meteoric Water Line (defined as $\delta^2H = 8\ \delta^{18}O + 10$; Craig 1961). Range of modern recharge from Kullin & Schmassmann (1991). Samples in circles are less reliable owing to experimental artefacts (*cf.* Section 4.8). See text for details on the numbering of red arrows (depth trend).

6 Final remarks and main conclusions

RWI team

High-quality cores could be extracted from the BAC1-1 borehole as planned between the «Felsenkalke» + «Massenkalk» and the top of the Zeglingen Formation. Groundwater could be sampled from the Klettgau Formation (Keuper aquifer) and the Schinznach Formation (Muschelkalk aquifer). The porewater samples enabled to acquire high quality mineralogical, petrophysical and porewater data using a well-established procedure. Drilling operations proceeded down to a maximum depth of 1'306.26 m (MD – bgl) (Weitenau Formation, Permian).

As in previous boreholes, a number of systematic depth trends were observed for the contents of clay minerals, quartz and calcite. Above a strong upward decrease of clay minerals in the Staffelegg Formation, the base of the Opalinus Clay marks a major mineralogical discontinuity towards high clay-mineral contents. Within the Opalinus Clay, trends are less well defined in comparison to other boreholes. The «Parkinsoni-Württembergica-Schichten» show a distinct upward increase of the ratio quartz/clay minerals. The ratio of the illite-to-kaolinite end-member clays also shows a systematic variation with depth. A substantial upward decrease is identified within the Klettgau and Staffelegg Formations, reaching a minimum in the centre of the Opalinus Clay. From there, the ratio increases towards the top of the Wildegg Formation. It is noteworthy that while most other boreholes show a near-constant illite-to-kaolinite ratio within the Opalinus Clay, a distinct minimum (around 1) is found in the case of BAC1-1, evolving to a ratio of about 2 at the base and top of the formation.

The depth trends of mineral contents correlate well with those of petrophysical parameters and can be even clearer (e.g. water content). Water content and porosity correlate positively with the clay-mineral content, even though the correlation is far from perfect. This indicates that apart from clay-mineral content, other rock characteristics, such as depositional environment, pore-space architecture and diagenesis have an influence on porosity. The most prominent deviations towards high porosity include dolostones of the Schinznach and Zeglingen Formations, where diagenetic dissolution occurred, as well as dolomitic marls and sandstones of the Klettgau Formation. In contrast, anhydrite-rich samples from the Bänkerjoch Formation show markedly low porosities.

Nitrogen adsorption data were obtained for 11 samples from the upper and lower confining units of the Opalinus Clay only. The samples are lithologically very different, but the general trends match with those observed for the larger dataset from the BUL1-1 borehole. There is a broadly positive correlation of the external specific surface area (BET, N_2 adsorption) with clay-mineral contents and, when excluding two outliers, with water contents. Due to the small sample number, no clear trends of average radii of external pores (assuming negligible interlayer water) with water content or with clay-mineral content are visible, but values in similar ranges as noted for other boreholes are observed.

Drilling fluid contamination was not identified in aqueous extraction samples. It was noticed that aqueous extraction on dried rock yielded substantially lower Br and somewhat lower Cl concentrations compared to extracts conducted on wet rock, especially in the samples of the Rietheim Member. This might be related to complexation with transformed organic matter during the heating to 105 °C and oxidation, but further investigations would be needed to test this hypothesis.

From the «Felsenkalke» + «Massenkalk» to the Klettgau Formation both $\delta^{18}O$ and $\delta^{2}H$ values of the porewater show well defined, slightly curved profiles, with a maximum in the Villigen Formation. None of the isotope tracers show any irregularities or excursions in the deformation zone (911.63 – 912.16 m) of the Opalinus Clay. Porewaters in the Malm and the «Brauner

Dogger» are enriched in ^{18}O and ^{2}H and plot far to the right of the Global Meteoric Water Line (GMWL) indicating long residence times. From the «Brauner Dogger» to the base of the Klettgau Formation the porewater isotope composition continuously evolves towards lower values of $\delta^{18}O$ and (less so) $\delta^{2}H$. It does not fully approach the GMWL but matches very well with the groundwater value in the Keuper aquifer. The different behaviour of $\delta^{18}O$ and $\delta^{2}H$ porewater values in this section of the borehole may reflect inherited trends resulting from the earlier evolution (i.e., before the isotope signatures in the confining aquifers changed to present-day values). From the Keuper aquifer towards the Muschelkalk aquifer, the porewater values increase first slightly in the Bänkerjoch Formation before dropping sharply towards the more depleted meteoric signature (below modern recharge) in the Muschlkalk aquifer. The gradients between the lower part of the Bänkerjoch Formation and the upper part of the Schinznach formation appear very steep, but the number and reliability of data in this part is, unfortunately, low. The isotope composition of porewater and groundwater in the Muschelkalk falls on or slightly to the right of the GMWL and is somewhat depleted relative to modern recharge, indicative for infiltration under cold-climate conditions.

Anion-accessible porosities could be derived from squeezed (SQ) and advectively displaced (AD) porewaters from the interval «Brauner Dogger» – Klettgau Formation. These yielded Cl-accessible porosity fractions (f_{Cl}) with a mean value of ~ 0.51 ± 0.07. This is in a comparable range as derived for previous boreholes from the TBO programme. The same linear relationship of f_{Cl} with clay-mineral content as for the three other boreholes from the Nördlich Lägern siting region (BUL1-1, STA3-1, STA2-1) was used to derive Cl and Br concentrations per accessible porewater from aqueous extraction.

Broadly consistent Cl and Br profiles are revealed from squeezing, advective displacement and re-calculated aqueous extraction data. Using pycnometer porosities instead of water-loss porosities when scaling the aqueous extract data to concentrations per bulk porewater or accessible porewater leads to a similar profile but with slightly more scatter in the upper part of the profile. The Cl profile exhibits near-to-constant concentrations between the lower Malm (Villigen Formation) and the Keuper aquifer, with values scattering around 10 g/L. Below a decrease towards the Muschelkalk aquifer is observed, with Cl concentrations reaching ~ 1 g/L in the porewaters and groundwater. The Br profile is comparable with that of Cl. Overall, analogous profiles were derived for $\delta^{18}O$ and $\delta^{2}H$, which, however, show steadily decreasing values with depth towards the Keuper aquifer.

The depth profile of the Br/Cl ratio reveals consistency between AqEx and SQ and AD data. The Br/Cl profile shows less scatter than that of Cl or Br due to the fact that no assumptions on anion accessibility need to be made and the uncertainty regarding re-calculation to the rock porosity cancels out. Constant Br/Cl ratios close to modern seawater are found in the upper part of the profile and decrease slightly in the Opalinus Clay towards the Keuper aquifer. Below, the profile shows a positive excursion in the Bänkerjoch Formation and upper Schinznach Formation, followed by a strong decrease towards the Muschelkalk aquifer where both porewaters and the groundwater exhibit very low ratios. The very low Br/Cl concentrations in this aquifer and below are indicative of the imprint of halite dissolution from the salt layer in the underlying Zeglingen formation.

The sulphate profile obtained from SQ and AD, which covers the sequence «Brauner Dogger» – Staffelegg Formation, indicates constant SO_4 concentrations (~ 2 g/L) across the «Brauner Dogger» down to the lower part of the Opalinus Clay. From there, a slightly increasing trend reaching ~ 3 g/L in the Keuper aquifer can be observed, but with a negative excursion in the Staffelegg Formation. Conversely, AqEx data yield systematically higher and more variable concentrations, as has been observed in the previous boreholes and the Mont Terri Rock Laboratory. SO_4/Cl ratios deduced from SQ and AD exhibit a similar shape as the SO_4 profile with values of ~ 0.1 (molar units) in the «Brauner Dogger» and Opalinus Clay.

Cation data representative of the porewater could be obtained from SQ and AD experiments. These generally indicate rather flat profiles for the major cations Na and Ca as well as for K across the sampled «Brauner Dogger» – Klettgau Formation sequence. Mg shows a slightly decreasing trend with depth.

The cation exchange capacity (CEC) correlates positively with the clay-mineral content. An even better correlation can be deduced with the sum of illite and smectite end-member mineral contents, the main carriers of the CEC. The main exchangeable cations are Na and Ca, followed by Mg and K. The exchanger composition (cation occupancies) is approximately constant across the «Brauner Dogger» – Opalinus Clay but indicates a shift towards enrichment of Na and Mg at the expense of Ca in the Staffelegg-Klettgau sequence. The exchanger composition determined from extraction methods exhibits the same trends as the "back-calculated" exchanger composition obtained from modelling of the SQ and AD porewater data.

The porewaters in the Opalinus Clay and confining units display moderate salinities and ionic strengths with Cl concentrations of about 8 – 11 g/L. These chloride levels in the BAC1-1 are slightly higher than the ones of STA2-1 and STA3-1 (maximum concentration ~ 8 g/L) and slightly lower than the ones of BUL1-1 from the same siting region (maximum concentration ~ 12 g/L). The porewaters are of Na-(Ca)-Cl-(SO_4) type (according to the nomenclature of Jäckli 1970) in the interval sampled for SQ and AD («Parkinsoni-Württembergica-Schichten» – Staffelegg Formation).

The pH/pCO_2 conditions deduced for the SQ and AD experiments indicate values ~ 7 – 7.5 and ~ -2 to -2.8 log(bar) for pH and pCO_2, respectively. For SQ data, however, a correction procedure by geochemical modelling was necessary to account for CO_2 degassing that had occurred during the squeezing process.

SQ experiments yield porewater TOC concentrations of 130 – 170 mg C/L whereas data from AD experiments show higher concentrations (200 – 800 mg C/L). Concentrations from both experiments are not thought to reflect in situ porewater conditions, but rather the easily mobilisable fraction from the solid organic matter (that is, values are higher than in situ).

SQ and isotope diffusive exchange experiments were performed on a core subjected to advective displacement to increase the understanding of methodological differences in some results. Although this core showed close to complete Cl, Br and isotope breakthrough based on AD exfiltration concentrations, consecutive squeezing and isotope diffusive exchange still revealed a significant signature of the in situ porewater. This indicates the existence of preferential pathways for advective transport under the experimental conditions (very high hydraulic gradients), and domains where the equilibration with the APW is more diffusion-controlled and slower.

An in-depth interpretation and comparison with data from boreholes from the same or other siting areas is beyond the scope of this report. Here, a short summary of a few points is presented:

- In the BAC1-1 borehole, groundwater samples could be extracted from packed-off sections in the Keuper and in the Muschelkalk. At both localities tracer profiles as well as structural observations confirm the presence of aquifers in the Klettgau Formation and in the Schinznach Formation. The geochemical gradients towards the Keuper aquifer are low for many porewater tracers. In contrast, there is a sharp and distinct gradient from the Bänkerjoch Formation towards Muschelkalk aquifer.
- From the SQ and AD data, the f_{Cl} value (~ 0.51 for clay-mineral contents > 30 wt.-%) is similar as derived for the BUL1-1 borehole (0.52), but slightly higher than observed for other investigated boreholes.
- The porewaters in the Opalinus Clay from BAC1-1 show chloride concentrations of ~10 g/L fitting well within the range of concentrations (8 – 12 g/L) displayed by the other three boreholes (BUL1-1, STA2-1, STA3-1) of the Nördlich Lägern siting region.
- The profiles of $\delta^{2}H$ and $\delta^{18}O$ in BAC1-1 are broadly similar to profiles in other boreholes of the Nördlich Lägern region, but BAC1-1 shows a flat profile above the local Keuper aquifer in contrast to STA2-1. This probably relates to the lower hydraulic conductivity in BAC1-1 (8×10^{-9} m/s) compared to STA2-1 (6×10^{-8} m/s).

7 References

Allison, J.D., Brown, D.S. & Novo-Gradac, K.J. (1991): MINTEQA2/PRODEFA2, a geochemical assessment model for environmental systems: Version 3.0 user's manual. Environmental Research Laboratory, Office of Research and Development, U.S. Environmental Protection Agency, 106 p.

Aschwanden, L. & Wersin, P. (2020): Experimental study of sulphate in the Opalinus Clay: Results from extraction tests. Nagra Arbeitsbericht NAB 20-17.

Aschwanden, L., Camesi, L., Gimmi, T., Jenni, A., Kiczka, M., Mäder, U., Mazurek, M., Rufer, D., Waber, H.N., Wersin, P., Zwahlen, C. & Traber, D. (2021): TBO Trüllikon-1-1: Data report Dossier VIII. Rock properties, porewater characterisation and natural tracer profiles. Nagra Arbeitsbericht NAB 20-09.

Aschwanden, L., Camesi, L., Gaucher, E., Gimmi, T., Jenni, A., Kiczka, M., Mäder, U., Mazurek, M., Rufer, D., Waber, H.N., Wersin, P., Zwahlen, C. & Traber, D. (2022): TBO Stadel-3-1: Data report Dossier VIII. Rock properties, porewater characterisation and natural tracer profiles. Nagra Arbeitsbericht NAB 22-01.

Aschwanden, L., Waber, H.N., Eichinger, F. & Gimmi, T. (2023): Isotope diffusive exchange experiments for deriving porewater isotope composition in low-permeability rocks – Improvements in experimental procedure and data processing. Applied Geochemistry, *accepted*.

Bradbury, M.H. & Baeyens, B. (1998): A physicochemical characterisation and geochemical modelling approach for determining porewater chemistries in argillaceous rocks. Geochim. Cosmochim. Acta 62, 783-795.

Courdouan-Merz, A. (2008): Nature and reacivity of dissolved organic matter in clay formations evaluated for the storage of radioactive waste. PhD thesis. ETH Zurich.

Courdouan, A., Christl, I., Meylan, S., Wersin, P. & Kretzschmar, R. (2007a): Characterization of dissolved organic matter in anoxic rock extracts and in situ pore water of the Opalinus Clay. Applied Geochemistry 22, 2926-2939.

Courdouan, A., Christl, I., Meylan, S., Wersin, P. & Kretzschmar, R. (2007b): Isolation and characterization of dissolved organic matter from the Callovo-Oxfordian formation. Applied Geochemistry 22, 1537-1548.

Craig, H. (1961): Isotopic variations in meteoric waters. Science 133, 1702-1703.

Debure, M. & Gailhanou, H. (2019): GD experiment: Experimental study of sulphate in Opalinus Clay. Unpubl. Mont Terri Technical Note. Mont Terri Project, Switzerland.

Deniau, I., Devol-Brown, I., Derenne, S., Behar, F. & Largeau, C. (2008): Comparison of the bulk geochemical features and thermal reactivity of kerogens from Mol (Boom Clay), Bure (Callovo–Oxfordian argillite) and Tournemire (Toarcian Shales) underground research laboratories. Science of the Total Environment 389, 475-485.

Gimmi, T. & Alt-Epping, P. (2018): Simulating Donnan equilibria based on the Nernst-Planck equation. Geochim. Cosmochim. Acta 232, 1-13.

Gimmi, T. & Waber, H.N. (2004): Modelling of tracer profiles in porewater of argillaceous rock in the Benken borehole: Stable water isotopes, chloride and chlorine isotopes. Nagra Technical Report NTB 04-05.

Gimmi, T., Waber, H.N., Gautschi, A. & Rübel, A. (2007): Stable water isotopes in pore water of Jurassic argillaceous rocks as tracers for solute transport over large spatial and temporal scales. Water Resources Research 43, W04410, doi:10.1029/2005WR004774.

Gimmi, T., Leupin, O.X., Eikenberg, J., Glaus, M., Van Loon, L.R., Waber, H.N., Wersin, P., Wang, H.A.O., Grolimund, D., Borca, C.N., Dewonck, S. & Wittebroodt, C. (2014): Anisotropic diffusion at the field scale in a four-year multi-tracer diffusion and retention experiment. I: Insights from the experimental data. Geochim. Cosmochim. Acta 125, 373-393.

Gimmi, T., Aschwanden, L., Camesi, L., Gaucher, E.C., Jenni, A., Kiczka, M., Mäder, U., Mazurek, M., Rufer, D., Waber, H.N., Wersin, P., Zwahlen, C. & Traber, D. (2022): TBO Bözberg-2-1: Data report Dossier VIII. Rock properties, porewater characterisation and natural tracer profiles. Nagra Arbeitsbericht NAB 21-22.

Gimmi, T., Aschwanden, L., Waber, H.N., Gaucher, E., Ma, J. & Traber, D. (2024): Profiles of $\delta^{18}O$ and $\delta^{2}H$ in porewater of a Mesozoic rock sequence: Regional variability and relation to large-scale transport regimes. Applied Geochemistry 160, 105846.

Hadi, J., Wersin, P., Mazurek, M., Waber, H.N., Marques Fernandes, M., Baeyens, B., Honty, M., De Craen, M., Frederickx, L., Dohrmann, R. & Fernandez, A.M. (2019): Intercomparison of CEC method within the GD project. Mont Terri Technical Report TR 2017-06. Mont Terri Project, Switzerland.

Heidinger, M. & Eichinger, F. (*in prep.*): Krypton-81 model ages of groundwaters from the TBO boreholes (working title). Nagra Arbeitsbericht.

Isler, A., Pasquier, F. & Huber, M. (1984): Geologische Karte der zentralen Nordschweiz 1:100'000. Herausgegeben von der Nagra und der Schweiz. Geol. Komm.

Jäckli, H. (1970): Kriterien zur Klassifikation von Grundwasservorkommen. Eclogae Geol. Helv. 63/2, 389-434.

Jenni, A., Aschwanden, L., Lanari, P., de Haller, A. & Wersin, P. (2019): Spectroscopic investigation of sulphur-containing minerals in Opalinus Clay. Nagra Arbeitsbericht NAB 19-23.

Kiczka, M., Wersin, P., Mazurek, M., Zwahlen, C., Jenni, A. & Mäder, U. (2023): Porewater composition in clay rocks explored by advective displacement and squeezing experiments. Applied Geochemistry 159, 105838.

Kullin, M. & Schmassmann, H. (1991): Isotopic composition of modern recharge. *In:* Pearson, F.J., Balderer, W., Loosli, H.H., Lehmann, B.E., Matter, A., Peters, Tj., Schmassmann, H.-J. & Gautschi, A. (1991): Applied Isotope Hydrogeology – A Case Study in Northern Switzerland. Studies in Environmental Science 43, Elsevier, Amsterdam, 65-89.

Lorenz, G.D. (*in prep.*): Borehole BAC1-1 (Bachs-1-1): Fluid sampling and analytical hydrochemical data report. Unpubl. Nagra Interner Bericht.

Mäder, U. (2018): Advective displacement method for the characterisation of porewater chemistry and transport properties in claystone. Geofluids 2018, Article ID 8198762, doi.org/10.1155/2018/8198762.

Mäder, U. & Waber, H.N. (2017): Results of advective displacement / multi-component transport experiments from claystone samples of the Schlattingen borehole. Nagra Arbeitsbericht NAB 17-16.

Mäder, U. & Wersin, P. (2022). Reference porewaters for SGT Stage 3 of the Opalinus Clay for the siting regions Jura Ost (JO), Nördlich Lägern (NL) and Zürich Nordost (ZNO). Nagra Arbeitsbericht NAB 22-47.

Mäder, U., Aschwanden, L., Camesi, L., Gimmi, T., Jenni, A., Kiczka, M., Mazurek, M., Rufer, D., Waber, H.N., Wersin, P., Zwahlen, C. & Traber, D. (2021): TBO Marthalen-1-1: Data report Dossier VIII. Rock properties, porewater characterisation and natural tracer profiles. Nagra Arbeitsbericht NAB 21-20.

Marques Fernandes, M. & Baeyens, B. *(in prep.*): Sorption of Cs(I), Ni(II), Eu(III), Th(IV) and U(VI) on rock samples of Opalinus Clay and confining units from deep boreholes at the potential siting regions Jura Ost, Nördlich Lägern and Zürich Nordost: Measurements and predictive sorption model. Nagra Technischer Bericht NTB 23-01.

Mazurek, M. (2017): Gesteinsparameter-Datenbank Nordschweiz – Version 2. Nagra Arbeitsbericht NAB 17-56.

Mazurek, M. & Aschwanden, L. (2020): Multi-scale petrographic and structural characterisation of the Opalinus Clay. Nagra Arbeitsbericht NAB 19-44.

Mazurek, M., Oyama, T., Wersin, P. & Alt-Epping, P. (2015): Pore-water squeezing from indurated shales. Chemical Geology 400, 106-121.

Mazurek, M., Aschwanden, L., Camesi, L., Gimmi, T., Jenni, A., Kiczka, M., Mäder, U., Rufer, D., Waber, H.N., Wanner, P., Wersin, P. & Traber, D. (2021): TBO Bülach-1-1: Data Report Dossier VIII. Rock properties, porewater characterisation and natural tracer profiles. Nagra Arbeitsbericht NAB 20-08.

Mazurek, M., Gimmi, T., Zwahlen, C., Aschwanden, L., Gaucher, E., Kiczka, M., Rufer, D., Wersin, P., Marques Fernandes, M., Glaus, M., Van Loon, L., Traber, D., Schnellmann, M. & Vietor, T. (2023): Swiss deep drilling campaign 2019–2022: Geological overview and rock properties with focus on porosity and pore-space architecture. Applied Geochemistry 159, 105839.

Naef, H., Büchi, M., Bläsi, H.R., Deplazes, G. & Gysi, M. (2019): Lithology Manual – Lithological description of drill cores and cuttings in Northern Switzerland. Nagra Arbeitsbericht NAB 19-11.

Nagra (2008): Vorschlag geologischer Standortgebiete für das SMA- und das HAA-Lager. Geologische Grundlagen. Nagra Technischer Bericht NTB 08-04.

Nagra (2014): SGT Etappe 2: Vorschlag weiter zu untersuchender geologischer Standortgebiete mit zugehörigen Standortarealen für die Oberflächenanlage. Geologische Grundlagen. Dossier II: Sedimentologische und tektonische Verhältnisse. Nagra Technischer Bericht NTB 14-02.

Parkhurst, D.L. & Appelo, C.A.J. (2013): Description of input and examples for PHREEQC Version 3: A computer program for speciation, batch-reaction, one-dimensional transport, and inverse geochemical calculations. No. 6-A43. US Geological Survey.

Pearson, F.J. (1999): What is the porosity of a mudrock? *In*: Aplin, A.C., Fleet A.J. & Macquaker, J.H.S. (eds.): Muds and Mudstones: Physical and Fluid Flow Properties. Geological Society, London, Special Publications 158, 9-21.

Pearson, F.J., Arcos, D., Bath, A., Boisson, J.Y., Fernandez, A.M., Gäbler, H.E., Gaucher, E., Gautschi, A., Griffault, L., Hernan, P. & Waber, H.N. (2003): Mont Terri project – geochemistry of water in the Opalinus Clay formation at the Mont Terri rock laboratory. Federal Office for Water and Geology Rep. 5, Bern, Switzerland.

Pearson, F.J., Tournassat, C. & Gaucher, E.C. (2011): Biogeochemical processes in a clay formation in situ experiment: Part E – Equilibrium controls on chemistry of pore water from the Opalinus Clay, Mont Terri underground research laboratory, Switzerland. Applied Geochemistry 26, 990-1008.

Pietsch, J. & Jordan, P. (2014): Digitales Höhenmodell Basis Quartär der Nordschweiz – Version 2013 (SGT E2) und ausgewählte Auswertungen. Nagra Arbeitsbericht NAB 14-02.

Rufer, D. (2019): Field Manual: Drillcore sampling for analytical purposes. Nagra Arbeitsbericht NAB 19-13.

Rufer, D. & Mazurek, M. (2018): Pore-water extraction and characterization: Benchmarking of the squeezing and adapted isotope diffusive exchange methods. NWMO Technical Report NWMO-TR-2018-14. Nuclear Waste Management Organization, Toronto, Canada.

Thoenen, T., Hummel, W., Berner, U. & Curti, E. (2014): The PSI/Nagra Chemical Thermodynamic Database 12/07. PSI Bericht Nr. 14-04, Paul Scherrer Institut, Villigen, Switzerland.

Thommes, M., Kaneko, K., Neimark, A.V., Olivier, J.P., Rodriguez-Reinoso, F., Rouquerol, J. & Sing, K.S. (2015): Physisorption of gases, with special reference to the evaluation of surface area and pore size distribution (IUPAC Technical Report). Pure and Applied Chemistry 87, 1051-1069.

Tournassat, C., Vinsot, A., Gaucher, E.C. & Altmann, S. (2015): Chemical conditions in clayrocks. *In:* Tournassat, C., Steefel, C.I., Bourg, I.C. & Berrgaya, F. (eds.): Natural and Engineered Clay Barriers. Developments in Clay Science 6, Chapter 3, 71-100. Elsevier.

Waber, H.N. (ed.) (2020): SGT-E3 deep drilling campaign (TBO): Experiment procedures and analytical methods at RWI, University of Bern (Version 1.0, April 2020). Nagra Arbeitsbericht NAB 20-13.

Wersin, P., Mazurek, M., Waber, H.N., Mäder, U.K., Gimmi, T., Rufer, D. & de Haller, A. (2013): Rock and porewater characterisation on drillcores from the Schlattingen borehole. Nagra Arbeitsbericht NAB 12-54.

Wersin, P., Mazurek, M., Mäder, U.K., Gimmi, T., Rufer, D., Lerouge, C. & Traber, D. (2016): Constraining porewater chemistry in a 250 m thick argillaceous rock sequence. Chemical Geology 434, 43-61.

Wersin, P., Pekala, M., Mazurek, M., Gimmi, T., Mäder, U.K., Jenni, A., Rufer, D. & Aschwanden, L. (2020): Porewater chemistry of Opalinus Clay: Methods, modelling & buffering capacity. Nagra Technical Report NTB 18-01.

Wersin, P., Aschwanden, L., Camesi, L., Gaucher, E.C., Gimmi, T., Jenni, A., Kiczka, M., Mäder, U., Mazurek, M., Rufer, D., Waber, H.N., Zwahlen, C. & Traber, D. (2022a): TBO Bözberg-1-1: Data report Dossier VIII. Rock properties, porewater characterisation and natural tracer profiles. Nagra Arbeitsbericht NAB 21-21.

Wersin, P., Mazurek, M. & Gimmi, T. (2022b): Porewater chemistry of Opalinus Clay revisited: Findings from 25 years of data collection at the Mont Terri Rock Laboratory. Applied Geochemistry 138, 105234.

Wersin, P., Gimmi, T., Ma, J., Mazurek, M., Zwahlen, C., Aschwanden, L., Gaucher, E. & Traber, D. (2023): Porewater profiles of Cl and Br in boreholes penetrating the Mesozoic sequence in northern Switzerland. Applied Geochemistry 159, 105845.

Zwahlen, C., Aschwanden, L., Camesi, L., Gaucher, E., Gimmi, T., Jenni, A., Kiczka, M., Mäder, U., Mazurek, M., Rufer, D., Waber, H.N., Wersin, P. & Traber, D. (2023a): TBO Stadel-2-1: Data report Dossier VIII. Rock properties, porewater characterisation and natural tracer profiles. Nagra Arbeitsbericht NAB 22-02.

Zwahlen, C., Gimmi, T., Jenni, A., Kiczka, M., Mazurek, M., van Loon, L., Mäder, U. & Traber, D. (2023b): Chloride accessible porosity fractions across the Jurassic sedimentary rocks of northern Switzerland. Applied Geochemistry, accepted.